

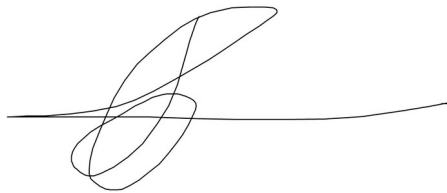
# Title Page: An alternative approach for assessing drug-induced seizures, using non-protected larval zebrafish

Submitted by Joseph Pinion to the University of Exeter as a thesis for the degree of Doctor of Philosophy in Biological Sciences, December 2022.

This thesis is available for Library use on the understanding that it is copyright material and that no quotation from the thesis may be published without proper acknowledgment.

I certify that all material in this thesis which is not my own work has been identified and that any material that has previously been submitted and approved for the award of a degree by this or any other University has been acknowledged.

Signed, Joseph Pinion:

A handwritten signature in black ink, consisting of a series of loops and a long horizontal line extending to the right.

## Abstract

As many as 9% of epileptic seizures occur as a result of drug toxicity. Identifying compounds with seizurogenic side effects is imperative for assessing compound safety during drug development, however, multiple marketed drugs still have clinical associations with seizures. Moreover, current approaches for assessing seizurogenicity, namely rodent EEG and behavioural studies, are highly resource intensive. This being the case, alternative approaches have been postulated for assessing compound seizurogenicity, including *in vitro*, *in vivo*, and *in silico* methods.

In this thesis, experimental work is presented supporting the use of larval zebrafish as a candidate model organism for developing new seizure liability screening approaches. Larval zebrafish are translucent, meaning they are highly amenable to imaging approaches while offering a more ethical alternative to mammalian research. Zebrafish are furthermore highly fecund facilitating capacity for both high replication and high throughput. The primary goal of this thesis was to identify biomarkers in larval zebrafish, both behavioural and physiological, of compounds that increase seizure liability.

The efficacy of this model organism for seizure liability testing was assessed through exposure of larval zebrafish to a mechanistically diverse array of compounds, selected for their varying degrees of seizurogenicity. Their central nervous systems were monitored using a variety of different techniques including light sheet microscopy, local field potential recordings, and behavioural monitoring. Data acquired from these measurements were then analysed using a variety of techniques including frequency domain analysis, clustering, functional connectivity, regression, and graph theory. Much of this analysis was exploratory in nature and is reflective of the infancy of the field.

Experimental findings suggest that larval zebrafish are indeed sensitive to a wide range of pharmacological mechanisms of action and that drug actions are reflected by behavioural and direct measurements of brain activity. For example, local field potential recordings revealed electrographic responses akin to pre-ictal, inter-ictal and ictal events identified in humans.  $\text{Ca}^{2+}$  imaging using light sheet microscopy found global increases in fluorescent intensity and functional connectivity due to seizurogenic drug administration. In addition,

further functional connectivity and graph analysis revealed macroscale network changes correlated with drug seizurogenicity and mechanism of action. Finally, analysis of swimming behaviour revealed a strong correlation between high-speed swimming behaviours and administration of convulsant compounds.

In conclusion, presented herein are data demonstrating the power of functional brain imaging, LFP recordings, and behavioral monitoring in larval zebrafish for assessing the action of neuroactive drugs in a highly relevant vertebrate model. These data help us to understand the relevance of the 4 dpf larval zebrafish for neuropharmacological studies and reveal that even at this early developmental stage, these animals are highly responsive to a wide range of neuroactive compounds across multiple primary mechanisms of action. This represents compelling evidence of the potential utility of larval zebrafish as a model organism for seizure liability testing.

## Acknowledgements

I would like to thank my supervisors, Charles Tyler, Andrew Randall, Matt Winter, and Marc Goodfellow for their help and guidance. In particular, Matt, for his seemingly inexhaustible patience, his understanding, and his unique brand of straightforward pragmatism. It is safe to say my Ph.D. would have been vastly more challenging without him. I also feel extremely fortunate to have had my lab mates and all the ARC staff, without whom zebrafish husbandry would have been immensely more tiresome.

I would also like to extend my gratitude to my friends\*, who made my 4 years in Exeter a period of profound joy, and whose comradeship contributed in a very real way to the completion of this thesis. I would especially like to thank my lab mate Callum and flatmate Milena: Callum for his contribution, advice, and infectious enthusiasm, and Milena for her openness, understanding and companionship, without which lockdowns would have been infinitely less enjoyable. In addition, I feel compelled to thank my friends Josh, Liam and Sam, whose kindness and hospitality made my transitions between homes and countries times of happiness and festivity.

While writing my thesis, I feel blessed to have shared the home of my brother Sam and his wife Marika. Our shared meals, surfs and ski trips transformed, what could have been a stressful time, into something altogether more relaxed and happy.

Finally, I would like to thank my parents, whose unconditional support and love is the reason I have enjoyed the life that I have.

*\* Ed, Toddy, Dan, Laski, Callum, Alastair, Erica, Tess, Milena, Hazel, James, Sophie, Charles, Jenni, Josh, Liam, Sam, Meryn, Matilde, Michael, Mike and Hannah.*



# Contents

Title Page: An alternative approach for assessing drug-induced seizures, using non-protected larval zebrafish

Abstract

Acknowledgements

Contents

List of Tables

Authors Declaration

List of Abbreviations

Chapter 1: General Introduction

1.1 Drug Induced Seizures

1.2 The Role of Neurotransmitters in Seizure

1.2.1 Gamma aminobutyric acid (GABA)

1.2.1.1 Glutamate

1.2.1.2 Ionotropic

1.2.1.3 Metabotropic

1.2.2 Acetylcholine

1.2.3 Opioids

1.2.4 Monoamines

1.2.4.1 Serotonin

1.2.4.2 Dopamine

1.2.4.3 Noradrenaline

1.2.4.4 Histamine

1.3 Current approaches for detecting drug-induced seizure liability

1.3.1 Rodent EEG

1.3.2 Rodent Behavioural Assays

1.4 *In vitro* Seizure Liability testing

1.4.1 Receptor-ligand binding assays

1.4.2 Brain slice

- 1.4.3 Cell culture – Rodent
- 1.4.4 Cell culture – Human Induced Pluripotent Stem Cells (hiPSC)
- 1.5 Zebrafish and seizure liability testing: the story so far.
  - 1.5.1 Zebrafish behavioural assessment
  - 1.5.2 Zebrafish Electrophysiology
  - 1.5.3 Utilising Ca<sup>2+</sup> for studying brain activity
  - 1.5.4 Zebrafish Ca<sup>2+</sup> Imaging
  - 1.5.5 In Silico and molecular markers of seizure
- 1.6 Summation
- 1.7 Thesis Aims

Chapter 2: Functional brain imaging in larval zebrafish for characterising the effects of seizurogenic compounds acting via a range of pharmacological mechanisms

- 2.1 Introduction
- 2.2 Methods
  - 2.2.1 Experimental animals
  - 2.2.2 Test compounds
  - 2.2.3 Selection of exposure concentration ranges and durations
  - 2.2.4 Drug treatment and light sheet microscopic imaging
  - 2.2.5 Light sheet microscopic imaging settings
  - 2.2.6 Image processing and peak parameter measurements
  - 2.2.7 Data analysis - Describing the resting state network
  - 2.2.8 Data analysis - Analysis of region-specific GCamp6s fluorescence across the whole larval brain
  - 2.2.9 Data analysis - Multivariate exploration of larval brain functional connectivity
  - 2.2.10 Data analysis - Post hoc assessment of phenotype-defining data features
  - 2.2.11 Data analysis - Overall functional connectivity as an indicator of altered network synchronicity

2.2.12 Materials

2.2.13 Nomenclature of targets and ligands

## 2.3 Results

2.3.1 The resting state network involves activation of hindbrain autonomic, sensory and motor centres

2.3.2 The 4 dpf larval zebrafish is responsive to a range of molecular mechanisms known to induce neural network hyperexcitation in mammals

2.3.3 Similarities in functional connectivity phenotypes of larvae exposed to monoaminergics and cholinergics

2.3.4 Alterations in brain region functional connectivity after exposure to cholinergic and monoaminergic compounds

2.3.5 Differences in patterns of brain functional connectivity between most non-seizurogenic and pro- seizurogenic compounds

## 2.4 Discussion

## 2.5 Supplementary Analysis

2.5.1 Network Based Statistic

2.5.2 Classification Algorithms: Neural networks and support vector machines

2.5.3 K-means clustering

## 2.6 Supplementary Results

# Chapter 3: Differential Electrographic Signatures Generated by Mechanistically-Diverse Seizurogenic Compounds in the Larval Zebrafish Brain

## 3.1 Introduction

## 3.2 Materials and Methods

3.2.1 Experimental animals

3.2.2 Test compounds and concentration range selection

3.2.3 In vivo LFP recordings from zebrafish brains

3.2.4 Data analysis: event detection

3.2.5 Data analysis: wavelet of selected events

3.2.6 Data analysis: number of selected events

3.2.7 Data analysis: comparisons of area under the curve (AUC) of the LFP baseline and exposure period

3.2.8 Data analysis: spectral analysis

3.2.9 Data analysis: classical multidimensional scaling (MDS) of baseline normalized spectral data

3.2.10 Code accessibility

### 3.3 Results

3.3.1 Mean event and wavelet analysis

3.3.2 Number of detected events

3.3.3 Changes in AUC between baseline and exposure

3.3.4 Spectral frequency band analysis

3.3.5 Classical MDS

### 3.4 Discussion

3.4.1 Electrographic phenotypes of representative traces

3.4.2 Trace amplitude and seizure

3.4.3 Neural oscillations zebrafish versus mammals

3.4.4 Study limitations

Chapter 4: The development and application of a within animal control-based approach for improving the sensitivity and specificity of functional brain imaging in larval zebrafish.

### 4.1 Introduction

### 4.2 Methods

4.2.1 Experimental animals

4.2.2 Test compounds and concentration range selection

4.2.3 In vivo  $\text{Ca}^{2+}$  light sheet imaging

4.2.4 Image processing

4.2.5 Data Analysis: Peak and Functional Connectivity Analysis

4.2.6 Data Analysis: Peak Analysis

4.2.7 Data Analysis: Functional Connectivity

4.2.8 Data Analysis: Graph Measures

## 4.3 Results

4.3.1 Mean fluorescent intensity

4.3.2 Peak Parameters

4.3.1 Multidimensional scaling of peak parameters

4.3.2 Functional connectivity changes in individual connections

4.3.3 Changes in Mean Functional connectivity

4.3.4 Graph measures

## 4.4 Discussion

## Chapter 5: Behavioural Profiling of Seizurogenic Compounds

5.1 Introduction

5.2 Methods

5.2.1 Model Organism

5.2.2 Experimental methodology

5.2.3 Data Analysis

5.2.4 Data Preparation

5.2.5 Data Analysis: PTZ vs Control (Positive Control vs Negative Control)

5.2.6 Data Analysis: Polynomial Linear Regression

5.2.7 Data Analysis: Logistic Regression

5.3 Results

5.3.1 PTZ vs Control

5.3.2 Polynomial Linear Regression

5.3.3 Logistic Regression

5.4 Discussion

## Chapter 6: General Discussion

## Bibliography

## List of Tables

**Table 2.1** Summary of the test chemicals and experimental exposure conditions used in the current study

**Table 3.1** Test compounds and exposure concentration ranges used for *in vivo* electrophysiological recording in 4 dpf *elavl3:GCaMP6s* zebrafish larvae

**Table 3.2:** All statistical test outputs from frequency band analyses

**Table 3.3** Summary of information comparing the effect of selected drugs on EEG in mammals from published data with the data obtained for zebrafish in this study

**Table 4.1:** Test compounds and exposure concentration ranges used for *in vivo* Ca<sup>2+</sup> light sheet imaging, in addition to evidence of seizure liability as reported from the literature sources listed. Reproduced and expanded from (Pinion et al., 2022).

**Table 5.1:** Compounds and concentration ranges used

**Table 5.2:** Table of variable abbreviations and descriptions

## Authors Declaration

**Chapter 1:** (General Introduction), was written by J.P.

**Chapter 2:** M.J.W. conceived the project, developed the concept and designed the experiments with input from K.T. and W.S.R., M.J.W., C.R.T., A.D.R. and M.J.H. obtained the funding. M.J.W., A.T., J.P., A.Ta. and J.S.B. conducted the experiments, processed resultant images and analysed the data using univariate statistical analyses. J.M. coded and modified the image processing pipeline. J.P., M.G. and P.G. designed and undertook multivariate statistical analyses. A.T., M.T. and M.J.H. undertook analysis of internal compound concentrations. M.J.W., J.P., A.D.R and C.R.T. interpreted the data and drafted the manuscript with further input from all other authors.

**Chapter 3:** A.D.R., C.R.T., and M.J.W. designed research; J.P. performed research; J.P. analysed data with input from C.W., and M.G.; J.P. wrote the paper.

**Chapter 4:** Written by J.P. with input from C.R.T. and M.J.W. All experimental work and data analysis for this chapter was performed by J.P. J.M. coded and modified the image processing pipeline.

**Chapter 5:** Written by J.P. with input from C.R.T. and M.J.W. All experimental work was performed by M.J.W. All data analysis was performed by J.P.

**Chapter 6:** (General Discussion) was written by J.P.

### Authors

(J.P) Joseph Pinion

(K.T.) Karen Tse

(M.J.W) Matthew J. Winter

(W.S.R.) Will S. Redfern

(A.T) Anna Tochwin

(M.J.H) Malcolm J. Hetheridge

(A.Ta) Aya Takesono

(M.G.) Marc Goodfellow

(J.S.B) Jonathan S. Ball

(A.D.R.) Andrew D. Randall

(P.G.) Piotr Grabowski

(C.R.T.) Charles R. Tyler

(J.M.) Jeremy Metz

(M.T) Maciej Trznadel

## List of Abbreviations

MDS - multi dimensional scaling

PTZ - pentylenetetrazol

CAS - Chemical abstracts service

NSAID - Non-steroidal anti-inflammatory drugs

CNS - Central nervous system

GABA - Gamma aminobutyric acid

GAD - glutamic acid decarboxylase

IPSP - inhibitory post-synaptic potential

EPSP - excitatory postsynaptic potential

LTP - long term potentiation

EAATs - excitatory amino acid transporters

mGlu - Metabotropic glutamate receptors

NMDA - N-methyl-D-aspartate

AChE - acetylcholinesterase

NOPr - nociceptin opioid peptide receptor

EEG - electroencephalogram

FOB - functional observation battery

MEA - multi-electrode arrays

hiPSCs - human induced pluripotent stem cells

Fb - forebrain

TeO - optic tectum

Mb - midbrain

Hb - hindbrain



MUX - multichannel amplifier

ADC - analog-to-digital converter

GECIs - genetically encoded Ca<sup>2+</sup> sensors

GFP - green fluorescent protein

MRI - magnetic resonance imaging

GCaMPs - genetically encoded Ca<sup>2+</sup> sensors

LSM - light sheet microscopy

fMRI - functional magnetic resonance imaging

ROIs - regions of interest

mNG - mNeonGreen

SVM - Support vector machine

dpf - days post fertilisation

DAT - dopamine

NET - norepinephrine

SERT - serotonin

AP - area postrema

C - cerebellum

CC - corpus cerebelli

DT - dorsal thalamus

E - eyes

EG - eminentia granularis

ET - eminentia thalami

H - habenulae

IH - intermediate hypothalamus

IO - inferior olive

IPN - interpeduncular

nucleus

LC - lobus caudalis cerebelli

Lco - locus coeruleus

LRN - lateral reticular nucleus

Mt - Mauthner

MVN - medial vestibular nucleus

NIV - noradrenergic neurons of the interfascicular and vagal areas

Np - Spinal cord neuropil

OB - olfactory bulb

OE - olfactory epithelium

P - pineal

PA - preoptic area

pa - pallium

PT - pretectum

RI - raphe inferior

Ro - rostral hypothalamus

RS - raphe superior

SC - spinal cord

Sp - subpallium

PT - posterior tuberculum

TL - torus longitudinalis

tm - tegmentum

TN - tectum neurophil

TSC - torus semicircularis

TSP - tectum stratum periventriculare

TVN - tangential vestibular nucleus

V - Valvula cerebelli

VG - vagal ganglia

VT - ventral thalamus

AUC - area under the curve

RST - (RS)-(tetrazol-5-yl)glycine

VGCCs - voltage gated Ca<sup>2+</sup> channels

SEM - standard error of the mean

## Chapter 1: General Introduction

An alternative approach for assessing drug-induced seizures, using non-protected larval zebrafish

## 1.1 Drug Induced Seizures

Seizures are defined as periods of excessive or hyper-synchronous brain activity (Fisher et al., 2014a). This aberrant brain activity has a considerable rate of mortality and injury (Thurman et al., 2017) and places a high financial burden on health care services (Begley and Durgin, 2015). Approximately 6% of new-onset seizures and 9% of status epilepticus cases are as a result of drug toxicity (Chen et al., 2016), including multiple marketed drugs (Easter et al., 2009; Ruffmann et al., 2006).

In the California Poison Control System, for example, 386 cases of drug induced seizure were reported over the course of 2003, amounting to around one drug induced seizure, per 100 thousand people, per year, for which poison control centre consultation was requested. Notably, a wide variety of mechanistically diverse compounds were involved in the 386 cases, including antidepressants (e.g. venlafaxine), amphetamines, antibiotics (e.g. isoniazid), and pain killers (e.g. tramadol) (Thundiyil et al., 2007). Of these cases, 65.5% involved suicide attempts and 14.8% involved drug abuse, so it can be assumed that most cases involved the excessive consumption of the compounds in question. Moreover, it may also account for the high proportion of antidepressant medication (23% bupropion, 7.7% tricyclic antidepressants) involved in seizure incidence, given the increased likelihood of deliberate overdose. Indeed, the proportions of compounds involved in incidence of seizure is likely reflective of the cultural and medical practices of different regions, in addition to the inherent seizurogenicity of the drugs themselves. For example, a Swiss study of seizure incidence, after single-agent exposure, listed the non-steroidal anti-inflammatory (NSAID) drug mefenamic acid as the most prevalent seizure inducing compound (16%), a compound not present in the Californian study (Reichert et al., 2014; Thundiyil et al., 2007). Although, antidepressants were still the most prolific group of drugs accounting for 43% of the recorded cases (Reichert et al., 2014). Interestingly, the incidence of drug induced seizures was three times lower than that seen in California, a figure likely reflective of cultural and socio-economic factors in addition to different drug prescription practices. The high risk of mefenamic acid induced seizure has also been highlighted by case studies in the UK, which suggest there is a

higher likelihood of central nervous system (CNS) toxicity in mefenamic acid overdose compared to other NSAIDs (Kamour et al., 2017). Mefenamic acid's purported seizurogenicity is notable, given that it is not a drug designed to treat CNS related disorders. By contrast, another problematic drug, the antidepressant bupropion, is psychoactive by design. Bupropion, was the leading cause of drug induced seizure in California in 2003, while in Switzerland it caused seizures in 6 out of the 19 cases reported to the poisoning department (Reichert et al., 2014; Thundiyil et al., 2007). Bupropion has also been reported to induce seizures at therapeutic doses in at risk individuals, leading to its withdrawal from the United States market in 1986 (Onakpoya et al., 2016; Pesola and Avasarala, 2002).

Bupropion, however, is not the only drug removed from the market due to reports of nervous system toxicity. In a worldwide study looking into drugs removed from circulation between 1953 and 2013, 12% of the 462 drugs identified were removed from the market due to CNS toxicity (Onakpoya et al., 2016). This figure is corroborated by another study observing that between 1960 and 1999, 10% of all drugs withdrawn from the market were withdrawn due to CNS toxicity (Fung et al., 2001).

Again, the pharmacodynamics of these drugs varied greatly with compounds designed as antimicrobials, antispasmodics, antidepressants and immune system modulators all featuring prominently (Onakpoya et al., 2016). Moreover, drug targets that prominently feature include opioid, muscarinic, acetylcholine, dopamine and serotonin receptors (Onakpoya et al., 2016). It should be noted however that most of these drugs were released onto the market between 1945 and 1990 (Figure 1.1A), and thus are therefore somewhat dated. However, there is a significant delay between date of release and removal from the market for problematic compounds (Figure 1.1B), and therefore it is possible on a global scale that some problematic drugs released after 1990 were still in circulation around the time this study was published. The mechanistically diverse array of marketed drugs that still show problematic levels of seizurogenicity, despite having completed extensive preclinical and clinical testing, highlights the extent of the issue and the need for further development and innovation of seizure liability screening methodology. Furthermore, it

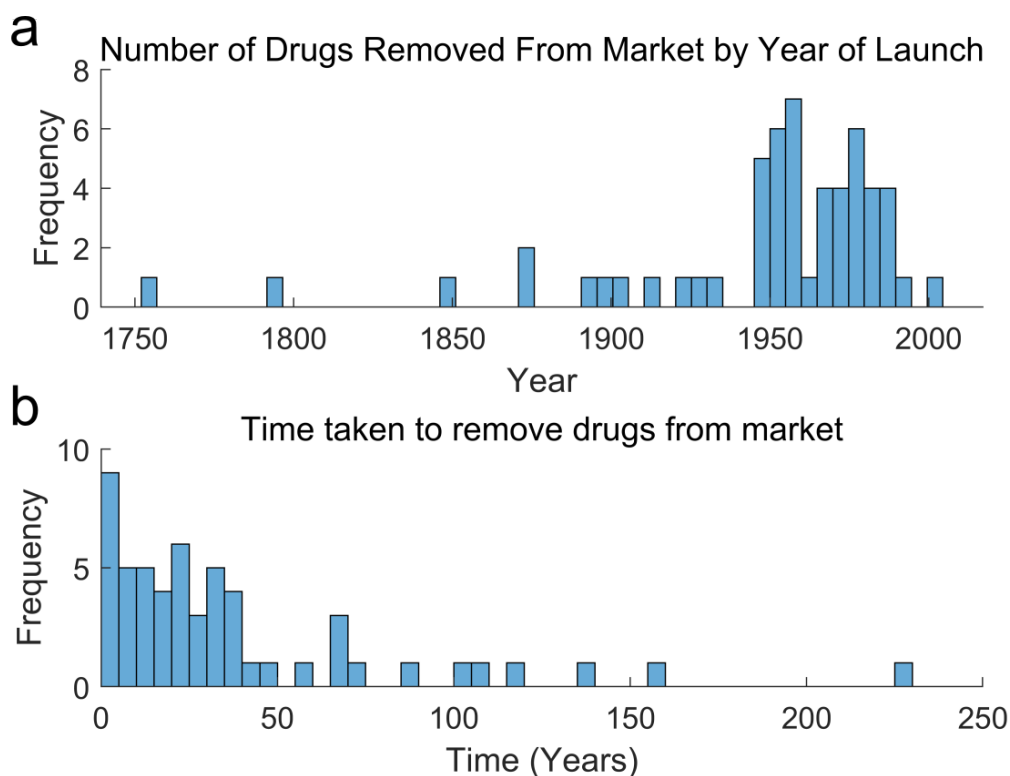


**Figure 1.1:** (a) Histogram showing the frequency of drugs removed from the market for CNS related side effects. (b): the time taken for their withdrawal from market. Data for each extracted from Onakpoya IJ et al (Onakpoya et al., 2016).

reveals the necessity of more adequate appraisal of seizurogenicity in marketed drugs, in order to inform safer clinical practice, both in terms of appropriate prescription practices and overdose treatment strategies.

In addition to seizure liability involving marketed drugs, drug developers also face high levels of drug attrition, caused by the detection of unacceptable levels of seizurogenicity during the development process. In an analysis of four major pharmaceutical companies, failure during non-clinical safety assessment contributed to around 40% of drug development termination before phase IV of the drug development process (Waring et al., 2015). Among the contributors to this high attrition rate is drug-induced seizure liability (Kreir et al., 2018).

Moreover, seizure liability assessment typically occurs during the later stages of pre-clinical drug testing. Consequently, if a compound fails due to a propensity to induce seizures, a great deal of resources are wasted in terms of time, money and animals used. This is because current approaches – predominantly *in vivo* assays in rodents and dogs - are expensive, low throughput, require

large amounts of compound, and have poor animal welfare profiles. *In vivo* electrophysiological approaches, in particular, are highly invasive, requiring the surgical implantation of electrodes into the brain (Haumesser et al., 2017).

If seizure liability could be detected earlier in development, seizurogenic compounds could be fast-tracked to mammalian *in vivo* assays, avoiding the intervening safety testing. Moreover, efforts could be made to modify the chemical structure of compounds in order to reduce seizurogenicity, or, alternatively, compounds with fewer side effects could be selected for progression, in cases where several analogues are available.

There is, therefore, a demand for higher throughput, lower cost, and more ethical seizure liability assessments that are viable for use in the early stages of pre-clinical testing. Numerous approaches have been developed to fit this mandate, including several *in vitro*, *in vivo*, and *in silico* methods and assays (Easter et al., 2009). These assays aim to determine whether compounds increase the likelihood of seizures occurring in brain tissue. Additionally, the ideal seizure liability test will provide some understanding of the biological mechanisms by which test compounds illicit seizures. Improved understanding of these mechanisms allows drug developers to make more informed decisions concerning chemical optimisation and compound selection.

## **1.2 The Role of Neurotransmitters in Seizure**

A delicate balance of excitatory and inhibitory neurotransmission exists within the brain which, if interfered with, can result in seizures (Staley, 2015). Excitatory neurotransmission provokes an influx of cations that causes neurons to depolarise. This reduces the negative transmembrane potential and increases the likelihood of an action potential to occur. Conversely, inhibitory neurotransmission increases the negative charge across the neuronal membrane, increasing the size of depolarisation required to reach threshold and fire an action potential. A variety of neurotransmitter interactions favour excitatory neurotransmission mechanisms such as GABA<sub>A</sub> receptor antagonism, ionotropic glutamate receptor agonism, muscarinic acetylcholine receptor agonism, acetylcholine esterase inhibition, and  $\mu/\delta$ -opioid receptor agonism (Barker-Haliski and White, 2015; Boison, 2016; Easter et al., 2009; Friedman et al., 2007; Ruffmann et al., 2006). Drugs that influence seizure liability may act on one or multiple neurotransmission systems. The following



section outlines the roles of each of these systems in mammals and zebrafish and how they may relate to seizure development.

### *1.2.1 Gamma-aminobutyric acid (GABA)*

Gamma aminobutyric acid (GABA) is the primary inhibitory neurotransmitter in the vertebrate CNS. GABA is produced by glutamic acid decarboxylase (GAD), which catalyses the synthesis of GABA from glutamate (Erlander and Tobin, 1991). There are two main receptor subtypes that GABA binds to: GABA<sub>A</sub> and GABA<sub>B</sub>.

When bound to the GABA<sub>A</sub> receptor, GABA hyperpolarises neurons by causing Cl<sup>-</sup> to move into the cell via ligand-gated ion channels inducing an inhibitory post-synaptic potential (IPSP) (Johnston, 1996). IPSPs increase the negative charge across the neuronal cell membrane, increasing the positive charge required to reach threshold potential and cause an action potential to fire (Sieghart, 1994). Thus, if GABA function is diminished, neuronal inhibition is reduced, limiting the brain's ability to regulate excitation, thus increasing the chance of seizure induction (Samokhina and Samokhin, 2018). Multiple pro-convulsant compounds used in research exploit this approach to chemically induce seizures including pentylentetrazole (PTZ), gabazine and picrotoxin (Ridler et al., 2018; Samokhina and Samokhin, 2018). Equally, increasing GABAergic neurotransmission reduces seizure liability, a mechanism that has been exploited for certain antiepileptic therapies. These are typically in the form of benzodiazepine-derived compounds that are GABA<sub>A</sub> positive allosteric modulators (Haut et al., 2016). Allosteric modulators change the agonist binding affinity or the efficacy of the receptor action, in the case of benzodiazepines, they increase the flow of Cl<sup>-</sup> ions into neurons when GABA is bound, thus increasing hyperexcitation (Haut et al., 2016).

In contrast with the ionotropic GABA<sub>A</sub> receptors, GABA<sub>B</sub> receptors are metabotropic as they are G protein-coupled. Metabotropic receptors use signal transduction mechanisms such as G-proteins to induce an intracellular cascade that implements the receptors' function, in contrast, ionotropic receptors form an ion channel pore in cell membranes which directly influences the movement of ions. As such, metabotropic receptors have a longer, slower and more widely disseminated effect within the cell compared with the faster, localised and more

transient effects of ionotropic receptors. GABA<sub>B</sub> receptors work through Gβγ to open K<sup>+</sup> channels and close Ca<sup>2+</sup> channels (Bettler et al., 2004). This causes membrane hyperpolarisation and reduction of neurotransmitter release. GABA<sub>B</sub> receptors also activate and inhibit adenylyl cyclase via the G<sub>i</sub>α/G<sub>o</sub>α and Gβγ subunits, causing a range of effects including some that influence synaptic plasticity (Bettler et al., 2004).

In zebrafish, GABA is distributed throughout the CNS and has functionally established inhibitory properties (Kim et al., 2004). Indeed, the zebrafish has GAD, GABA, GABA<sub>A</sub> and GABA<sub>B</sub> equivalents that have CNS mRNA levels homologous with mammals (Cocco et al., 2017). Zebrafish contain two GAD genes. These genes possess 84% sequence homology with human GAD65 and GAD67 (Martin et al., 1998). The zebrafish GABA<sub>A</sub> receptor α subunits also show over 80% amino acid sequence homology with the human equivalents, including the histidine residue which is critical for benzodiazepine binding (Renier et al., 2007). The genes for the two heterodimers that make up GABA<sub>B</sub>, GABBR1 and GABABR2, also have highly homologous sequences, with over 80% and over 70% amino acid homology on average respectively across two loci (Renier et al., 2007).

Moreover, immunostaining shows that the distribution of the GABAergic system in the zebrafish cerebellum is similar to mammals, with GABAergic neurons spread throughout the cerebellar corpus, valve and vestibulolateral lobe with staining concentrated in the molecular layer (Delgado and Schmachtenberg, 2008). However, GABA<sub>A</sub> receptor concentration appears lower in the granular layer and higher in the molecular layer, in zebrafish, relative to mammals (Delgado and Schmachtenberg, 2008).

GABAergic neurons have been detected in zebrafish embryos as early as 30 hours post fertilisation (hpf). At this time point, *in situ* hybridisation reveals GABA and GAD are most abundant in Kolmer-Agduhr neurons (a subgroup of interneurons connected to the spinal cord), but they are also present in the mediodorsal region (Higashijima et al., 2004). Interestingly, optogenetic stimulation of zebrafish Kolmer-Agduhr (KA) cells has been observed to induce symmetrical tail beating similar to spontaneous slow forward swimming, suggesting these neurons help drive spontaneous locomotion (Wyart et al., 2009). In behavioural assays, GABA<sub>A</sub> receptor antagonists appear to increase

movement of larval zebrafish in a dose dependent manner, although this varies depending on the specific chemical used (Winter et al., 2008). At 4 dpf, GAD is present in the dorsal two thirds of the spinal cord in addition to the KA neurons. GAD is also expressed throughout the mid- and hindbrain, with GAD positive neurons orientated in stripes along the rostrocaudal axis (Higashijima et al., 2004). These stripes are consistent with stripe-like clustering of GABA expressing neurons in mammals (Katarova et al., 2000). Moreover, there was also evidence of co-expression of GABA and glycine in spinal neurons, similar to that seen in mammals (Todd et al., 1996).

By 3 dpf, immunostaining reveals GABA distributed throughout the larval zebrafish brain. In the diencephalon: the posterior epiphysis, habenula, pretectum and ventral thalamus all contain GABA cells, as does the ventral part of the posterior tuberculum (Figure 1.2). All parts of the hypothalamus contain GABA positive cells which accumulate in the periphery (Mueller et al., 2006).

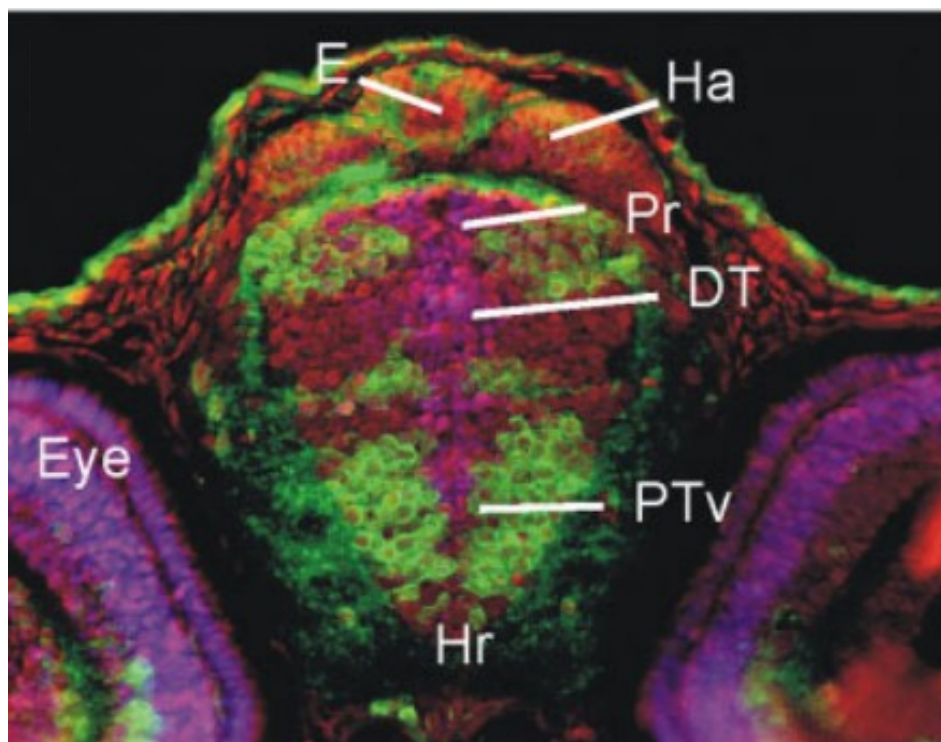


**Figure 1.2:** Immunostaining of the diencephalon region of a 3dpf larval zebrafish. GABA-positive cells are green, Nissl staining is red, and DAPI-staining is purple. Abbreviations are as follows: E – epiphysis, Ha – habenula, Pr – pretectum, DT – dorsal thalamus, PTV - ventral part of posterior tuberculum, Hr – rostral hypothalamus. Picture taken from Mueller et al., 2006.

In the mesencephalon: the central part of the optic tectum, the torus semicircularis and the basal plate tegmentum contain GABA-positive cells (Figure 1.3) (Mueller et al., 2006).

Moreover, in the cerebellum and rhombencephalon: the valvular cerebelli, corpus cerebelli and medulla oblongata also contain many GABA-positive cells (Figure 1.3) (Mueller et al., 2006). The wide spread of GABA-positive cells throughout the CNS at this life stage highlights the potential sensitivity of larval zebrafish to GABAergic compounds, and their utility for screening for activity associated with GABAergic pharmacology. In support of this, embryo-larval (3-7 dpf) zebrafish appear highly responsive to PTZ and picrotoxin exposure, both of which are well-established GABA<sub>A</sub> antagonists used as chemoconvulsants in mammalian seizure models (Baraban et al., 2005; Winter et al., 2017).

#### 1.2.1.1 Glutamate

The main excitatory neurotransmitter of the vertebrate CNS system is glutamate. Glutamate is involved in a variety of physiological processes including learning and memory, motor coordination and neural development

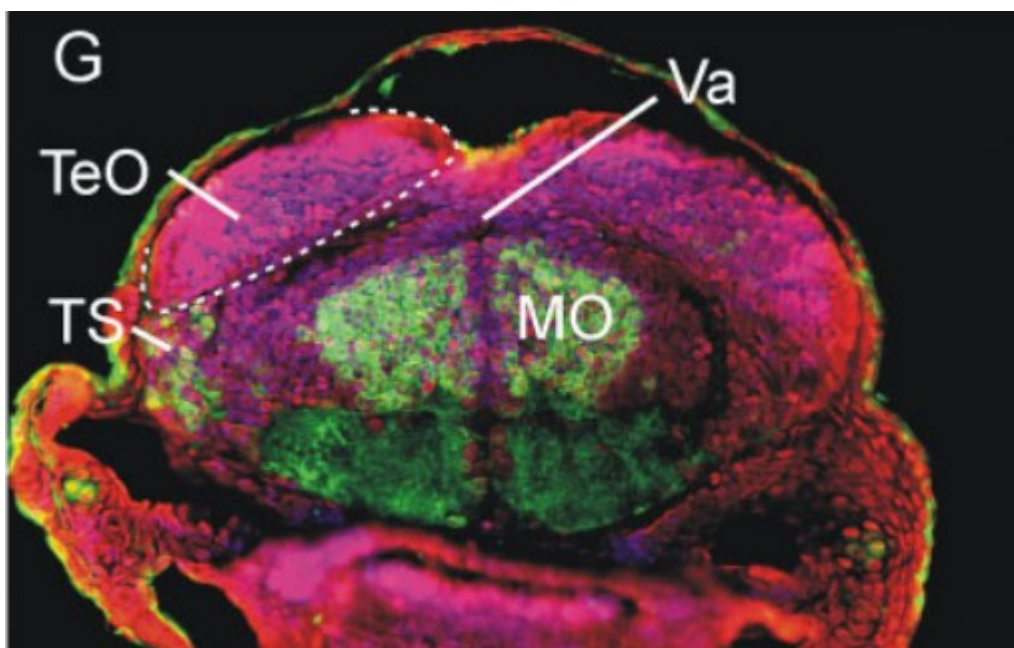


**Figure 1.3** Immunostaining of the midbrain region of a 3dpf larval zebrafish. GABA-positive cells are green, Nissl staining is red and DAPI-staining is blue. Abbreviations are as follows: TS – torus semicircularis, MO - Medulla Oblongata, TeO – optic tectum, Va - Valvula Cerebelli. Picture taken from Mueller et al., 2006.

(Ozawa et al., 1998). Glutamate receptors fall into two categories: ionotropic and metabotropic.

#### *1.2.1.2 Ionotropic*

There are three main classes of ionotropic glutamate receptor - NMDA, AMPA and kainate receptors. The AMPA and kainate receptors are named for the agonists that bind them, AMPA and kainic acid respectively.

When activated by a ligand, ionotropic glutamate receptors allow cations to enter neurons initiating depolarisation. All ionotropic glutamate receptors are agonised endogenously by glutamate, while kynurenic acid is the endogenous antagonist (Baran et al., 1995). Both Kainate and AMPA receptors are activated by kainic acid and multiple other kainoids (Swanson and Sakai, 2009). Aspartic acid and glycine also activate glutamate endogenously (Swanson and Sakai, 2009). NMDA can also be agonised by Aspartate at the receptor site, or Glycine/D-Serine at the modulatory site (Ritter et al., 2018). Furthermore, NMDA receptors are heteromeric and therefore are made up of multiple subunits of which there are three sub-classes (Chen and Wyllie, 2006). Most notably NMDA receptors made up of both GluN1 and GluN2 subunits require both glycine and glutamate to be active (Chen and Wyllie, 2006).

Each of these receptor classes has various subtypes and while each class has distinct properties, all three can influence neuronal excitation, and thus the potential for seizure induction (Hanada, 2020; Sperk, 1994). NMDA receptor activation results in a relatively slow release of cations, particularly  $\text{Ca}^{2+}$ , into the neuron - a process critical for synaptic plasticity (Furukawa et al., 2005; Paoletti et al., 2013). By contrast, AMPA receptors, which often co-localise with NMDA, cause fast excitatory postsynaptic potentials (EPSPs) and can be impermeable to  $\text{Ca}^{2+}$  when accommodating a GluR2 subunit (Hanada, 2020). Similarly, kainate receptors cause a fast influx of cations and have low  $\text{Ca}^{2+}$  permeability, however, unlike AMPA receptors, they can exist on the presynaptic terminal and thus influence subsequent neurotransmitter release (Lerma, 2006). Both AMPA and kainate receptor antagonists are being explored as novel therapeutic targets for antiepileptic drugs (Chang et al., 2016; Madsen et al., 2012; Twele et al., 2015).

In mammals, there are five NMDA receptor genes, one encoding the NMDAR1 subunit and four encoding four NMDAR2 subunits (Ozawa et al., 1998). In zebrafish, two paralogous genes encode the NMDAR1 subunit and these share 90% homology with their human counterparts. By comparison, the eight NMDAR2 genes expressed in the zebrafish are more divergent from their mammalian equivalents, with the NR2C sequences showing approximately 50% identity to the human receptor. However, the transmembrane regions and the Mg<sup>2+</sup> binding site are highly conserved, with around 90% similarity to the human equivalent. The NR2B and NR2D subunits, however, have 50% and 35% identity between humans and zebrafish respectively. Encouragingly, the majority of these genes are expressed to some extent, in larval zebrafish, at under 48 hours post-fertilisation (Cox et al., 2005). Moreover, NMDA, like in mammals, mediates long-term potentiation (LTP) in the telencephalon, the zebrafish brain region homologous with the mammalian hippocampus and amygdala (Nam et al., 2004). As such, it seems the NMDA receptor is largely functionally conserved.

Similar to NMDA, Kainate receptors are found in high densities in the zebrafish olfactory bulb. The different proportions of these two receptor types play an important role in the function of the olfactory system in both zebrafish and mammals (Edwards and Michel, 2003). Crucially, Kainate receptor activation induces clonic seizures in zebrafish, similar to that in rodent models (Alfaro et al., 2011).

Zebrafish contain 8 AMPA receptors genes compared with just four in mammals, due to the presence of paralogous pairings. Paralogous pairs of genes in zebrafish, each orthologous to a single mammalian equivalent, is common due to a tetraploidization event (doubling of chromosomes) that took place early on in the zebrafish lineage (Postlethwait et al., 1999). The distribution of these transcribed paralogous proteins are different, however, suggesting the possibility of subfunctionalisation. For example, unlike *gria1a*, *gria1b* is not detectable in the cerebellar plate or in the hypothalamus (Hoppmann et al., 2008). Despite this, AMPA receptor distribution in the zebrafish medulla oblongata and spinal cord during development mirrors the situation in their mammalian analogues, as does the complete representation of AMPA subunits in retinal ganglion cells and the forebrain (Hoppmann et al.,

2008). In early developmental stages, rat pyramidal neurons contain AMPA receptors that are deficient in GluR2 and thus possess  $\text{Ca}^{2+}$  permeability. However, by postnatal day 16, AMPA receptors undergo subunit alteration that abolishes  $\text{Ca}^{2+}$  migration (Kumar et al., 2002). Evidence of AMPA subunit switching has also been reported during embryonic development in zebrafish Mauthner cells (Patten and Ali, 2007).

In addition to glutamate receptors, several glutamate transporters exist, known as excitatory amino acid transporters (EAATs). These play an important homeostatic role ensuring that levels of glutamate do not become cytotoxic. Given that glutamate is not metabolised extracellularly, reuptake is the sole mechanism of reducing glutamate concentration outside the cell. There are five known subtypes of mammalian EAATs that dynamically control the temporal and spatial profile of glutamate in the extracellular space, including the synaptic cleft, thus, also controlling the extent of receptor activation (Divito and Underhill, 2014). Zebrafish possess homologues of four of the five mammalian EAATs, which are expressed throughout the zebrafish nervous system, including the telencephalon (Rico et al., 2010). Moreover, it appears these perform much the same functions in zebrafish as in mammals, as they are concerned mostly with the movement, and specifically reuptake, of glutamate in the extracellular space (Rico et al., 2010).

#### *1.2.1.3 Metabotropic*

Metabotropic glutamate receptors are endogenously agonised by 3,5-dihydroxyphenylglycine (DHPG) and (RS)-2-chloro-5-hydroxy-phenylglycine (CHPG, group 1), eglumetad (group 2) and L-2-amino-4-phosphonobutyric acid (L-AP4) and (S)-3,4-dicarboxyphenylglycine (4-DCPG, group 3) (Ritter et al., 2018). Metabotropic glutamate receptors (mGlu) mostly confer their function via modulation of ionotropic receptors, primarily NMDA (Ambrosini et al., 1995; Lea IV et al., 2002; Shigemoto et al., 1997). Group 1 mGlu receptors are largely excitatory, modifying responses through NMDA by increasing intracellular  $\text{Ca}^{2+}$  while Group 2 and Group 3 mGlu receptors tend to reduce synaptic transmission and neuronal excitability (Ritter et al., 2018).

### 1.2.2 Acetylcholine

Like glutamate, acetylcholine is an excitatory neurotransmitter. There are two main classes of acetylcholine receptors, nicotinic (nAChRs) which are ionotropic, and muscarinic (mAChRs), which are metabotropic. Nicotinic and muscarinic receptors get their names from their exogenous ligands, nicotine (Dani and Bertrand, 2007) and muscarine (Jin, 2011).

Ligand binding induces a conformational change in nAChR subunits, causing a pore in the receptor to open, which allows cations to enter. Because nAChRs exist at both the presynaptic and postsynaptic terminals, they influence neurotransmitter release, as well as inducing EPSPs (Dani and Bertrand, 2007). As such, nAChR agonism can induce seizures in animal models (Dani and Bertrand, 2007).

In contrast to nAChRs, the metabotropic muscarinic acetylcholine receptors are relatively slow-acting and have a wide array of potential functions. The muscarinic receptor agonist pilocarpine, which agonises four of the five mammalian muscarinic receptor subtypes, has been shown to induce spontaneous seizures (Leite et al., 1990). Muscarinic receptors have multiple exogenous ligands, with agonists including carbachol and oxotremorine (Maehara et al., 2008), while scopolamine is a commonly used antagonist (Renner et al., 2005). Of the four known mammalian receptors, the one most implicated in seizure induction is the M1 receptor. Indeed, pilocarpine-induced seizures are dependent on the presence of the M1 receptor, which may induce seizurogenesis via blockage of M-type  $K^+$  channels (Hamilton et al., 1997). This widely expressed  $K^+$  channel subtype is open at rest and during depolarisation. Moreover, it is highly important for returning to and increasing threshold potential (Greene and Hoshi, 2017). As such, M1 receptor activation instigates longer-lasting depolarisations and the induction of post-action potential depolarisations (Smith and Araneda, 2010).

Another important component of the ACh system is the enzyme acetylcholinesterase (AChE) which is responsible for the breakdown of acetylcholine, hydrolysing acetylcholine esters, and thus, terminating receptor activation (Daniel, 1987). As such, AChE is particularly important for modulating acetylcholine receptor activation. This being the case, AChE inhibitors, that are



often exploited for their cognition-enhancing effects, can in some cases cause seizure (Ashford, 1998). AChE inhibitors prevent acetylcholine breakdown increasing both the duration and quantity of acetylcholine in the synapse (Ota et al., 2010).

It has been postulated that acetylcholine may have an important neuromodulatory role during embryonic development in zebrafish. Indeed, the early presence of acetylcholine esterase, as identified by ChAT immunostaining (Figure 1.4), supports this hypothesis. Cholinergic neurons are present in the preoptic area, optic tectum and tegmentum from 60 hpf and in the spinal cord from 48 hpf (Arenzana et al., 2005).

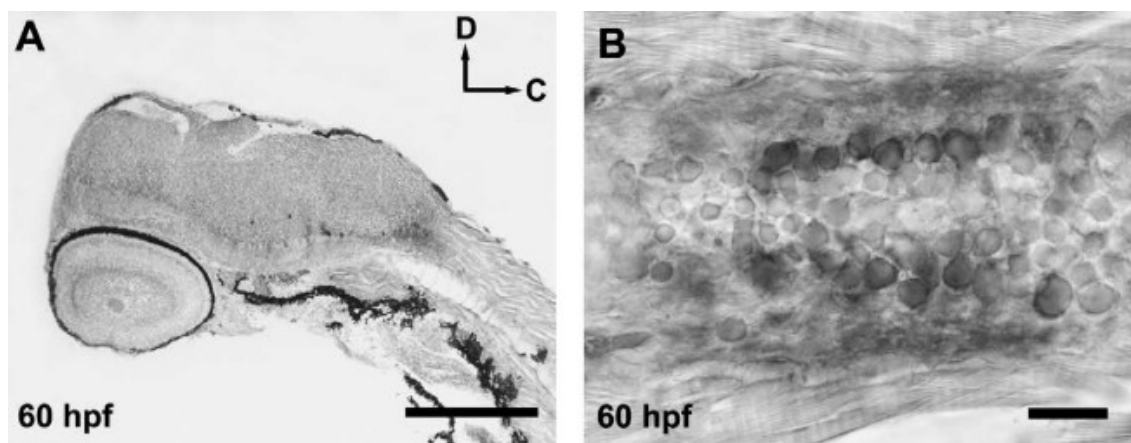


**Figure 1.4 . ChAT-immunoreactivity during zebrafish brain development. (A)** Parasagittal section showing the immunolabeled elements for ChAT in the embryonic rhombencephalon at 60 hpf: D, dorsal; C, caudal. **(B)** Magnification of the spinal cord of a 60 hpf embryo showing ChAT-ir motor neurons. Image from Arenzana et al., 2005.

Moreover, in radioligand binding assays, when exposed to a variety of established muscarinic pharmacophores, the binding affinity of muscarinic receptors compares favourably with mammalian equivalents (Williams and Messer, 2004). The muscarinic antagonist scopolamine has been shown to impair memory in zebrafish during behavioural assays, a result similar to those expected in mammals (Richetti et al., 2011). This is further supported by a study demonstrating the modulation of memory by nicotine in zebrafish, which is another a result that mirrors those in rodents, monkeys and humans (Levin and

Chen, 2004). This suggests that the cholinergic system has both a similar function and similar molecular binding properties in zebrafish as in mammals.

### 1.2.3 Opioids

In mammals there are four types of opioid receptor:  $\delta$ -opioid,  $\mu$ -opioid,  $\kappa$ -opioid receptor and the nociceptin opioid peptide receptor (NOPr). In contrast to acetylcholine receptors,  $\mu/\delta$ -opioid receptor agonism typically induces inhibitory activity (Shang and Filizola, 2015), however paradoxically some agonists at these receptors have also been associated with seizures (Jutkiewicz et al., 2006; Snead, 1986; Tortella et al., 1987). Opioid receptors promote  $K^+$  channel activation (causing potassium discharge) and prevent  $Ca^{2+}$  channels from opening, inducing hyperpolarisation of the neuron and reducing action potential firing probability, while also preventing neurotransmitter release (Shang and Filizola, 2015).

Despite this inhibitory activity, some, but not all (Saitoh et al., 2018),  $\delta$ -opioid receptor agonists induce convulsions and seizures (Jutkiewicz et al., 2006). There is evidence that this seizure activity is mediated by  $\delta$ -opioid receptor inhibition of GABAergic neurons in the forebrain; as a reduction in GABA mediated inhibitory activity can induce seizures (Chu Sin Chung et al., 2015).

Moreover,  $\mu$ -opioid receptor agonists such as morphine, have also been demonstrated to induce seizure; doing so independently of  $\delta$ -opioid receptor activity (Snead, 1986). Indeed, a study looking at enkephalin induced seizures, showed that  $\mu$ -opioid receptor-specific agonists can cause seizures; a process blocked by  $\mu$ -opioid receptor antagonism (Tortella et al., 1987). This suggests a mechanism of  $\mu$ -opioid receptor-mediated seizurogenesis, possibly again through inhibition of GABAergic neurons, although the exact mechanisms are yet to be elucidated.

Interestingly, both  $\mu$  and  $\delta$ -opioid agonists have also been shown to prevent seizures in convulsant treated rats. However, in this instance, the doses were around half that of those demonstrated to cause seizure and were administered after seizure induction (Tortella et al., 1988). This highlights the importance of the dose and context of drug administration when studying drug induced seizure induction.

By contrast,  $\kappa$ -opioid receptor agonism seems to be mostly anti-convulsant with little evidence of seizurogenicity. In fact, the endogenous opioid peptide dynorphin has been shown to effectively inhibit seizures in some models (Simonato and Romualdi, 1996). Moreover, a selective  $\kappa$ -opioid receptor agonist was shown to prevent seizure, dose dependently, in bicuculline treated mice (Yajima et al., 2000).

Of the four mammalian opioid receptors, NOPr is unique in that it has no affinity for morphine, although, like the others, it does appear to have a role in neuronal excitability (Butour et al., 1997). NOP receptor antagonism or genetic knockout have been shown to reduce the susceptibility of mice to Kainate induced seizures (Bregola et al., 2002). It would seem, therefore, that NOP has at the very least, a role to play in the propagation of glutamate driven seizures.

In zebrafish, there are four comparable types of opioid receptor ( $\delta 1$ ,  $\delta 2$ ,  $\mu$  and  $\kappa$ ) (Sanchez-Simon and Rodriguez, 2008). Opioid receptors are widely distributed throughout the brain from around 24 hpf and, like in mammals, are proposed to play a role in the development of the CNS and digestive tract (Sanchez-Simon and Rodriguez, 2008). This suggestion is supported by the fact that there are peaks in mRNA levels of different opioid receptors throughout the developmental process (Sanchez-Simon and Rodriguez, 2008).

There are multiple endogenous ligands to opioid receptors that play a crucial role in regulatory mechanisms governing pain, many of which are peptides such as  $\beta$ -endorphin, met-enkephalin, and dynorphin (Stein et al., 1993). Zebrafish endogenous peptides are broadly similar to mammals (Gonzalez-Nunez et al., 2003; Gonzalez-Nuñez et al., 2007; Gonzalez Nuñez et al., 2003). The zebrafish dynorphin-A peptide differs from the mammalian equivalent by only two amino acids. Moreover, like the mammalian dynorphins, the two zebrafish dynorphins bind  $\delta$ ,  $\mu$  and  $\kappa$  opioid receptors with varying affinities (Gonzalez-Nuñez et al., 2007). Similarly, there are zebrafish genes for proenkephalin and pronociceptin that are highly homologous with the mammalian equivalents (Gonzalez-Nunez et al., 2003; Gonzalez Nuñez et al., 2003).

Pharmacological binding data shows that zebrafish opioid receptors are sensitive to multiple broad acting agonists including morphine and enkephalin (Pinal-Seoane et al., 2006; Rodriguez and Gonzalez-Nunez, 2006). However, it

appears that receptor-selective synthetic opioids such as U69,593, DPDPE and DAMGO have low affinity for zebrafish  $\kappa$ -opioid,  $\delta$ -opioid or  $\mu$ -opioid receptors respectively (Rodriguez and Gonzalez-Nunez, 2006). As such, it seems that zebrafish lack affinity for highly selective opioid ligands, despite their demonstrable affinity for mammalian receptors. Meanwhile, non-selective ligands bind both mammalian and zebrafish opioid receptors with high affinity. This suggests that the binding sites of opioid receptors in mammals and zebrafish are similar, however, the extracellular domains that are selective with respect to ligand binding are perhaps more divergent.

#### *1.2.4 Monoamines*

Monoamines are a subgroup of neurotransmitters that includes histamine, dopamine, adrenaline, noradrenaline and serotonin. Monoamines are classed together because they all have a single amino group attached to an aromatic ring by a two-carbon chain and are often derived from single amino acids (Ritter et al., 2018). The amino acid tyrosine is converted into dopamine and noradrenaline, whereas serotonin is derived from tryptophan (Libersat and Pflueger, 2004). Due to this chemical similarity monoamines share transporters and enzymes involved in their uptake, transport and synthesis (Ritter et al., 2018). They are pharmacological targets for almost all antidepressant medications as they are implicated in the pathophysiology of depression (Elhwuegi, 2004).

##### *1.2.4.1 Serotonin*

Serotonin receptors are among the most diverse found in the body with at least 14 receptor subtypes, with varying specialisations (Nichols and Nichols, 2008). Serotonin receptors modulate a wide range of other neurotransmitter systems including GABA, glutamate, dopamine and acetylcholine with a range of functional effects (Filip and Bader, 2009). Due to the variety of receptor subtypes, there is a tremendous number of ligands. One of the most selective is the 5HT-2<sub>A</sub> agonist lysergic acid diethylamide (Liechti, 2017). Agonism of the 5HT-2<sub>A</sub> receptor causes alterations in global and thalamic brain connectivity resulting in an altered state of human consciousness (Preller et al., 2018). As such, second generation antipsychotic drugs, such as risperidone, target 5HT-2<sub>A</sub> by stabilising the inactive conformation of the receptor in order to prevent

transition into a psychotic state (Kimura et al., 2019). Notably, examples of both first and second generation antipsychotic medications have been shown to lower seizure threshold (Bloechliger et al., 2015).

Serotonin depletion has been associated with increased seizure susceptibility in rats (Maia et al., 2017). Moreover, serotonin reuptake blockers, which increase serotonergic transmission, have been shown to reduce the number of fast ripple events in rats, a phenotype of temporal lobe epilepsy (Pardo-Peña et al., 2014). However, serotonin neurotransmission can be deemed to either increase or decrease seizure liability depending on the receptor subtype activated, the specific serotonin agonists used, and the type of seizure model used for assessment (Gharedaghi et al., 2014). The variability of outcomes in studies looking at serotonergic mechanisms of seizurogenesis highlights the complexity of this neurotransmitter system. Antidepressants that predominantly target serotonin, have varied associations with seizure induction (Johannessen Landmark et al., 2016; Vermoesen et al., 2011), suggesting that it isn't quite as simple as 'more serotonin results in an increased risk of seizure'. Antidepressants generally have an effect on a variety of receptors types, including multiple monoamines other than serotonin (Elhwuegi, 2004). It is likely that when seizurogenicity does occur, it arises from an array of receptor interactions and how these manifest within the physiology of specific individuals. *In vivo testing* is therefore beneficial for elucidating complex multi-subtype metabotropic receptor systems, as it is the only way to assess all receptor subtypes in conjunction with one another. Zebrafish have serotonin systems functionally and structurally similar to mammals, with serotonergic neurons appearing to be present as early as 4 dpf (McLean and Fetcho, 2004; Panula et al., 2006). Like in humans, serotonin modulating compounds, such as the widely prescribed antidepressant fluoxetine, have been shown to affect anxiety in zebrafish (Maximino et al., 2013b). Structurally, the raphe nuclei in zebrafish are homologous with part of the raphe nuclei in mammals and both areas contain large clusters of serotonergic neurons (Kaslin and Panula, 2001). However, zebrafish contain serotonergic neurons in some additional areas to mammals, including the posterior tuberculum and the pretectal area (Figure 1.5, Kaslin and Panula, 2001). In mammals, 5-HT<sub>2</sub> receptor agonism appears to confer anti-seizure properties (Gharedaghi et al., 2014). This tallies with the reports that clemizole and other 5-HT<sub>2B</sub>R agonists have been shown to

suppress seizure activity in *snc1lab* zebrafish mutant larvae, a genetic model of Dravet syndrome (Griffin et al., 2019). Moreover, *snc1lab* mutant zebrafish are also effectively treated for seizure by the drug fenfluramine, which has been demonstrated to treat Dravet syndrome in clinical trials (Polster, 2019; Sourbron et al., 2017). Like clemizole, fenfluramine appears to modulate serotonin in zebrafish, as selective serotonin antagonists inhibit its anti-seizure effects (Sourbron et al., 2017).

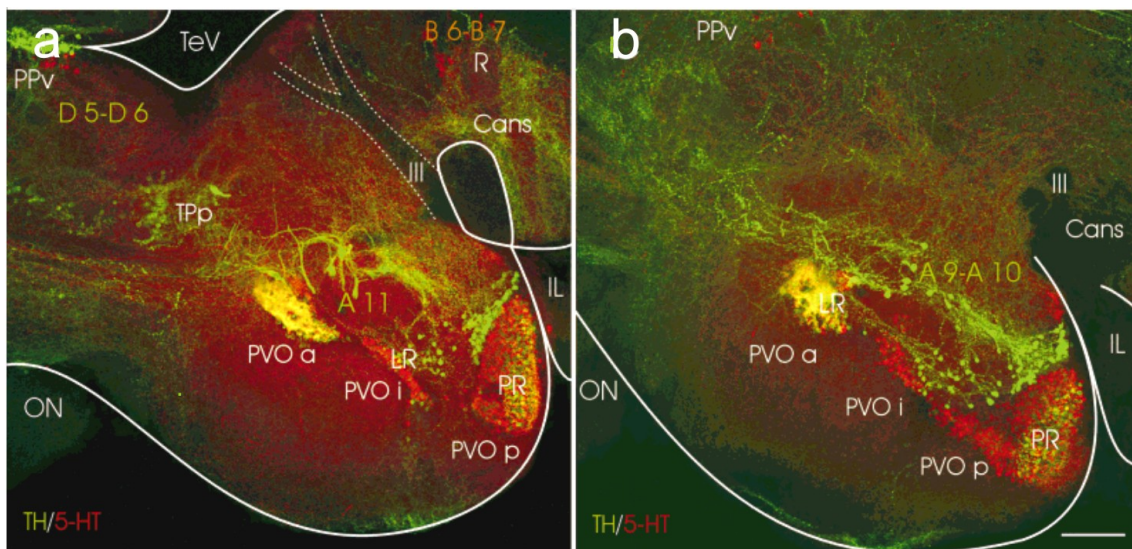


**Figure 1.5: Immunostaining of zebrafish midbrain for serotonin and tyrosine (a)** A sagittal view of serotonin-immunoreactive (ir. red) and tyrosine hydroxylase-ir (green) in periventricular cell groups in the vicinity of the ventricle and the recesses. **(b)** A sagittal section showing a cluster of tyrosine hydroxylase-ir (green) neurons with extensive ascending projections located in the dorsocaudal hypothalamus. Scale bar 50  $\mu$ m. Abbreviations: A9-A11 – catecholaminergic cell groups, B6-B7 serotonergic cell groups, Cans – ansulate commissure, D5-D6 – cell groups corresponding to mammalian dopa decarboxylase containing cell groups, IL – inferior hypothalamic lobe, LR – lateral recess of the diencephalic ventricle, ON – optic nerve, PPa - parvocellular preoptic nucleus anterior part, PPp - parvocellular preoptic nucleus posterior part, PPd - periventricular prepectal nucleus dorsal part, PPV – periventricular prepectal nucleus ventral part, TPp periventricular nucleus of posterior tuberculum. Figure from Kaslin and Panula, 2001.

#### 1.2.4.2 Dopamine

Dopamine binds to two groups of receptors containing a total of five different receptor subtypes, the D1-like family containing D1 and D5, and the D2-like family, containing D2, D3 and D4. These subtypes have varying effects on seizure generation (Barone et al., 1991). Early studies suggested that D2 receptor antagonism and D1 receptor agonism can contribute to the development of seizures (Starr, 1996). D1 receptor agonists, such as SKF 81297, have been shown to induce epileptiform activity, a state inhibited by the D1 antagonist SCH 23390 (Gangarossa et al., 2011). Moreover, some involvement of D5 receptors has been implicated in seizure induction, although to a lesser extent than D1 (Gangarossa et al., 2011). In zebrafish, dopaminergic neurons are present as early as 18 hpf, with several clusters present by 4 dpf. The distribution of dopaminergic neurons in the zebrafish brain broadly mirrors mammals, as tyrosine positive cells can be found in the posterior tuberculum, hypothalamus, sympathetic ganglia, pretectum and medulla oblongata of the larval zebrafish, even at 4 dpf (Figure 1.6, Schweitzer and Driever, 2009). There are some exceptions to this, namely the absence of dopamine on the mesencephalon and ventral midbrain (Schweitzer and Driever, 2009). An additional difference is that zebrafish lack a substantia nigra, a dopamine receptor rich region in mammals (Schweitzer and Driever, 2009). Despite this, zebrafish dopamine receptors, corresponding to the mammalian D1, D2, D3, and D4 receptors, have been identified each with unique distributions throughout the zebrafish CNS (Boehmier et al., 2004; Boehmler et al., 2007; Li et al., 2007).

Pharmacologically, zebrafish respond to dopaminergic compounds in a similar manner to mammals. For example, cocaine, amphetamine and ethanol have been shown to increase the locomotor activity of zebrafish, at low concentrations, in a similar fashion to their mammalian counterparts (Irons et al., 2010). The dopamine antagonist clozapine ablates locomotor activity in zebrafish, as is the case in mammals, an effect that can be reversed through D4 receptor agonism (Nabinger et al., 2020). Notably, the dopamine reuptake inhibitor GW12909 has been shown to have anti-convulsant effects in both zebrafish and rodent models of generalised epilepsy, thus supporting the

homologous role of dopamine in seizure regulation between zebrafish and mammals (Goldsmith et al., 2007).

#### 1.2.4.3 Noradrenaline

The neurotransmitter noradrenaline is typically associated with arousal and is one of the drivers of the sympathetic nervous system (Esler et al., 1985). Noradrenaline is synthesised from dopamine by dopamine- $\beta$ -hydroxylase and binds to a class of G-protein coupled receptors. There are 3 main receptor types  $\alpha_1$ ,  $\alpha_2$ , and  $\beta$ , which in mammals each contain three different receptor subtypes (Ritter et al., 2018).

The noradrenaline system is highly conserved between mammals and zebrafish. Noradrenergic cells are present in the medulla oblongata, area postrema and locus coeruleus from as early as 16 hpf, and are present throughout the nervous system by 4 dpf (Figure 1.6, Kaslin and Panula, 2001; Schweitzer et al., 2012). Zebrafish contain homologous genes for all the mammalian  $\alpha_1$ ,  $\alpha_2$  and  $\beta$  receptor subtypes (Horzmann and Freeman, 2016), however, zebrafish contain a fourth  $\alpha_2$  receptor subtype represented by two paralogous genes (Jori O Ruuskanen et al., 2005). Each of the three mammalian  $\alpha_2$  sub-types,  $\alpha_{2A}$ ,  $\alpha_{2B}$  and  $\alpha_{2C}$ , are coded for in zebrafish by an orthologous *adra2* gene. Two additional *adra2* genes code for  $\alpha_{2Da}$ - and  $\alpha_{2Db}$ -adrenoceptors, representing a duplicated, fourth  $\alpha_2$ -adrenoceptor subtype. It has been hypothesised that this subtype was present in the common ancestor of vertebrates and has since been lost in mammals, wherein its function is now performed by the  $\alpha_{2A}$  receptor (Jori O. Ruuskanen et al., 2005).

Noradrenaline and adrenaline both signal through adrenergic receptors (Ritter et al., 2018), which are also the targets of a plethora of marketed drugs, mostly targeting the cardiovascular system. For example, isoprenaline is a non-selective  $\beta$ -receptor agonist used to increase cardiac output in cases where the heart may have slowed (Arnold et al., 1985), while  $\beta$ -receptor antagonists are used to lower blood pressure (Ram, 2010).

Typically, zebrafish respond to noradrenergic acting compounds similarly to mammals. For example, the  $\alpha_2$  agonist, dexmedetomidine, causes sedation,



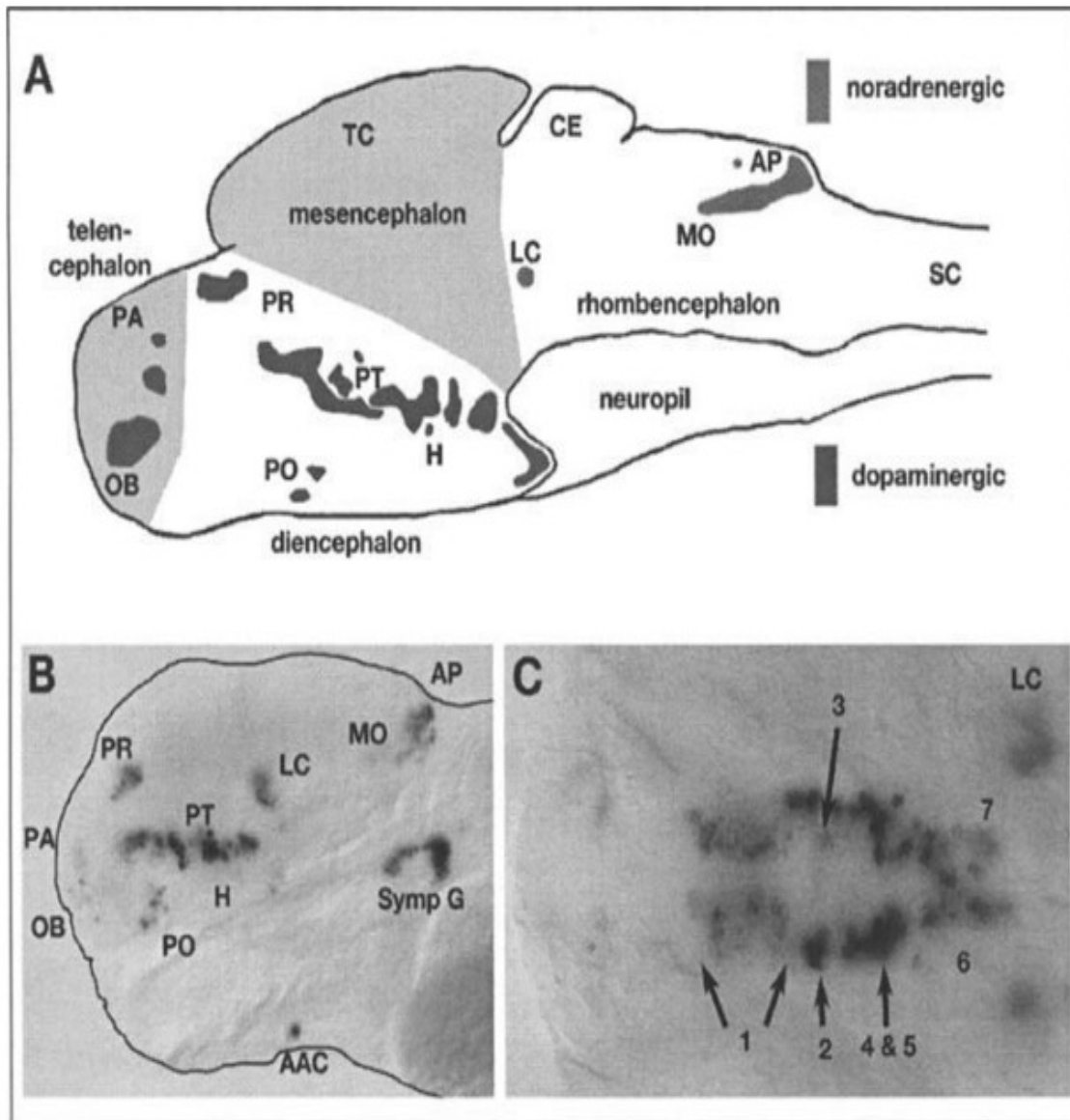


**Figure 1.6 Dopaminergic and noradrenergic cells groups of the 4 day old zebrafish larvae. (A)** Schematic drawing of 4-day old zebrafish brain with major brain subdivisions and locations of catecholaminergic groups highlighted.

Anterior at left, dorsal at top. **(B/C)** Detection of tyrosine hydroxylase expression in catecholaminergic neurons of 4-day old zebrafish larva. **(B)** Lateral view anterior at left, dorsal at top. The circumference of the head is emphasized by a black line. **(C)** Dorsal view of same embryo as in A, magnified posterior tuberculum and hypothalamus, anterior at left.

Abbreviations: Numbers 1-7 indicate DA subgroups of ventral diencephalon according to the numbering of (6); AAC: arch associated NA cells (carotid body); AP: area postrema; CE: cerebellum; H: hypothalamus; LC: locus coeruleus; MO: medulla oblongata ; OB: olfactory bulb; PA: pallium; po: preoptic area; PR: pretectum; PT: posterior tuberculum; TC: tectum; SC: spinal cord; SympG: sympathetic ganglia.

(Jori O. Ruuskanen et al., 2005) and the  $\beta_1$  antagonist propranolol reverses tachycardia, (Mann et al., 2010) in both mammals and zebrafish.

In mammals, noradrenaline appears to be protective of seizure. Indeed, depletion of noradrenaline increases seizure susceptibility in rodents *in vivo*, as well as the speed at which seizures enter the convulsive stage. A finding that has been replicated in hippocampal slice models (Corcoran, 1988; McIntyre and Edson, 1982). Noradrenergic drugs have also been shown to potentiate the effects of anticonvulsants in both mice and humans (Weinshenker and Szot, 2002). However, in zebrafish there has been little work in this area. One study performing a pharmacological analysis of the antiepileptic mechanisms of fenfluramine found that fenfluramine seizure attenuation was correlated with a 50% reduction in noradrenaline (Sourbron et al., 2017). However, the data were merely correlative and occurred in the context of many other drug mechanisms and confounding factors (Sourbron et al., 2017).

#### 1.2.4.4 Histamine

Histamine is an important modulator of the immune system, in addition to being a centrally acting neurotransmitter. Histamine is derived via a decarboxylation reaction of the amino acid histidine (Ritter et al., 2018). In mammals, there are four known receptor subtypes that histamine binds in the CNS, labelled  $H_1$ ,  $H_2$ ,  $H_3$  and  $H_4$ , all of which are G-protein coupled receptors (Brown et al., 2001). Histamine in the mammalian brain is found predominantly in the hypothalamus (Mochizuki et al., 1991), where it has been implicated to have a role in satiety and homeostatic control of energy metabolism (Sakata et al., 1997).

In a PTZ treated mouse model of seizure, it was shown that treatment with the histamine receptor agonist histidine increased seizure threshold, while  $H_1$  receptor antagonists reduced seizure threshold. However, antagonists of  $H_2$ ,  $H_3$  and  $H_4$  had no effect on seizure susceptibility, suggesting a role of the  $H_1$  receptor specifically, in neuronal excitability (Scherkl et al., 1991). Interestingly, despite its anti-seizure effects,  $H_1$  receptor activation is typically excitatory, causing large depolarisations via blockade of potassium conductance (Brown et al., 2001). As such, it presumably mitigates neuronal excitability via its action on other neurotransmitter systems. In contrast to the activity of the  $H_1$  receptor,  $H_3$

receptor antagonists appear to have anticonvulsant activity in rats exposed to PTZ (Sadek et al., 2016).

Zebrafish H<sub>1</sub>, H<sub>2</sub>, and H<sub>3</sub> receptors, have between 40% and 50% amino acid homology with the corresponding human receptors and are present as early as 3 hpf (Scherkl et al., 1991). A zebrafish H<sub>4</sub> receptor has not yet been identified. Distribution of histaminergic neurons is confined to a single cluster in the vicinity of the posterior recess in zebrafish, whereas the rat brain has five distinct clusters (Kaslin and Panula, 2001). In mammals, histamine receptors are distributed most densely in the thalamus, hippocampus and cerebellum, whereas in zebrafish histamine receptors have been identified in the optic tectum, hypothalamus, locus coeruleus and the superior reticular formation (Maximino and Herculano, 2010).

Similarly to mammals, antagonism/reverse agonism of histamine induces sedation in zebrafish, reflected by reduced swimming behaviour (Peitsaro et al., 2007). Indeed, H<sub>1</sub> receptors have been shown to regulate wakefulness and orexin/hypocretin neuron development in both zebrafish and mice (Sundvik et al., 2011). Notably, the H<sub>1</sub> receptor antagonist clemizole was shown to inhibit seizures in *snc1Lab* mutant zebrafish (Baraban et al., 2013a), a finding at odds with the previous studies wherein H<sub>1</sub> antagonists reduced seizure threshold (Scherkl et al., 1991). However, the anti-convulsant effects of clonidine have been postulated to be due to 5-HT<sub>2B</sub>R agonism, as opposed to its effects on histamine (Baraban et al., 2013a). This highlights the importance of context when studying compound seizurogenicity as these studies were performed using different seizure models: PTZ induced seizures in rodents (Scherkl et al., 1991) vs spontaneous seizures in *snc1Lab* mutant larval zebrafish (Baraban et al., 2013a). This also highlights the importance of secondary pharmacology, as each study used different H<sub>1</sub> antagonists with different secondary pharmacological profiles: clonidine (Baraban et al., 2013a) vs dimethindene and promethazine (Scherkl et al., 1991).

### **1.3 Current approaches for detecting drug-induced seizure liability**

Given the complexity of the nervous system and the plethora of ways in which compounds can interact with it, assessing the potential for compounds to cause seizures is non-trivial. It is imperative that accurate assessment of seizure liability occurs early in drug development; as seizures are a serious side effect

and their detection often results in a compound being dropped from further development. Therefore, maximising information as early as possible in the drug development process is important, in order to minimise the resources expended on a compound that subsequently fails. There are multiple different tools that have been developed and applied for seizure liability testing. These range from radioligand binding assays, to the assessment of drug-receptor interactions, through to *in vivo* studies in mammals and zebrafish (Easter et al., 2009). Of these approaches, the current gold standard is rodent *in vivo* electroencephalogram (EEG) (Fonck et al., 2005). However, due to the resource intensive nature of this approach, this typically occurs later in preclinical testing when fewer candidate drugs require assessment due to other sources of attrition. Although several approaches have historically been used to discern seizure liability in new drugs, each method has its limitations (Easter et al., 2009). Moreover, the fact that drugs are still failing later in development (Figure 1.1), suggests that better (and practical) methods of detection for early deployment in drug development are still very much needed.

### 1.3.1 Rodent EEG

As brain activity is, by its very nature, electrically charged, measurement of changes in voltage offers the most direct measure for assessing brain physiological activity. These voltage changes are typically measured via highly sensitive electrode screws surgically implanted directly into the CNS as part of a process known as electroencephalography (or EEG). If surgeries are successful, animals are left to recover (usually for ~5 days) and are subsequently attached via wires to an amplifier and recording unit. Brain activity is measured for a baseline period after which animals are exposed to test compound (Fonck et al., 2005). A variation is the proconvulsant or sub-threshold PTZ, assay in which animals are also treated with low concentrations of a chemoconvulsant, such as PTZ, in order to assess the effect of the compound on seizure threshold. This approach has been repeatedly shown to be a highly effective strategy for assessing adverse CNS effects, including increased seizure liability, and as such is considered the gold standard method for detecting seizure liability for new drugs with a high degree of translation to human (Bassett et al., 2014; Easter et al., 2009; Fonck et al., 2015, 2005; Hu et al., 1992; Kamendi et al., 2010; Lundt et al., 2016; Markgraf et al., 2014; Talos

et al., 2013; Vermoesen et al., 2011). Seizure morphology is highly diverse and varies depending on specific pathology or triggering mechanism (Fisher et al., 2014b).

Ictal activity, as measured via *in vivo* EEG recording in rodents, can often be characterised by trains of spiking activity as shown in Figure 1.7 (Markgraf et al., 2014). These may be seen on spectrograms (a frequency domain representation of a timeseries) as increases in amplitude in higher frequency bands. Changes in the frequency profiles of electrographic traces are popular method for assessing seizure dynamics, with patterns of frequencies such as rhythmical evolving theta delta and alpha frequencies commonly being seen preceding seizure events. In addition, high frequency high amplitude events are commonly seen in conjunction with seizures with spectrograms registering frequencies as high as 500hz (Fisher et al., 2014b).

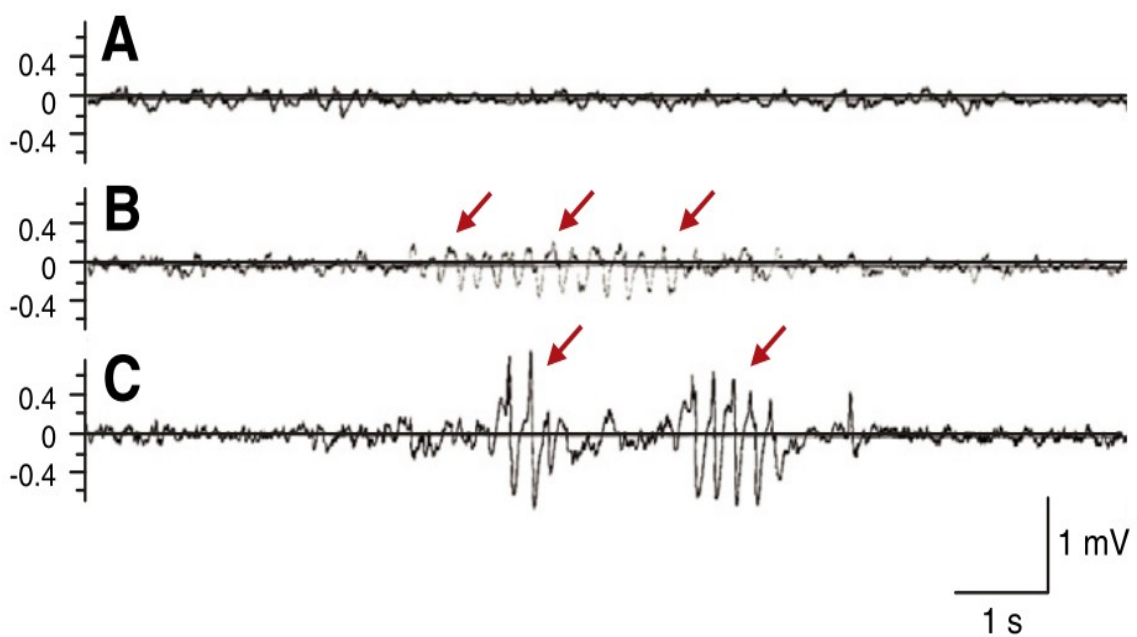


**Figure 1.7** Representative EEG traces from the rats in the Org 306039 group on Day 10. (A) Normal awake rat EEG is displayed in the top trace. (B) Arrows indicate presence of a train of sharp waves. (C) Arrows indicate presence of a train of spikes. Figure taken from Markgraf et al., 2014.

Efforts have been made to develop non-invasive scalp EEG caps for rodents (Sumiyoshi et al., 2011), which would significantly reduce the degree of invasiveness of EEG recordings in rodents. These approaches have been shown to be effective and can be used to generate topographical maps of brain activity (Mégevand et al., 2008; Paulson et al., 2018). However, they are fraught

with technical difficulty due to the small scalp area and proximity of the electrodes to the brain tissue. As such they require bespoke precision-engineered equipment that makes implementation at scale in a commercial setting highly challenging.

### *1.3.2 Rodent Behavioural Assays*

In addition to the direct electrographic measurement of seizure activity from neurons using electrophysiology, seizures can be measured by proxy through EEGs. Despite its considerable translational power, rodent EEGs require a large amount of compound when compared with alternative assays such as hippocampal slice and zebrafish assays. This is highly relevant as during the early stages of preclinical testing, compound availability can be scarce. Moreover, EEG requires surgical implantation of electrodes. Not only is this extremely invasive, but it also requires a great deal of technical expertise. If done poorly, surgeries can themselves result in adverse effects, such as seizures, which has obvious implications for false positive test results. The recording process itself can also be stressful as animals are attached to wires which limit natural movement. In addition, these approaches are extremely low throughput and therefore costly, typically requiring up to a fortnight to test a single compound, per set of animals. As a result of these limitations, this approach is typically not employed until late on in pre-clinical testing.

the assessment of the behavioural manifestations of aberrant electrical activity, such as convulsions. There are two main types of rodent behavioural assays used in drug development that can provide a degree of insight into the presence of seizure liability amongst new drugs: the functional observation battery (FOB) and the Irwin test (Irwin, 1968; Sette, 1989). Both approaches are broadly similar and rely on wide variety of behavioural parameters in order to assess adverse CNS effects. However, the FOB was developed more recently, by the United States Environmental Protection Agency, in response to concerns about inadequate neurotoxicity testing, and has a greater focus on cage-side observations (Sette, 1989). The consistency and effectiveness of these approaches has been meticulously assessed and standardised in an international collaborative study in which all participants could identify and describe the effects of known neurotoxic compounds (Moser, 2000; Moser et

al., 1997). Behavioural approaches convey multiple advantages over EEG: the lack of invasive surgery, expensive equipment and costly training. However, due to the large differences between human and rodent behaviour it is clear that some end points do not always translate well to humans (Ross, 2000). As behavioural endpoints can often be subjective there can be a large amount of inter-individual differences in their measurement (Moser et al., 1997). In the area of seizure detection, behavioural parameters can be misleading as convulsion-like motor behaviours can be attributed to causes other than true electrographic seizure and conversely (electrographic) seizures may not induce convulsions, thus increasing the risk of false positive and negative test results (Scholtes et al., 1996). Furthermore, mammals have expensive housing and upkeep requirements in addition to breeding and maturing at a relatively low rate compared to fish. Finally, as mentioned previously, rodents require relatively large amounts of compound to induce a physiological effect and so are less well suited to front-loaded approaches wherein compound is potentially scarce.

#### **1.4 *In vitro* Seizure Liability testing**

The complex nature of seizures and epilepsy mean that *in vivo* models are always likely to offer the most faithful recapitulation of the actual events. However, there have been moves over recent years to develop *in vitro* methods that can recreate specific aspects of seizurogenesis. *In vitro* approaches offer a cheaper and more ethical way of assessing seizure liability, while also generally using less compound (Accardi et al., 2016). Additionally, these approaches are typically higher throughput than *in vivo* models, and in some cases can use human cells for perceived better translation to the potential clinical impact (Tukker et al., 2020).

##### *1.4.1 Receptor-ligand binding assays*

Pharmacological profiling in the form of receptor-ligand binding assays can provide useful information on the effects of compounds based on their affinity for known receptors which are known to carry increased seizure risk. There are many different types of binding assays which follow the same general principles. These assays combine a source of receptors and a ligand, and then

measure the efficiency of ligand binding. This may be via the concentration of a drug that occupies 50% of the available receptors (EC50) (Davenport, 2012).

For example, radioligand binding assays have been used to compare the receptor affinities of endogenous ligands between zebrafish and mammals (Gonzalez-Nuñez et al., 2007). This is useful as it helps to confirm the presence of orthologous ligands between two different model organisms, while assessing the pharmacological translatability between them.

Receptor-ligand binding assays are typically used in the earliest stages of drug development to screen many compounds and identify promising drug candidates (Davenport, 2012). Moreover, information about compound receptor affinity can be a useful indicator of seizure liability, as certain receptors have known seizurogenic profiles as discussed previously. What is more, such assays require very little compound, are low cost and are high throughput (Armstrong et al., 2007).

Despite these advantages, these approaches can only verify that a specific ligand binds to a receptor. They fail to take into account how multiple targets may interact with one another to encourage seizure and are limited by the available literature on receptor function. They also provide no information on the impact of pharmacokinetics of a compound in an organism, which are highly important, as compounds may be inactive on ligands until further processing inside the body. For example, the psychotropic drug psilocybin is converted into its metabolically active form in the body via dephosphorylation (Horita and Weber, 1960).

#### 1.4.2 *Brain slice assays*

Other *in vitro* approaches, such as brain slice assays, use sections of living tissue (typically from the hippocampus of mice) in combination with electrical stimulation and recording to test seizure liability. The hippocampus is often selected because it can remain viable *ex vivo* for several hours, is easily identifiable which allows for consistent electrode positioning, and is associated with seizure induction (Schwartzkroin, 1994) and temporal lobe epilepsy (Engel, 1996).



As multiple slices can be harvested from a single animal, brain slice electrophysiology is considerably more efficient and more ethical (through reduction) than *in vivo* testing in mammals. Since the technique allows for interrogation of living tissue, it provides a simulation of seizure under relatively physiological conditions (Ridler et al., 2018). Additionally, the selection of specific anatomical regions is enabled, allowing for electrophysiological examination of the epileptiform properties of specific brain areas (Ridler et al., 2018).

Advancements in technology, such as multi-electrode arrays (MEAs), have allowed the simultaneous recording of multiple regions of a brain slice (Steidl et al., 2006). This allows assessment of the direction of depolarisations and the synchronicity of activity, the latter which is an important determinant and hallmark of seizures. As such, MEAs have been shown to effectively detect seizurogenic compound induced seizure activity in hippocampal slices and cultured neurons (Fan et al., 2019).

Due to the ease of seizure detection in this model and its physiological relevance, several studies have been produced applying it to seizure liability testing (Avoli and Jefferys, 2016; Easter et al., 2007; Fan et al., 2019; Gao et al., 2017). The application of a semi-automated, relatively high-throughput approach for simultaneous recording of seizure events from multiple brain slices yielded positive results. All of the compounds tested evoked statistically significant changes in biomarkers of seizure, however, there was no representation of CNS-active seizure-negative compounds (Easter et al., 2007).

In more recent years, with the popularisation of advanced machine learning approaches for scientific research, powerful discriminative models have been built using data garnered from slice electrophysiology (Gao et al., 2017). Gao *et al* used MEAs to record local field potentials (LFPs) from neocortical-hippocampal slices perfused with compounds of varying seizurogenicity. Using machine learning techniques they were able to develop a 100% predictive discriminative model that could identify seizurogenic compounds from pictures of their LFPs (Gao et al., 2017). While these results are very promising, only 14 compounds were included and many of the seizure negative compounds selected had no known effects on the CNS or were anti-epileptic drugs. A more thorough examination of this model should include non-seizurogenic

compounds that are still CNS-active, as well as a greater number of compounds overall.

There is clear evidence that slice electrophysiology is highly useful for assessing seizure liability however there are several limitations. Primarily, it fails to capture the seizure physiology of a complete set of brain regions in conjunction with one another as slicing severs the majority of signalling pathways, a process during which some damage is inevitably sustained. Secondly, if testing is confined to the hippocampus, the involvement of other brain areas is overlooked. This, therefore, biases this approach to receptors present in high numbers in the hippocampus and may overlook compounds that stimulate receptors which are not well represented in this tissue. Finally, slice electrophysiology still requires the sacrifice of a protected species, which, where possible, should be replaced or partially replaced in line with the 3Rs (Prescott and Lidster, 2017).

#### *1.4.3 Rodent cell culture assays*

Similar to slice electrophysiology, primary cell culture assays using rodent based cells also require the sacrifice of animals. However, as thousands of cells are dissociated from a single animal and sustained in culture, a significantly larger number of experiments can be performed per animal (Hogberg and Bal-Price, 2011). Cultured cells are then amenable to electrophysiological recordings. One such study utilised rat cortical neurons cultured on multi electrode array 48-well plates which were then exposed to a variety of seizurogenic drugs. Subsequent analysis showed significant changes in measures of electrical activity associated with seizure in response to less than half of the compounds. The assay, therefore, showed relatively poor sensitivity, failing to yield markers of seizurogenicity for several convulsant compounds (Kreir et al., 2018). This is perhaps unsurprising given the anatomical homogeneity of rat neuronal cultures lacks physiological synonymity.

In contrast, a similar study utilising cultured rat cortical tissue exposed to convulsant compounds reported a detection rate of more than 90% (Bradley et al., 2018). This study utilised MEAs for electrophysiological recordings initially measuring 39 different spike train descriptors, ultimately selecting the 12 most informative. These measures were altered significantly in 14 of the 15

convulsant compounds. However, while there were changes in specific spike train descriptors for the majority of convulsants tested, they did not subsequently test these measures in a separate set of compounds, so it is unclear whether these measures are generalizable. Moreover, the control data consisted of two neurotoxic compounds and two compounds that have no known effect on the brain. As such, it is unclear whether these descriptors are specific to seizurogenic compounds or merely to compounds with effects on neurons.

It is clear that further work in this area needs to be completed, with larger numbers of compounds and appropriate validation protocols.

#### *1.4.4 Human induced pluripotent stem cell (hiPSC) culture assays*

In recent years there has been a great deal of interest in human induced pluripotent stem cells (hiPSCs). This is with good reason, as these cells are generated from human cells, there are no issues with inter-species translatability, as well as no need for the use of any animals. This means no need for expensive animal containment facilities or animal sacrifice, thus fulfilling the 'replacement' tier of the 3Rs (Prescott and Lidster, 2017). Additionally, the development of co-culture, a process whereby cells of different types are cultured together, has improved the physiological relevance of this approach. In particular, the inclusion of astrocytes is highly relevant for seizure liability testing due to their involvement in glutamate regulation (Eid et al., 2013). Co-cultures of this type have already been utilised for seizure liability assessment with comparisons being made between different manufacturers (Tukker et al., 2020). In one such study, co-cultures contained varying proportions of glutamatergic cells, GABAergic cells and astrocytes. All cultures displayed some spontaneous neural activity, and most responded as expected to strychnine and picrotoxin, but not to 4-AP. This approach does appear, therefore, to be sensitive to at least some convulsants, however, a much wider array of compounds needs to be tested in order to fully interrogate the model and assess its predictive value.

A problematic aspect of most neuronal cell cultures, while of obvious physiological relevance, is a lack of clear three-dimensional structure inherent to most tissues. For example, the hippocampus has a very defined neuronal

structure consisting of a u-shape of tightly packed pyramidal neurons (Schwartzkroin, 1994). This lack of a clear neuronal architecture has been addressed, to a degree, via the development of brain organoids, some of which are designed to mimic specific anatomical regions such as the hippocampus (Sakaguchi et al., 2015). Typically, brain organoids are made from hiPSCs which are cultured in contact with growth factors specific to the desired output tissue (Kelava and Lancaster, 2016). In order to encourage growth in 3D, the cells have to be grown in a specialised culture environment, such as microplate moulds, or spinner flasks (Alhaque et al., 2018). This allows the hiPSCs to self-organise into complex structures that can begin to replicate the organisation of specific brain regions. However, it should be noted that brain organoids can't yet fully replicate the complex and diverse cellular architecture of a complete nervous system, wherein multiple brain regions interact with one another across a complex array of connections. Nonetheless, cerebral organoids have been shown to be responsive to PTZ, and to have PTZ-induced seizures reversed using anti-epileptic drugs (Yokoi et al., 2021). Electrical activity from these organoids was measured using a MEA, which allowed for recordings from multiple regions simultaneously at extremely high frequencies - up to 500Hz (Yokoi et al., 2021). This represents a highly promising modality through which drug induced seizures could be studied, however, this approach needs to be tested with a wider array of compounds to really begin to assess its efficacy for drug screening.

### **1.5 Zebrafish and seizure liability testing: the story so far**

One of the most promising non-mammalian models assessed for its utility in testing seizure liability in drugs is the small tropical fish species, the zebrafish (*Danio rerio*). In particular, the larval form is proving most popular as larval zebrafish have several features that make them amenable as an early stage *in vivo* approach for the assessment of drug toxicity. Zebrafish can reproduce in very large numbers, their embryos can be used at a non-protected life stage (< 5 dpf), and they have orthologues of up to 70% of all human proteins (MacRae and Peterson, 2015). What is more, due to their small size they require very small amounts of compounds. As such, zebrafish have already been used in a wide variety of contexts for informing mammalian neuropsychopharmacology and central nervous system (CNS) drug discovery (Khan et al., 2017). Initial

forays into seizure liability assessment in zebrafish have broadly yielded positive results and to date have mainly been focussed on behavioural assessment and small-scale electrophysiological assessments.

### *1.5.1 Zebrafish behavioural assessment*

Behaviour assays, like the aforementioned FOB and Irwin tests, have been shown to be a useful first step in assessing psychoactive compounds (Ahmad et al., 2012). Moreover, automated video analysis allows for the objective calculation of variables that represent zebrafish swimming behaviour thus increasing throughput and reducing subjectivity. By comparison, there is more scope for the FOB and Irwin tests to suffer from inconsistent user interpretation of rodent behaviour, owing to the subjective nature of the measurements (Moser et al., 1997). Zebrafish behavioural assays have shown to be a sensitive approach for assessing anaesthetics, convulsants and other psychoactive compounds (McCarroll et al., 2019; Tran et al., 2017; Winter et al., 2008).

Indeed, zebrafish behavioural assays have been used to assess a variety of drug-induced cognitive and emotional states. For example, they have been used to identify the sedative effects of high doses of antidepressants (Suryanto et al., 2021), to identify GABA and serotonin ligands related to sedation and paradoxical excitation (McCarroll et al., 2019) and to identify the anxiogenic effects of donepezil in zebrafish (Giacomini et al., 2020).

In the area of convulsant screening, a behavioural assay on an array of 25 compounds, with mixed seizurogenicity, returned 72% predictivity for compounds that increased seizure liability (Winter et al., 2008). Utilising measurements such as number of high-speed movements, total swimming distance and time spent in different areas of the recording chamber can provide an indirect measure of neuronal excitability.

However, despite being reasonably successful, behavioural screening, suffers from multiple drawbacks, primarily the lack of translatability of most zebrafish behaviour to humans and the lack of a direct measure of brain activity. Specifically, it is difficult to identify behavioural differences in zebrafish that relate to specific drug mechanisms and associated changes in brain activity. For example, with regard to convulsant screening, these assays may be able to identify in some cases if a compound is seizurogenic, but it cannot reveal much

else about mechanism of action. Moreover, drugs may induce seizures but not necessarily increase swimming movement or conversely not cause seizures but increase swimming.

### 1.5.2 Zebrafish electrophysiology

Despite its long history in neuroscience, the use of electrophysiological recordings in zebrafish for seizure research has been uncommon until relatively recently. However, multiple studies performing local field potential (LFP) recordings (highly sensitive measures of voltage changes occurring in tissue) in larval zebrafish with *snc1a* mutations have identified clemizole and other serotonin modulators as potentially effective treatments for Dravet syndrome (Baraban et al., 2013b; Griffin et al., 2017, 2019). While clemizole is yet to stand clinical trials for this application, the relevance of serotonin receptor involvement in treating Dravet syndrome may help inform future clinical studies. Similarly, an LFP-based high-throughput approach utilising larval zebrafish and measures of temporal complexity was predictive of compounds with the highest efficacy and least side effects for the treatment of seizures in a zebrafish model of Dravet syndrome. However, it should be noted the success of this assay was measured against behavioural data from zebrafish, and not clinical data (Eimon et al., 2018).

Similar studies have been performed screening coumarins derivatives for anti-seizurogenic properties, using LFP recordings, in a PTZ exposure model of seizures, in larval zebrafish (Kozioł et al., 2021). It should be noted, this is a relatively simple model of seizure and as such anti-epileptic drug efficacy is biased to the pharmacological mechanism of seizure induction.

In addition to drug screening, LFP recordings have also been used in screening for genes implicated in childhood epilepsy (Griffin et al., 2021). In this case, as in many of the aforementioned studies, LFP recordings were used to measure electrical activity and identify aberrant electrophysiological signatures that implicate seizurogenesis. This is more easily done using LFP, than any other method due to the wealth of electrophysiological studies assessing seizures in other animal models. As such electrophysiological seizure phenotypes, varied as they are, are relatively well categorised (Fisher et al., 2014b).

Recent advancements in the brain coverage of electrophysiological recordings in zebrafish have been made with the development of multi-electrode recording devices designed specifically for zebrafish (Cho et al., 2017; Hong et al., 2016). Multi-electrode setups allow for recordings to be taken from numerous brain regions simultaneously, which allows for network analyses measuring how brain regions are behaving relative to one another. This is especially useful for seizure research, as often one of the defining aspects of seizures is hyper-synchronous activity. One of the more refined approaches utilises microfluidics to restrain and 'dose' zebrafish while simultaneously recording using multiple electrodes. Reminiscent of human EEG devices, this procedure is non-invasive, with electrodes resting on the head of larvae trapped in a 3-D fluidic channel see Figure 1.8 (Hong et al., 2016). This approach is high-throughput and records from multiple sites, it also doesn't require the use of drugs to immobilise zebrafish to allow for recording. When used for seizure modelling, this approach was shown to be sensitive for seizures and showed increases in cross-correlation between recording sites, suggesting elevated brain synchronicity (Hong et al., 2016). It should be noted, however, that the nature of the system means electrode placement will vary depending on the size and shape of the head, as well as its exact positioning in the chamber. Moreover, the lack of intracranial electrodes and prior paralysis may mean this approach detects muscle and movement artefacts in addition to brain activity. Some of these issues can be avoided by direct implantation of electrodes onto the heads of adult zebrafish, however, this requires the use of anaesthesia and is relatively slow and invasive procedure in addition to taking place at a protected life-stage. This means it is less high throughput and therefore less viable as a frontloaded drug screening approach (Cho et al., 2017).

In addition to the limitations listed above, a fundamental issue with electrophysiological recording is the lack of spatial resolution due to the recording taking place from a limited number of brain regions. As such, the specific involvement of various brain regions in the propagation of seizures is difficult to delineate. An emerging method that provides much greater spatial coverage and, when coupled with high-speed microscopy, acceptable temporal resolution is whole brain  $\text{Ca}^{2+}$  imaging.

### 1.5.3 Utilising $\text{Ca}^{2+}$ for studying brain activity.

Calcium ions are involved in a plethora of biological processes, ranging from gene expression to the cardiac cycle (Dulhunty, 2006; Hardingham et al., 1997). Notably,  $\text{Ca}^{2+}$  is necessary for exocytosis in a variety of secretory cells including pancreatic  $\beta$ -cells, rod photoreceptors, and neuronal axons (Neher and Sakaba, 2008).

In the neuron, exocytosis of neurotransmitter occurs when the arrival of an action potential at the presynaptic terminal causes depolarisation, which, induces opening of voltage-dependent ion channels, allowing the passage of  $\text{Ca}^{2+}$  into the neuron.  $\text{Ca}^{2+}$  influx into the presynaptic terminal initiates neurotransmitter release via the calcium sensing synaptotagmin 1, which binds

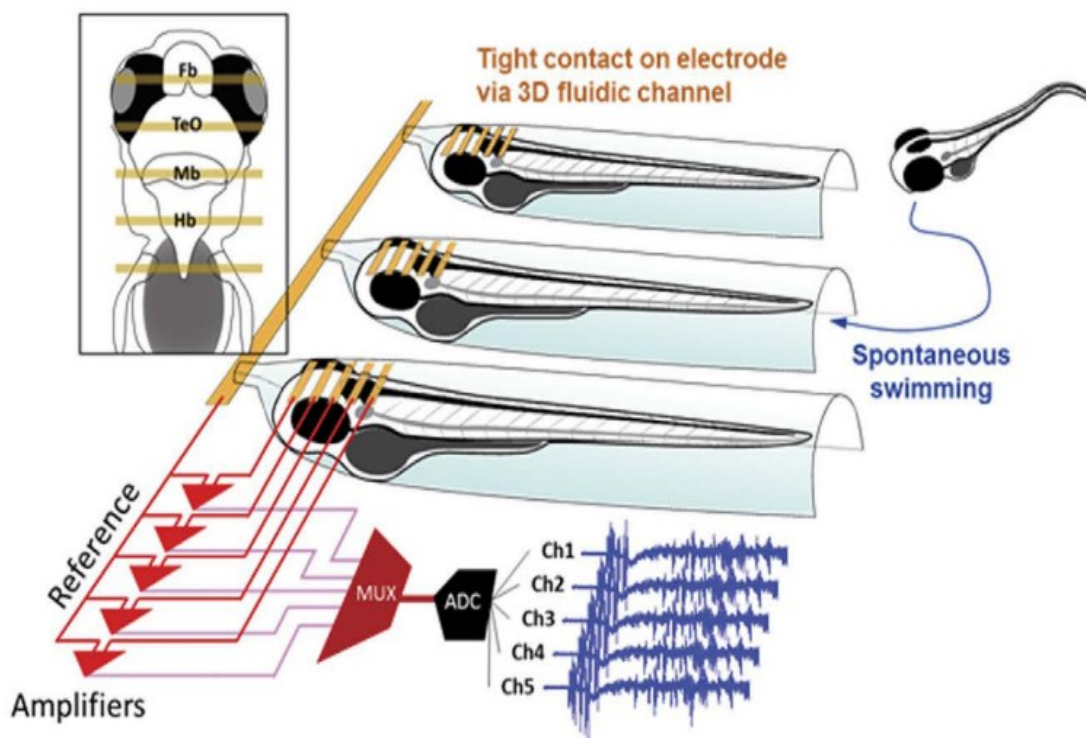


**Figure 1.8 Non-invasive multichannel EEG.** The graphic shows the relative position of surface electrodes to zebrafish brain (Fb, forebrain; TeO, optic tectum; Mb, midbrain; Hb, hindbrain) and a multichannel amplifier (MUX, multiplexer; ADC, analog-to-digital converter) (Hong et al., 2016).



$\text{Ca}^{2+}$  and activates the membrane fusion machinery. Synaptotagmin works in conjunction with the cofactor complexin to activate and clamp SNARE proteins, which mediate the fusion of neurotransmitter containing vesicles to the cell membrane, initiating exocytosis of the neurotransmitter (Südhof, 2012). This process requires high levels of rapid  $\text{Ca}^{2+}$  influx, which remains in the presynaptic terminal only transiently. However, slow accumulation of  $\text{Ca}^{2+}$  at excitatory hippocampal synapses has been identified as a determining factor in synaptic strength and can be induced via trains of action potentials. The slow accumulation of  $\text{Ca}^{2+}$  encourages pooling of exocytosis-ready vesicles (containing neurotransmitter). leading to subsequent activation inducing an increased release of neurotransmitter (Stevens and Wesseling, 1998). The increased basal amount of  $\text{Ca}^{2+}$  consequently leads to a higher probability of neurotransmitter release during action potential, as  $\text{Ca}^{2+}$  is more likely to reach the threshold concentration required for  $\text{Ca}^{2+}$  dependent exocytosis. These slower  $\text{Ca}^{2+}$  transients, therefore, induce short term facilitation and are involved in manipulation of synaptic plasticity (Neher and Sakaba, 2008).

With the role of  $\text{Ca}^{2+}$  intrinsically linked to action potentials and neuronal activation,  $\text{Ca}^{2+}$  can provide a useful, if indirect, measure of neuronal activity. The development of  $\text{Ca}^{2+}$  sensors, which emit or absorb light, in the presence of  $\text{Ca}^{2+}$ , allow for the visualisation of  $\text{Ca}^{2+}$  transients. Using a variety of microscopy techniques,  $\text{Ca}^{2+}$  in tissue can be quantified and localised with extremely high spatial resolution (Grienberger and Konnerth, 2012).  $\text{Ca}^{2+}$  sensors can be split into two broad categories: loadable dye and genetically encoded.

One of the more popular loadable dyes used in neuroscience is Fura-2 (Wokosin et al., 2004). Fura-2 absorbs light at wavelengths 340 nanometers (nm) and 380 nm subsequently emitting light at 510 nm. However, the amount of light absorbed at each of these wavelengths is different and the ratio of absorption at each of these wavelengths changes in response to  $\text{Ca}^{2+}$  binding (Wokosin et al., 2004). Thus, quantifying  $\text{Ca}^{2+}$  is a case of measuring light emissions from fura-2 when stimulated at 340nm and (separately) 380nm then calculating the ratio between the two. This provides a highly sensitive and fast measure for quantifying  $\text{Ca}^{2+}$  in target tissues. However, this approach requires loading of fura-2 into the target tissue, which can be invasive. Moreover, fura-2

is sensitive to photobleaching over long periods of imaging, which can lead to inaccurate estimation of  $\text{Ca}^{2+}$  concentration (Becker and Fay, 1987).

In contrast, genetically encoded  $\text{Ca}^{2+}$  sensors (GECIs) are much less prone to photobleaching, and do not require invasive introduction of exogenous chemicals, which is particularly advantageous for imaging over longer time periods and *in vivo*. GECIs can be expressed under the control of specific promoters, meaning that they can be expressed in genetically defined neuronal cell types in a stable and replicable manner (Dana et al., 2014). However, up until very recently, GECIs have not been as sensitive as the equivalent dyes (such as fura-2), while also suffering from slower kinetics meaning that fast  $\text{Ca}^{2+}$  transients were not detectable (Dana et al., 2018). The most widely used form of GECI are the GCaMP family of  $\text{Ca}^{2+}$  sensors, which were created from the fusion of green fluorescent protein (GFP), m13 and calmodulin (Nakai et al., 2001). When  $\text{Ca}^{2+}$  is present it binds to calmodulin which undergoes a conformational change resulting in GFP-mediated fluorescence (Akerboom et al., 2009).

Alongside the development of  $\text{Ca}^{2+}$  sensors has been the development of advanced microscopy techniques that allow for fast imaging of tissue in the three dimensions (Grienberger and Konnerth, 2012). Confocal, two photon and light sheet microscopes have either been developed, improved or sped up alongside improvement in  $\text{Ca}^{2+}$  sensors. In the area of  $\text{Ca}^{2+}$  imaging in zebrafish, light sheet microscopes in particular have proven highly effective and became popular due to their ability to image large volumes of tissue at relatively high temporal resolutions (Hillman et al., 2019). The reason this high temporal resolution is achievable, is because, unlike point scanning approaches such as confocal and two-photon microscopy, light sheet microscopes illuminate an entire plane of tissue at a time (Hillman et al., 2019). Light sheet microscopes utilise a laser beam focussed into a sheet of light which is used to optically section the sample. In addition to the improved speed relative to point scanning techniques, selective plane illumination is less phototoxic, reducing the risk of photobleaching. This is due, in part, to the fact that light only passes through the part of the sample intended for illumination, meaning reduced exposure of other parts of the tissue to light (Hillman et al., 2018). These factors make light sheet microscopy amenable to functional imaging, allowing videos of active tissue to

be recorded across three dimensions, in a manner similar to functional MRI (Reynaud et al., 2014). Given the highly dynamic nature of brain activity, this approach is highly useful as it can detect fluorescence from  $\text{Ca}^{2+}$  sensors at sub cellular resolution and track their activity over time, an approach already being practiced in larval zebrafish (Ahrens et al., 2013).

#### *1.5.4 Zebrafish $\text{Ca}^{2+}$ imaging*

The combination of genetically encoded  $\text{Ca}^{2+}$  sensors (GCaMPs) and light sheet microscopy (LSM) in larval zebrafish has allowed for functional imaging of the whole CNS at sub-cellular resolution at increasingly rapid speeds (Ahrens et al., 2013). Zebrafish are uniquely suited for functional imaging of this kind, offering a 1 mm<sup>3</sup> CNS containing discrete anatomical divisions, with some functional homology to their mammalian peers, at a mere seven days post fertilisation (Kalueff et al., 2014). The resultant output, using this approach, is a series of images containing fluorescent intensity information encapsulated in each pixel. This information can be used to generate timeseries' that represent changes in fluorescent intensity, and thus  $\text{Ca}^{2+}$  activity, over time. How these pixels are spatially resolved is dependent on the goals of the researcher, as this approach provides a unique opportunity to observe  $\text{Ca}^{2+}$  dynamics at both the single cell and whole brain network scales, allowing assessment of how brain networks are integrated across these gradations. Indeed, PTZ induced seizure dynamics in larval zebrafish have been categorised in these terms, identifying abrupt surges in neural synchrony at the level of both single cell and wider brain regions (Diaz Verdugo et al., 2019).

In terms of drug profiling, some initial work has been undertaken using  $\text{Ca}^{2+}$  functional imaging to assess a limited range of convulsant compounds, yielding distinct spatio-temporal patterns of activity for compounds with disparate mechanisms of action. This preliminary work highlights the potential sensitivity, of whole-brain functional imaging in zebrafish, for the pharmacodynamic properties of CNS-active drugs. Moreover, it pioneered the use of whole brain anatomically selected regions of interest in larval zebrafish  $\text{Ca}^{2+}$  functional imaging (Winter et al., 2017). This provides an opportunity to perform network analysis in the context of our understanding of larval zebrafish anatomy, allowing knowledge of receptor distribution to inform our understanding of the

effects of different drug mechanisms on larval zebrafish brain networks, something not addressed in this initial study (Winter et al., 2017).

Network analyses on these timescales typically utilise correlation coefficients to measure the magnitude of similarity between different timeseries', a technique known as functional connectivity. Functional connectivity is an approach commonly applied to functional magnetic resonance imaging (fMRI) (Chalovich and Eisenberg, 2007). However, the excellent spatial-resolution provided by light sheet microscopy, and the small volume of the zebrafish brain, allows for FC analyses to be performed at sub-cellular resolution for the first time in a complete CNS. However, analyses are typically performed on a coarser set of regions of interest (ROIs), due to the computationally expensive nature of performing FC analyses on thousands of neurons. ROI determination is a process that will need to be refined and tested to identify the most informative output, with multiple methods already in use, including clustering-based approaches, anatomical registration or combinations of the two (Burgstaller et al., 2019; Ghannad-Rezaie et al., 2019; Winter et al., 2017).

One of the ways functional connectivity measures can be analysed further is by using graph theory. Graph theory uses functional connectivity information to elucidate the nature of a network as a whole. For example, the graph measure modularity reveals how modular a network is, that is to say, does the network have ROIs that are 'more' connected to each other than the rest of the network? In a zebrafish transgenic model of depression and anxiety, modularity was significantly increased, an effect that was reversed by administration of antidepressant drugs (Burgstaller et al., 2019).

Functional connectivity in larval zebrafish has been shown to increase in response to PTZ exposure (Liu and Baraban, 2019; Turrini et al., 2022), an effect for which efforts have been already made to develop generative mathematical models (Rosch et al., 2018). Notably, in all these cases correlation analysis was performed between relatively large anatomical regions of interest, employing between 5-12 ROIs in total. Moreover, PTZ exposure has also been shown to generate caudo-rostral ictal waves, that may account for the increased functional connectivity seen in previous studies (de Vito et al., 2022). This study, in contrast, not only looked at wider brain regions but also individual neurons. In addition, it developed the use of ultra-high speed two photon LSM

able to perform volumetric imaging of the zebrafish brain at 5 Hz. However, this technique was not amenable to baseline recordings due to the use of capillary tubes to mount larvae. As such, larvae would have been insulated from the *in situ* exposure of compound, meaning that periods could not be used within animal controls. Despite this, the use of two photon microscopy and the immense speed of the system reflect the rapid development of light sheet microscopes and the implications this has for neuroscientific work in zebrafish. Indeed, two photon light sheets have a distinct advantage over one photon, as one photon microscopes suffer from higher levels of crosstalk from neuropil, resulting in increases in signal to noise and artefactual correlations of neural activity (Shemesh et al., 2020).

The efficacy of one photon light sheet systems can be improved through the use of soma-targeted GCaMP, which results in an improved signal to noise ratio and a reduction in artefactual correlations (Shemesh et al., 2020). In addition to targeting GCaMP in the cell body, GCaMP itself is being developed further to improve its dynamic range, contrast and sensitivity to  $\text{Ca}^{2+}$  (Barykina et al., 2020). Moreover, development of alternative GECI sensors to GCaMP is also in the pipeline in order to address the issues GCaMP has with  $\text{Ca}^{2+}$  buffering. The term  $\text{Ca}^{2+}$  buffering refers to the phenomena wherein calmodulin competes with endogenous proteins for  $\text{Ca}^{2+}$  binding, which, in the case of long term or high expression of GCaMP, can result in abnormal neuronal phenotypes (Yang et al., 2018). Reducing the expression of GCaMP does solve this problem, however, it also results in reduced brightness. As such the development of GECIs using brighter alternative fluorescent proteins, such as mNeonGreen (mNG) has begun with preliminary studies suggesting comparable performance to GCaMP6s with improved brightness, however, further improvements need to be made in order to substantially improve on GCaMPs (Subach et al., 2020; Zarowny et al., 2020).

It is clear, therefore, that the zebrafish LSM approach offers a unique insight into neuronal networks and macro-scale brain function by elucidating functional interactions between brain regions (Betzl, 2019). However, current light sheet systems, while they are the fastest of the imaging approaches for recording in four dimensions (Friedrich et al., 2017), still have limited temporal resolution. By comparison, electrophysiology studies use sample rates thousands of times

higher, allowing them to perform frequency domain analyses and identify highly dynamic brain activity that cannot be detected using whole-brain imaging (Cho et al., 2017; Griffin et al., 2017; Liu and Baraban, 2019). Indeed, for LSM setups to increase temporal resolution, brain coverage is sacrificed, in a trade-off between the number of neurons imaged and the speed of imaging. As such, it may be the case that the use of such systems for assessing seizure liability focus imaging on specific brain regions in order to maximise temporal resolution. While it may be necessary to sacrifice some spatial coverage it is still possible to image in multiple planes at kHz speeds. A study performing volumetric imaging of the zebrafish heart utilised multiple laser sheets and multiple cameras, focusing each camera individually on a single illuminated plane, as such they were able to perform recordings at the maximum acquisition speed of each camera (Sacconi et al., 2022). This is highly promising in terms of high-speed imaging, however, will result in increased photobleaching and photo-toxicity. Moreover, the approach relies on deconvolution to fully separate information into their separate planes, which increases the likelihood of imaging artefacts.

The high spatial resolution offered by LSM and the ability to image an entire intact brain *in vivo* offers a unique tool for modelling non-drug induced seizures. One such study has assessed seizure activity caused by Dravet syndrome, a rare form of childhood epilepsy (Ghannad-Rezaie et al., 2019). Transgenic zebrafish expressing GCaMP and containing the Dravet syndrome-causing *scn1a* mutations have allowed for the identification of novel approaches to epilepsy treatment. This includes multi-drug approaches informed by functional connectivity analyses (Ghannad-Rezaie et al., 2019).

#### 1.5.5 *In silico* and molecular markers of seizure

Generative computational models are among the useful approaches for improving understanding of how seizures can develop and propagate. Such models provide a simplified mathematical representation of neural systems that can be utilised to gain an understanding of the mechanisms underpinning specific pathophysiological perturbations (Stefanescu et al., 2012). Indeed, *in silico* approaches have demonstrated a potential utility for identifying the optimal location of surgical resection in pharmacologically intractable epilepsy treatment

(Goodfellow et al., 2016), as well as the ability to diagnose specific epilepsy types (Lopes et al., 2019). Despite their obvious utility in other areas, no generative models exist that can predict seizure liability of compounds based purely on their chemical structure. However, there has been work developing discriminative models for these purposes (Heikamp and Bajorath, 2014).

Discriminative models separate representatives of different categories based on their features. For example, Zhang *et al* selected a set of 855 compounds (328 seizure positives and 527 seizure negatives) and generated a set of 434 molecular descriptors for each compound, including geometrical, topological and electrical properties. From these molecular descriptors, they removed the parameters that were highly correlated with each other or that had very low standard deviation across compounds, finally fine-tuning their feature set using an additional feature selection algorithm. They subsequently 'trained' an optimised support vector machine classifier (a machine learning algorithm) using 680 of the compounds. Support vector machines (SVMs) function by creating a multidimensional feature space containing the training data and drawing a line (known as a hyperplane) in the feature space separating representatives of the different categories. New compounds can subsequently be plotted into this feature space and where they are relative to the hyperplane dictates the category they are assigned. When Zhang *et al* tested their trained SVM using their test set of 175 compounds they achieved 86.9% predictivity for seizurogenic compounds (Zhang et al., 2011). Despite this, application in a real-world drug development context is yet to be demonstrated. This approach potentially allows for an accurate predictive model than can identify potentially seizurogenic compounds based solely on their molecular properties without the use of animal models or any compounds. However, that is not to say this approach could not be adapted for use with data obtained from animal models, as combining molecular measures and data generated from animals' models could yet further improve its efficacy.

However, the black-box nature of machine learning algorithms means that few elucidations can be made about what causes compounds to be seizurogenic, as outputs from such algorithms are only categorisations. Indeed, the true performance of such models in drug discovery programmes is yet to be carefully evaluated, particularly when testing compounds with weak or

infrequent seizure liability. In addition, more must be known about compound seizurogenicity, with regards to dosages and mechanism of action, to inform the decision-making process and this goes beyond binary answers around the propensity to cause seizures alone.

## **1.6 Summary**

The role drugs can play in either initiating seizures or increasing seizure risk is often complex and can involve interactions from multiple receptor sub-types, neurotransmitters and brain regions. With this being the case, approaches taken to assess seizure liability need to include *in vivo* models, with inclusions of distinct anatomical regions. Current seizure liability testing includes this, utilising *in vivo* EEG approaches in rodents. However, such approaches are expensive and low throughput and as such are typically utilised late in preclinical testing. Neuroscientific approaches in larval zebrafish offer an *in vivo* model much more amenable as frontloaded approach, which offers good similarity to their mammalian counterparts and contain representatives of the majority of relevant neurophysiological systems. What is more, due the development of more and more effective GECIs and volumetric imaging techniques, larval zebrafish offer unique insight into the network activity of a complete CNS. With this being the case, larval zebrafish may well offer an additional solution for early identification of compounds that influence seizure liability. However, most of the current  $\text{Ca}^{2+}$  imaging studies on seizures in larval zebrafish only use one or two convulsant compounds with little emphasis on the broad spectrum of drug classes that increase seizure liability. As such, there is a still a need to test this approach more thoroughly and to identify if  $\text{Ca}^{2+}$  imaging outputs reflect drug seizurogenicity or pharmacology. This being the case,  $\text{Ca}^{2+}$  imaging in larval zebrafish needs to be performed on an array of different compounds with varying mechanisms of action and assessed for biomarkers that indicate drug pharmacology or seizurogenicity.

## **1.7 Thesis aims**

In this thesis the first overarching aim, addressed in Chapter 2, was to test the hypothesis that the spatiotemporal patterns of neural activity observed in the larval zebrafish brain following drug exposure are linked to specific mechanisms of action that induce seizures in mammals, including humans. In order to do this  $\text{Ca}^{2+}$  functional imaging data were generated using GCaMP6 larval zebrafish



exposed to a variety of compounds and used the resultant spatiotemporal patterns of activity produced by each agent, to identify commonalities between compounds with similar pharmacodynamics.

It was further hypothesised that changes in spatiotemporal patterns of  $\text{Ca}^{2+}$  activity upon compound exposure would align with the current understanding of zebrafish receptor distribution. As such, the spatiotemporal patterns of  $\text{Ca}^{2+}$  activity elicited by specific receptor ligands were compared with immunohistochemical studies of the corresponding receptors in larval zebrafish. This was performed in the discussion portions of chapters 2 and 4.

In chapter 3, the thesis studies also sought to demonstrate concordance between the  $\text{Ca}^{2+}$  imaging of functional responses to drugs and direct electrophysiological measurement of network hyperexcitability using in vivo electroencephalography (EEG) in 4 dpf larvae. This would allow confirmation of the electrographic basis of observed  $\text{Ca}^{2+}$  activity and provide data to help translate to more established non-clinical/clinical measures of seizuregenesis.

In a final analysis in chapter 5 an existing behavioural dataset from 7 dpf zebrafish larvae was analysed and compared with neurophysiological data from EEG and  $\text{Ca}^{2+}$  imaging in 4 dpf larvae. This work was undertaken to compare the efficacy of different methodologies (behaviour, EEG,  $\text{Ca}^{2+}$  imaging) for identifying seizurogenic compounds and to assess the behavioural impact of specific neurophysiological phenotypes.

Throughout the thesis research work there was furthermore a focus on developing and refining the methodologies used to keep pace with this rapidly developing field.

## Chapter 2: Functional brain imaging in larval zebrafish for characterising the effects of seizurogenic compounds acting via a range of pharmacological mechanisms

### 2.1 Introduction

Functional brain imaging using genetically encoded  $\text{Ca}^{2+}$  sensors in optically transparent larval zebrafish offers an extremely powerful approach for analysing the *in vivo* response of the vertebrate brain to drug treatment. Despite its power, this approach has yet to be widely used in neuropharmacological studies. A research area that is beginning to exploit this methodology is the study of seizures and the chronic seizurogenic condition, epilepsy (Burrows et al., 2020).

Traditionally, seizures have been classified as the culmination of abnormal neuronal excitation that progresses to hyper-synchronous excitation across large-scale neural circuits. Most animal models of seizures and epilepsy rely upon unbalancing excitatory and inhibitory synaptic influences using pharmacological (or electrical) stimulation (Staley, 2015). Whilst this process is often exploited for anti-epileptic drug development (Kandratavicius et al., 2014), this can also occur through the inadvertent action of chemicals, including drugs (Ruffmann et al., 2006). The exact mechanisms that lead to seizures are not fully understood (Scharfman, 2007) and a major challenge is that, to understand the mechanistic basis of seizure generation and identify novel drug targets, studies of brain networks linking local and global scales are crucial (Rossi et al., 2018; Staley, 2015). Importantly, and in contrast with other current animal models, functional brain imaging in the larval zebrafish allows this and also provides a more direct indicator of neural activity than, for example, behavioral assessments of convulsions (Winter et al., 2008). Consequently, multiple recent studies have focused on functional imaging in the zebrafish larval brain after exposure to the model seizure-precipitant and  $\text{GABA}_A$  antagonist pentylentetrazole (PTZ), as well as a small number of other

seizurogenic tool compounds (Diaz Verdugo et al., 2019; Liu and Baraban, 2019; Rosch et al., 2018; Turrini et al., 2017; Winter et al., 2017) or have demonstrated the application of this methodology in assessing the efficacy of anti-epileptic drugs in genetic or PTZ-induced epilepsy (Ghannad-Rezaie et al., 2019; Lin et al., 2018). The fact that functional brain imaging studies using larval zebrafish have focused on one or two mechanisms of initiation, however, means that we still do not have a clear idea of whether neural network hyperexcitation induced by other drug types can be detected using this approach and what those neural imaging signatures look like (Burrows et al., 2020). Such information is critical both for assessing the validity of this approach for the detection of unwanted neuroactivity during drug development, and its application for the discovery of new antiepileptic drugs. Furthermore, understanding the neuropharmacological responsiveness of the larval zebrafish provides important validation data on the applicability of this model for more fundamental mechanistic studies of seizures and epilepsy, and on the translational power of the larval zebrafish for use in imaging-focused neuroscience studies more widely.

To address this knowledge gap using four-dimensional functional brain imaging, we systematically tested the responsiveness of 4 days post fertilisation (dpf) larval zebrafish to 57 compounds with a known link to seizure generation in mammals and spanning more than 12 drug classes, alongside eight compounds with no such link. We opted to use 4 dpf zebrafish as these are not considered protected vertebrates under European animal legislation and are therefore ethically preferable, particularly for use in higher throughput screens where animal usage can be high. In addition, the use of 4 dpf larvae allows unfettered functional imaging in the vertebrate brain in the absence of the confounding effects of a general anaesthetic. With this experimental approach, we sought to address these key questions: (1) Are 4 dpf larval zebrafish responsive to a range of molecular mechanisms linked to network hyperexcitation in mammals? (2) Are there phenotypic features that allow for differentiation between non-seizurogenic and pro-seizurogenic compounds

and/or particular pharmacologies? (3) Are there brain regions that appear particularly important for the initiation and/or propagation of seizure-like network activity regardless of the initiating mechanism? (4) Are the resultant spatiotemporal patterns of neural activity consistent with our knowledge of neurotransmitter-specific brain circuitry in the larval zebrafish?

## 2.2 Methods

The experimental approach is detailed in the following sections and the process is summarised in Figure 2.1. Throughout, the data shown in graphs and tables are the means  $\pm$  SEM of data points from individual animals ( $n$ ). Statistical analysis was undertaken using larvae as the individual replicate values and only where the sample size was at least  $n = 5$ . Due to data loss, one dataset contained an  $n = 4$  (picrotoxin at the lowest treatment level of 15  $\mu$ M) and in this case, the treatment was not subject to statistical assessment. Outliers were not excluded from the analyses or presentation of data. This manuscript complies with the *British Journal of Pharmacology* recommendations and requirements on experimental design and analysis (Curtis et al., 2018).

### 2.2.1 Experimental animals

4 dpf transgenic zebrafish with a pan-neuronal  $\text{Ca}^{2+}$  sensor (*elavl3:GCaMP6s*) were used for the imaging. Adult *elavl3:GCaMP6s* broodstock (Ahrens et al., 2014), originally obtained from Dr. Misha Ahrens (Janelia Research Campus, Howard Hughes Medical Institute, Ashburn, Virginia, USA), were held in aquaria at the University of Exeter, at  $28^{\circ} \pm 1^{\circ}\text{C}$  under optimal conditions for spawning (12-h light: 12-h dark cycle, with 20-min dusk–dawn transition periods). Culture water consisted of mains tap water which was filtered by reverse osmosis (Environmental Water Systems UK Ltd.) and then reconstituted with Analar-grade mineral salts to a standard synthetic freshwater composition (final ion concentrations: 117  $\text{mg L}^{-1}$   $\text{CaCl}_2 \cdot 2\text{H}_2\text{O}$ , 25.0  $\text{mg L}^{-1}$   $\text{NaHCO}_3$ , 50  $\text{mg L}^{-1}$   $\text{MgSO}_4 \cdot 7\text{H}_2\text{O}$ , 2.3  $\text{mg L}^{-1}$   $\text{KCl}$ , 1.25  $\text{mg L}^{-1}$  Tropic Marine Sea Salt, giving a conductivity of 300 mS). The culture water was aerated and heated to  $28^{\circ}\text{C} \pm 1^{\circ}\text{C}$  before being supplied to individual zebrafish tanks on a

semi recirculatory system. Water was routinely monitored for temperature, pH, conductivity, ammonia, nitrite and nitrate, all of which were maintained within appropriate limits for zebrafish. Spawning occurred at the time of lights on and was encouraged by provision of a spawning substrate. Fertilized eggs were collected shortly after spawning, bleached for 1 min in 1% w/v chloramine T (Sigma-Aldrich, Poole, UK) in culture water, rinsed with fresh culture water and transferred to Petri dishes which were filled with culture water and held at  $28^{\circ} \pm 1^{\circ}\text{C}$ , under the same lighting conditions, until use in experiments at 4 dpf. All work was undertaken under project and personnel licenses granted by the UK Home Office under the UK Animals (Scientific Procedures) Act and approved by the University of Exeter's Animal Welfare and Ethical Review Body and with the recommendations made by the *British Journal of Pharmacology* (Lilley et al., 2020).

### 2.2.2 Test compounds

The range of drug types assessed spanned agents targeting multiple mechanisms implicated in the initiation of neural network hyperexcitation (Easter et al., 2009) and comprised many compounds which have not, to our knowledge, been tested before in zebrafish. The compounds tested encompassed those implicated in the induction of seizures in humans or nonclinical models via a range of molecular mechanisms and those with no known association with seizures (Table 2.1). Compounds were selected following an extensive review of available published data. This review allowed us to identify compounds with a link to seizures in preclinical or clinical studies and select appropriate pharmacological probes known to act via mechanisms implicated in the generation of neural network hyperexcitation. The compiled list was not considered exhaustive but rather designed to encompass several examples acting through related mechanisms of action. Based on the strength of the supporting literature, we categorised the selected compounds as follows: category A - tool compounds typically used in animal models of seizures or epilepsy; category B - compounds for which there is strong evidence for an association with seizures from clinical or nonclinical animal

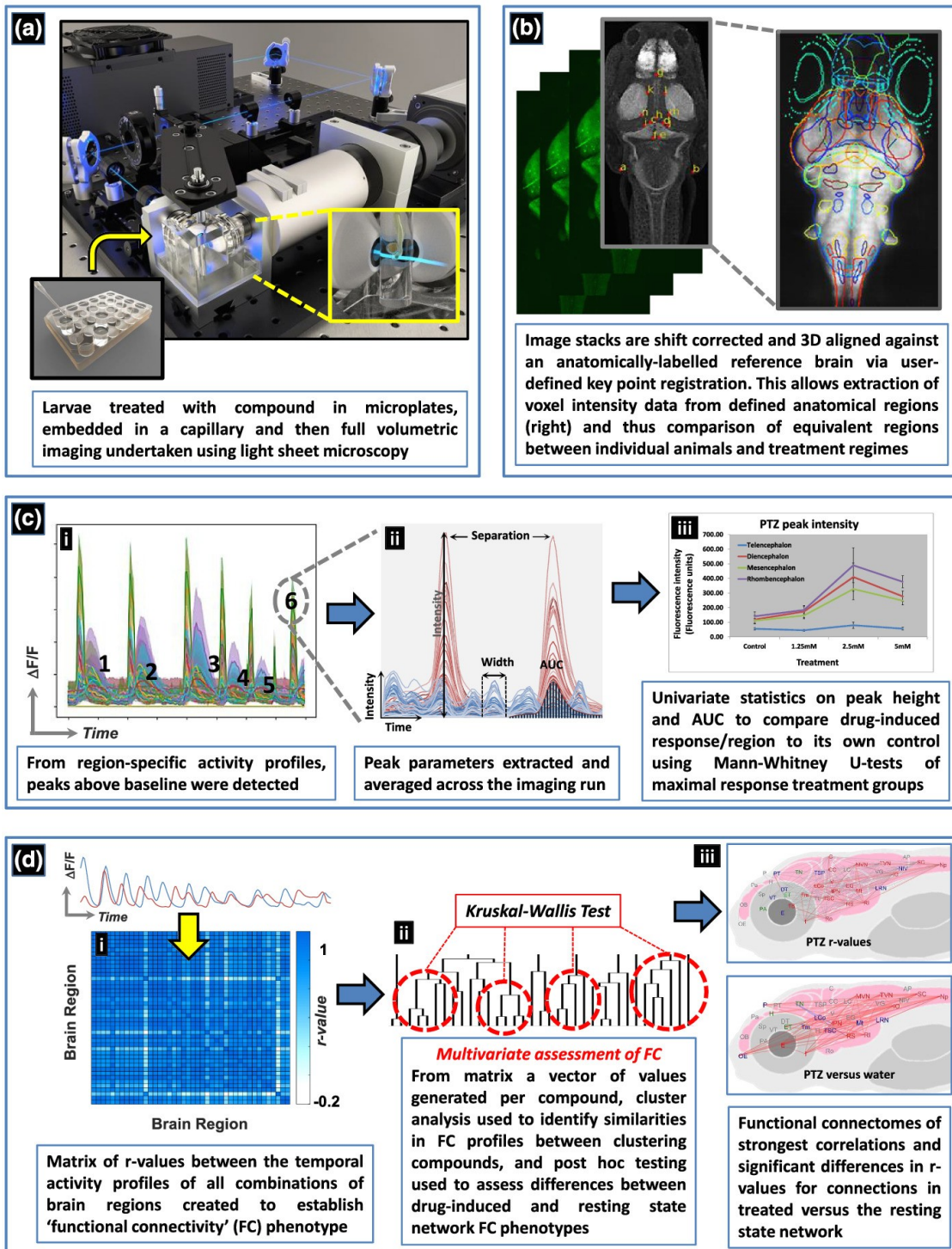


**Figure 2.1:** Schematic of the experimental process used to obtain 4D whole brain neural activity data from drug treated larval *elav13: GCaMP6s* zebrafish. The experimental process and resultant data analysis procedures are summarised in panels a–d. (a) Animals were first exposed to the compound

and then imaged using light sheet microscopy. (b) The resultant image stacks were 3D aligned to a standardised brain image library (Z-brain atlas) and subsequent 3D registration allowed extraction of anatomical region-specific fluorescence data. (c) The extracted region-specific fluorescence intensity temporal profiles were then analysed to reveal regional changes between treated and untreated animals. (i) Peaks were automatically identified from the temporal profiles (e.g. labelled 1–6) and (ii) peak parameters for each profile extracted. (iii) Peak height and area under the curve (AUC) were then analysed using univariate statistics to identify brain regions showing altered neural activity versus the same area in the corresponding group of control animals. (d) For the analysis of functional connectivity (FC), (i) Pearson's correlation coefficients ( $r$ ) were calculated between the temporal activity profiles of each pair of regions to provide a matrix summarising measures of the level of functional connectivity between each pair of nodes. An  $r$  value of  $>0.7$  between two regions suggested these areas were functionally connected as both showed correlated temporal activity profiles. (ii) Multivariate statistical analysis of the FC data was then undertaken, followed by cluster analysis of the resultant Euclidean distances, to assess similarities in the resultant phenotypes and whether groupings contained compounds sharing common mechanisms of pharmacological action. Post hoc testing of the resultant groupings using Kruskal–Wallis tests then revealed the brain regions and/or connections driving these similarities/differences. (iii) The  $r$  values from the FC matrices generated for each compound were visualised in the form of a connectivity map of the brain (a functional connectome ~ upper panel) and as exposed animal data versus the resting state network by comparing the  $r$  values for each connection between treated and untreated groups using Mann–Whitney  $U$  tests (lower panel)

Compound	Categorized strength of link to seizures in mammals	CAS No.	Abbreviation	Class	Primary mechanism of Action	Light sheet exposure conditions	
						External conc.	Duration
Bicuculline	A	40709-69-1	BICC	Analeptics	GABA <sub>A</sub> R antagonism	250, 125, 62.5µM	30mins
Pentylenetetrazole	A	54-95-5	PTZ		GABA <sub>A</sub> R antagonism	5, 2.5, 1.25mM	20mins
Picrotoxin	A	124-87-8	PICR		GABA <sub>A</sub> R antagonism	60, 30, 15µM	20mins
Bemegride	A	64-65-3	BEM		GABA <sub>A</sub> R antagonism	1, 0.5, 0.25mM	20mins
Gabazine	A	104104-50-9	GABA		GABA <sub>A</sub> R antagonism	1, 0.5, 0.25mM	20mins
DMCM*	A	1215833-62-7	DMCM		GABA <sub>A</sub> R negative allosteric modulation	1, 0.5, 0.25µM	20mins
Strychnine	A	60-41-3	STRY	Glycine antagonist	GlyR antagonism	200, 100, 50µM	20 mins
Kainic acid	A	58002-62-3	KAIN	Glutamate agonists	KAR activation	0.5, 0.25, 0.125mM	30mins
N-methyl-D-aspartate	A	6384-92-5	NMDA		NMDAR activation	2, 1, 0.5mM	30mins
Domoic acid	B	14277-97-5	DOMO		KAR activation	100, 50, 25µM	1hour
Cis-ACPD**	E	477331-06-9	CisA		NMDAR activation	1, 0.5, 0.25mM	1 hour
(RS)-Tetrazol-5-ylglycine	E	138199-51-6	RST		NMDAR activation	62.5, 31.25, 15.6µM	20mins
4-aminopyridine	A	504-24-5	4AP	K+ channel blockers	Non-selective Kv blockade	500, 250, 125µM	20mins
Tetraethylammonium Cl	C	56-34-8	TEA		Non-selective Kv blockade	1, 0.5, 0.25mM	1 hour
XE991***	D	122955-13-9	XE991		Kv <sub>v</sub> (KCNQ) channel blockade	1, 0.5, 0.25mM	20mins
Pilocarpine	A	54-71-7	PILO	Muscarinic agonists	mAChR agonism (non selective)	5, 2.5, 1.25mM	30mins
Bethanechol	C	590-63-6	BETH		mAChR agonism (non selective)	1, 0.5, 0.25mM	1 hour
Carbachol	C	51-83-2	CARB		mAChR and nAChR agonism	1, 0.5, 0.25mM	1 hour
Oxotremorine	C	17360-35-9	OXO		mAChR and nAChR agonism	1, 0.5, 0.25mM	1 hour
Muscarine	E	2936-25-6	MUSC		mAChR agonism (non selective)	1, 0.5, 0.25mM	1 hour
PF06767832****	E	1859081-58-5	PF67		M1 selective mAChR agonist	500, 250, 125µM	20mins
BW373U86*****	A	155836-50-3	BW373	Opioid analgesics	δ-opioidR agonism	500, 250, 125µM	1 hour
SNC80*****	A	156727-74-1	SNC80		δ-opioidR agonism	100, 50, 25µM	20mins
Fentanyl	C	85951-63-9	FENT		µ-opioidR agonism	125, 62.5, 31.25µM	20mins
Meperidine	C	50-13-5	MEP		µ-opioid R agonism	250, 125, 62.5µM	20mins
Morphine	D	52-26-6	MORP		µ-δ-opioidR activation	1, 0.5, 0.25mM	2 hours
SB205607*****	E	1217628-73-3	SB20		δ-opioidR agonism	500, 250, 125µM	20mins
Donepezil	B	884740-09-4	DONE	ACh esterase inhibitors	Reversible AChE inhibition	125, 62.5, 31.25µM	30mins
Physostigmine	C	57-64-7	PHYS		Reversible AChE inhibition	500, 250, 125µM	20mins
Tacrine	C	1684-40-8	TACR		Reversible AChE inhibition	1, 0.5, 0.25mM	20mins
Galantamine	D	217-780-5	GALA		Reversible AChE inhibition	1, 0.5, 0.25mM	20mins
Neostigmine	D	114-80-7	NEO		Reversible AChE inhibition (no BBB penetration)	1, 0.5, 0.25mM	1 hour
Phenserine	E	101246-66-6	PHEN		Reversible AChE inhibition	125, 62.5, 31.25µM	20mins
Bupropion	B	31677-93-7	BUPR	NDRJ Antidepressant	NA/DA reuptake inhibition	60, 30, 15µM	30 mins
Nomifensine	D	32795-47-4	NOMI		NA/DA reuptake inhibition	100, 50, 25µM	20mins
Maprotiline	B	10347-81-6	MAPR	Tetracyclic Antidepressant	NA reuptake inhibitor (weak 5-HT), mAChR, α <sub>1/2</sub> R/H <sub>1</sub> R antagonism	31.25, 15.6, 7.8µM	20 mins
Amoxapine	B	14028-44-5	AMOX	Tricyclic antidepressants	NA/5-HT reuptake inhibitor, DAR/5-HT/α <sub>1/2</sub> R/H <sub>1</sub> R antagonism	62.5, 31.25, 15.6µM	20mins
Amitriptyline	C	549-18-8	AMIT		NA/5-HT reuptake inhibitor, 5-HT/α <sub>1</sub> R/H <sub>1</sub> R/mAChR antagonism	125, 62.5, 31.25µM	20mins
Clomipramine	C	17321-77-6	CLOM		NA/5-HT reuptake inhibitor, 5-HT/α <sub>1</sub> R/DAR/H <sub>1</sub> R/mAChR antagonism	15.6, 7.8, 3.9µM	20mins
Desipramine	C	58-28-6	DESI		NA/5-HT reuptake inhibitor, α <sub>1</sub> R/H <sub>1</sub> R/mAChR antagonism	125, 62.5, 31.25µM	20mins
Protriptyline	C	1225-55-4	PROT		NA/5-HT reuptake inhibitor, 5-HT <sub>1</sub> R/α <sub>1</sub> R/DAR/H <sub>1</sub> R/mAChR antagonism	250, 125, 62.5µM	20mins
Chlorpromazine	C	69-09-0	CPZ		Phenothiazine antipsychotic	D <sub>1/2/3/4</sub> R/α <sub>1/2</sub> R/H <sub>1</sub> R/mAChR/5-HT <sub>1/2</sub> R antagonism	125, 62.5, 31.25µM
Clozapine	B	5786-21-0	CLOZ	Atypical antipsychotics	D <sub>1/2</sub> R/α <sub>1/2</sub> R/H <sub>1</sub> R/mAChR/5-HT <sub>1/2</sub> R antagonism	100, 50, 25µM	20mins
Olanzapine	C	132539-06-1	OLAN		D <sub>2</sub> R/α <sub>1</sub> R/H <sub>1</sub> R/mAChR/5-HT <sub>1/2</sub> R antagonism	250, 125, 62.5µM	20mins
Risperidone	C	106266-06-2	RISP		D <sub>2</sub> R/α <sub>1/2</sub> R/H <sub>1</sub> R/mAChR/5-HT <sub>1/2</sub> R antagonism	500, 250, 125mM	20mins
Aminophylline	B	317-34-0	AMIN	Methylxanthine derivatives	P1 antagonism and PDE inhibition	2, 1, 0.5mM	30mins
Theophylline	B	58-55-9	THEO		P1 antagonism and PDE inhibition	1, 0.5, 0.25mM	1 hour
Caffeine	D	58-09-2	CAFF		P1 antagonism and PDE inhibition	1, 0.5, 0.25mM	20mins
Theobromine	D	83-67-0	THBR		P1 antagonism and PDE inhibition	1, 0.5, 0.25mM	1 hour
Paraxanthine	D	611-59-6	PARA		P1 antagonism and PDE inhibition	1, 0.5, 0.25mM	1 hour
Cocaine	B	53-21-4	COCA	Illicit drugs	DA/NA/5-HT reuptake inhibitor and Na <sup>+</sup> channel blockade	250, 125, 62.5µM	20mins
Amphetamine	B	51-63-8	AMPH		DA/NA/5-HT reuptake inhibitor	1, 0.5, 0.25mM	20mins
Phencyclidine	D	656-90-1	PCP		NMDAR antagonism	125, 62.5, 31.25µM	20mins
Apomorphine	D	41372-20-7	APOM	Mixed classes, unclear link to seizures	D <sub>1/2</sub> R/5-HT/α <sub>1</sub> R agonism	50, 25, 12.5µM	1hour
Ethanol	D	64-17-5	ETOH		GABA <sub>A</sub> R positive allosteric modulation	1.5, 0.75, 0.375% v/v	20 mins
Rollipram	D	61413-54-5	ROLI		PDE-4 inhibition	150, 75, 37.5µM	24hours
Yohimbine	D	65-19-0	YOHI		α <sub>2</sub> R antagonism	62.5, 31.25, 15.6µM	20mins
4-Aminophenyl sulfone	F	80-08-0	4AMS	Mixed classes, no known link to seizures	Antibiotic (sulfonamide-like)	1, 0.5, 0.25mM	20mins
Cisplatin	F	15663-27-1	CISP		DNA cross linking chemotherapeutic	500, 250, 125µM	2hours
Clonidine	F	4205-91-8	CLOM		α <sub>2</sub> R agonism (in CNS)	1, 0.5, 0.25mM	20mins
Emetine	F	316-42-7	EMET		Alkaloid antiprotozoal	500, 250, 125µM	1hour
Ketamine	F	1867-66-9	KETA		NMDAR antagonism	62.5, 31.25, 15.6µM	20mins
Ketoconazole	F	65277-42-1	KETO		Cytochrome P450 inhibitor	100, 50, 25µM	20mins
Mizolastine	F	108612-45-9	MIZO		H <sub>1</sub> R antagonism	100, 50, 25µM	20mins
Quinine HCl	F	6119-47-7	QUIN		Alkaloid antimalarial	1, 0.5, 0.25mM	20mins

**Table 2.1:** Summary of the test chemicals and experimental exposure conditions used in the current study. Information shown left to right: compound name; strength of the association with seizure induction in mammals (see below); Chemical Abstracts Service (CAS) registry number; abbreviation as used in other figures; pharmacological class; primary mechanism of action; and exposure concentration and times used the Ca<sup>2+</sup> imaging. The strength of the association with seizure induction in mammals based on the scientific literature is classified as follows: A - strong link—tool compounds/precipitants; B - clear association in clinic/nonclinical studies; C - measurable association in clinic and/or some nonclinical evidence; D - limited clinical/non clinical data,



but weak or conflicting and/or seizure-inducing only under specific circumstances (e.g., overdose or withdrawal); E - mechanistic link only, no published confirmatory data; and F - no known link to seizures (seizure negative). Abbreviations: AChE = acetylcholine esterase; DR = dopamine receptor;  $\alpha R$  =  $\alpha$ -adrenoreceptor;

HR = histamine receptor; mAChR = muscarinic acetylcholine receptor; 5-HTR = 5-hydroxytryptamine receptor; GABAR =  $\gamma$ -aminobutyric acid receptor; KAR = kainic acid receptor; NMDAR = glutamatergic *N*-methyl-D-aspartate receptor; GLYR = glycine receptor; Kv = voltage-gated K<sup>+</sup> channel; NA = noradrenaline; DA = dopamine; 5-HT = 5-hydroxytryptamine (serotonin); P1 = adenosine receptor; PDE = phosphodiesterase;  $\mu/\delta$ -opioidR = mu/delta-opioid receptor; LOQ = limit of quantification. \*DMCM (methyl-6,7-dimethoxy-4-ethyl-beta-carboline-3-carboxylate); \*\*cis-ACPD (( $\pm$ )-1-Aminocyclopentane-cis-1,3-dicarboxylic acid); \*\*\*XE991 (10,10-bis(4-Pyridinylmethyl) -9(10*H*)-anthracenone dihydrochloride); \*\*\*\*PF-06767832 (1,5-Anhydro-2,3-dideoxy-3-[[[5-methyl-4-[[4-(4-thiazolyl)phenyl]methyl]-2-pyridinyl]carbonyl]amino]-L-threo-pentitol, *N*-((3*R*,4*S*)-3-hydroxytetrahydro-2*H*-pyran-4-yl)-5-methyl-4-[4-(1,3-thiazol-4-yl)benzyl]-pyridine-2-carboxamide); \*\*\*\*\*SNC80 ((+)-4-[( $\alpha R$ )- $\alpha$ -((2*S*,5*R*)-4-Allyl-2,5-dimethyl-1-piperazinyl)-3-methoxybenzyl]-*N,N*-diethylbenzamide); \*\*\*\*\*SB205607 or TAN-67, ((*R*<sup>\*</sup>,*S*<sup>\*</sup>)-( $\pm$ )-2-methyl-4aa-(3-hydroxyphenyl)-1,2,3,4,4a,5,12,12aa-octahydroquinolino[2,3,3-*g*]isoquinoline dihydrobromide); \*\*\*\*\*BW373U86 4-[( $\alpha R$ <sup>\*</sup>)- $\alpha$ -((2*S*<sup>\*</sup>,5*R*<sup>\*</sup>)-4-Allyl-2,5-dimethyl-1-piperazinyl)-3-hydroxybenzyl]-*N,N*-diethylbenzamide). All test chemicals were obtained from sigma-Aldrich (Gillingham, UK) or Tocris (Bristol, UK)

data; category C - compounds for which there is some evidence supporting a link with (non) clinical seizures; category D - compounds for which there are limited reports of an association or where seizures are induced only under specific exposure scenarios such as during overdose (e.g. morphine) or withdrawal (e.g. ethanol); category E compounds for which there is a clear mechanistic link but for which literature data on seizure induction are absent

(typically pharmacological probes) and category F compounds for which no evidence or mechanistic association with seizure induction was evident (negative controls). The final classification was agreed *a priori* by all study participants based upon the information available following the reviewed literature.

### 2.2.3 Selection of exposure concentration ranges and durations

The concentration ranges and exposure durations used in the functional imaging in 4 dpf larvae were selected using information gained from a separate assessment of compound effects on locomotion in 7 dpf larval, using a previously described standardised assay see (Winter et al., 2008). Bioanalysis of internal (whole body) compound concentrations were carried out in the same 7 dpf animals using liquid chromatography with tandem mass. The results of this work on 7 dpf larvae are summarised in Table 2.1 and the methods used briefly outlined in the Supporting Information. The internal compound concentrations in 7 dpf larvae only provide an estimate of actual internal compound concentrations in the 4 dpf larvae, but collectively, these data helped both to select the initial exposure conditions used for the 4 dpf functional imaging assessment (e.g., high uptake supported a short exposure period and lower concentration range and vice versa), and to interpret the resultant functional imaging data (e.g., where the absence of a biological effect might be explained by poor compound uptake).

### 2.2.4 Drug treatment and light sheet microscopic imaging

We aimed to generate equally sized datasets of  $n = 8$  animals per treatment in our exposures for which the imaging logistics required the treatments to be run over two separate days on two batches of embryos (i.e. from two separate spawnings). Each treatment was equally represented over the 2 days of experimentation and the experimental process undertaken identically. Although treatments were not blinded, each larva was randomly selected and assigned to test compound at one of three concentrations or to a fish culture system water (vehicle) control for the exposure durations detailed in Table 2.1.

Following exposure, each animal was imaged as described below. The order in which animals were exposed and imaged was rotated through all treatments on each day to remove any bias associated with the time of day used for assessment. The need to hold larvae motionless during imaging to avoid movement artefacts, whilst avoiding introducing the widespread confounding effects of using a general anaesthetic, necessitated the use of a neuromuscular blocker. Tubocurarine was selected as a non-depolarizing neuromuscular blocker (nicotinic acetylcholine antagonist) with a stable and long duration of action (Appiah-Ankam and Hunter, 2004) and was applied at a concentration of 4 mM to induce rapid paralysis appropriate for the acute exposure regimen of our study. Although tubocurarine has been associated with histamine release and resultant hypotension clinically, importantly it exhibits no muscarinic receptor (mAChR) antagonist activity and is water soluble. Furthermore, it has been used to paralyse zebrafish in previous functional imaging studies (Favre-Bulle et al., 2018; Miyazawa et al., 2018; Tao et al., 2011; Vanwalleghem et al., 2020). Adding to this, we observed no evidence of the attenuated neuromuscular blockade during acetylcholinesterase (AChE) inhibitor application over the time scale we use for imaging after neuromuscular blocker application. Each larva was transferred to an aqueous mixture of compound and tubocurarine (4 mM) until muscle tone was lost (typically ~1 min), then moved to tubocurarine and test compound in 1.4% low melting point agarose and finally drawn into a clear borosilicate glass capillary plugged with 2% low melting point agarose. No organic solvents were employed to minimise potential confounding effects and vehicle (water) control larvae were treated identically (including the presence of neuromuscular blocker) but without test compound. Larvae were positioned on the light sheet microscope (Figure 2.1a) and dorsal-ventral optical sectioning undertaken in the horizontal plane (10 equidistant Z-slices across 220µm taken in 1.875 s, repeated 200 times). Following imaging, larval health was confirmed through observation of a normal heart rate and blood flow.

In any functional imaging study, there is trade-off between spatial coverage and temporal resolution. Our imaging conditions were optimised to obtain the

fastest cycle time whilst maintaining whole brain volume coverage at an appropriate temporal resolution. Some previous studies have chosen to obtain higher temporal resolutions across single focal plains, however, to fully capture the spatial component of neural network hyperexcitation and answer specific questions about regional importance in seizure generation, we opted for whole brain volume imaging at a mesoscale spatial resolution. The importance of this scale of interrogation in the study of seizures has recently been highlighted by (Wykes et al., 2019) who pointed out that seizure foci do not 'operate in isolation', exhibiting connectivity with 'short and long range projections' and that mesoscale study is required in order to 'record propagation pathways', areas of the brain that are recruited during seizure development and to detect abnormalities between 'functionally connected but distant areas of the brain'. Similarly, (Rosch et al., 2018) acknowledged that epileptic seizures are an emergent property at the level of neuronal populations and mesoscale modelling may provide insights that assessments at the microscale do not. Accordingly, we used anatomically anchored image registration to provide mesoscale segmentation of the whole brain in 3D and which provided the ability to compare equivalent regions across different larvae and treatments using anatomical location as the reference point for comparison. Further to this, in initial studies we undertook in support of this work we identified that a 6-min assessment period was sufficient to capture seizure-like activity after drug treatment, whilst providing datasets of a manageable size (Winter et al., 2017).

#### *2.2.5 Light sheet microscopic imaging settings*

The light sheet microscope was custom built using the Open Access platform for SPIM (Huisken, 2012; Pitrone et al., 2013) as previously detailed in (Winter et al., 2017). The system comprised a 488 nm Argon laser (Melles Griot, Didam, Netherlands) for illumination, a 20×/0.5 NA objective lens (Olympus, Southend-on-Sea, UK) with an intermediary magnification of 1×, followed by a 525/50 nm emission filter and 495 nm bandpass filter (Chroma, Olching, Germany) to collect emitted light and a 5.5-MP Zylas CMOS camera (30 frames per second, 640 × 540 pixels, 4 × 4 binning, 40-ms exposure, Andor,

Belfast, Northern Ireland) to capture images. The camera and rotational axis (Picard Instruments, Albion, USA) were controlled through  $\mu$ Manager and the OpenSPIM plugin (Pitrone et al., 2013). The Point Spread Function of our system was determined by performing Z-stacks of  $50 \times 0.5\mu\text{m}$  fluorescent beads, embedded in 1% low melting point agarose within a glass capillary. Images were acquired at z-intervals of  $1.5\mu\text{m}$  using the same system settings employed during data acquisition (detailed above) and the PSF calculated using the MOSAIC suite point spread function tool ([http://imagej.net/MOSAIC\\_suite](http://imagej.net/MOSAIC_suite)). The spatial resolution of our system was measured using a segment from a multi-grid stage micrometer (Edmund Optics, UK) with  $100\text{-}\mu\text{m}$  divisions. The grid was imaged in the sample chamber using the same optics and medium to determine the pixel length of each  $100\text{-}\mu\text{m}$  division. Each  $100\text{-}\mu\text{m}$  division at  $1 \times 1$  binning was 304 pixels and at  $4 \times 4$  binning was 76 pixels.

#### *2.2.6 Image processing and peak parameter measurements*

Data extraction from resultant images was undertaken automatically using a custom Python image processing pipeline developed at the University of Exeter and as previously detailed in Winter et al. (2017) (available at: <https://gitlab.com/exeter-zebrafish-research/zebrafish-neuroanalyser3d>) (Figure 2.1b). Briefly, each image was initially down-sampled ( $3 \times 3 \times 1$ ) and then 3D-aligned against a labelled reference brain (Randlett et al., 2015) using registration against 14 user-selected key points from a representative 3D image stack. This brain atlas was established for use in 5-7 dpf larvae, so we undertook a full 3D affine transformation (optimised using the Umeyama algorithm) that enabled alignment of our image series to the reference brain and allowed extraction of voxel intensity data from defined anatomical regions of interest selected to encompass only major (larger) brain structures. This brain atlas has been widely used for anatomical registration including for multiple previous functional imaging studies (Migault et al., 2018; Rosch et al., 2018; Vanwalleghem et al., 2020). During processing, images were automatically shift-corrected to account for any sample drift. For this, the shape index function as defined by (Koenderink and van Doorn, 1992) was used to

simultaneously correct for x, y and z- drift using functions from the Scikit-image library (van der Walt et al., 2014). Next, quantitative data were extracted for each region of interest as the mean of incorporated voxels for each time point, to generate a temporal profile of activity for that region. These profiles were baseline subtracted using a sliding minimum filter comprising 50 time-points or the signal length if less than 50 time-points and peaks in activity were subsequently identified and analysed (Figure 2.1c (i)). Fluorescence-intensity profiles then underwent fine-scale smoothing using Gaussian filtering ( $\sigma = 1.5$ ) to remove high-frequency noise and activity peaks spanning 2 or more consecutive imaging cycles were identified by subtracting the baseline and applying a threshold of  $2\sigma$ . From the identified activity peaks in the profiles for each region of interest, time-averaged peak height and Area Under the Curve (AUC—calculated as the sum of the intensity values within each defined peak region) were calculated for each animal (referred to as ‘peak parameters’) as these two metrics were found to be the most useful for defining activity phenotypes (Figure 2.1c (ii)). We have previously described the performance characteristics of our imaging process (Winter et al., 2017). Briefly, the error of the 3D affine registration processes was calculated as  $27.56 \pm 0.43 \mu\text{m}$ , the theoretical point spread function was  $0.751 \mu\text{m}$ , the measured lateral resolution was 0.76 pixels per micrometre and the temporal resolution was 1.875 s per full brain volume.

### *2.2.7 Data analysis - Describing the resting state network*

To describe the resting state network of 4 dpf larvae analysed using this methodology, analysis of the peak parameters across all vehicle (water) control groups was undertaken. This analysis allowed us to describe the relative levels of neural activity in different brain regions under ‘resting’ conditions to establish which regions were comparatively (in)active during imaging. When comparing between regions of interests under such circumstances, it is important to control for potential regional variations in *eIavI3:GCaMP6s* expression and, therefore, data were first normalised by subtracting each voxel's baseline, estimated using a sliding minimum filter

(comprising 50 time-points or the signal length if less than 50 timepoints) and then dividing by this baseline value. Functional connectivity in vehicle control larval brains was also assessed using the method detailed below.

#### *2.2.8 Data analysis - Analysis of region-specific GCamp6s fluorescence across the whole larval brain*

To identify the neural network activity profile induced by each compound and therefore measure the responsiveness of larvae across a range of pharmacological mechanisms of action, univariate analysis of the concentration–response relationships within each regions of interest was undertaken (Figure 2.1c (iii)). For this, Kruskal–Wallis coupled with Dunn's multiple comparisons tests (where an overall difference was detected) were undertaken on the mean fluorescence peak height or AUC value averaged across animals at each concentration, versus the mean of the corresponding water control group (Bonferroni individual  $\alpha = .017$ ). Baseline correction, as used to compare between control animal regions of interests, was not undertaken for within-regions of interest comparison of untreated and treated animal neural activity to ensure due consideration of compound-induced changes in 'baseline' fluorescence. Furthermore, all treatment-related comparisons undertaken were between corresponding regions of interests and consequently, no comparison of fluorescence was undertaken between regions of interests in treated animals, thus avoiding potential bias associated with regional differences in GCaMP expression in these cases.

#### *2.2.9 Data analysis - Multivariate exploration of larval brain functional connectivity*

Functional connectivity in the context of neuroimaging pertains to the relationship between the neuronal activity patterns of anatomically separated brain regions, which in turn reflects the level of communication between these regions (van den Heuvel and Hulshoff Pol, 2010). Practically, these relationships can be represented by measures of correlation that reveal

information on mesoscale or macroscale networks responding to stimulation, in this case mediated by the action of seizurogenic compounds. Here, multivariate analysis of functional connectivity phenotypes was hypothesised to reveal information about the activation or suppression of specific neural circuits following compound treatment, by reflecting the spatial distribution of targets across the brain.

First, a connectivity matrix was generated for each animal by calculating the Pearson's correlation coefficient ( $r$ ) between the time series of all possible pairs of regions of interests (Figure 2.1d (i)). Initial assessment of concentration response curves showed that in most cases the maximal response of larvae (versus control data) to compound treatment was apparent at the highest or second highest treatment concentrations. Consequently, it was decided to use these two treatment levels in the exploratory multivariate analysis. The lowest treatment concentration data were not included as in most cases activity levels were indistinguishable from controls and as such would likely reduce the ability to distinguish the phenotypic effect of drug treatment. The data for DMCM, domoic acid, Cis-ACPD, TEA, bethanechol, theobromine and paraxanthine were also excluded from these analyses as we found no evidence of compound uptake (see Section 3).

Multivariate analysis required a consistent number of regions of interests across all experiments and therefore, regions of interests that were inconsistently registered (i.e. were absent in >2% of larvae analysed) during image processing as they occurred at the limits of Z-plane penetration were excluded prior to analysis, leaving 39 analysed regions of interests per animal. All values from each connectivity matrix were then reshaped into a connectivity vector (generating 741 regions of interest connections per larva) and the mean of the vectors for all animals calculated to provide one vector per compound (Figure 2.1d (ii)). To allow visualisation of similarities or differences between resultant profiles and to generate groups on which post hoc statistical analysis could be undertaken, a simple unsupervised agglomerative hierarchical cluster analysis ('unweighted pair group method with arithmetic mean' or UPGMA) was undertaken. This was considered the best approach where no prior information



on the relative importance of any particular data feature was known. For this, the Euclidean distances between vectors of all of the compounds were calculated to provide a value for similarity between each compound within the multivariate feature space, and UPGMA cluster analysis undertaken. The same analysis was also undertaken on all control animal data to provide confidence that the observed clustering of 'related' compounds was not driven by potential differences in the baseline levels of GCaMP fluorescence between experimental runs (Figure S2).

#### *2.2.10 Data analysis - Post hoc assessment of phenotype-defining data features*

Next, to assess whether the groupings identified by cluster analysis were based upon phenotypic similarities amongst grouped compounds, and to test the hypothesis that certain data features differ between primary pharmacological mechanisms of action, post hoc statistical comparisons between compound-treated larvae and the resting state network were undertaken (Figure 2.1d (ii)). For this, Mann–Whitney  $U$  tests with a highly conservative Bonferroni correction ( $\alpha = .000055$ ) (due to the high number of comparisons undertaken on each matrix) were used to identify statistically significant differences between compound-treated and control functional connectivity phenotypes, by comparing the  $r$  values obtained for all pairs of regions of interests. A difference between these two values would suggest an increase or decrease in the strength of that connection between the two groups and help to determine whether any brain regions or functional connections were particularly prevalent within a specific grouping and provide more confidence in the significance of groupings identified from the cluster analyses.

#### *2.2.11 Data analysis - Overall functional connectivity as an indicator of altered network synchronicity*

Traditionally, a key defining feature of seizures is the occurrence of hypersynchronicity between disparate brain regions. It has, however, been

acknowledged that the interictal–ictal cycle is likely to incorporate aspects of both hypersynchronicity and hyposynchronicity depending on the point in the cycle at which assessment is made and the spatiotemporal resolution of the detection methods used (Jiruska et al., 2013). With this in mind and given there is currently no universally accepted classification of epileptiform brain activity within Ca<sup>2+</sup> imaging datasets (Burrows et al., 2020), here we compared compound-treated and resting state network average functional connectivity (both average *r* values and numbers of connections with an *r* value > 0.7) using Mann–Whitney *U* tests (*p* < .05) (Figure 2.1d (iii)). These data were taken as an indicator of the degree to which hypothesizedon between regions was occurring compared with that observed in the resting state network. It was hypothesized that an increase in the number of functional connections and/or the strength of those connections may allow differentiation between non-seizurogenic and pro-seizurogenic compounds acting via a range of primary initiating mechanisms. Analysis of average functional connectivity was undertaken across all brain regions combined and also separately on the average of those connections that involve only regions within the telencephalon, diencephalon, mesencephalon, or the rhombencephalon, in order to assess changes in macroscale functional connectivity.

### *2.2.12 Materials*

All test chemicals are detailed in full, along with their Chemical Abstracts Services (CAS) registry numbers, in Table 2.1 and its accompanying legend. All test chemicals and reagents were obtained from Sigma-Aldrich (Gillingham, UK) or Tocris (Bristol, UK).

### *2.2.13 Nomenclature of targets and ligands*

Key protein targets and ligands in this article are hyperlinked to corresponding entries in the IUPHAR/BPS Guide to PHARMACOLOGY <http://www.guidetopharmacology.org> and are permanently archived in the Concise Guide to PHARMACOLOGY 2019/20 (Alexander et al., 2019a, 2019b, 2019c, 2019d).

## 2.3 Results

### 2.3.1 *The resting state network involves activation of hindbrain autonomic, sensory and motor centres*

Analysis across all vehicle (water) control larvae was undertaken to describe the resting state network of animals analysed using our experimental setup. Analysis of the peak parameter data revealed low-magnitude, high-frequency neural activity, most frequently in hindbrain regions functionally associated with homeostatic control, sensory processing, arousal and motor activity (Figure 2.2a). Analysis of functional connectivity (Figure 2.2b) further supported this with the strongest functional connections and most connected regions also predominantly associated with these physiological processes.

### 2.3.2 *The 4 dpf larval zebrafish is responsive to a range of molecular mechanisms known to induce neural network hyperexcitation in mammals*

Peak parameter analysis revealed that many compound-treated larvae exhibited increases (net regional activation) or in some cases decreases (net regional inhibition) in GCaMP6s fluorescence in specific anatomical regions, when compared with the corresponding vehicle (water) controls (Figure 2.3). In the majority of cases, concentration–response relationships were also evident supporting compound-induced modification of neural activity (Figure S3). Exposure to GABA<sub>A</sub> receptor, glycine receptor, AChE and NA/5-HT/DA modulating compounds generally resulted in a higher number of changes in activity within specific brain regions when compared with other pharmacological classes. Also of note, neural activity in hindbrain regions and in particular the cerebellum and its sub regions, the corpus cerebelli and valvula cerebelli, were more frequently altered after exposure to compounds associated with seizure induction (Figure S4). In contrast, multiple potentially seizurogenic compounds showed no alteration of fluorescence intensity versus the water controls in any brain region. Of these DMCM, domoic acid, Cis-ACPD, TEA, bethanechol, theobromine and paraxanthine showed no observable effects in the separate

maximum tolerated concentration or locomotor assessment of 7 dpf animals and no differences in GCaMP6s fluorescence peak height or AUC. There was also no evidence of uptake for these compounds (<2% of the external concentration or not measurable) in 7 dpf animals suggesting a lack of internal exposure might explain the inactivity observed in 4 dpf larvae here (compound name highlighted in light grey in Table 2.1). Low internal exposure, however, was less likely to explain an absence of altered peak height or AUC after exposure to 4-AP, PF-06767832, SNC80, meperidine, physostigmine, maprotiline, cocaine and theophylline. Exposure to clonidine and quinine, two compounds not normally associated with CNS excitation in mammals, conversely resulted in significantly elevated GCaMP-fluorescence in certain brain regions, especially in the case of clonidine

When the number of brain regions exhibiting an increase or decrease in peak height or AUC were assessed (AUC data in Figure S5), strongly seizurogenic compounds generally showed more regions with elevated activity and fewer with reduced activity compared with the non-seizurogenic compounds. Notable exceptions were clonidine and quinine, as mentioned, and the 'positive' compounds fentanyl, carbachol and amitriptyline, which showed reductions in activity across multiple brain regions. Weaker seizurogenics and those categorised as showing seizure liability only under specific circumstances (category D in Table 2.1) tended to locate away from the two extremes showing fewer significant changes in brain activity per se.

### *2.3.3 Similarities in functional connectivity phenotypes of larvae exposed to monoaminergics and cholinergics*

The functional connectomes resulting from exposure to each compound are shown in Figure S6 with an overview of published data on target distribution summarised in the Supporting Information. In addition, functional connections showing a difference compared with the resting state network are shown in Figure S7. Cluster analysis revealed multiple groupings in which similar pharmacologies co-located (Figure 2.4), most notably containing close groupings of monoaminergics (groups 3 and 8 in Figure 2.4) and cholinergics

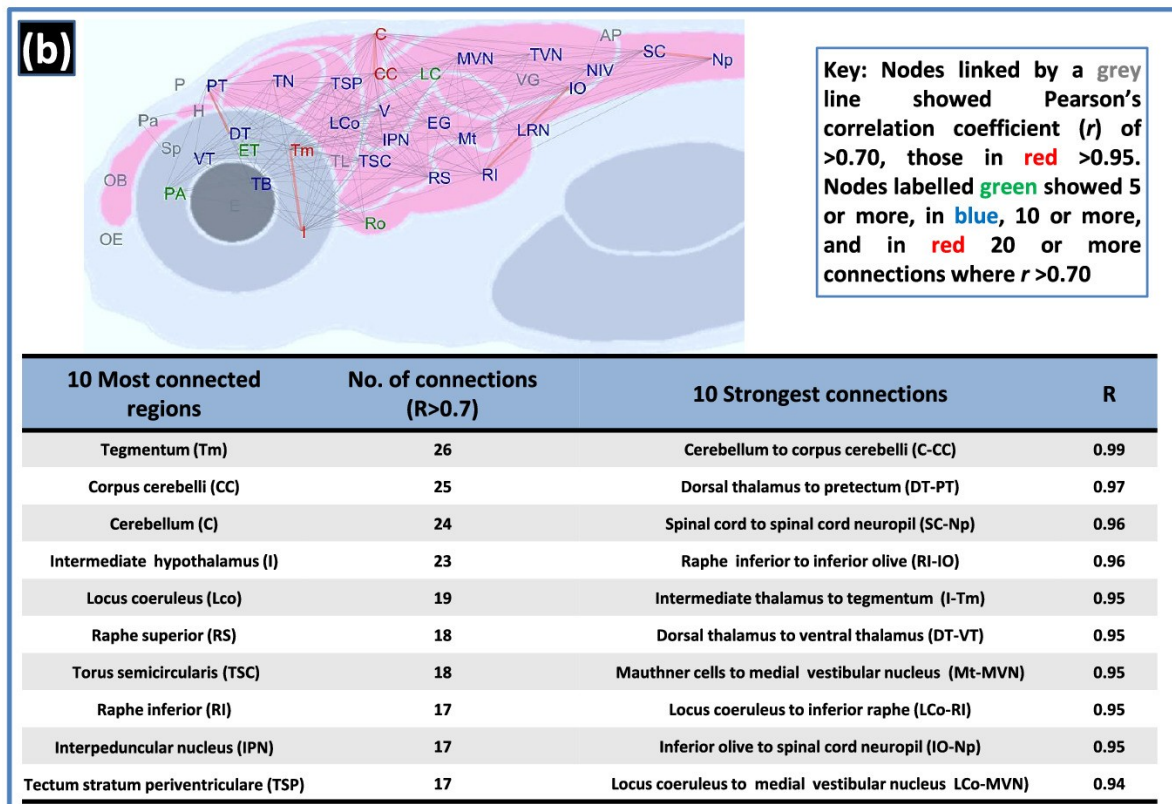
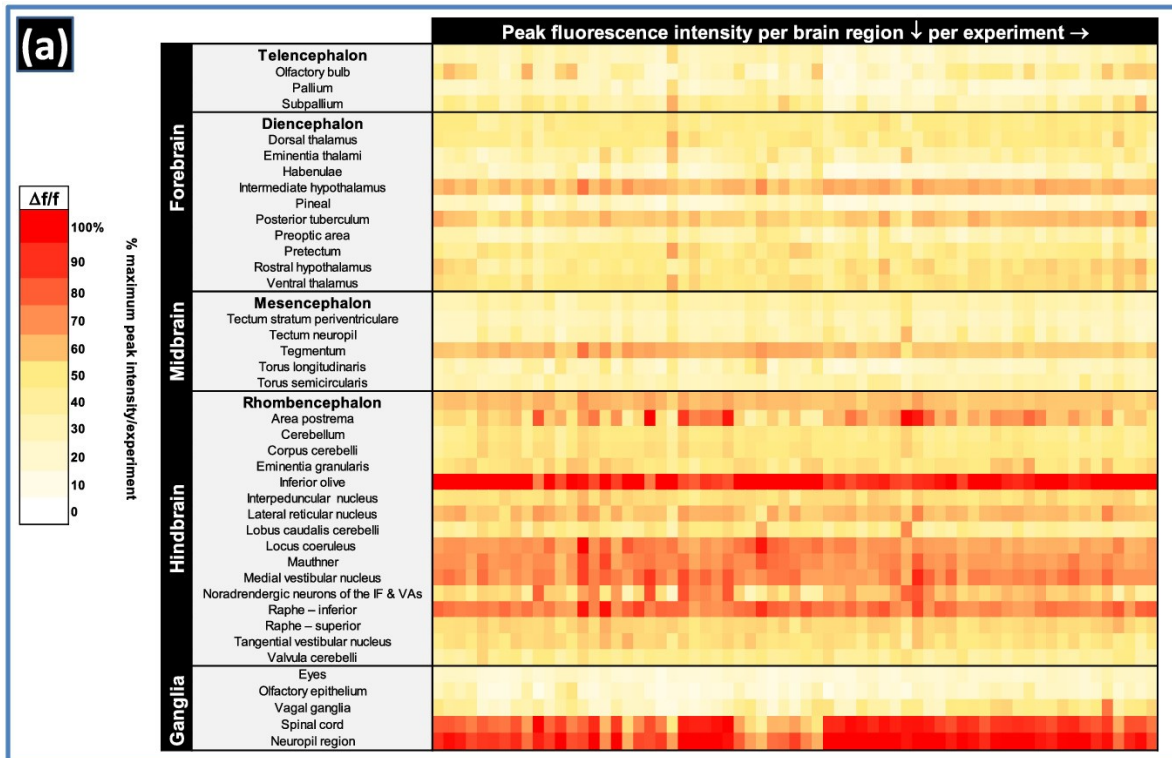


**Figure 2.2:** Summary of peak fluorescence intensity and functional connectivity data from vehicle (water) control larvae tested across 65 experimental datasets. Panel (a) shows the peak fluorescence intensity data per brain region of interest

(ROI) as the average baseline-corrected fluorescence intensity ( $\Delta f/f = (f_1 - f_0)/f_0 * 100$ , where  $f_1$  = peak fluorescence intensity and  $f_0$  = baseline fluorescence intensity within each ROI) of larvae within each control group (per column), presented as the % of the maximum peak intensity shown within that experimental dataset ( $n = 7-9$  larvae per group). The most active brain region in each dataset is represented by 100%, with decreasing red/orange colour intensity representing ROIs with lower levels of comparative activity. Note the high consistency across experiments in brain regions exhibiting elevated basal activity, especially those that showed a mean peak intensity of >33% higher basal activity than the overall mean across all regions: intermediate hypothalamus, area postrema, inferior olive, locus coeruleus, Mauthner cells, medial vestibular nucleus, inferior raphe, spinal cord and spinal cord neuropil. Panel (b) shows the resting state functional connectome of control larvae presented as the average across 65 experimental datasets along with a table summarising the 10 most connected brain regions and the 10 strongest functional connections ( $n = 516$  larvae). Abbreviated brain regions are as follows: area postrema (AP); cerebellum (C); corpus cerebelli (CC); dorsal thalamus (DT); eyes (E); eminentia granularis (EG); eminentia thalami (ET); habenulae (H); intermediate hypothalamus (I); inferior olive (IO); interpeduncular nucleus (IPN); lobus caudalis cerebelli (LC); locus coeruleus (Lco); lateral reticular nucleus (LRN); Mauthner (Mt); medial vestibular nucleus (MVN); noradrenergic neurons of the interfascicular and vagal areas (NIV); spinal cord neuropil (Np); olfactory bulb (OB); olfactory epithelium (OE); pineal (P); preoptic area (PA); pallium (pa); pretectum (PT); raphe inferior (RI); rostral hypothalamus (Ro); raphe superior (RS); spinal cord (SC); subpallium (Sp); posterior tuberculum (TB); torus longitudinalis (TL); tegmentum (tm); tectum neurophil (TN); torus semicircularis (TSC); tectum stratum periventriculare (TSP); tangential vestibular nucleus (TVN); Valvula cerebelli (V); vagal ganglia (VG); ventral thalamus (VT). Note: Positions of regions approximate to allow spacing of nodes and visualisation of connections.

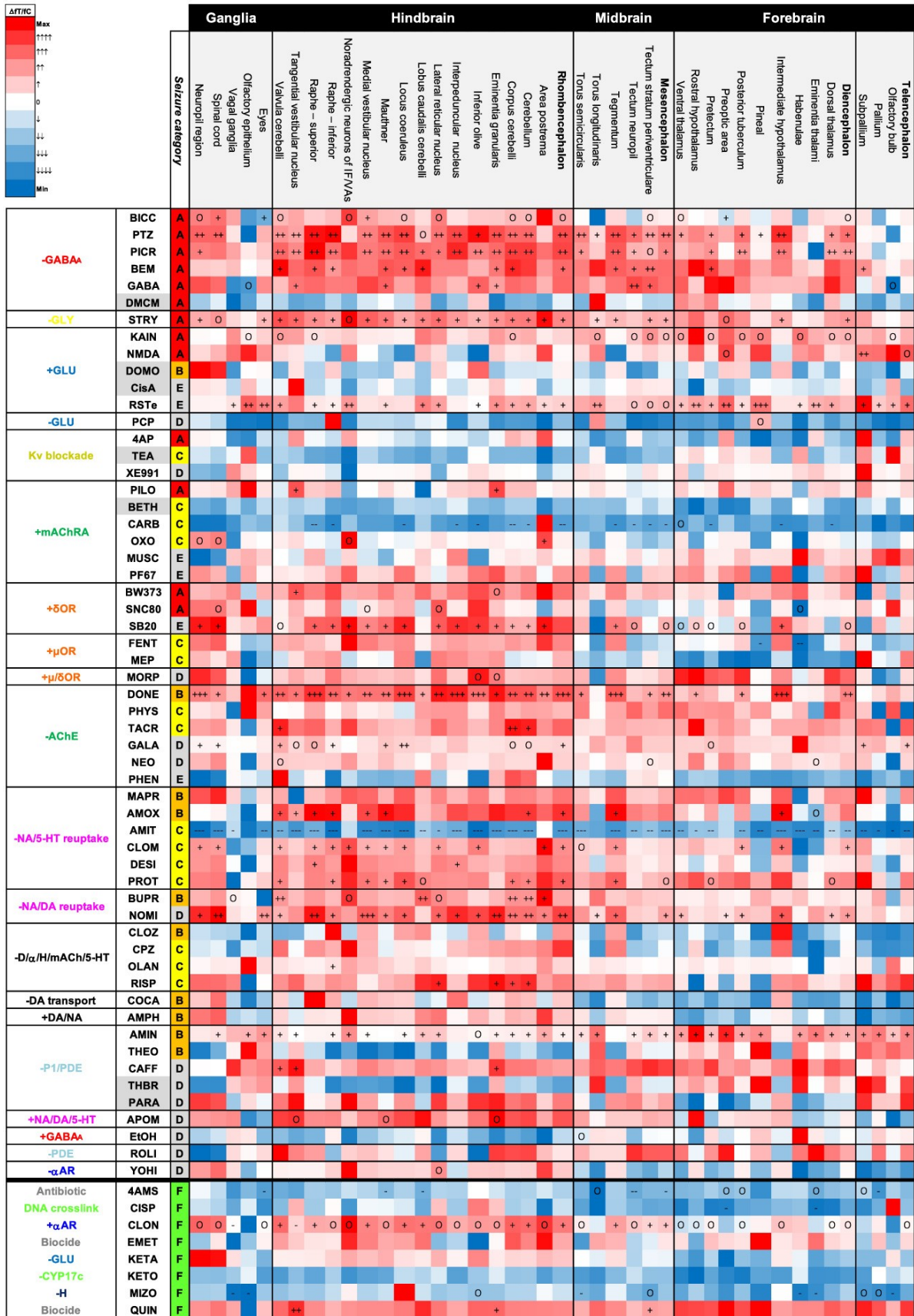




**Figure 2.3:** Summary of peak GCaMP6s fluorescence intensity data measured in brain regions of larvae exposed to a range of neuroactive test compounds. Column 1 (left) shows the primary pharmacological mechanism of action; column 2, the abbreviated compound name; column 3, the strength of association with seizure induction in mammals according to the categories in Table 2.1. Data (column 4 onwards) are expressed as % increase over the same regions of interest (ROI) from the corresponding water control group ( $\Delta fT/fC = (f_1 - f_0)/f_0 * 100$ , where  $f_1$  = treated group and  $f_0$  = control group, mean fluorescence peak height) (n = 6–10 larvae per group). Colour coding signifies the magnitude of effect with increasing red colour intensity signifying an increase, white no change and blue a decrease compared to the control. Within each box, statistically significant differences between compound-treated and control groups are shown (p < .017): + signifying a significant increase at one concentration, ++ at two and +++ at three. -, -- and --- signifies a significant decrease for the same categories. O signifies an overall difference only, following Kruskal–Wallis analysis. Abbreviations are as follows: GABA =  $\gamma$ -aminobutyric acid; GLU = glutamate; ACh = acetylcholine; P1/PDE = adenosine/ phosphodiesterase; NA/DA/5-HT = noradrenaline/dopamine/5-hydroxytryptamine (serotonin); Kv = potassium channels; OR = opioid receptor;  $\alpha$ R =  $\alpha$ -adrenoreceptor; H = histamine; CYP = cytochrome P450).

(both mAChR agonists and AChE inhibitors, groups 4 and 5). The majority of drugs that inhibit dopamine (DAT) norepinephrine (NET) and 5-HT (serotonin; SERT) transporters located in group3, along with phencyclidine and two  $\mu$  receptor agonists (fentanyl and meperidine). In contrast with all other antidepressants, amitriptyline exhibited a reduced activity across almost all brain regions versus the control state (Figure 2.3), despite widespread modulation of regional functional interconnectivity (Figures S6 and S7, panel 33). The grouping of several muscarinic agonists and AChE inhibitors together also indicated a common phenotype amongst some cholinergics, although other class members located elsewhere (e.g. PF-06767832 and Donepezil, Figures S6 and S7, panels 16 and 23, respectively).



Notably, the GABA<sub>A</sub> receptor modulators (Figure S6, Figure S7, panels 1–5) failed to show common functional connectivity phenotypes despite showing very high neuroactivity when other metrics were assessed. Similarly, neither NMDA nor (*RS*)-(tetrazol-5-yl)glycine exhibited any particularly strong functional connections (Figure S6, panels 8 and 9) despite being highly active, perhaps due to the absence of signal oscillation resulting in a flat waveform (see Video S1).

#### 2.3.4 *Alterations in brain region functional connectivity after exposure to cholinergic and monoaminergic compounds*

Figure 2.4b shows the number of functional connections for each brain region that differed after compound treatment, compared with the same connection in the resting state network. Furthermore, the blue and red colours, respectively, indicate whether the majority of those connections exhibited an increase or decrease in the *r* value compared with the resting state network and thus whether these connections were strengthened or weakened by compound treatment. The cholinergics generally showed a reduction in the strength of connectivity across most brain regions, with the most commonly connected regions being the tectum stratum periventriculare, the locus coeruleus, medial vestibular nucleus and the inferior raphé. Donepezil, in stark contrast showed a widespread and large increase in functional connectivity across virtually all brain regions, whilst muscarine and PF-06767832 showed no effect. The main grouping of monoaminergic drugs (group 3) generally exhibited increased *r* values compared with the resting state network suggesting an increase in the strength of functional connections after compound treatment. Amongst these, the most consistently connected regions were in the hindbrain, except for the tegmentum and the intermediate hypothalamus which were also prominently connected within the close pairing of amoxipine and nomifensine (group 8). Amitriptyline was unusual amongst the monoaminergic reuptake inhibitors in that there was widespread reduction in functional connections particularly from posterior hind brain regions, although many of the most interconnected regions were in common with other mood enhancing drugs.

### *2.3.5 Differences in patterns of brain functional connectivity between most non-seizurogenic and pro-seizurogenic compounds*

Many of the more active seizurogenic compounds exhibited an increase in the average number of connections and/or in the average  $r$  value per connection compared with the resting state network (Figure 2.5), suggesting a tendency towards excitatory synchronization between brain regions. Moreover, the weaker acting pro-seizurogenic and 7/8 non-seizurogenic compounds showed no altered network activity with respect to either metric used. Assessment of macroscale functional connectivity (Figure S8) also suggested that seizurogenic compounds were more likely to exhibit changes in mesencephalic and, to a lesser degree, diencephalic, functional connectivity compared with nonseizure-associated compounds. Interestingly, however, the well-known seizurogenic compounds pilocarpine and bicuculline showed reductions in the average number and strength of functional connections.

## **2.4 Discussion**

Analysis of the resting state network suggested stimulation from the imaging environment, with elevated activity apparent in regions involved in motor coordination and control (Heap et al., 2013), sensory processing (Yokogawa et al., 2012) and physiological homeostasis. Collectively, this mirrors other studies reporting activation of sensory-motor networks in conscious, immobilised larval zebrafish following external stimulation and subsequent functional imaging (Ahrens et al., 2012; Migault et al., 2018).

Analysis of GCaMP-indicated brain activity suggested that 4 dpf zebrafish larvae are responsive to a wide range of pharmacologies associated with the induction of neural network hyperexcitation in mammals. The mechanistic classes that showed the most consistent induction of neural activity were the NMDA receptors and GABA<sub>A</sub> receptor agonists, glycine receptor agonist, AChE inhibitors and NA/5-HT/DA reuptake inhibitors. Although not a definitive measure of brain exposure in 4 dpf larvae, the data for whole body compound uptake in 7 dpf larvae provided an indication of where low compound uptake

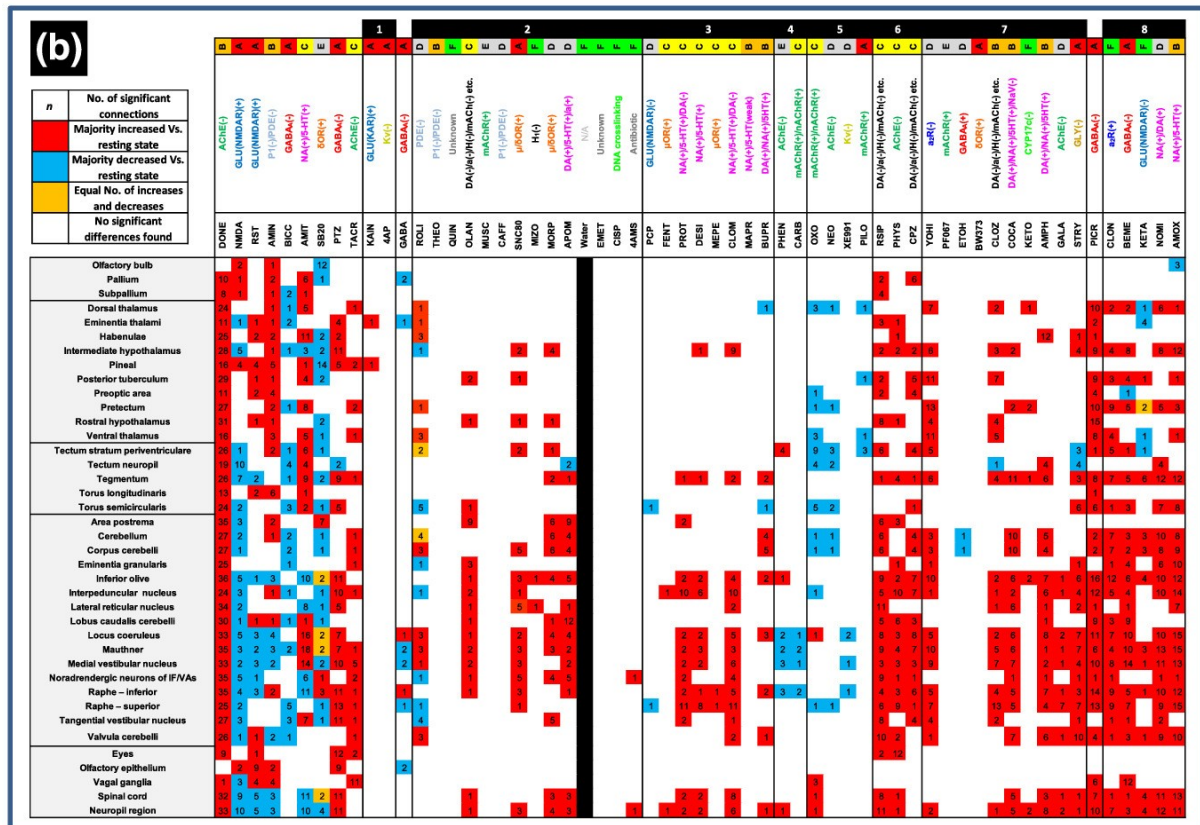
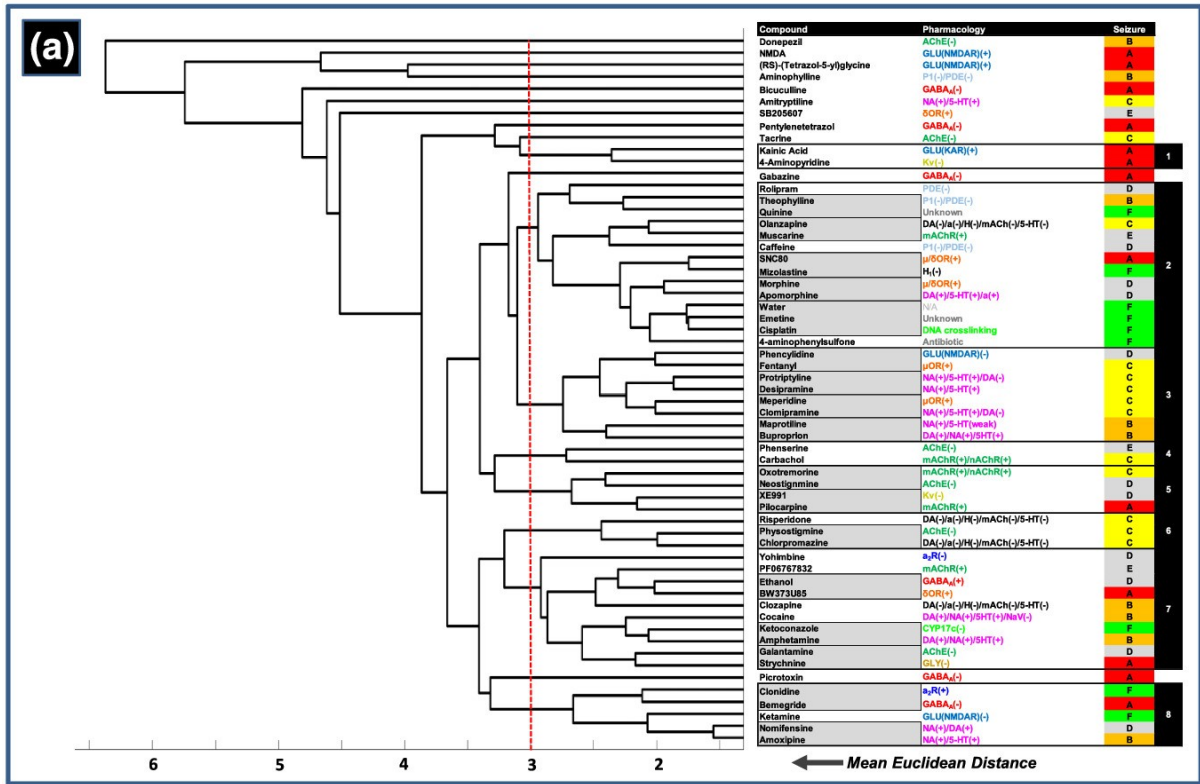


**Figure 2.4:** Results of the hierarchical cluster and post-hoc analysis of the functional connectivity data. Panel (a) shows the dendrogram resulting from the cluster analysis on the Euclidean distances between mean  $r$  values for each of the compounds assessed. Identified groupings showing a mean Euclidean distance of no more than 3 (represented by the red dotted line in the dendrogram) are shown in the right hand table denoted by borders, along with the corresponding primary pharmacological mechanism of action and seizure liability category (as defined in Table 2.1). Grey boxes represent the closest sub groupings. Numbers in the right hand column are references for each defined grouping that occurs in the corresponding dendrogram. Note in particular, the grouping of specific compounds that share a primary mechanism of action (e.g., especially groups 3, 4 and 5). Panel (b) shows the results of the post hoc assessment of changes in functional connectivity of each brain region in compound-treated animals, versus the same region in the resting state network. Abbreviated compound names, along with the primary pharmacological mechanism of action, seizure liability category and dendrogram group number are shown along the top of the table, with each registered brain region shown down the left-hand side of the table. Each cell shows the number of connections to that region for which the mean  $r$  value had significantly changed versus the equivalent connection in the resting state network. Those boxes coloured red showed a majority of increased  $r$  values, blue a majority of decreases and orange an equal number of increases and decreases (see Figures S6 and S7 for all compound connectomes). These data reveal the brain regions in which functional connectivity was most significantly changed after compound treatment. Comparisons were undertaken using Mann–Whitney  $U$  tests with a Bonferroni correction applied (significance at  $p < .00006$ ). A blank cell signifies there was no change in functional connectivity with any other region when compared to the resting state network.  $n = 12$ – $19$  larvae per drug exposed group and  $n = 516$  for the resting state network.

may be the reason for a relative lack of biological responsiveness (e.g. in the case of DMCM, domoic acid, Cis-ACPD, TEA, bethanechol, theobromine and

paraxanthine). This highlights the importance of having some information on relative compound penetration for the interpretation of zebrafish chemical screens and for identifying false negatives that may occur as the consequence of low compound uptake (Berghmans et al., 2008; Cassar et al., 2020). Another important observation is the frequency with which the cerebellum and related regions exhibited elevated neural activity after treatment with seizurogenic compounds. These changes in cerebellar subregions are likely reflective of activity in the region as a whole as full differentiation of cerebellar cellular layers is not thought to be complete until around 6dpf (Volkman et al., 2008). Nevertheless, the frequent activation of these regions after exposure to seizurogenic compounds supports a role for cerebellar circuitry in neural network hyperexcitation. Previous work in mammals has suggested the cerebellum may play an important role in seizures and epilepsy (Rijkers et al., 2015), and this structure is a recognised target for deep brain stimulation to treat refractory epilepsy (Fisher, 2013). Furthermore, activation of the cerebellum has been reported in previous studies of PTZ-induced seizures in zebrafish (Baraban et al., 2005) and of the five large brain regions examined by Diaz Verdugo et al. (2019), the optic tectum and cerebellum appeared influential in the progression from preictal to ictal states. Liu and Baraban (2019) also observed propagation of PTZ-induced seizures from the pallium, via the cerebellum, to the hind brain perhaps further suggesting that the cerebellum, along with other regions (Diaz Verdugo et al., 2019), may constitute a key facilitator for the transition from focal to generalised hypersynchronous excitation.

The absence of any changes in brain activity after exposure to several other seizurogenic compounds that showed evidence of uptake suggests that pharmacological insensitivity could be a factor. Within-class individual compound-insensitivity could be due to subtle interspecies differences in receptor subtype homology, differences in the level of local tissue distribution, or temporal methodological insensitivity. For example, the larval zebrafish  $\delta$  receptor has previously been shown to have a low affinity for SNC80 (Sanchez-Simon et al., 2012), PF6767832 is selective for the  $M_1$  receptor alone and larval

zebrafish have previously been shown to be insensitive to cocaine perhaps due to differential tissue partitioning resulting in reduced central stimulatory activity (Kirla et al., 2016). 4-AP, a well-known seizurogenic compound, has previously been shown to induce generalised CNS hyperexcitation, but without consistent induction of seizures (Liu and Baraban, 2019). Moreover, Liu and Baraban (2019) reported that fast spiking was detected using electrophysiological, but not  $\text{Ca}^{2+}$  imaging approaches and that 4-AP exposure results in dispersed small activated neuronal clusters. This perhaps suggests that the mesoscale segmentation and temporal resolution of our system is not sufficient for the consistent capture of fast ictal events induced by 4-AP and certain other compounds; therefore, faster, higher resolution systems may be needed for full neuropharmacological functional imaging coverage. In contrast, exposure to the centrally acting  $\alpha_2$ -adrenoceptor agonist clonidine resulted in a surprisingly high degree of CNS activation. Analysis of 7 dpf larval locomotor activity, however, revealed a biphasic response comparable to that following  $\text{Ca}^{2+}$  imaging and such a dose–response relationship has been reported previously in relation to anxiolysis versus angiogenesis in rats (Soderpalm and Engel, 1988). Furthermore, although clonidine is a putative anticonvulsant, there are very limited data suggesting seizure induction under specific circumstances (Feron et al., 2008). Quinine exposure also resulted in elevated CNS activity in a small number of brain regions perhaps due to its known blockade of several  $\text{K}^+$  channels (Zou et al., 2018). The most strongly activated region was the medial vestibular nucleus, which is of particular interest given the known potent inhibitory effect of quinine on mechanosensory hair cells of the lateral line (Thomas et al., 2013) and may point to compensatory activation linked to vestibular inhibition in these animals.

Most of the D-classified compounds showed relatively low levels of CNS activation or suppression with the exception of nomifensine, galantamine and caffeine. Nomifensine is a NA/DA reuptake inhibitor which has been linked with seizures in the clinic (Guy Edwards and Glen-Bott, 1987) and is known to increase locomotion in mice (Kitanaka et al., 2012) supporting the potential for

neural-excitation. Similarly, caffeine predominantly exerts its CNS stimulatory effects through adenosine receptor antagonism and has a well-established association with seizures but only at high dose levels (van Koert et al., 2018).

Amitriptyline and carbachol rather unexpectedly exhibited decreases in activity across multiple brain regions. Of these, amitriptyline also showed an inhibitory effect on larval locomotion and very high compound uptake. A sedative-like effect has previously been seen in adult zebrafish exposed to amitriptyline (Demin et al., 2017) and its known sedative effects in mammals are likely driven by activity at the histamine H<sub>1</sub> receptor (Lawson, 2017). Similarly, carbachol is also known to be a sedative in rats, an effect likely driven by action on the M<sub>2</sub> receptors of the brainstem (Ma et al., 2001).

To date, functional connectivity analysis of zebrafish neural activity has been limited to few studies. Rosch et al. (2018) for example used dynamic causal modelling to reveal the optic tectum may be central in driving network wide synchronisation and Diaz Verdugo et al., (2019) used pairwise correlation analysis (as used here) to show that glia may play an important role in the transition to a seizure. Our assessment of functional connectivity served two purposes: first, we hypothesised that functional connectivity phenotypes would reflect mechanism-specific circuit activation or inhibition in 4 dpf larvae and thus reveal differences between mechanisms of action, and second, that changes in overall functional connectivity would support a trend for the mesoscale and macroscale hypersynchronisation characteristic of seizure induction after activation via a range of pharmacological mechanisms of action. Our functional connectivity data revealed that larvae exposed to certain cholinergics, and monoaminergic reuptake inhibitors showed common features within their phenotypes. Notably, both muscarinic agonists and AChE inhibitors grouped together suggesting a common cholinergic phenotype. The most prominent regions showing altered connectivity after exposure to cholinergics were the tectum stratum periventriculare, locus coeruleus, medial vestibular nucleus and the inferior raphe. The development of the cholinergic system in the zebrafish CNS was described by (Arenzana et al., 2005), who reported that spatiotemporal development from 2dpf to 5dpf followed a caudorostral gradient. Our data also



Compound	Pharmacology	Seizure group	Total no. of connections		Average r-values	
			% size difference Vs Water	p Vs water	% size difference Vs Water	p Vs water
Donepezil	AChE(-)	B	74.02	0.0000	37.06	0.0000
Physostigmine	AChE(-)	C	36.54	0.0000	17.77	0.0002
Risperidone	DA(-)/a(-)/H(-)/mACh(-) etc.	C	35.33	0.0003	14.83	0.0047
RST	GLU(NMDAR)(+)	A	30.64	0.1299	5.74	0.2413
Picrotoxin	GABA <sub>A</sub> (-)	A	29.50	0.0009	13.02	0.0082
Chlorpromazine	DA(-)/a(-)/H(-)/mACh(-) etc.	C	28.62	0.0026	16.80	0.0023
Tacrine	AChE(-)	C	27.04	0.0029	16.23	0.0006
Aminophylline	P1(-)/PDE(-)	B	25.07	0.1051	8.59	0.4148
Nomifensine	NA(+)/DA(+)	D	24.67	0.0054	7.07	0.1986
Bemegride	GABA <sub>A</sub> (-)	A	23.91	0.0042	10.42	0.0207
Clonidine	a <sub>2</sub> R(+)	F	23.51	0.0035	9.17	0.0375
PTZ	GABA <sub>A</sub> (-)	A	23.49	0.0029	15.26	0.0008
Amphetamine	DA(+)/NA(+)/5HT(+)	B	20.85	0.0106	11.22	0.0170
Strychnine	GLY(-)	A	20.18	0.0310	10.53	0.0284
Amoxipine	NA(+)/5-HT(+)	B	19.83	0.0024	7.63	0.0371
Yohimbine	a <sub>2</sub> R(-)	D	19.61	0.0029	10.05	0.0090
Kainic Acid	GLU(KAR)(+)	A	18.54	0.0577	11.17	0.0275
Galantamine	AChE(-)	D	17.86	0.0389	10.03	0.0415
Clozapine	DA(-)/a(-)/H(-)/mACh(-) etc.	B	16.71	0.0279	6.81	0.1682
Cocaine	DA(+)/NA(+)/5HT(+)/NaV(-)	B	15.38	0.0687	5.70	0.3269
4-AMS	Antibiotic	F	14.53	0.2205	6.50	0.3126
BW373U85	δOR(+)	A	14.41	0.1455	5.35	0.2925
Ketoconazole	CYP17c(-)	F	12.93	0.0638	7.81	0.0720
Olanzapine	DA(-)/a(-)/H(-)/mACh(-) etc.	C	12.86	0.0517	6.28	0.0990
4-AP	Kv(-)	A	11.35	0.2423	6.84	0.1884
Ketamine	GLU(NMDAR)(-)	F	9.48	0.1335	1.97	0.6244
Protriptyline	NA(+)/5-HT(+)/DA(-)	C	9.02	0.2985	4.10	0.4348
Amityriptiline	NA(+)/5-HT(+)	C	7.79	0.4265	4.54	0.3529
Morphine	μ/δOR(+)	D	7.77	0.1450	2.90	0.4160
Clomipramine	NA(+)/5-HT(+)/DA(-)	C	7.51	0.1977	0.54	0.8513
Apomorphine	DA(+)/5-HT(+)/a(+)	D	7.04	0.2573	3.98	0.3882
Desipramine	NA(+)/5-HT(+)	C	6.15	0.5544	0.58	0.8358
Quinine	Unknown	F	6.13	0.6697	1.48	0.8823
Emetine	Unknown	F	5.82	0.2098	0.99	0.5683
Rolipram	PDE(-)	D	4.97	0.6989	0.19	0.7677
Bupropion	DA(+)/NA(+)/5HT(+)	B	4.41	0.4925	-0.62	0.9490
Caffeine	P1(-)/PDE(-)	D	4.39	0.6418	1.90	0.6702
Muscarine	mAChR(+)	E	4.22	0.9369	1.92	0.7997
SNC80	μ/δOR(+)	A	3.50	0.4928	0.67	0.8747
SB205607	δOR(+)	E	2.26	0.7641	-8.40	0.0519
Ethanol	GABA <sub>A</sub> (+)	D	1.86	0.7524	1.20	0.8825
Mizolastine	H <sub>1</sub> (-)	F	1.86	0.6593	-1.31	0.9073
Meperidine	μOR(+)	C	1.09	0.9401	-0.64	0.8552
Maprotiline	NA(+)/5-HT(weak)	B	0.12	0.6480	-4.78	0.1131
Theophylline	P1(-)/PDE(-)	B	-0.85	0.9577	-0.67	0.9810
Phencylidine	GLU(NMDAR)(-)	D	-2.52	0.6024	-6.06	0.1044
PF0676782	mAChR(+)	E	-2.91	0.5649	-2.23	0.4314
NMDA	GLU(NMDAR)(+)	A	-3.47	0.3390	-13.07	0.2201
Fentanyl	μOR(+)	C	-3.73	0.6080	-6.69	0.2162
Gabazine	GABA <sub>A</sub> (-)	A	-3.82	0.5814	-6.79	0.1855
Phenserine	AChE(-)	E	-4.92	0.7573	-5.63	0.5937
Cisplatin	DNA cross-linking agent	F	-5.64	0.5443	-0.52	0.9319
Oxotremorine	mAChR(+)/nAChR(+)	C	-9.51	0.1651	-0.89	0.7644
Neostigmine	AChE(-)	D	-13.75	0.0788	-2.02	0.6058
XE991	Kv(-)	D	-14.05	0.0319	-5.60	0.1318
Carbachol	mAChR(+)/nAChR(+)	C	-17.02	0.0307	-11.11	0.0662
Pilocarpine	mAChR(+)	A	-20.23	0.0050	-8.17	0.0422
Bicuculline	GABA <sub>A</sub> (-)	A	-26.26	0.0008	-17.07	0.0002

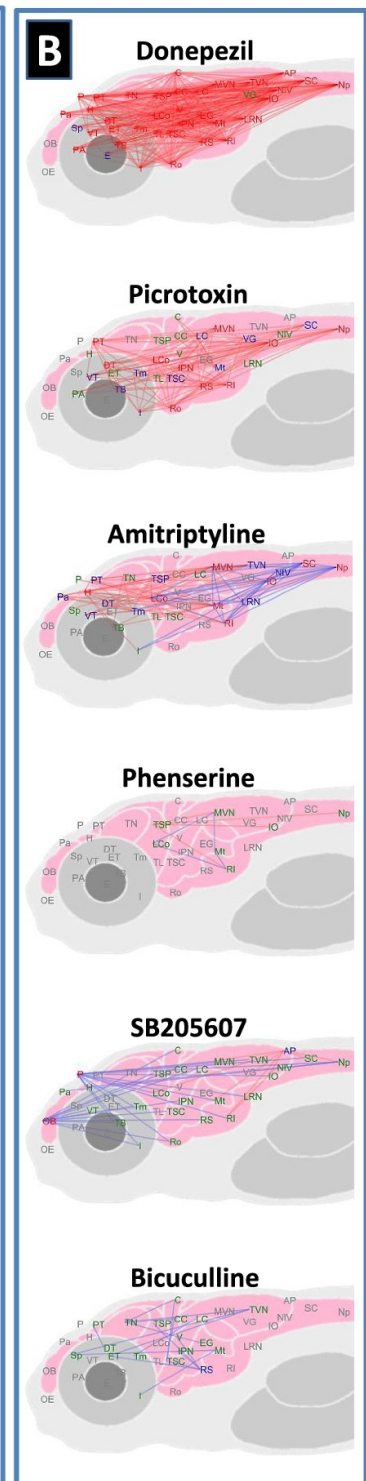


**Figure 2.5:** Assessment of average functional connectivity across the whole brain. Panel (a) shows a comparison of the functional connectivity across the whole brain of larvae exposed to each compound compared with the resting state network animals. Data are shown as the % difference in the number of



functional connections between the two groups (where  $r > .7$ ) along with the corresponding  $p$  value generated after Mann–Whitney  $U$  testing, along with the same parameters for the average  $r$  value of the two groups. Compounds are listed in order of the % size difference from the highest to lowest with values highlighted in red signifying increases and those in a blue decrease compared with the control value.  $p$  values highlighted in pale yellow were statistically significant ( $p < .05$ ). Note that most compounds with no known association to seizure showed no change in functional connectivity versus the resting state network, whereas the stronger seizurogenic compounds (especially the precipitants) generally showed an increase in functional connectivity. Note also that some known seizurogenic compounds also exhibited a decrease in functional connectivity compared with the resting state network. Panel (b) shows representative connectomes from compounds across the full range of values from those showing a large increase in functional connectivity (top), to those showing a large decrease in functional connectivity (bottom). Data shown are connections that exhibited a different mean  $r$  value compared with the equivalent connection as a mean of all the vehicle (water) control animals tested. Nodes connected with a red line represent significant increases and blue significant decreases in the  $r$  value compared with the control. Nodes labelled in green showed 1 or more significantly different connections, in blue, 5 or more and in red 10 or more. Comparisons here were undertaken using Mann–Whitney  $U$  tests with a Bonferroni correction applied (significance at  $p < .00006$ ).  $n = 12$ – $19$  larvae per drug exposed group and  $n = 516$  for the resting state network. Abbreviated brain regions as detailed in Figure 2.2. Note: Positions of regions approximate to allow spacing of nodes and optimal visualisation of connectivity.

support preferentially altered functional connectivity in hind brain regions after treatment with cholinergic agents but of course reflect wider synaptic connectivity, as exemplified by the widespread activity of donepezil, rather than discrete distributions of cell bodies or subcellular receptor populations. Also of note was the close grouping of the Kv blocker XE991 and pilocarpine.

Importantly, XE991 is Kv<sub>7</sub>-selective and inhibition of Kv<sub>7</sub> is known to be excitatory, functionally mimicking the direct agonism of muscarinic receptors, which in turn initiates channel closure and aspects of cholinergic stimulation (Brown, 2018).

The other class of compounds showing notable similarities amongst their functional connectivity phenotypes were the monoaminergic reuptake inhibitors. There was also subdivision of these compounds that may be reflective of the subtle balance in efficacy against each (zebrafish) transporter (Huot et al., 2015) and further work with more selective modulators would help to clarify this. Analysis of the brain regions showing the greatest changes in functional connectivity supported effects on noradrenaline and 5-HT circuitry. Aminergic neurons are also amongst the first to develop in zebrafish. Noradrenergic pathways mainly originate from the locus coeruleus; dopaminergic projections from the posterior tuberculum (Tay et al., 2011) and 5-HT neurons from the raphé nuclei (Maximino and Herculano, 2010). Linking these regions is the important relay station, the interpeduncular nucleus (Bianco and Wilson, 2009), which was also prominently connected here. Altered functional connectivity with the tegmentum is also notably associated with compounds showing relative dopaminergic activity (e.g. cocaine, amphetamine and nomifensine). Given that the tegmentum is known to be relatively rich in zebrafish D<sub>2A</sub> receptors (Maximino and Herculano, 2010), this may suggest that dopaminergic activity is influencing these phenotypes in contrast with other groupings where the more subtle balance between NET and SERT activity is the predominant driving force. The co-location of fentanyl, meperidine and phencyclidine with several monoaminergic reuptake inhibitors could be explained by interactions between these neurotransmitter systems, for example, the reported inhibition of the human SERT and NET by meperidine at low µM concentrations (Rickli et al., 2018) and the inhibition of NA and DA reuptake at low µM concentrations in rat hippocampus (Snell et al., 1988).

Using our analysis method, some pharmacological classes showed few similarities in their functional imaging phenotypes despite being extremely

neuroactive in 4 dpf larvae. Amongst the GABA<sub>A</sub> modulators tested, for example, this dissimilarity may be driven by differences in receptor subtype distribution and relative ligand efficacy (Bandara et al., 2020; Johnston, 2013). Alternatively, this may be reflective of the broad distribution of GABA<sub>A</sub> receptors across the CNS, meaning that targets with a more punctate spatial distribution, such as with the monoaminergics, are more easily differentiated using functional connectivity analysis. Similarly, despite being neuroactive neither NMDA nor (*RS*)-(tetrazol-5-yl)glycine exhibited any particularly strong functional connections. This could be the result of agonism-induced global depolarization resulting in blockade of synaptic transmission in which the Ca<sup>2+</sup> rise (and associated GCaMP fluorescence) would remain due to Ca<sup>2+</sup> entry via the NMDAR itself and depolarization-mediated gating of voltage-gated Ca<sup>2+</sup> channels.

Extending previous findings using PTZ (Diaz Verdugo et al., 2019; Liu and Baraban, 2019), here we demonstrate altered functional connectivity resulting from compound treatment across a wide range of pharmacological mechanisms of action implicated in seizure generation, particularly amongst compounds used as precipitants in animal models of seizure and epilepsy. The presence of abnormal synchronisation is a key feature of seizure networks, as reported in experimental and clinical assessments of epileptic seizures (Jiruska et al., 2013). Our data also revealed an increased prevalence of altered functional connectivity involving nodes within the mesencephalon, in particular, as well as in the diencephalon after exposure to compounds associated with seizures. This echoes the results of previous authors using broader scale segmentation (Diaz Verdugo et al., 2019; Rosch et al., 2018), who have suggested large midbrain structures, such as the optic tectum, play an important role as hubs in the transition of preictal to ictal network dynamics after exposure to the GABA<sub>A</sub> antagonist PTZ. Whole brain connectivity analysis also revealed a reduced overall functional connectivity after exposure to several compounds, most notably pilocarpine and bicuculline. Cymerblit-Sabba and Schiller, (2012) found that overall network synchronicity decreased in the initial stages of a seizure after systemically

applied pilocarpine or an intrahippocampal applied mixture of pilocarpine, kainate and picrotoxin in rats and that hypersynchronisation developed only as seizures progressed and intensified. It may, therefore, be the case here that longer term exposure of some compounds is required in order to reach the advanced stages of a seizure and allow a hypersynchronous phenotype to emerge.

Concluding, we present data demonstrating the power of functional brain imaging in larval zebrafish for assessing the action of neuroactive drugs in a highly relevant vertebrate model. These data help us to understand the relevance of the 4 dpf larval zebrafish for neuropharmacological studies and reveal that even at this early development stage, these animals are highly responsive to a wide range of neuroactive compounds across multiple primary mechanisms of action. The 4 dpf larva appears a particularly relevant model for the study of drugs affecting the monoaminergic and cholinergic systems and has potential utility for the assessment of new drugs targeting these circuits. Furthermore, the assessment of neural activity levels and overall network functional connectivity could help to identify unwanted seizure liability in drugs as part of a new drug CNS safety assessment cascade, as well as aiding in the identification and characterisation of new anti-epileptic drugs and therapeutic targets (Ghannad-Rezaie et al., 2019). This approach also has high potential as an *in vivo* model for the study of seizurogenic and epileptogenic mechanisms more widely, especially with advances in spatiotemporal resolution driving a move towards real time-imaging of large-scale neuronal assemblies at cellular, or even subcellular, resolutions.

## **2.5 Supplementary Analysis**

In addition to the analyses undertaken and detailed in Winter *et al.* (2021), multiple other analysis methods were investigated as part of method development activities for this chapter. Broadly these additional analyses were assessed, but ultimately considered unsuitable as they were either not considered appropriate for the type of data that were generated or did not yield results that were better than those ultimately presented in the publication.

Specifically, designing analyses for this dataset was particularly challenging due to its highly multivariate, hierarchically structured nature, and the fact that there were multiple treatment groups requiring analysis. The methods investigated during method development but not ultimately detailed in Winter et al. (2022) are outlined in this supplementary methods section, along with some brief details as to why they were not selected for definitive application.

### *2.5.1 Network Based Statistic*

Network based statistics constitute a statistical method for comparing the components of functional connectomes, while controlling for the false discovery rate (Zalesky et al., 2010). The method produces a p-value for the null hypothesis that the components of two groups of connectivity matrices are the same. As analysing functional connectivity involves calculating pairwise measures of similarity across all ROIs within a functional imaging dataset, it often produces a large number of pairwise comparisons (in Winter et al. (2022) there were 741). Statistical tests can be performed on these individually in order to make elucidations about the overall difference between two networks. However, the large number of statistical tests means it is necessary to control for the false discovery rate, which can mean a significant loss of statistical power. Network based statistic overcomes this problem by making comparisons of the connected components of the difference between groups.

This approach was implemented by selecting each treatment group to compare (e.g., PTZ vs control) and calculating the pairwise functional connectivity for each ROI. Then for each connection a Mann Whitney u-test was performed comparing the two treatment groups. This produced a matrix of p-values identical in size to each of the functional connectomes. This matrix was then thresholded to select for elements where  $p < 0.01$ . Connected components of this matrix were then identified and the number of nodes present counted in each component.

Next permutation testing was undertaken, wherein connections were randomly swapped between treatment groups, creating a randomised version of each

treatment group while maintaining the original connections across both groups. The above steps were then repeated, performing Mann Whitney tests and finding connected components, identifying the largest component. This was repeated 5000 times, each time taking note of the largest component. This generates a comparative dataset we can use to assess the probability that our original observed difference components occur at random. If the original component was larger than 95% of the randomly generated components, it is considered to be significantly different between treatment groups.

While this approach was highly useful it was not used as there was sufficient statistical power to perform functional connectivity analysis without it. As such NBS was not used in order to avoid adding additional complexity into the analysis pipeline.

### *2.5.2 Classification Algorithms: Neural networks and support vector machines*

Additional analyses that were performed included training a classification algorithm on the data set in order to discriminate between seizurogenic and non-seizurogenic compounds. In order to do this all the compounds in the dataset were labelled either seizurogenic or non-seizurogenic based on the clinical and pharmacological information already available. Data was then split into two equally sized sets, a training and test set. The neural network was trained using the training data set using measures of peak size and shape. The neural network consisted of 500 nodes, and used a scaled conjugate gradient algorithm to optimise network weights (Møller, 1993). The network performance was measured using cross entropy (Nasr et al., 2002). The resultant network performed extremely poorly with high sensitivity but very low specificity. This suggests the model was over-trained on the seizurogenic compounds. This is unsurprising given the much larger volume of data available for these compounds. Moreover, not all of the data was accurately labelled, as some compounds with clinical/ pharmacological associations with seizure in the literature did not reflect this in the Ca<sup>2+</sup> imaging outputs.

Similarly, a quadratic support vector machine was also trained. Support vector machines work by separating data points in multivariate feature space using a hyperplane that maximally separates the classes, in this case seizurogenic and non-seizurogenic compound exposed larva. In this case data points were mapped into higher dimensional space using the radial basis function kernel (Tao, 2002). This was chosen as it's among the most commonly used kernels and can map into infinitely a high dimensional space.

This approach is certainly promising and could have been refined further with this dataset, however, as the aim of the publication was to perform exploratory analysis of the dataset to identify features that are indicative of seizures it was decided to abandon this approach. Neural networks, while highly effective predictive models, are black box algorithms with little descriptive value and thus didn't fit within the narrative of the publication. Moreover, in order to train an accurate neural network, it is necessary to have a data set where the ground truth is well understood. Without first exploring our data set and identifying which compounds resulted in seizure like states and how these states manifest within the zebrafish CNS, it is impossible to make an informed decision about feature selection or labelling data. As such, neural networks are a model earmarked for future use when zebrafish  $\text{Ca}^{2+}$  imaging data is sufficiently refined and well understood, and a highly discriminatory training data set can be generated.

### 2.5.3 *K-means clustering*

In addition to the hierarchical clustering presented in the original paper Winter *et al.* (2021), k-means clustering was also trialled. This was performed on the average of the top two concentrations of each compound. Initially, the euclidean distances between every compound was calculated for each set of parameters (peak or functional connectivity). Then the k-means ++ algorithm was performed on the distances to identify cluster affiliations of each fish. The k-means ++ algorithm was chosen as opposed to Lloyd's algorithm as it achieves faster convergence to a lower sum of within-cluster sum of squares, than traditional k-means (Lloyd's algorithm) (David and Vassilvitskii, 2007). The number of

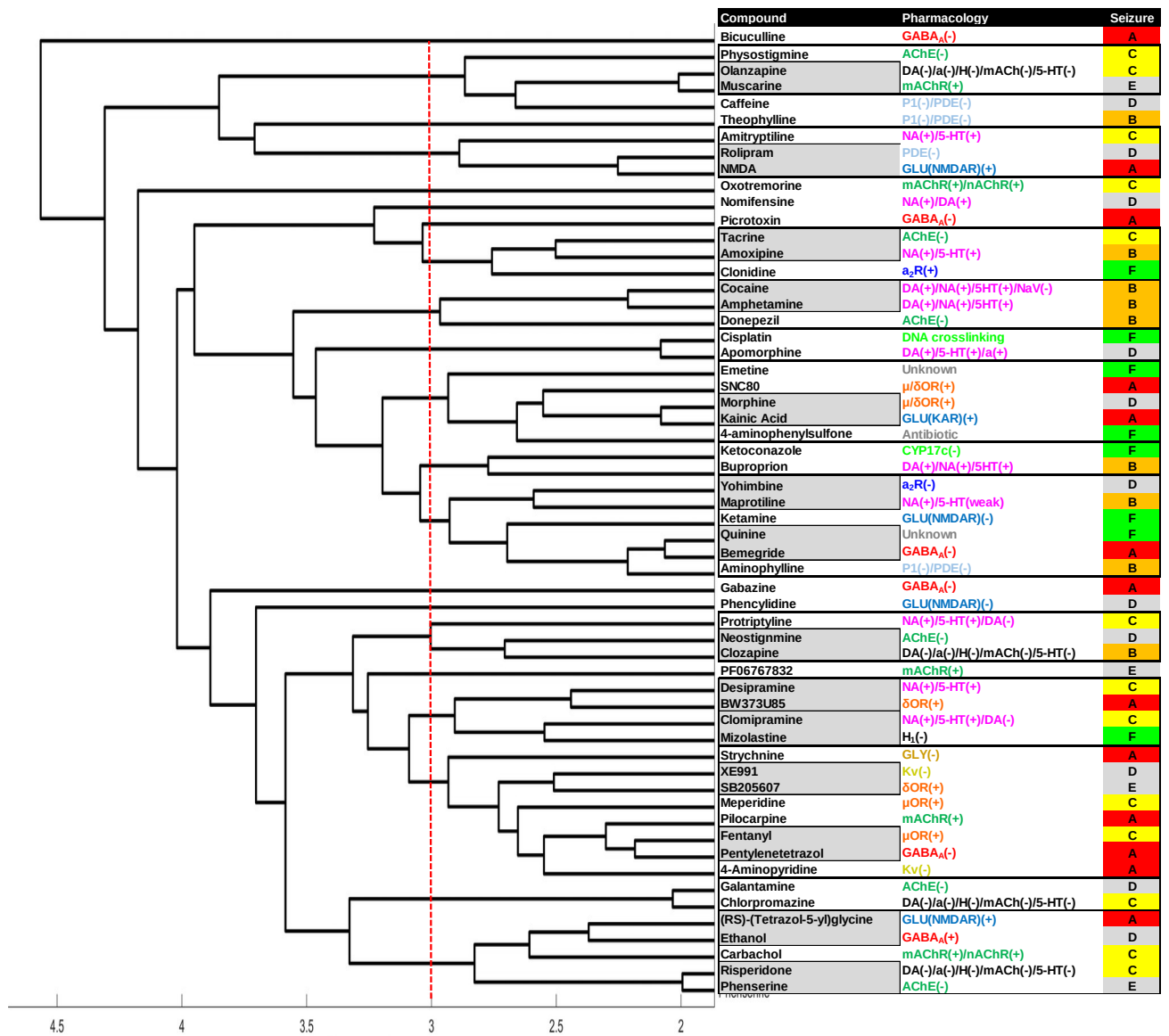
clusters chosen was two in order to differentiate between seizurogenic and non-seizurogenic compounds. Ultimately however, hierarchical clustering was selected as it provided a more descriptive output, showing the distances between individual data points. Moreover, hierarchical clustering naturally selects clusters and sub-clusters based on the structure of the dataset. This allows fewer assumptions to be made about the nature of the dataset, specifically, how many clusters it should consist of.



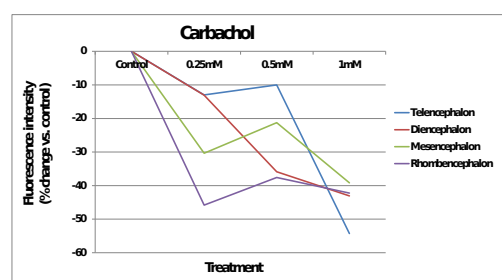
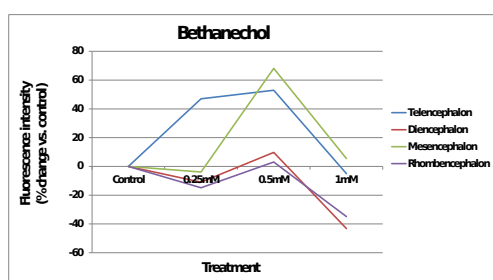
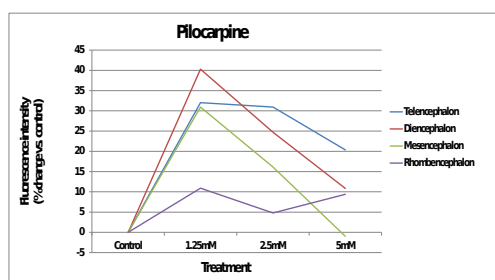
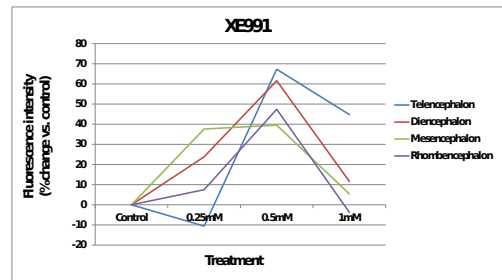
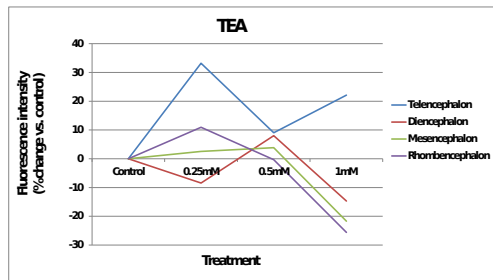
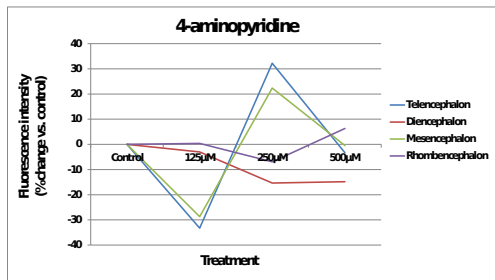
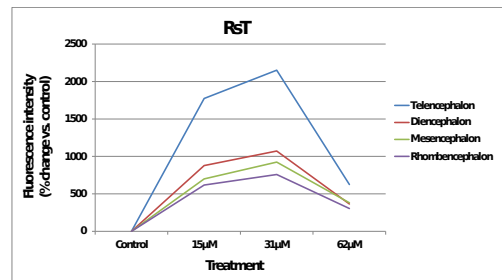
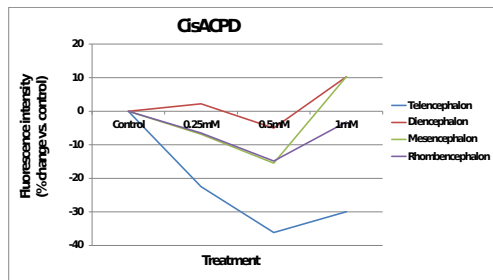
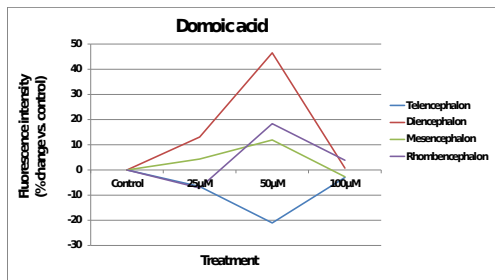
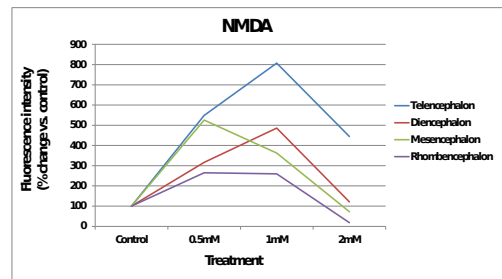
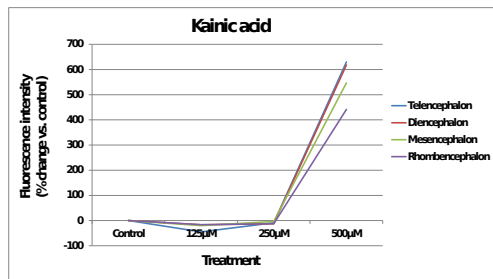
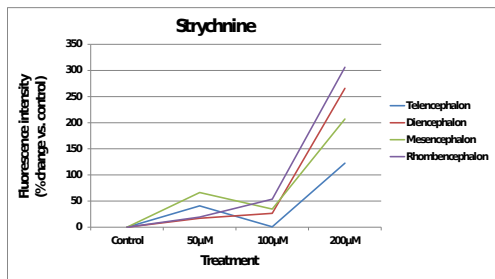
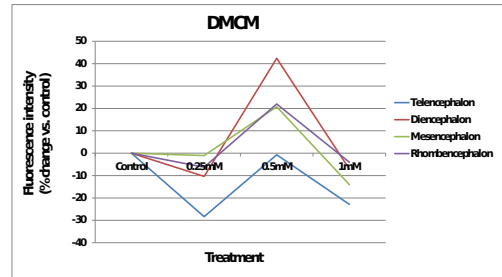
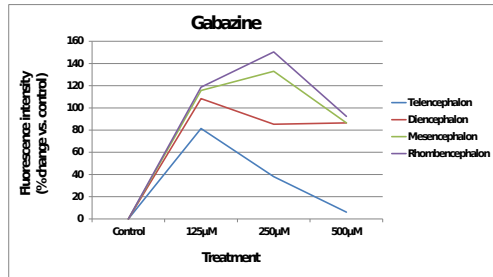
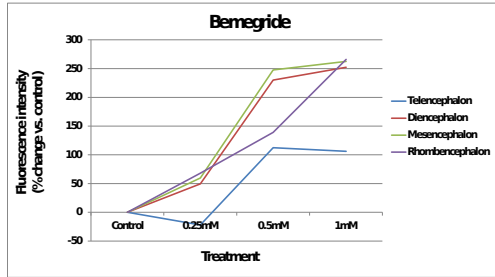
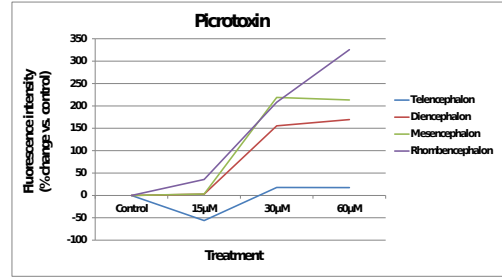
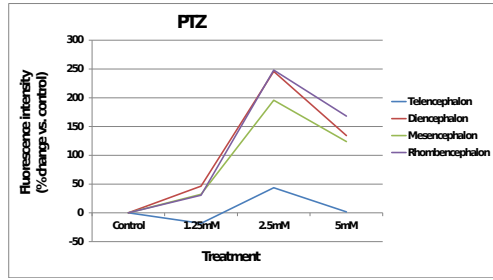
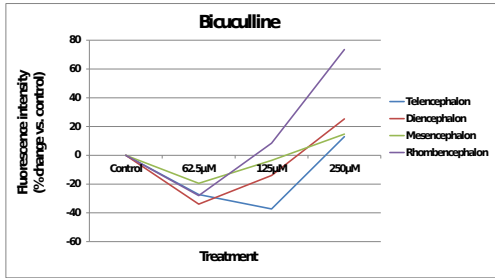
## 2.6 Supplementary Results

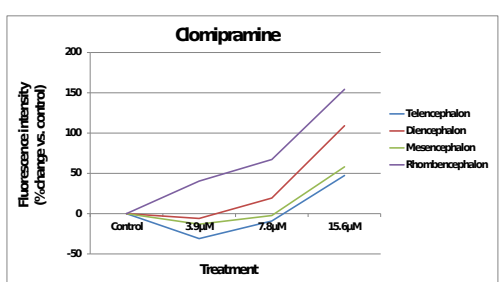
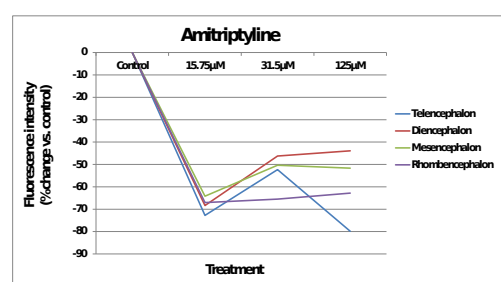
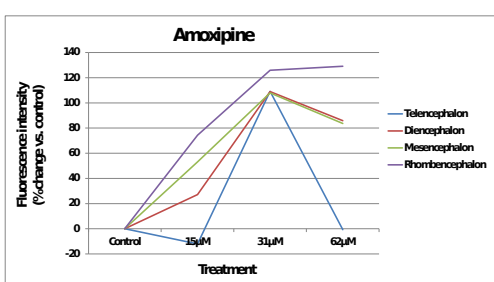
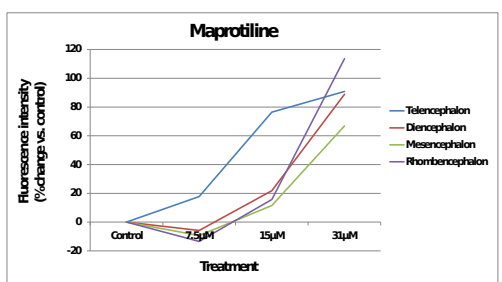
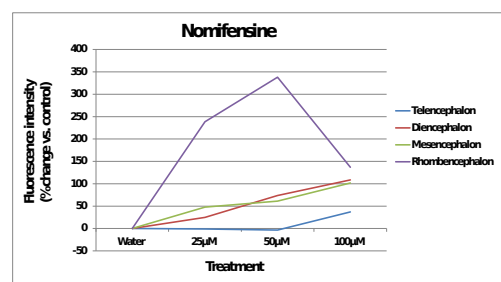
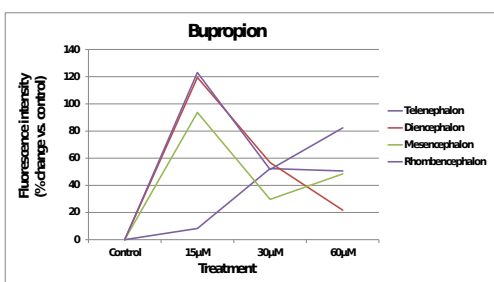
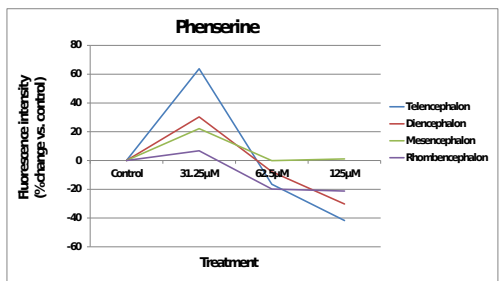
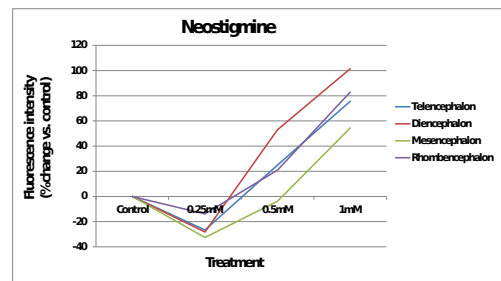
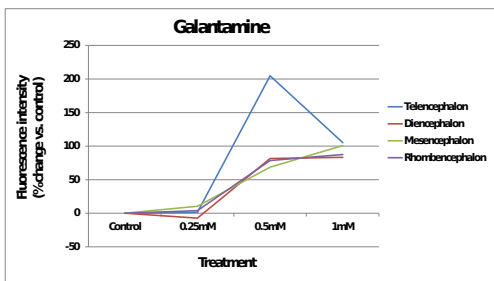
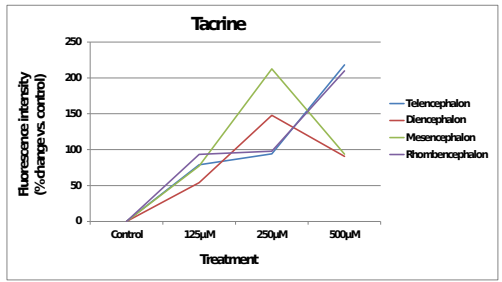
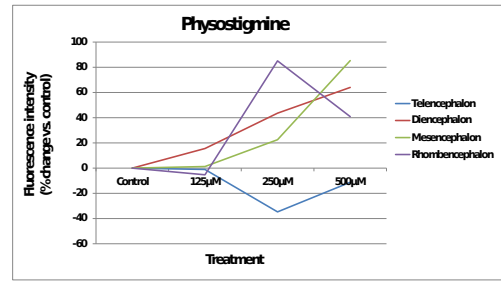
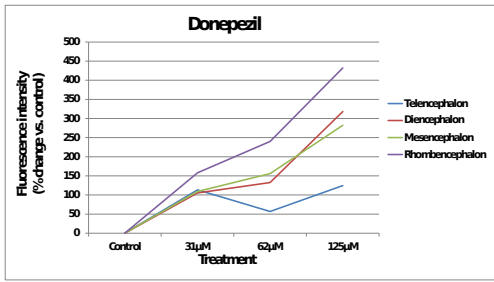
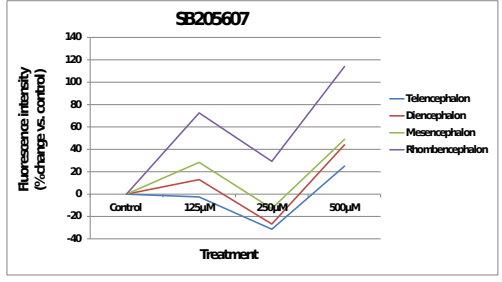
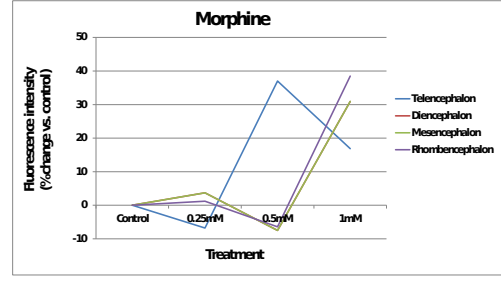
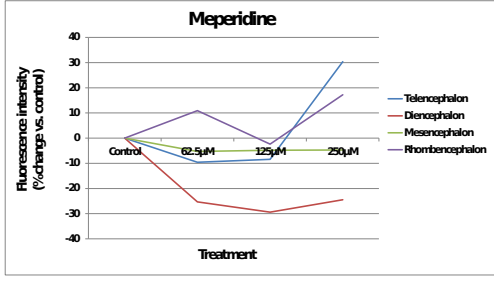
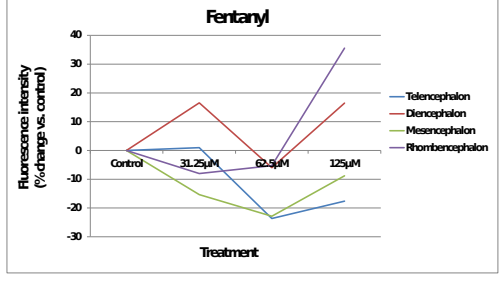
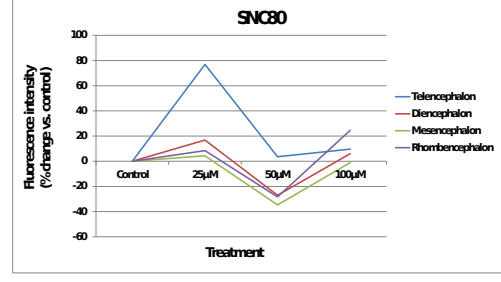
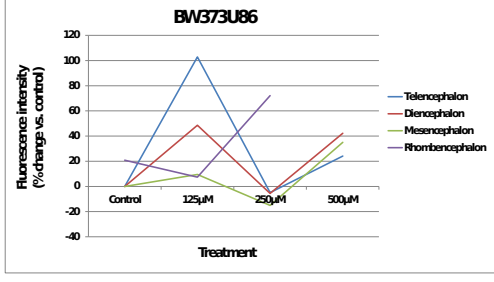
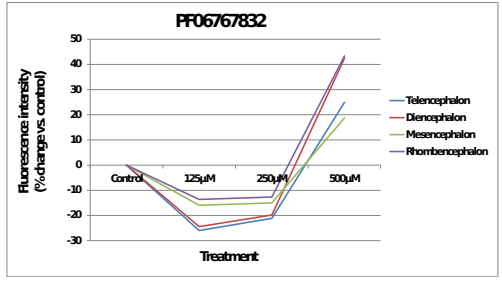
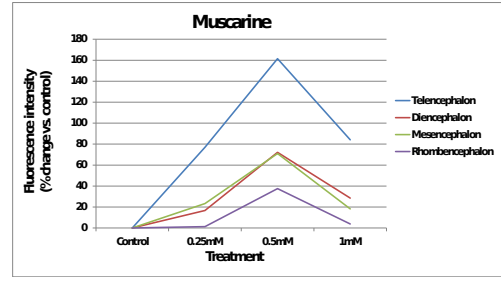
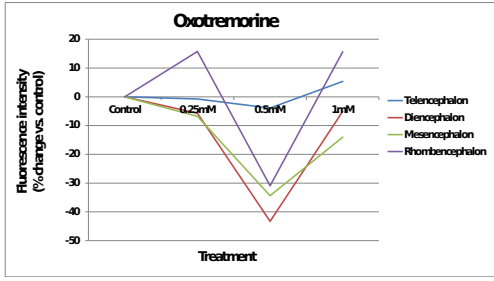
Compound	Categorized strength of link to seizures in mammals	CAS No.	Abbreviation	Assessment of locomotor activity in 7 dpf larvae		Bioanalysis of compound uptake in 7 dpf larvae		
				Effect on high speed distance	MTC	External conc.	Internal conc	% uptake
Bicuculline	A	40709-69-1	BICC	31.25µM***	>500µM	250µM	2µM	1
Pentylentetrazole	A	54-95-5	PTZ	1mM**	5mM	5mM	195µM	4
Picrotoxin	A	124-87-8	PICR	60µM***	120µM	60µM	2µM	2
Bemegride	A	64-65-3	BEM	500µM***	>1mM	1mM	N/A	N/A
Gabazine	A	104104-50-9	GABA	>500µM	>500µM	500µM	4µM	1
DMCM*	A	1215833-62-7	DMCM	>500µM	>500µM	75µM	N/A	N/A
Strychnine	A	60-41-3	STRY	28µM*** (reduction)	28µM	14µM	5µM	36
Kainic acid	A	58002-62-3	KAIN	>1mM	0.5mM	1mM	<LOQ	<LOQ
N-methyl-D-aspartate	A	6384-92-5	NMDA	Overall/no NOEC	1mM	2mM	N/A	N/A
Domoic acid	B	14277-97-5	DOMO	>250µM	>250µM	125µM	<LOQ	<LOQ
Cis-ACPD**	E	477331-06-9	CisA	>1mM	>1mM	1mM	<LOQ	<LOQ
(RS)-(Tetrazol-5-yl)glycine	E	138199-51-6	RST	>1mM	1mM	62.5µM	N/A	N/A
4-aminopyridine	A	504-24-5	4AP	500µM***	>1mM	500µM	11µM	2
Tetraethylammonium Cl	C	56-34-8	TEA	>1mM	>1mM	1mM	N/A	N/A
XE991***	D	122955-13-9	XE991	>500µM	>500µM	75µM	N/A	N/A
Pilocarpine	A	54-71-7	PILO	5mM***	>5mM	5mM	407µM	8
Bethanechol	C	590-63-6	BETH	>1mM	>1mM	1mM	6µM	1
Carbachol	C	51-83-2	CARB	>1mM	>1mM	125µM	6µM	5
Oxotremorine	C	17360-35-9	OXO	>1mM	>1mM	1mM	12µM	12
Muscarine	E	2936-25-6	MUSC	>1mM	>1mM	1mM	8µM	1
PF06767832****	E	1859081-58-5	PF67	>500µM	>500µM	125µM	1mM	896
BW373U86*****	A	155836-50-3	BW373	>500µM	>500µM	150µM	53µM	35
SNC80*****	A	156727-74-1	SNC80	>100µM	100µM	100µM	486µM	486
Fentanyl	C	85951-63-9	FENT	31.25µM**	125µM	125µM	N/A	N/A
Meperidine	C	50-13-5	MEP	125µM*** (reduction)	250µM	250µM	460µM	184
Morphine	D	52-26-6	MORP	>1mM	>1mM	1mM	30µM	3
SB205607*****	E	1217628-73-3	SB20	250µM*	>500µM	5µM	5µM	15
Donepezil	B	884740-09-4	DONE	31.25µM**	62.5µM	62.5µM	130µM	208
Physostigmine	C	57-64-7	PHYS	>500µM	500µM	500µM	183µM	37
Tacrine	C	1684-40-8	TACR	31.25µM***	>1mM	1mM	165µM	17
Galantamine	D	217-780-5	GALA	250µM**	1mM	1mM	144µM	14
Neostigmine	D	114-80-7	NEO	>1mM	>1mM	1mM	5µM	0
Phenserine	E	101246-66-6	PHEN	15.63µM**	125µM	125µM	406µM	325
Bupropion	B	31677-93-7	BUPR	>56µM	>56µM	56µM	36µM	63
Nomifensine	D	32795-47-4	NOMI	Overall/no NOEC	125µM	62.5µM	247µM	394
Maprotiline	B	10347-81-6	MAPR	31.3µM*	<31.25µM	56µM	5µM	9
Amoxapine	B	14028-44-5	AMOX	62.5µM**	62.5µM	28µM	158µM	563
Amitriptyline	C	549-18-8	AMIT	0.97µM** (reduction)	31.25µM	31.25µM	264µM	845
Cloimpramine	C	17321-77-6	CLOM	>15.6µM	15.6µM	15.6µM	163µM	1043
Desipramine	C	58-28-6	DESI	Overall/no NOEC	125µM	125µM	224µM	179
Protriptyline	C	1225-55-4	PROT	8µM*** (reduction)	250µM	250µM	231µM	92
Chlorpromazine	C	69-09-0	CPZ	>125µM	125µM	31.25µM	382µM	1219
Clozapine	B	5786-21-0	CLOZ	25µM** (reduction)	125µM	50µM	611µM	1223
Olanzapine	C	132539-06-1	OLAN	25µM***	250µM	250µM	345µM	138
Risperidone	C	106266-06-2	RISP	125µM**	500µM	500µM	352µM	70
Aminophylline	B	317-34-0	AMIN	Overall/no NOEC	>2mM	900µM	18µM	2
Theophylline	B	58-55-9	THEO	Overall/no NOEC	>1mM	1mM	N/A	N/A
Caffeine	D	58-08-2	CAFF	250µM***	>1mM	1mM	152µM	15
Theobromine	D	83-67-0	THBR	>1mM	>1mM	1mM	N/A	N/A
Paraxanthine	D	611-59-6	PARA	>1mM	>1mM	1mM	2µM	0
Cocaine	B	53-21-4	COCA	62.5µM***	>250µM	125µM	191µM	153
Amphetamine	B	51-63-8	AMPH	31µM** (reduction)	>1mM	1mM	377µM	38
Phencyclidine	D	656-90-1	PCP	1mM**	125µM	125µM	95µM	77
Apomorphine	D	41372-20-7	APOM	13µM**	50µM	25µM	40µM	159
Ethanol	D	64-17-5	EIOH	0.125%***	1.50%	N/A	N/A	N/A
Rolipram	D	61413-54-5	ROLI	Overall/no NOEC	>150µM	150µM	35µM	24
Yohimbine	D	65-19-0	YOHI	62.5µM	125µM	62.5µM	27µM	43
4-Aminophenyl sulfone	F	80-08-0	4AMS	250µM** (reduction)	>1mM	1mM	104µM	10
Cisplatin	F	15663-27-1	CISP	>500µM	>500µM	100µM	2µM	2
Clonidine	F	4205-91-8	CLON	31µM** (reduction)	>1mM	1mM	365µM	37
Emetine	F	316-42-7	EMET	250µM***	>500µM	500µM	194µM	39
Ketamine	F	1867-66-9	KETA	20µM*** (reduction)	62.5µM	62.5µM	86µM	137
Ketocozazole	F	65277-42-1	KETO	Overall/no NOEC	100µM	50µM	445µM	891
Mizolastine	F	108612-45-9	MIZO	50µM**	>100µM	100µM	179µM	179
Quinine HCl	F	6119-47-7	QUIN	>1mM	>1mM	1mM	88µM	9

**Figure S1:** Summary of the data generated from the separate assessment of 7 dpf larval locomotion, maximum tolerated concentration (MTC) and whole body compound concentration used to inform the exposure condition settings used in the imaging study. Information shown left to right: compound name; strength of the association with seizure induction in mammals (see below); Chemical Abstracts Service (CAS) registry number; abbreviation as used in other figures; locomotor activity recorded in 7 dpf larvae along with the maximum tolerated concentration (MTC) measured in the same animals. The next columns show the external compound concentration used in the 7 dpf animal exposure, followed by the corresponding whole body internal concentration and % uptake based on these two values. Compound names highlighted in grey showed no evidence for compound uptake based on 7 dpf larval locomotor activity, MTC, bioanalysis or 4 dpf functional imaging assessments. The strength of the association with seizure induction in mammals is based on the scientific literature, the system of which is detailed in the main manuscript **Fig. 2**. Compound names are detailed in full in the main manuscript **Fig. 2** legend. All test chemicals were obtained from Sigma-Aldrich (Gillingham, UK) or Tocris (Bristol, UK).



**Figure S2:** Dendrogram produced from the cluster analysis of the functional connectivity data from the untreated (water control) larval groups. Along the y-axis are the compounds from which each control group was taken. Clustering is based upon Euclidean distances between mean *r* values, with identified groups showing a mean Euclidean distance of no more than 3 shown in the right hand table alongside each representative control group's name and primary mechanism of action (colour coded). Grey boxes represent especially close sub groupings. Note that mechanisms of action are generally distributed randomly across the dendrogram with few incidences of groupings comprising 2 or more control groups from experiments where there was shared pharmacology in the corresponding treated animal group. n = 7-9 larvae per group.





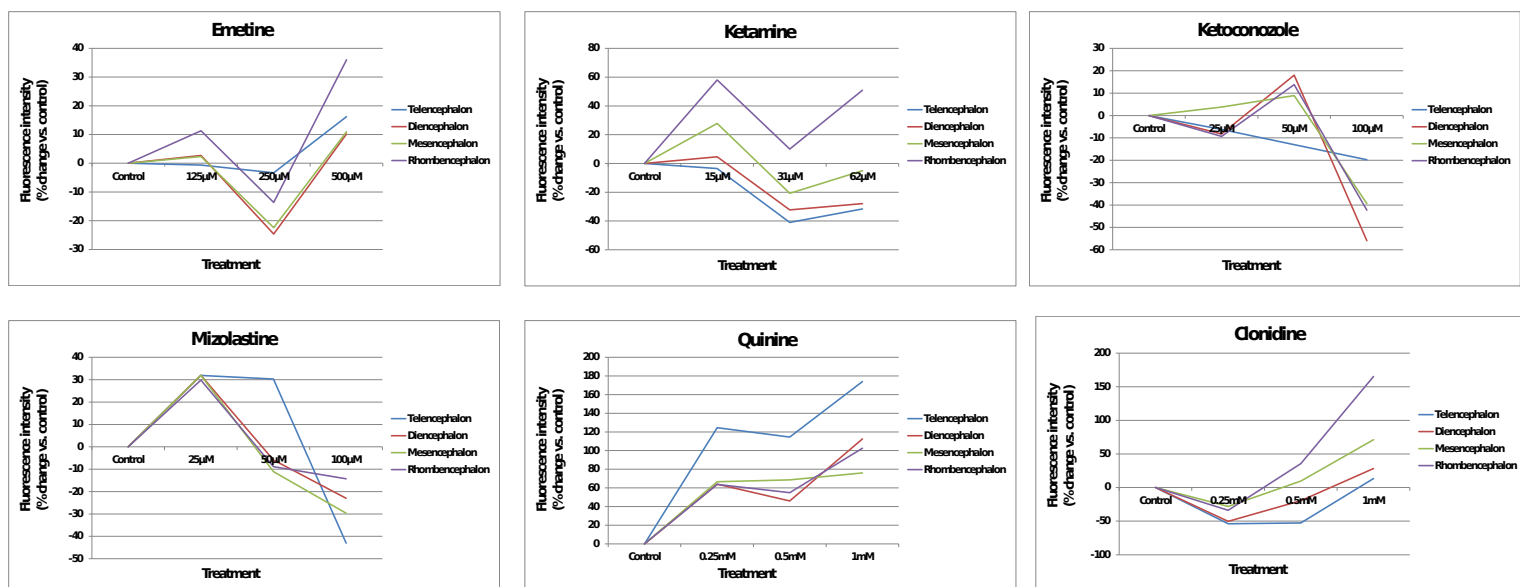


**Figure S3:** Concentration-response curves of fluorescence intensity measured in the telencephalon, diencephalon, mesencephalon and rhombencephalon following exposure to each of the compounds used in the current study. Data are shown as the mean peak fluorescence intensity measured in each region as the % increase or decrease compared with the corresponding vehicle (water) control group, and are presented to provide an indication of the general response of the brain to treatment with each compound. Where a concentration response relationship is evident, in most cases the maximal response observed occurred at the middle or highest treatment concentration. Graphs are shown in the order of presentation in Fig. 2 of the main manuscript.  $n = 6-10$  larvae per group. Note: lowest treatment concentration for picrotoxin had a low sample size of  $n = 4$  and should, therefore, be considered as preliminary.

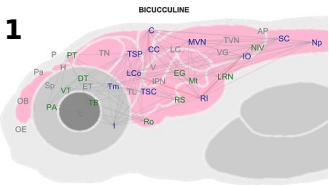
A	Seizure associated mechanisms	Regions showing a significant increase (+) or decrease (-) at x number of treatment levels, or overall (O)									
		+			-			O			All
		+	++	+++	% Sum (+)	-	--	---	% Sum (-)	O	
Forebrain	<b>Iencephalon</b>	2	0	0	5	0	1	0	2	1	9
	Olfactory bulb	2	0	0	5	1	0	0	2	2	11
	Pallidum	2	0	0	5	1	0	0	2	0	7
	Subpallidum	3	1	0	9	0	1	0	2	0	11
	<b>Diencephalon</b>	4	2	0	14	0	1	0	2	3	23
	Dorsal thalamus	3	1	0	9	1	1	0	5	2	18
	Eminentia thalami	1	1	0	5	0	1	0	2	1	9
	Habenulae	2	0	0	5	0	1	1	5	2	14
	Intermediate hypothalamus	4	2	1	16	1	0	1	5	0	20
	Pineal	2	0	1	7	1	1	0	5	1	14
	Posterior tuberculum	5	1	0	14	0	1	0	2	2	20
	Preoptic area	2	1	0	7	0	0	0	0	2	11
	Pretectum	5	0	0	11	1	1	0	5	3	23
Rostral hypothalamus	2	1	0	7	1	0	0	2	1	11	
Ventral thalamus	3	0	0	7	0	1	0	2	4	18	
Midbrain	<b>Mesencephalon</b>	3	2	0	11	1	0	1	5	4	25
	Tectum stratum periventriculare	4	2	0	14	1	1	0	5	4	27
	Tectum neuropil	4	1	0	11	1	1	0	5	3	23
	Tegmentum	6	2	1	20	1	0	1	5	0	25
	Torus longitudinalis	3	1	0	9	0	0	0	0	1	11
	Torus semicircularis	3	1	0	9	0	0	1	2	1	14
Hindbrain	<b>Rhombencephalon</b>	7	2	1	23	0	1	1	5	1	30
	Area postrema	7	1	0	18	0	0	0	0	0	18
	Cerebellum	8	4	0	27	1	0	1	5	1	34
	Corpus cerebelli	7	5	0	27	0	1	1	5	2	36
	Eminentia granularis	9	2	0	25	0	0	1	2	1	30
	Inferior olive	6	1	1	18	1	0	1	5	1	25
	Interpeduncular nucleus	3	2	1	14	1	0	1	5	0	18
	Lateral reticular nucleus	7	2	0	20	1	0	0	2	3	30
	Lobus caudalis cerebelli	6	1	0	16	0	1	0	2	2	23
	Locus coeruleus	6	2	1	20	1	0	1	5	1	27
	Mauthner	8	3	0	25	0	0	1	2	0	27
	Medial vestibular nucleus	7	3	0	23	0	0	1	2	1	27
	Noradrenergic neurons of F/VAs	4	1	0	11	0	0	0	0	4	20
Raphe – inferior	9	3	0	27	1	0	1	5	0	32	
Raphe – superior	7	2	1	23	0	1	1	5	1	30	
Tangential vestibular nucleus	7	2	0	20	0	0	1	2	0	23	
Valvula cerebelli	8	4	0	27	0	1	0	2	3	36	
Ganglia	Eyes	4	1	0	11	0	1	0	2	0	14
	Olfactory epithelium	1	1	0	5	0	0	0	0	2	9
	Vagal ganglia	1	0	0	2	1	0	0	2	1	7
	Spinal cord	5	1	0	14	0	0	1	2	3	23
	Neuropil region	4	1	1	14	0	0	1	2	2	20

B	Not linked to seizures	Regions showing a significant increase (+) or decrease (-) at x number of treatment levels, or overall (O)									
		+			-			O			All
		+	++	+++	% Sum (+)	-	--	---	% Sum (-)	O	
Forebrain	<b>Iencephalon</b>	0	0	0	0	0	0	0	0	0	0
	Olfactory bulb	0	0	0	0	0	0	0	0	0	0
	Pallidum	0	0	0	0	0	1	0	0	0	13
	Subpallidum	0	0	0	0	0	0	0	0	0	25
	<b>Diencephalon</b>	0	0	0	0	0	0	0	0	0	13
	Dorsal thalamus	0	0	0	0	0	0	0	0	0	13
	Eminentia thalami	0	0	0	0	2	0	0	25	1	38
	Habenulae	0	0	0	0	1	0	0	13	0	13
	Intermediate hypothalamus	0	0	0	0	0	0	0	0	0	13
	Pineal	0	0	0	0	0	0	0	0	0	0
	Posterior tuberculum	0	0	0	0	0	0	0	0	2	25
	Preoptic area	0	0	0	0	1	0	0	13	1	25
	Pretectum	0	0	0	0	0	0	0	0	0	13
Rostral hypothalamus	0	0	0	0	0	0	0	0	0	13	
Ventral thalamus	0	0	0	0	0	0	0	0	0	13	
Midbrain	<b>Mesencephalon</b>	1	0	0	13	1	0	0	13	0	25
	Tectum stratum periventriculare	2	0	0	25	0	0	0	0	1	38
	Tectum neuropil	0	0	0	0	0	1	0	13	1	25
	Tegmentum	1	0	0	13	0	0	0	0	0	13
	Torus longitudinalis	0	0	0	0	0	0	0	0	1	13
	Torus semicircularis	0	0	0	0	1	0	0	13	1	25
Hindbrain	<b>Rhombencephalon</b>	1	0	0	13	0	0	0	0	0	13
	Area postrema	0	0	0	0	0	0	0	0	0	13
	Cerebellum	1	0	0	13	0	0	0	0	0	13
	Corpus cerebelli	1	0	0	13	0	0	0	0	0	13
	Eminentia granularis	1	0	0	13	0	0	0	0	1	25
	Inferior olive	0	0	0	0	0	0	0	0	2	25
	Interpeduncular nucleus	0	0	0	0	0	0	0	0	1	13
	Lateral reticular nucleus	0	0	0	0	0	0	0	0	1	13
	Lobus caudalis cerebelli	1	0	0	13	1	0	0	13	0	25
	Locus coeruleus	1	0	0	13	0	0	0	0	0	13
	Mauthner	0	0	0	0	1	0	0	13	1	25
	Medial vestibular nucleus	1	0	0	13	0	0	0	0	0	13
	Noradrenergic neurons of F/VAs	0	0	0	0	0	0	0	0	0	13
Raphe – inferior	0	0	0	0	0	0	0	0	1	13	
Raphe – superior	1	0	0	13	0	0	0	0	0	13	
Tangential vestibular nucleus	0	1	0	13	1	0	0	13	0	25	
Valvula cerebelli	1	0	0	13	0	0	0	0	0	13	
Ganglia	Eyes	0	0	0	0	1	0	0	13	1	25
	Olfactory epithelium	0	0	0	0	1	0	0	13	0	13
	Vagal ganglia	0	0	0	0	2	0	0	25	0	25
	Spinal cord	0	0	0	0	0	0	0	0	1	13
	Neuropil region	0	0	0	0	0	0	0	0	1	13

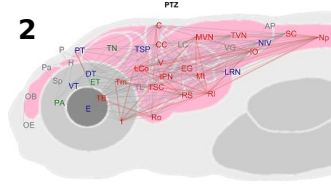
**Figure S4:** Summary of the statistically-significant effects of drug treatment on the peak intensity measured in various brain regions of the larval zebrafish. Data are shown either for drugs mechanistically linked to seizures (A), excluding those categorised as ‘D’ in the main manuscript Fig. 2, or those from category ‘F’ not linked to seizure (B). From the column headers, +, ++ and +++ show the number of compounds exhibiting a significant increase at 1, 2 or 3 concentrations in that brain region compared with the vehicle (water) control group ( $P < .017$ ), followed by the sum, represented as the % of the total number of compounds tested (% sum (+)); followed by the equivalent values for significant decreases. The column named ‘O’ shows the number of compounds exhibiting an overall significant difference following Kruskal Wallis analysis within that brain region, and the final column named ‘All’ is the sum of all significant differences (+, \_ and O) as a % of the total number of compounds tested. Cells highlighted in yellow are the top 5 values for each category used to show which regions were most consistently significantly activated. All statistical comparisons were undertaken using Kruskal-Wallis tests coupled with Dunn’s post hoc tests. Note when considering all significant increases, decreases and overall changes, the rhombencephalon, cerebellum, corpus cerebelli, lateral reticular nucleus, inferior and superior raphe and valvula cerebelli showed the most consistently altered activity in the seizure positive compounds.  $n = 6-10$  larvae per group per compound.



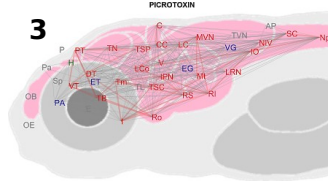




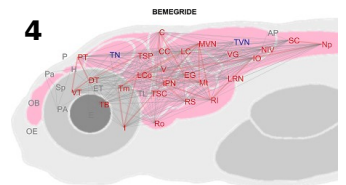
**Bicuculline**



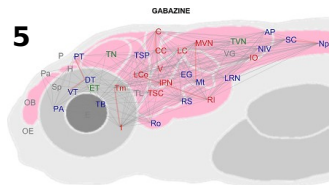
**PTZ**



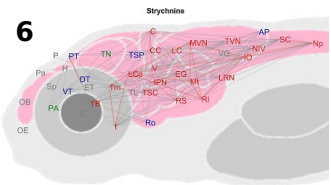
**Picrotoxin**



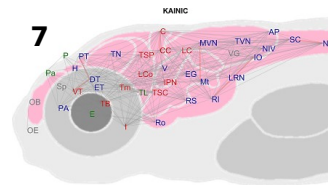
**Bemegride**



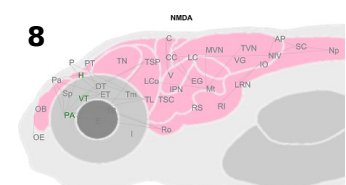
**Gabazine**



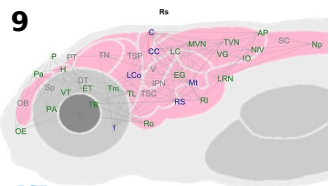
**Strychnine**



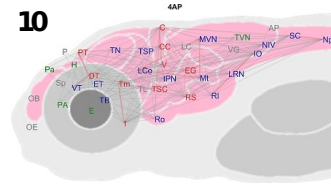
**Kainic acid**



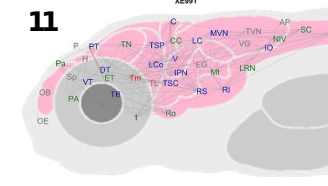
**NMDA**



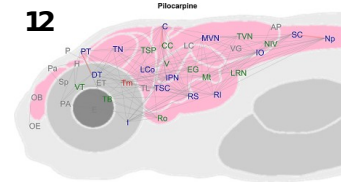
**RST**



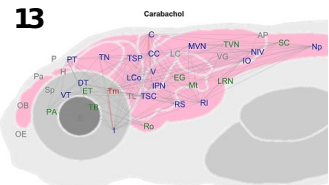
**4AP**



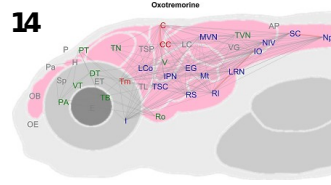
**XE991**



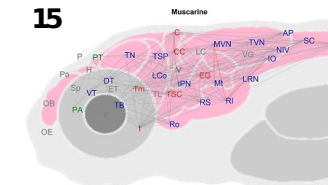
**Pilocarpine**



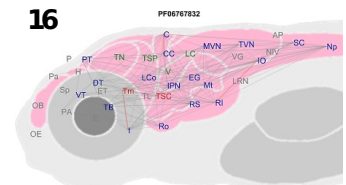
**Carbachol**



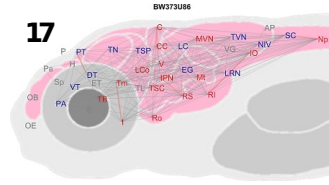
**Oxotremorine**



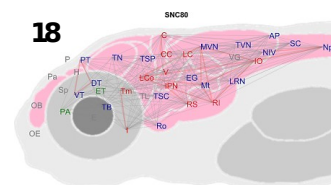
**Muscarine**



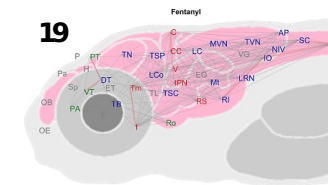
**PF067**



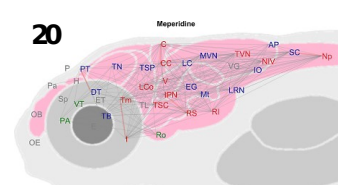
**BW373**



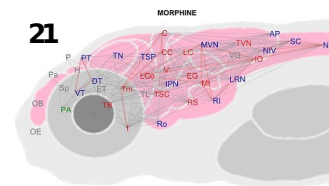
**SNC80**



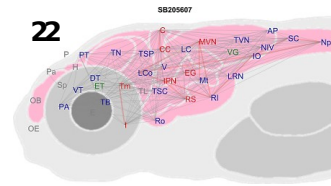
**Fentanyl**



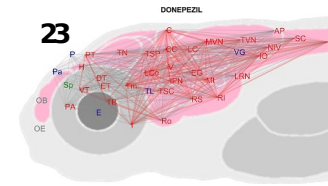
**Meperidine**



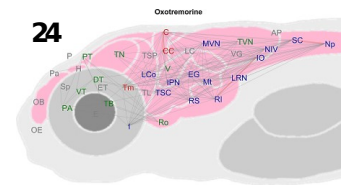
**Morphine**



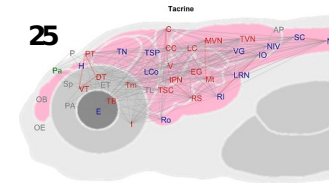
**SB205607**



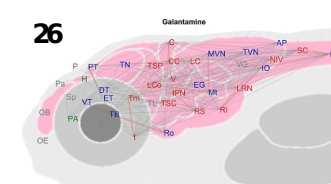
**Donepezil**



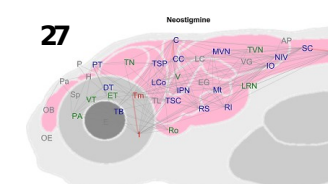
**Physostigmine**



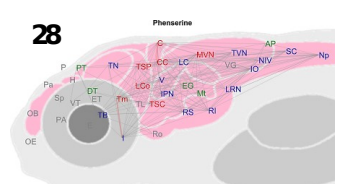
**Tacrine**



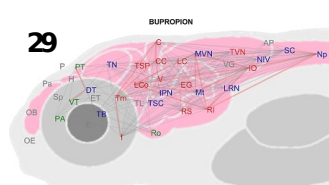
**Galantamine**



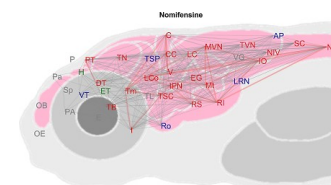
**Neostigmine**



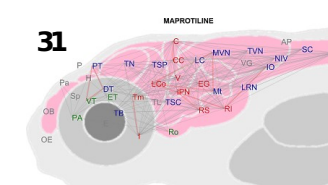
**Phenserine**



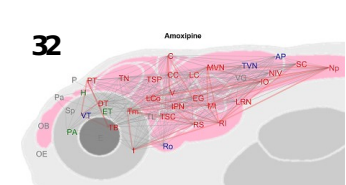
**Bupropion**



**Nonifensine**

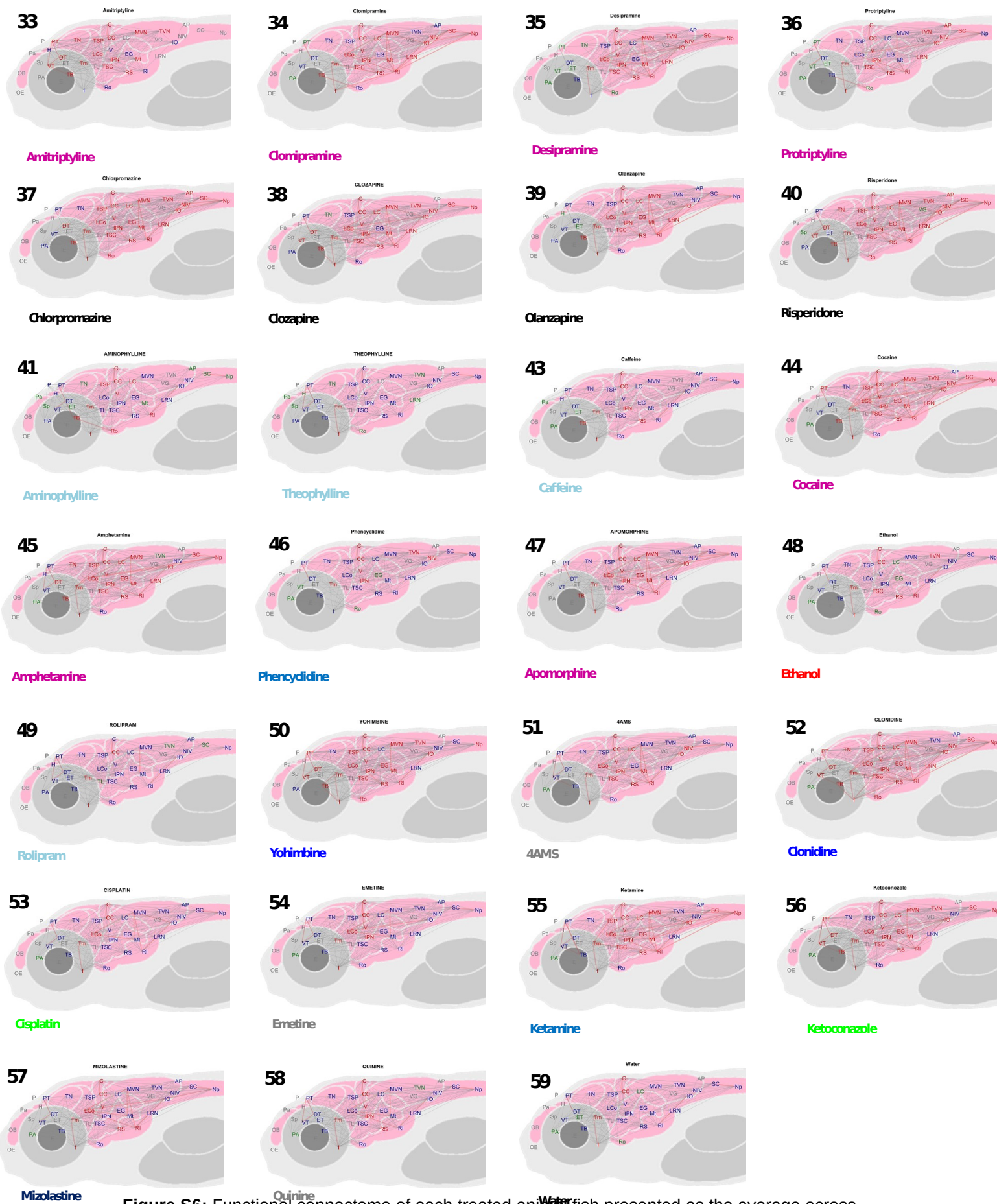


**Maprotiline**



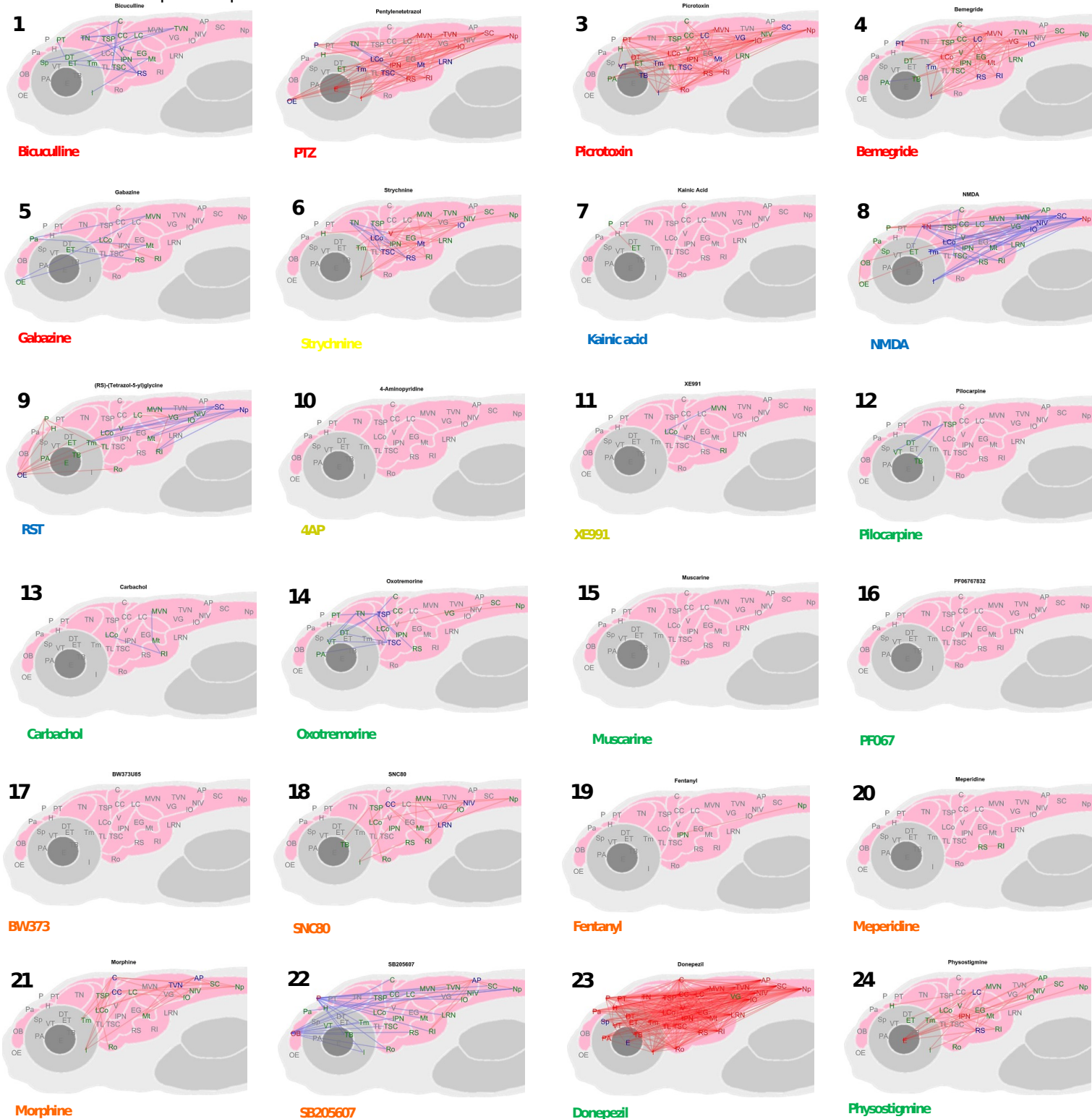
**Amoxipine**



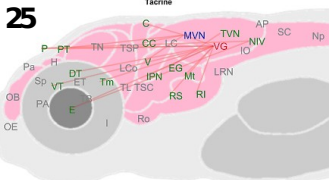


**Figure S6:** Functional connectome of each treated animal fish presented as the average across all fish treated at the medium and high concentrations per compound. Nodes linked by a grey line showed a mean Pearson's correlation coefficient ( $r$ ) of  $> .70$ , those in red  $> .95$ . Nodes labelled in Green showed 5 or more functional connections, in blue, 10 or more, and in red 20 or more connections ( $n = 12-19$  larvae per compound connectome, and  $n = 516$  for the water connectome). Abbreviated brain regions are: Area postrema (AP); Cerebellum (C); Corpus cerebelli (CC); Dorsal thalamus (DT); Eyes (E); Eminentia granularis (EG); Eminentia Thalami

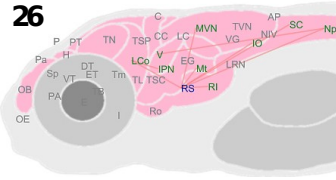
(ET); Habenulae (H); Intermediate hypothalamus (I); Inferior olive (IO); Interpeduncular nucleus (IPN); Lobus caudalis cerebelli (LC); Locus coeruleus (LCo); Lateral reticular nucleus (LRN); Mauthner (Mt); Medial vestibular nucleus (MVN); Noradrenergic neurons of the interfascicular and vagal areas (NIV); Spinal cord neuropil (Np); Olfactory bulb (OB); Olfactory epithelium (OE); Pineal (P); Preoptic Area (PA); Pallium (Pa); Pretectum (PT); Raphe inferior (RI); Rostral hypothalamus (Ro); Raphe superior (RS); Spinal cord (SC); Subpallium (Sp); Posterior tuberculum (TB); Torus longitudinalis (TL); Tegmentum (Tm); Tectum neurophil (TN); Torus semicircularis (TSC); Tectum stratum periventriculare (TSP); Tangential vestibular nucleus (TVN); Valvula cerebelli (V); Vagal ganglia (VG); Ventral Thalamus (VT) **Note:** positions of regions approximate to allow spacing of nodes and optimal visualisation of connectivity. **Note:** DMCM, domoic acid, Cis-ACPD, TEA, bethanechol, theobromine and paraxanthine are not shown as these compounds were excluded from these analyses as we found no evidence of compound uptake.



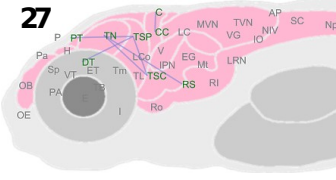




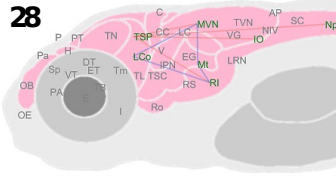
**Tacrine**



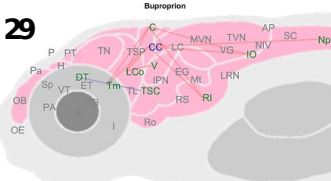
**Galantamine**



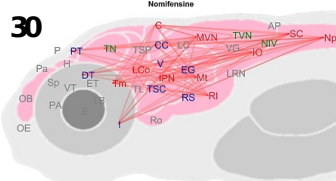
**Neostigmine**



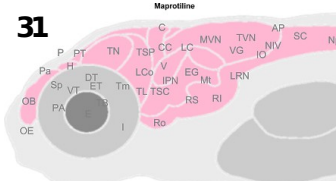
**Phenserine**



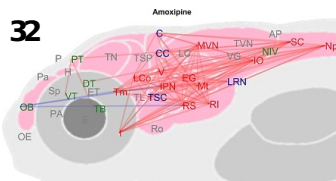
**Bupropion**



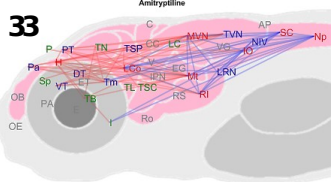
**Nonifensine**



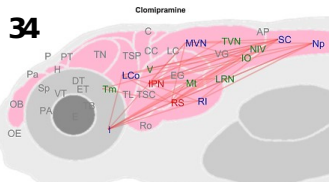
**Maprotiline**



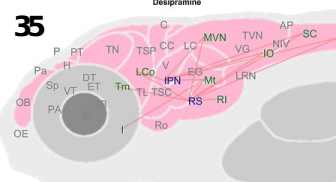
**Amoxipine**



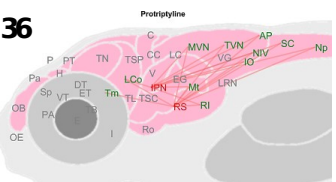
**Amitriptyline**



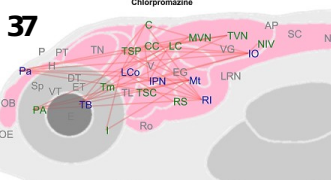
**Clonipramine**



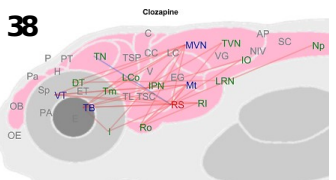
**Desipramine**



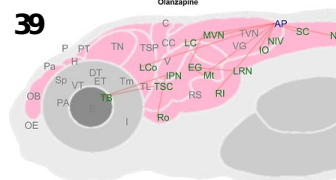
**Protriptyline**



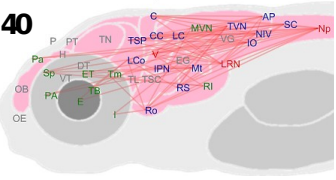
**Chlorpromazine**



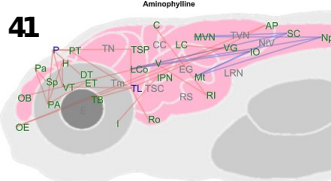
**Clozapine**



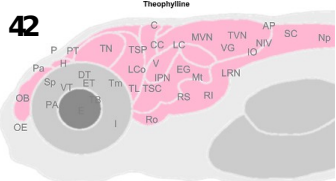
**Olanzapine**



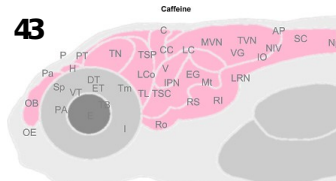
**Risperidone**



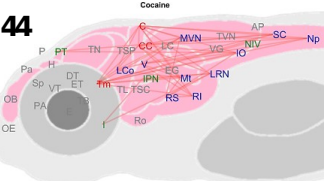
**Aminophylline**



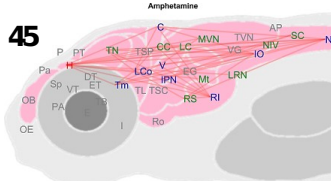
**Theophylline**



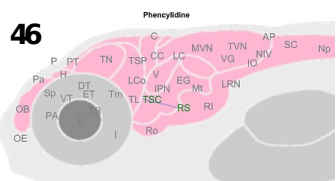
**Caffeine**



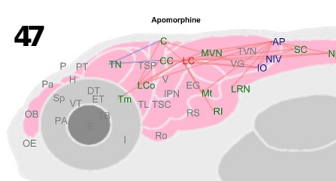
**Cocaine**



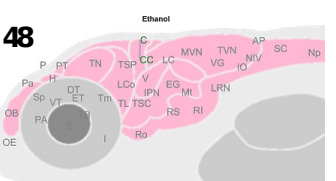
**Amphetamine**



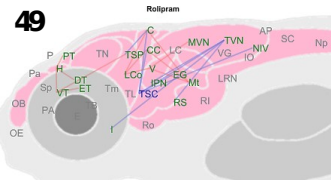
**Phencyclidine**



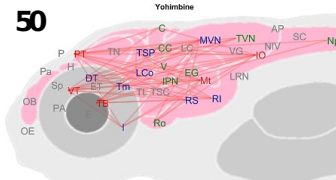
**Apomorphine**



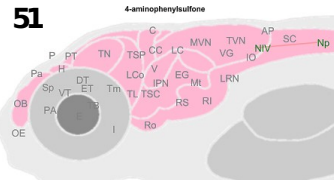
**Ethanol**



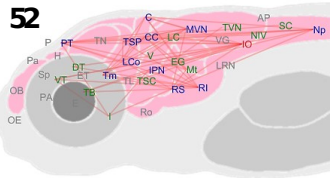
**Rolipram**



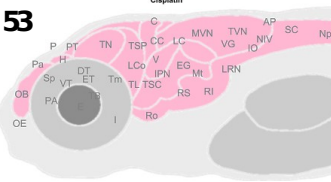
**Yohimbine**



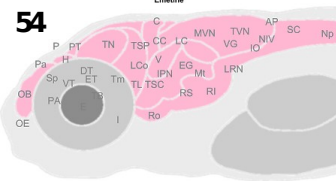
**4AMS**



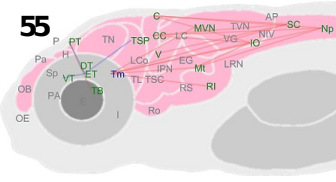
**Clonidine**



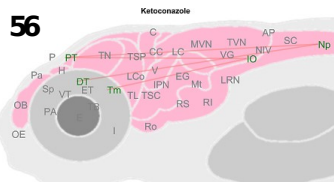
**Cisplatin**



**Emetine**



**Ketamine**



**Ketoconazole**

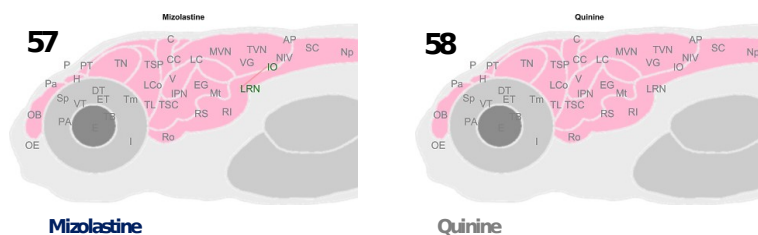


**Figure S7:** Post hoc analysis of functional connectivity (medium and high concentrations combined) in drug-treated versus vehicle (water) control larval brains. Data shown are connections that exhibited a significantly different mean  $r$  value compared with the equivalent connection as a mean of all the vehicle (water) control animals tested ( $n = 12-19$  larvae per compound exposed group, and  $n = 516$  for the resting state network). Nodes connected with a **red** line represent significant increases and **blue** significant decreases in the  $r$ -value compared with the control. Nodes labelled in **Green** showed 1 or more significant connections, in **blue**, 5 or more, and in **red** 10 or more. Comparisons were undertaken using Mann-Whitney U tests with a Bonferroni correction applied (significance at  $p < .00006$ ). Abbreviated brain regions are: Area postrema (**AP**); Cerebellum (**C**); Corpus cerebelli (**CC**); Dorsal thalamus (**DT**); Eyes (**E**); Eminentia granularis (**EG**); Eminentia Thalami (**ET**); Habenulae (**H**); Intermediate hypothalamus (**I**); Inferior olive (**IO**); Interpeduncular nucleus (**IPN**); Lobus caudalis cerebelli (**LC**); Locus coeruleus (**LCo**); Lateral reticular nucleus (**LRN**); Mauthner (**Mt**); Medial vestibular nucleus (**MVN**); Noradrenergic neurons of the interfascicular and vagal areas (**NIV**); Spinal cord neuropil (**Np**); Olfactory bulb (**OB**); Olfactory epithelium (**OE**); Pineal (**P**); Preoptic Area (**PA**); Pallium (**Pa**); Pretectum (**PT**); Raphe inferior (**RI**); Raphe superior (**RS**); Rostral hypothalamus (**Ro**); Spinal cord (**SC**); Subpallium (**Sp**); Posterior tuberculum (**TB**); Torus longitudinalis (**TL**); Tegmentum (**Tm**); Tectum neurophil (**TN**); Torus semicircularis (**TSC**); Tectum stratum periventriculare (**TSP**); Tangential vestibular nucleus (**TVN**); Valvula cerebelli (**V**); Vagal ganglia (**VG**); Ventral Thalamus (**VT**). **Note:** positions of regions approximate to allow spacing of nodes and optimal visualisation of connectivity. Also DMCM, domoic acid, Cis-ACPD, TEA, bethanechol, theobromine and paraxanthine are not shown as these compounds were excluded from these analyses as we found no evidence of compound uptake.



**Figure S8:** Results of the assessment of average brain functional connectivity involving the 4 main brain regions. The upper panel **(A)** shows the results of comparing the number of functional connections ( $r > .7$ ) involving regions in the 4 broad brain areas exposed to each compound, versus the corresponding data from the resting state network ( $n = 12-19$  larvae per compound exposed group, and  $n = 516$  for the resting state network). Panel **(B)** shows the same data as a comparison of the average  $r$ -values. Data are shown as the % difference between the two groups along with the corresponding  $p$ -value generated after Mann Whitney U-testing, along with the same values for the average  $r$ -value of the two groups. Compounds are listed in order of the seizure classification from the highest to lowest with values highlighted in red signifying increase and those in a blue a decreases compared with the control value.  $P$  values highlighted in yellow were statistically significant at the  $p < .05$  level.

## Chapter 3: Differential Electrographic Signatures Generated by Mechanistically Diverse Seizurogenic Compounds in the Larval Zebrafish Brain

### 3.1 Introduction

Seizures are defined as periods of excessive or hyper- synchronous brain activity (Fisher et al., 2014a), which, when recurrent and unprovoked, define the chronic disease epilepsy (Falco-Walter et al., 2018). In addition, seizure occurrences and myoclonus appear to be a feature of the pathophysiology of multiple other CNS diseases, including Alzheimer’s disease and other forms of dementia (Beagle et al., 2017). Seizures themselves have a wide-ranging etiology that includes a substantial proportion attributable to the adverse action of drugs. It has been estimated, for example, that ~6% of new-onset seizures and 9% of status epilepticus cases are as a result of drug toxicity (Chen et al., 2016), which includes the inadvertent action of multiple marketed drugs (Easter et al., 2009; Ruffmann et al., 2006). Seizures themselves can be definitively identified in human patients and nonclinical animal models using neurophysiological assessment techniques such as local field potential (LFP) recordings and electroencephalography (EEG; Lévesque and Avoli, 2019; Usman et al., 2019). Using these techniques, seizures can be observed to present diverse electrographic dynamics, with some common components including low-voltage fast activity, e.g., high- frequency oscillations (HFOs; Jiménez-Jiménez et al., 2015; Wang et al., 2020) in the fast ripple frequency bands (250– 500 Hz), or high-amplitude periodic spikes (Perucca et al., 2014; Jiménez-Jiménez et al., 2015; Wang et al., 2020). However, precisely how, and where, they are manifest can vary between different forms of epilepsy and different causes of seizure (Perucca et al., 2014; Jiménez-Jiménez et al., 2015; Wang et al., 2020).

In order to better understand why seizures occur and how to treat epilepsy, the use of experimental models is important. Such models should include an appropriate, often complex neural architecture, and the best models are those performed *in vivo*, preferably in the absence of confounds generated by anesthesia. With this in mind, a drive toward more ethical and cost-effective

approaches for studying complex neurologic disorders have increased interest in alternative, non-mammalian, vertebrate models for such studies. Of these models, the larval zebrafish offers considerable potential as a highly genetically tractable alternative for screening epilepsy related genes and for the study of genetic mutation-induced spontaneous seizures (Baraban, 2013; Griffin et al., 2021).

To date, zebrafish have been relatively widely used for assessing drug-induced neural activity, and various studies have described the effects of seizurogenic chemicals on their behavior (Alfaro et al., 2011; Baraban et al., 2013b; Berghmans et al., 2007; Winter et al., 2008), electrophysiology (Afrikanova et al., 2013; Baraban, 2013; Baraban et al., 2007; Cho et al., 2017; Copmans et al., 2019; Griffin et al., 2021; Hortopan et al., 2010; Hunyadi et al., 2017; Kim et al., 2010b; Liu and Baraban, 2019), and functional imaging phenotypes (Burgstaller et al., 2019; Burrows et al., 2020; Ghannad-Rezaie et al., 2019; Winter et al., 2021, 2017). Electrophysiological assessments, in particular, offer extremely high temporal resolution and allow direct comparison of zebrafish-derived data with that obtained from neurophysiological assessments undertaken in mammals. Consequently, the recording of larval zebrafish electrophysiological data offers the opportunity to directly compare abnormal electrographic dynamics between these two taxonomically diverse sets of model organisms. In larval zebrafish, typically, LFP recordings from small clusters of neurons in easily identified anatomic targets (such as the optic tectum) are used to measure the response of the brain to drug treatment. Indeed, LFP recordings have been used to assess the electrographic response of the larval zebrafish to a few seizurogenic compounds including picrotoxin, pilocarpine (Hortopan et al., 2010; Baraban, 2013), and, most often, pentylenetetrazole (PTZ; Baraban et al., 2007; Copmans et al., 2019; Kim et al., 2010; Liu and Baraban, 2019). Despite the relatively widespread use of electrophysiology in larval zebrafish, little is actually known about the specific electrographic characteristics of seizures induced by diverse chemicals in this model organism, other than the aforementioned exceptions. There are few published studies which characterize LFP profiles in larval zebrafish across a range of excitatory mechanisms, for example, or that have compared their characteristics with those used to define seizures in more traditional models of seizures and



epilepsy using mammalian electrophysiology and human EEG data. Here, we sought to address this knowledge gap by assessing the LFP-based response of 4-day post-fertilization (dpf) larval zebrafish, to treatment with a variety of seizurogenic compounds which act through a range of pharmacological mechanisms of action. Using frequency domain analysis on the resulting data we aimed to assess the similarities and differences in the electrographic signatures of LFPs between different pharmacologies, and to compare and contrast these characteristics with what is known from electrophysiological studies of seizures and epilepsy in mammals including humans, thereby adding considerably to our knowledge of the translational value of this model.

## **3.2 Materials and Methods**

The experimental approach used is detailed in the following sections and the process is summarized in Figure 3.1A. Throughout, the data shown in graphs and tables are the means  $\pm$  SEM of data points from individual animals (n). All analyses were performed using MATLAB (MATLAB version 9.8.0, 2020), including the signal processing toolbox 8.4 (MATLAB signal processing toolbox 8.4, 2020) and wavelet toolbox 5.4 (MATLAB wavelet toolbox 5.4, 2020).

### *3.2.1 Experimental animals*

For this work, 4 dpf transgenic zebrafish, of unknown sex, with a pan-neuronal  $\text{Ca}^{2+}$  sensor (*elavl3:GCaMP6s*) were used. This transgenic line allowed us to compare the electrographic recording data generated here, with functional imaging data obtained from a separate study (Winter et al., 2021). Four-day post-fertilization larval zebrafish were selected as these are not considered protected vertebrates under European animal legislation and as such are ethically preferable to the use of older, protected, animals. The use of 4 dpf larval zebrafish also enabled the use of neuromuscular blocking agents and for electrophysiological recordings to be performed in the absence of a potentially confounding general anesthetic. Adult *elavl3:GCaMP6s* broodstock (Ahrens et al., 2014; kindly supplied by Dr. Misha Ahrens, Janelia Research Campus, Howard Hughes Medical Institute, Ashburn, VA) were held in aquaria at  $28 \pm 1^\circ\text{C}$  under optimal conditions for spawning. Briefly, animals were held in dechlorinated mains tap water (referred to here as “culture water”),

which was routinely monitored for water quality parameters. Fertilized eggs were collected shortly after spawning and transferred to Petri dishes which were filled

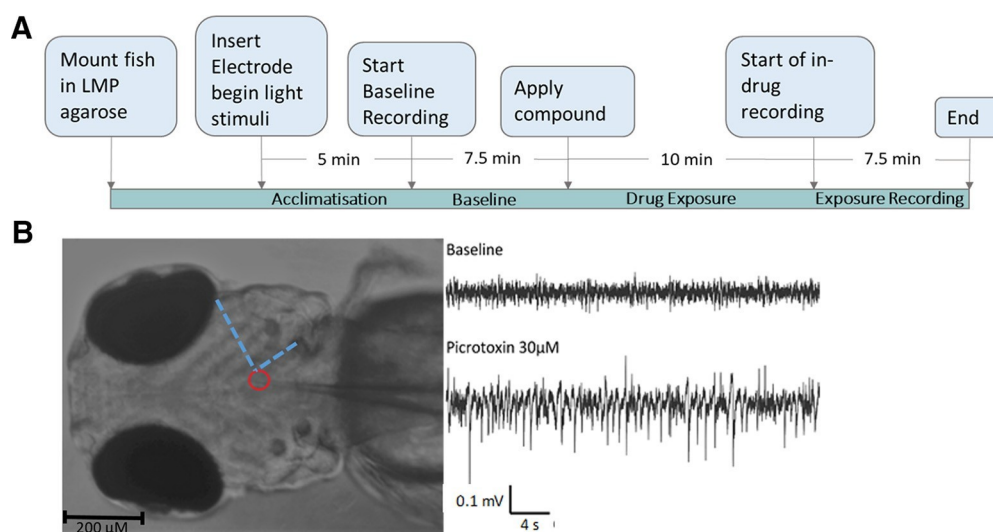


**Figure 3.1:** A schematic showing the experimental process and example data from in vivo electrophysiological recording in 4-d post fertilisation *elavl3:GCaMP6s* zebrafish larvae. A, The experimental process used. B, Left, A paralyzed, mounted zebrafish larva with glass electrode inserted into midbrain. The Red circle indicates the placement of the tip of the electrode, while the blue dashed line indicates landmarks used to consistently place the electrode. Right, local field potential recording (LFP) from midbrain of zebrafish larva at baseline and after administration of 30  $\mu\text{M}$  picrotoxin.

with culture water and held at  $28 \pm 1^\circ\text{C}$  until use in experiments at 4 dpf (for full details, see Winter et al., 2017). All work was undertaken under project and personal licences granted by the United Kingdom Home Office under the United Kingdom Animals (Scientific Procedures) Act.

### 3.2.2 Test compounds and concentration range selection

Test compounds were selected based on their known seizurogenic potential in mammals, including humans, as defined by case studies of seizure incidence and assays in model organisms as outlined in Table 3.1. Appropriate exposure concentration ranges ensuring CNS responsiveness without generalized toxicity were also selected based on previously published

data (Winter et al., 2021). The exposure conditions adopted are summarized in Table 3.1. All compounds were dissolved in extracellular solution (ECS) and pH adjusted to ~7.5 before use. The composition of ECS was: 1 mM NaCl, 2.9

Compound name	Pharmacodynamics	Concentrations used	Seizure liability
Aminophylline	Adenosine receptor antagonist and phosphodiesterase inhibitor	1, 2, 4 mM	Various cases of seizure in humans, and evidence of kindling in rats (Schwartz and Scott, 1974; Albertson et al., 1983)
Chlorpromazine	Dopamine, serotonin, histamine, Muscarinic and $\alpha$ 1- and $\alpha$ 2-adrenergic receptor antagonist	31.25, 62.5, 125 $\mu$ M	Increased risk of seizure in patients receiving anti-psychotic drug (APD) treatment, particularly polytherapy; seizure risk 5-fold higher in individuals receiving low/medium potency APDS such as chlorpromazine (Bloechliger et al., 2015; Druschky et al., 2019)
Donepezil	Acetylcholinesterase inhibitor	125, 62, 31 $\mu$ M	Among the top 10 drugs most commonly associated with seizures in World Health Organization adverse drug reaction database (Kumlien and Lundberg, 2010)
Picrotoxin	GABA <sub>A</sub> receptor antagonist	30, 60, 120 $\mu$ M	Commonly used convulsant compound used for modelling seizures (Mackenzie et al., 2002)
(RS)-(tetrazol-5-yl)glycine	NMDA receptor agonist	62.5, 125, 250 $\mu$ M	Convulsant compound used for modelling seizures (Schoepp et al., 1991)
SB205607 (TAN-67)	$\delta$ -Opioid receptor agonist	125, 250, 500 $\mu$ M	Increases incidence of convulsions in bicuculline kindled rats (Yajima et al., 2000)

Also shown are published evidence to support seizurogenicity. All compounds were sourced from Sigma-Aldrich or Tocris.

**Table 3.1** Test compounds and exposure concentration ranges used for *in vivo* electrophysiological recording in 4 dpf *elavl3:GCaMP6s* zebrafish larvae.

mM KCl, 10 mM HEPES, 1.2 mM MgCl<sub>2</sub>, 10 mM dextrose, and 2.1 mM CaCl<sub>2</sub> (Baraban, 2013). For each compound, there were three exposure concentrations, and for each experimental group, seven to eight larvae were used per treatment group. All test chemicals and other reagents were obtained from Sigma-Aldrich or Tocris.

### 3.2.3 *In vivo* LFP recordings from zebrafish brains

Individual 4 dpf larvae were paralyzed using 4 mM tubocurarine and then positioned dorsal side up in the recording chamber in 1.5% low melting point agarose containing ECS. Throughout recording, the mounted fish were kept in a static bath containing ECS. Under 4x magnification, a glass 2 M NaCl filled microelectrode (resistance of 3–5 MV) was inserted into the midbrain to record extracellular LFPs from a small network of neurons (Figure 3.1B). The area

chosen for electrode placement was based on clear anatomic landmarks, and the electrode was placed a small distance (~30 mm) lateral from the midline of the brain. This was decided on to ensure consistency of electrode placement in a specific brain area. Recordings were captured using an Axon CNS Multiclamp 700B amplifier and digitized using an Axon Digidata 1440A (Amplifier settings were Mode: I = 0, Gain: 20, Bessel: 2 kHz), and data were recorded with the Clampex 10.4 software. Following introduction of the recording electrode, larvae were equilibrated for 300 s before beginning data acquisition. The LFP recording procedure consisted of acquiring 7.5 min of baseline data following which the test compound was added to the ECS by pipette, followed by recording in the presence of compound for 17.5 min. The exposure epoch was defined as the period between 17.5 and 25 min, thus allowing 10 min for the test compound to penetrate the larva and reach equilibrium. All raw electrophysiological signals were recorded at 10 kHz, downsampled to 2 kHz and digitally filtered, using a Butterworth filter, with high pass at 1 Hz and low pass at 500 Hz, to filter out spiking activity from individual neurons while preserving LFP. Throughout recording and pre-equilibration larva were flashed with two flashes of blue light (488 nm), each lasting 100 ms and separated by a 500-ms gap, repeated every 4.5 s. This was undertaken for two purposes: to provide visual stimulation that could be detected using electrophysiology so as to ensure healthy nervous system functioning and to provide regular periodic CNS stimulation by a standard sensory pathway. Moreover, previous studies have successfully used light stimulation protocols to encourage spontaneous seizures in zebrafish expressing genes related to Dravet syndrome, thus we hypothesized it may also help to additionally sensitize animals to drug treatment (Eimon et al., 2018). Following completion of the compound exposure recording period, larval heart rate was visually assessed to confirm fish health. Additional vehicle- only experiments (identical except for no test compound exposure) were performed at regular intervals during the data acquisition phase to ensure that any changes in LFPs were not associated with the time/date of assessment.

#### *3.2.4 Data analysis: event detection*

The analysis described above was derived from averaging the activity over long periods. However, we also wanted to examine the presence of differences in the

LFP on shorter time scales, akin to examining the morphology of epileptiform spikes or rhythm. To achieve this, we algorithmically selected shorter time periods based on differences from baseline in their frequency components, which we defined as “events.” These events were defined as periods of time 1 s long whose frequency spectra deviated significantly from the baseline. Each larva has a “drug-free” baseline period and “events” that were considered significantly different from baseline were selected. In the case of control larva this “exposure period” was also a drug free baseline period. However, because of the sensitivity of the equipment used there were still some “events” that differed enough from the baseline in the control fish to be included, although compared with the drug treated fish, these were very few in number (Figure 3.4). These “erroneous” events are likely to be the result of electrical noise common in these kinds of recordings. For event detection, initially wavelet transformations were performed on the recorded voltage timeseries for both the exposure and the baseline periods to produce highly temporally resolved frequency spectra. For this a continuous 1-D wavelet transform was used, which was obtained using the analytic Morse wavelet with the symmetry parameter ( $g$ ) equal to 3, and the time-bandwidth product equal to 60, using 10 voices per octave. The frequencies of the resultant wavelets were binned into the following bands: 1–4, 4–7, 8–13, 15–30, 30–80, 80–150, and 150–500 Hz (Figure 3.2A). These bands broadly correlate with neural frequency bands used in mammalian models (Moffett et al., 2017; Wang et al., 2020) Next, the average over time in each of these frequency bands was calculated across the entire baseline period. Subsequently the Euclidean distance between the frequency spectra of every time point in the wavelets and the average baseline frequency spectra was calculated. This allowed identification of where in the wavelet transformations deviations from the mean of the baseline occurred. After plotting the resultant Euclidean distances as shown in Figure 3.2B, we used MATLAB’s findpeaks function to identify where the Euclidean distances were greater than two standard deviations from the mean of the baseline period, selecting 1s-long events. Next, taking all of the events selected using this first pass approach, the event wavelets for each fish were plotted separately in Euclidean space. From this, only the exposure events that were further from the centroid of the baseline events than the most distant baseline event, were selected. This process ensured we selected only the events whose

spectra were distinct from those that occurred during the drug-free baseline period.

### 3.2.5 Data analysis: wavelet of selected events

In order to better understand how the temporal profile of events differed between compounds, event epochs were selected from each treatment group of each compound. The events with the smallest Euclidean distance from

Frequency band	Compound	Concentration	P-value	Corrected p-value	Test statistic	Z-value
$\delta$	Chlorpromazine	62.5 $\mu\text{M}$	0.013812	0.03942	235	-2.46211
$\delta$	Chlorpromazine	125 $\mu\text{M}$	0.010224	0.035258	239	-2.56817
$\delta$	Picrotoxin	120 $\mu\text{M}$	0.013812	0.038106	235	-2.46211
$\theta$	Picrotoxin	120 $\mu\text{M}$	0.002566	0.013276	225	-3.01539
$\alpha$	Picrotoxin	120 $\mu\text{M}$	0.000544	0.003464	217	-3.45802
$\beta$	Aminophylline	2 mM	0.010089	0.036306	233	-2.57277
$\beta$	Chlorpromazine	31.25 $\mu\text{M}$	0.011825	0.037643	340	2.517311
$\beta$	Chlorpromazine	62.5 $\mu\text{M}$	0.00438	0.018126	332	2.849409
$\beta$	Chlorpromazine	125 $\mu\text{M}$	0.011825	0.036249	340	2.517311
$\beta$	Picrotoxin	120 $\mu\text{M}$	0.000442	0.003329	216	-3.51335
$\gamma$	Aminophylline	2 mM	0.002566	0.012495	225	-3.01539
$\gamma$	Chlorpromazine	31.25 $\mu\text{M}$	0.0001	0.002071	367	3.890389
$\gamma$	Chlorpromazine	62.5 $\mu\text{M}$	0.000188	0.002223	348	3.734663
$\gamma$	Chlorpromazine	125 $\mu\text{M}$	0.000053	0.004369	370	4.042954
$\gamma$	Picrotoxin	120 $\mu\text{M}$	0.00029	0.002668	214	-3.62401
$\gamma$	RST	250 $\mu\text{M}$	0.011825	0.034954	240	-2.51731
High $\gamma$	Aminophylline	2 mM	0.002566	0.011801	225	-3.01539
High $\gamma$	Aminophylline	4 mM	0.011821	0.039135	234	-2.51744
High $\gamma$	Chlorpromazine	31.25 $\mu\text{M}$	0.000081	0.002236	368	3.941244
High $\gamma$	Chlorpromazine	62.5 $\mu\text{M}$	0.000188	0.001945	348	3.734663
High $\gamma$	Chlorpromazine	125 $\mu\text{M}$	0.000053	0.002184	370	4.042954
High $\gamma$	Picrotoxin	120 $\mu\text{M}$	0.000442	0.003052	216	-3.51335
High $\gamma$	RST	250 $\mu\text{M}$	0.00293	0.012763	231	-2.975
HFO	Aminophylline	2 mM	0.001466	0.008088	222	-3.18138
HFO	Aminophylline	4 mM	0.008586	0.032303	232	-2.6281
HFO	Chlorpromazine	31.25 $\mu\text{M}$	0.0001	0.001657	367	3.890389
HFO	Chlorpromazine	62.5 $\mu\text{M}$	0.000995	0.00588	340	3.292036
HFO	Chlorpromazine	125 $\mu\text{M}$	0.000123	0.0017	366	3.839535
HFO	Picrotoxin	120 $\mu\text{M}$	0.00029	0.002401	214	-3.62401
HFO	RST	250 $\mu\text{M}$	0.004766	0.018784	234	-2.82244

**Table 3.2:** All statistical test outputs from frequency band analyses. Activity in each frequency band compared between test compound-treated and control fish using unpaired Wilcoxon rank sum test and corrected for multiple comparisons using the Benjamini and Hochberg method (Benjamini and Hochberg, 1995). The columns from left to right contain the relevant frequency band, compound, concentration of exposure, p-value, Benjamini and Hochberg corrected p-value, rank-sum test statistic, and corresponding z-statistic computed when the method is “approximate.” All statistics were undertaken using the MATLAB statistics and machine learning toolbox (MATLAB ranksum – MathWorks United Kingdom; Wilcoxon rank sum test, 2021). HFO, high frequency oscillation



the mean spectra of all the events selected for that treatment group (using the method outlined above), were selected as best representing events produced by that treatment. In addition to the presentation of the filtered timeseries, a heatmap of the wavelet transforms was also generated, as shown in Figure 3.3.

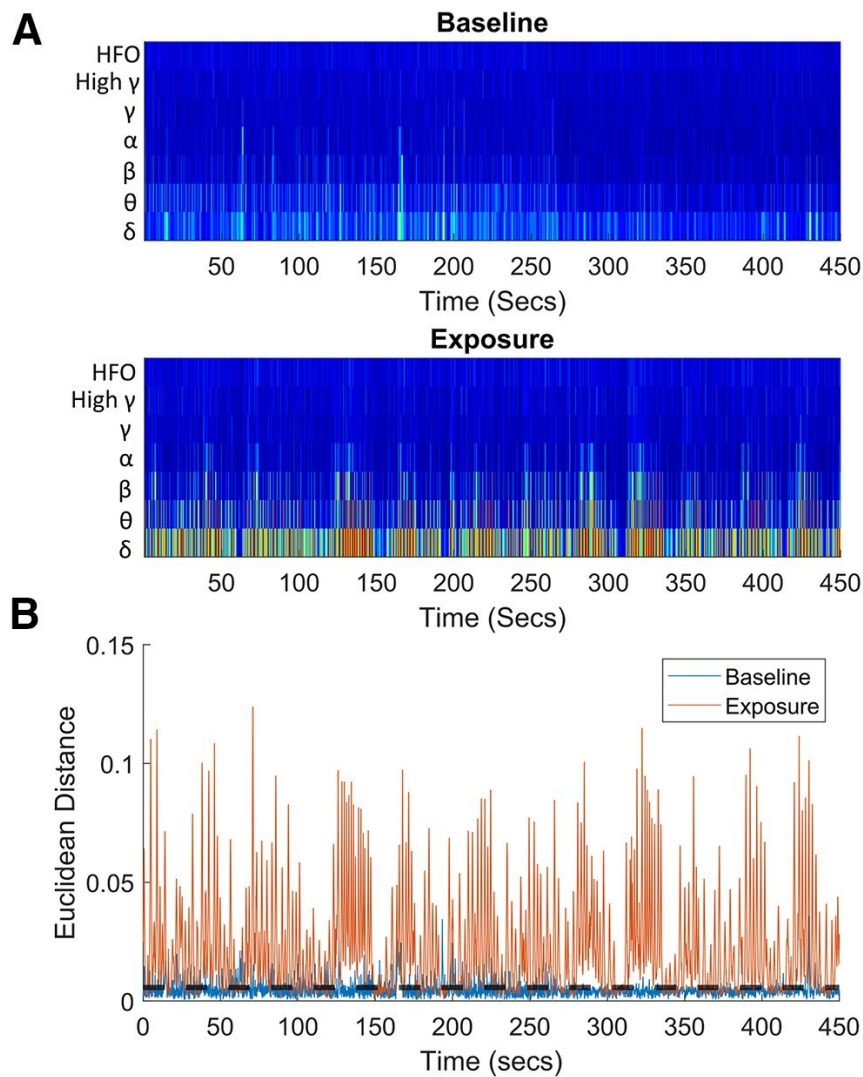


**Figure 3.2:** Example data obtained from in vivo electrophysiological recording in a 4 dpf *elavl3:GCaMP6s* zebrafish larva exposed to 62.5 mM donepezil. A, A representative frequency binned wavelet transformation from a single larva, the top graph shows the baseline and the bottom wavelet transform after drug administration. These transformations were used to identify events from the full timeseries. B, A plot of the Euclidean distance of each time point from the average of the baseline. The black dotted line represents the threshold for selecting events. All peaks above this line were selected and used to find events which were subsequently clustered.

### *3.2.6 Data analysis: number of selected events*

Moreover, the total number of detected events were calculated for each larva and compared between control and treatment groups (Figure 3.4) using a Wilcoxon rank sum test, corrected for multiple comparisons using the Benjamini and Hochberg method (Benjamini and Hochberg, 1995).

### *3.2.7 Data analysis: comparisons of area under the curve (AUC) of the LFP baseline and exposure period*

As a first step in our analyses, we aimed to assess whether the test compounds had an effect on the overall brain activity levels, over time. Seizures are associated with excessive hypersynchronous activity, therefore fish exposed to seizurogenic drugs might be expected to display a change in overall signal amplitude. The AUC was calculated, in 30-s time bins, for the absolute value of the Hilbert transform of the filtered LFP signal to allow an assessment of the “volume” of activity over time. This allowed us to visualize the time course of oscillatory activity, whether it was increasing or decreasing throughout the exposure or baseline periods (Figure 3.5A). Moreover, the total AUC over the baseline and exposure period was also calculated and a Wilcoxon signed-rank test (corrected for multiple comparisons using Benjamini and Hochberg method; Benjamini and Hochberg, 1995) was used to identify differences between baseline and drug- exposure recording epochs (Figure 3.5B).

### *3.2.8 Data analysis: spectral analysis*

Among the most commonly used approaches for assessing changes in neural activity patterns is frequency domain analysis, which allows investigation into the contribution of oscillations at different frequencies to the overall signal. Commonly in human EEG or mammalian animal model LFP datasets, oscillations are binned into bands of behavioral relevance, and changes in the power of these bands can correlate with transitions in behavioral or cognitive state (Başar et al., 2001). While the same frequency bands may not be as behaviorally relevant in zebrafish, we hypothesized that because of the similar underlying neurophysiology of mammals and zebrafish, interpreting spectral changes in the context of the same bands may provide useful insights into



underlying mechanisms of seizurogenesis. Furthermore, performing such analysis in the 4 dpf larval zebrafish served to provide a shared context which, it was hypothesized, would be important for making interspecies comparisons of electrophysiological responses to seizurogenic chemical treatment. Fourier transforms were performed on the signal from baseline and exposure periods of each fish, and the resulting spectra during each exposure period were normalized to the corresponding spectra of the baseline recordings. Next, the mean normalized spectra for each fish were averaged within treatment groups (Figure 3.6B). Finally, normalized spectra were binned into frequency bands used for studying mammalian and human EEG data (Moffett et al., 2017; Wang et al., 2020). These bands were:  $\delta$  (1–4 Hz),  $\theta$  (4–7 Hz),  $\alpha$  (8–13 Hz),  $\beta$  (15–30 Hz),  $\gamma$  (30–80 Hz) and high  $\gamma$  (80–150 Hz), and high frequency oscillations (HFO) (150–500 Hz). The activity in each band was then compared between test compound-treated and control fish using Mann–Whitney  $U$  tests corrected for multiple comparisons using the Benjamini and Hochberg method (Benjamini and Hochberg, 1995; Figure 3.6A; Table 3.2).

#### *3.2.9 Data analysis: classical multidimensional scaling (MDS) of baseline normalized spectral data*

In order to visualize the similarity or differences between representative spectra for each treatment group, classical multidimensional scaling was performed across the average normalized power spectra for each fish. Subsequently, the mean of the first two coordinates was calculated across treatments groups and plotted. The eigenvalues for these coordinates accounted for >74% of the sum of all the eigenvalues.

#### *3.2.10 Code accessibility*

The code/software described in the paper is freely available online at: <https://github.com/jp908/Ephys-Seizure-ZF>.

### **3.3 Results**

#### *3.3.1 Mean event and wavelet analysis*

The results of the mean event and wavelet analysis are summarized in Figure 3.3. Exposure to the compounds tested resulted in bursts of rhythmic activity of

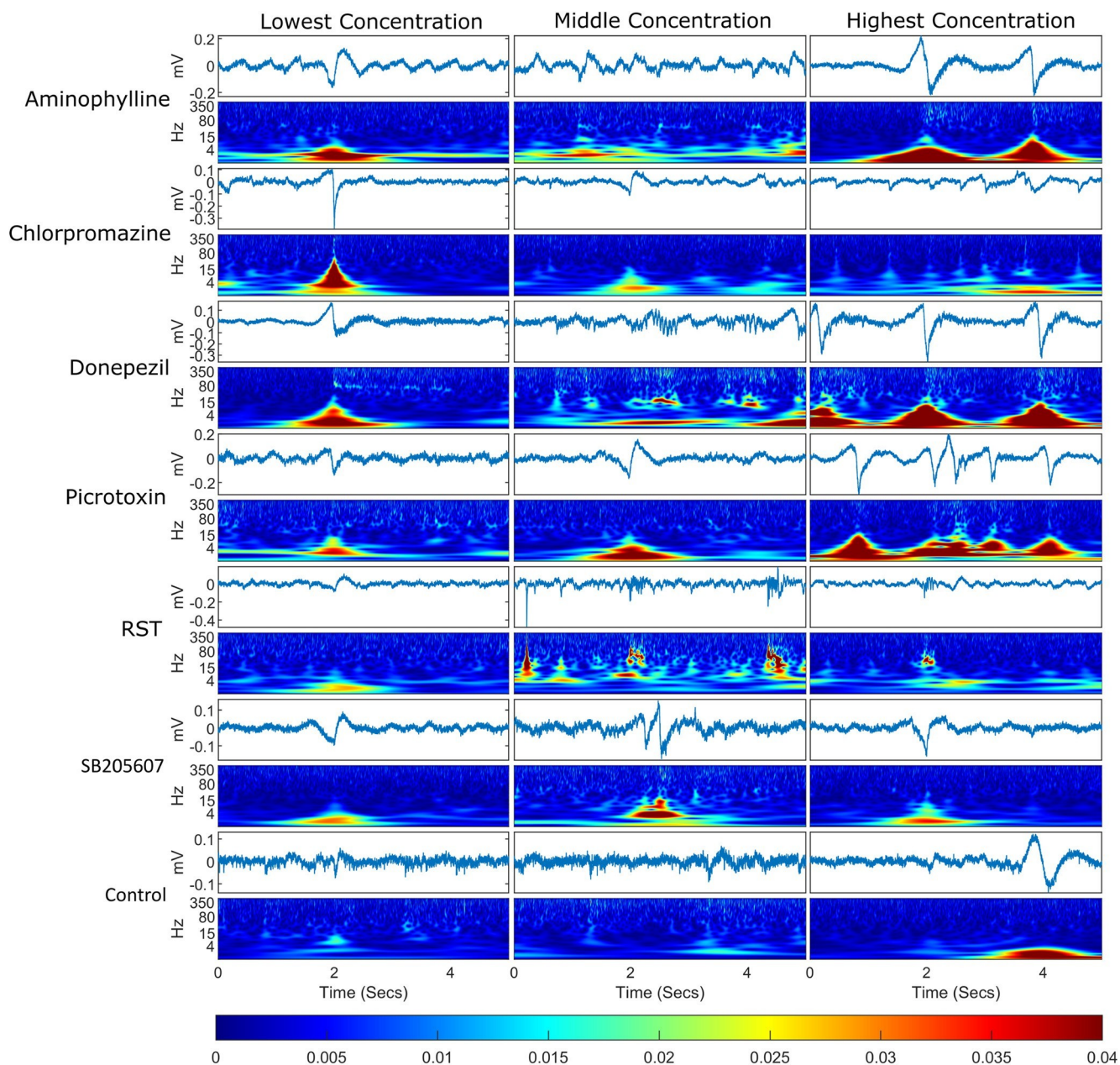


**Figure 3.3:** Example of an event plus 2 s either side for each treatment group. For each treatment group, the timeseries are displayed for each event with a wavelet transform below each one displaying the frequency domain over the same time period. The events selected were the events whose spectra were closest in Euclidean distance to the mean event spectra for that treatment group, meaning that these are representative of the events shown for each compound. The bottom bar shows the color scaling for the magnitude of the wavelet transformation. Each column represents a different concentration set and each row represents a different compound.

specific frequencies consistent with changes in the spectra observed in the previous analyses (Figure 3.6). Chlorpromazine's wavelet spectrograms, for example, showed a distinct amelioration of >80-Hz activity particularly in the higher concentrations, in addition to bursts of  $\theta$ ,  $\delta$ , and  $\alpha$  range activity. The events identified in animals exposed to donepezil were categorized by a gradual polarization followed by a large low-frequency event in the <15-Hz range with an additional high-frequency component at the peak of, and subsequent to, the main depolarization. However, there was also evidence of bursting type high-frequency activity. Picrotoxin exposure resulted in wavelet spectrograms characterized by a high-amplitude activity in the 80 Hz or less frequency range and appeared to show a distinct dose-dependent increase in activity. RST exposed animals were observed to contain a bursting type of high-frequency activity in addition to sharp spike-type discharges, as illustrated most clearly at the middle concentration. Notably RST appeared to lack much of the lower frequency component. Both aminophylline and SB205607 appeared to induce medium sized events, although notably the highest concentration of aminophylline appeared to have some similarities with donepezil's high concentration event profile.

### 3.3.2 *Number of detected events*

Exposure to aminophylline, chlorpromazine, donepezil, and RST appeared to increase the number of events detected in a dose-dependent manner (Figure 3.4). The highest concentrations of donepezil ( $p = 0.0354$ ,  $z$ -value = 2.764, test statistic = 239.5), picrotoxin ( $p = 0.0273$ ,  $z$ -value = 2.715, test statistic = 234), and RST ( $p = 0.0159$ ,  $z$ -value = -3.220, test statistic = 229.5) resulted in a significant increase in the number of detected events as compared with the control.

### 3.3.3 *Changes in AUC between baseline and exposure*

The results of the changes in AUC from baseline to exposure are summarized in Figure 3.5. Only picrotoxin ( $p = 0.0081$ , corrected- $p = 0.0104$ ,  $W = 51$ ,  $z$ -value = 2.6461) and SB205607 ( $p = 0.0006$ , corrected- $p = 0.0015$ ,  $W = 270$ ,  $z$ -value = 3.4286) exposure resulted in significant changes in AUC between the baseline

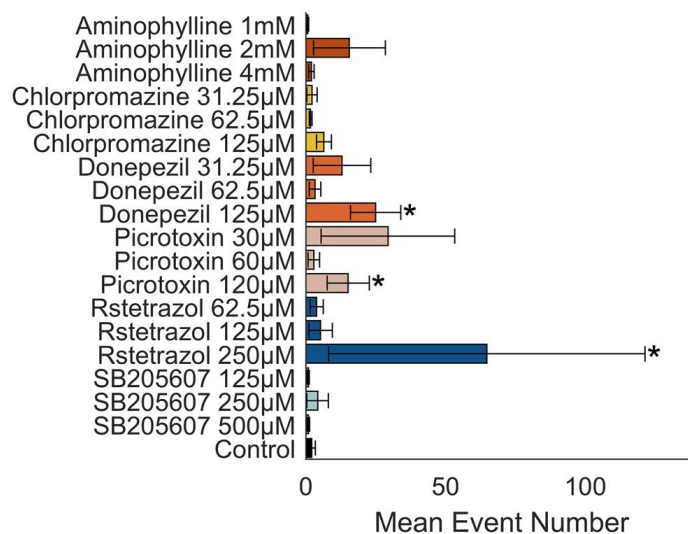


**Figure 3.4:** Mean number of events detected per treatment group. Bar graph showing the mean number of events per treatment group. Error bars represent the SEM (n = 7–8). Asterisks adjacent to the bars indicate a statistically significant difference from control (p < 0.05) using a Wilcoxon rank sum test corrected for multiple comparisons using the Benjamini and Hochberg method.

and exposure periods, exhibiting increased and decreased AUC, respectively. The AUC of picrotoxin appeared to oscillate slightly across 30s time bins with a slight upward gradient.

### 3.3.4 Spectral frequency band analysis

The results of the spectral analysis of the *in vivo* LFP data are summarized in Figure 3.6 and Table 3.2. From these data, it can be seen that exposure to the highest concentrations of chlorpromazine and picrotoxin resulted in a significant increase in activity in the slower  $\delta$ -frequency band compared with the control animals. In the higher frequency  $\gamma$ , high  $\gamma$ , and HFO bands, significant increases in activity were observed after exposure to (RS)-(tetrazol-5-yl)glycine (RST), picrotoxin and aminophylline. Interestingly, exposure to chlorpromazine resulted in significantly reduced,  $\beta$ ,  $\gamma$ , high  $\gamma$ , and HFO band activity at all of the concentrations tested, and this was not observed for any other compounds assessed here. Exposure to SB205607 and donepezil resulted in no significant changes in any of the frequency bands measured. In addition, exposure to picrotoxin resulted in increases in  $\alpha$  band oscillatory activity, while

aminophylline and picrotoxin exposure resulted in increases in  $\beta$  power. Notably, picrotoxin resulted in an increase in power in every single frequency band, but only at the highest concentration.

### 3.3.5 Classical MDS

Classical MDS of the spectral data revealed the distribution of each treatment

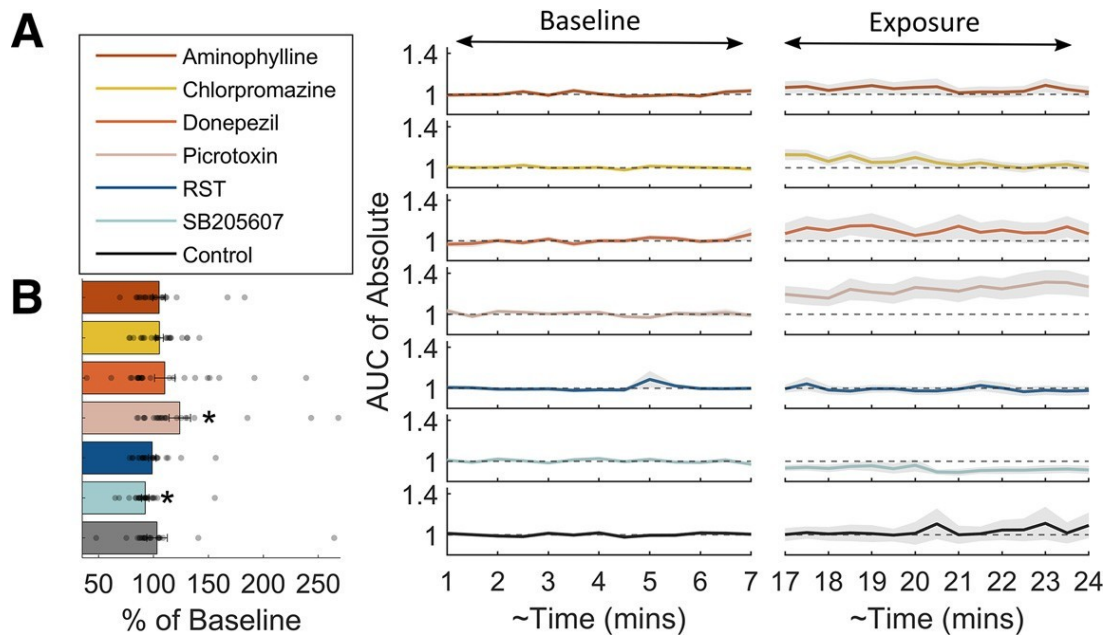


**Figure 3.5:** Analysis of the AUC of the Hilbert transform of the LFP recordings. *A*, Mean baseline normalized AUC of the absolute value of the Hilbert transform of the LFP averaged into 30-s time bins. The shadows represent the SEM ( $n = 20-24$ ). The left-hand side of the graph represents the baseline period, while the right-hand side represents the exposure period. The gap in time from 7 to 17 min is time allotted for compounds to take effect. *B*, Shows the baseline normalized AUC for each of the compounds tested. The bars show the normalized AUC averaged across all treatment groups for each compound, while the normalized AUC of individual larvae are represented as transparent grey circles. Data are shown as the mean with error bars depicting the SEM ( $n = 20-24$ ). An asterisk indicates a statistically significant difference between baseline and exposure periods ( $p < 0.05$ ) using Wilcoxon signed-rank test and corrected for multiple comparisons using the Benjamini and Hochberg method (Benjamini and Hochberg, 1995).



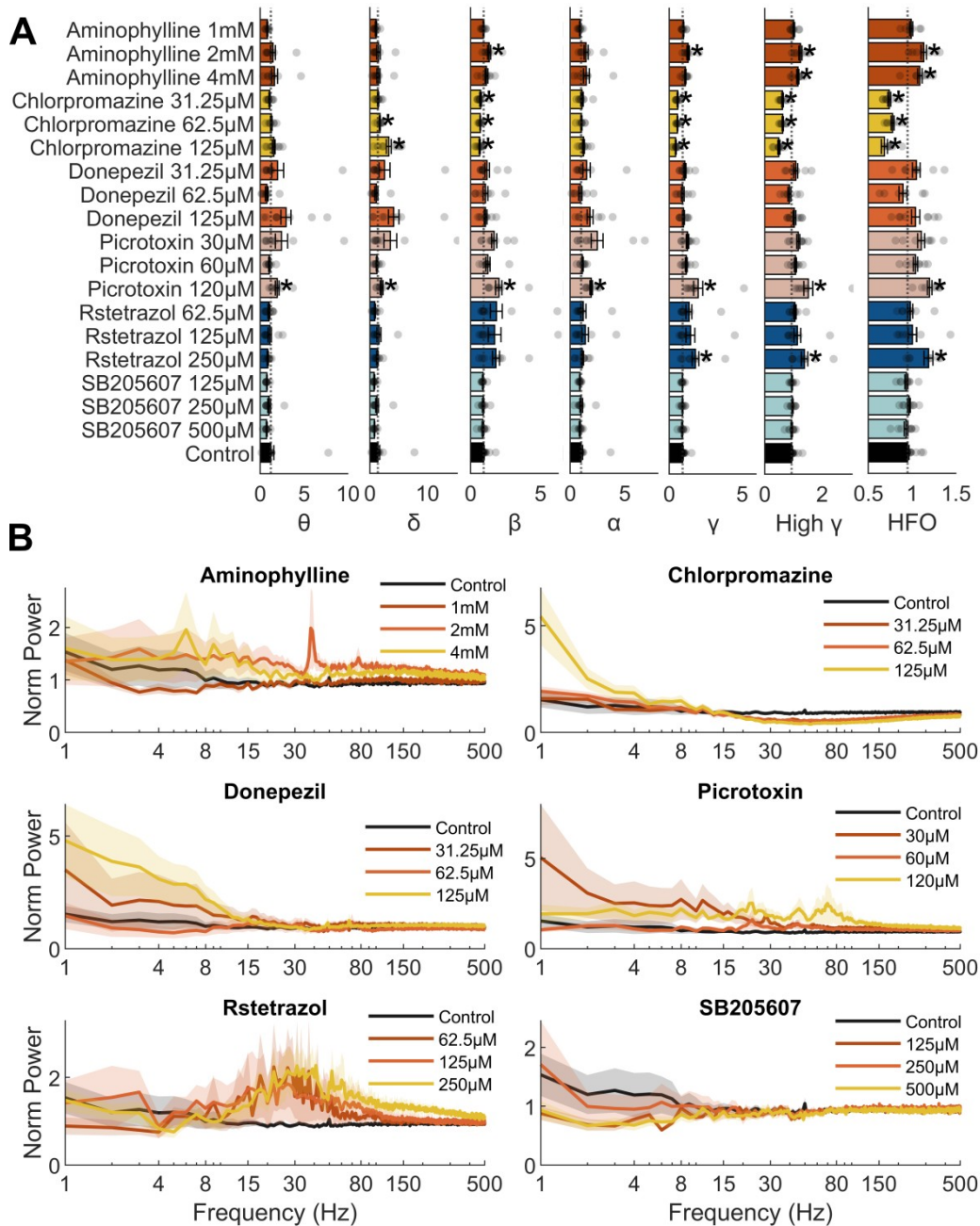


**Figure 3.6:** Data generated for larvae exposed to each of the test compounds after spectral analysis and categorization into specific frequency bands. A, The bars show the baseline normalized mean amplitude for each of the neural frequency bands frequently used for categorizing mammalian electrophysiological data (Moffett et al., 2017; Wang et al., 2020). Data are shown as the mean with error bars showing the SEM ( $n = 7-20$ ). The baseline normalized power for individual larvae are represented by the transparent grey circles. An asterisk indicates a statistically significant difference from control ( $p < 0.05$ ) using Mann–Whitney U tests and corrected for multiple comparisons using the Benjamini and Hochberg method (Benjamini and Hochberg, 1995). B,

Mean baseline normalized power spectra for each compound treatment group. In this case the x-axis is scaled to the common logarithm. Shading represents the SEM for each data point (n = 7–20) across the power spectra. Black lines here indicate the mean of the control animal power spectra and therefore are the same for each graph.

group in two dimensions. The outer regions of the resultant scatter plot (Fig. 3.7) are occupied by the highest concentration of chlorpromazine, donepezil, RST, and picrotoxin. Notably, there was overlap of the middle concentration of aminophylline and picrotoxin, likely because of similar increases in  $\beta$ ,  $\gamma$ , and high-frequency oscillations. SB205607 and the lowest concentration of aminophylline lie closest to the control reflecting the relative absence of induced effects on the parameters measured. The highest concentration of chlorpromazine is located furthest from RST and picrotoxin likely reflecting its reduction in oscillations at >15 Hz. Furthermore, RST and picrotoxin are located on the right-hand side of the scatterplot likely because of their notable induced increases in the magnitude of oscillations at >15 Hz.

### **3.4 Discussion**

Using *in vivo* mid-brain LFP recordings in 4 dpf larval zebrafish, we demonstrate responsiveness to a range of pharmacological agents implicated in the induction of seizures in mammals. The data we present show that exposure to chlorpromazine (a phenothiazine antipsychotic), donepezil (an acetylcholinesterase inhibitor), picrotoxin (a GABA<sub>A</sub>R antagonist) and RST (an NMDAR agonist) results in quantifiable, concentration-dependent, altered neuronal electrophysiology. Furthermore, the electrographic responses exhibited differed between each drug, and in some cases exhibited characteristics commensurate with the induction of interictal and ictal electrophysiology phenotypes similar to those classified in humans (Fisher et al., 2014b).

#### *3.4.1 Electrographic phenotypes of representative traces*

Although seizure phenotypes from electrographic recordings are extremely diverse, the main aim of our study was to explore what “abnormal” LFP recordings might emerge following exposure of zebrafish larvae to drugs acting via known seizurogenic mechanisms. Furthermore, from these phenotypes, we

aimed to classify such patterns in the context of their frequency components, and to compare these components to human EEG data and models of seizure in mammals. To this end, we compared the representative traces that were selected using our event detection algorithm with specific examples of preictal, interictal, and ictal type waveforms, as reported previously (Fisher et al., 2014b). The representative trace for the highest concentration of chlorpromazine, for example, appeared to comprise of rhythmical evolving  $\theta$ ,  $\delta$ , and  $\alpha$  frequencies, which is an electrophysiological phenotype commonly seen

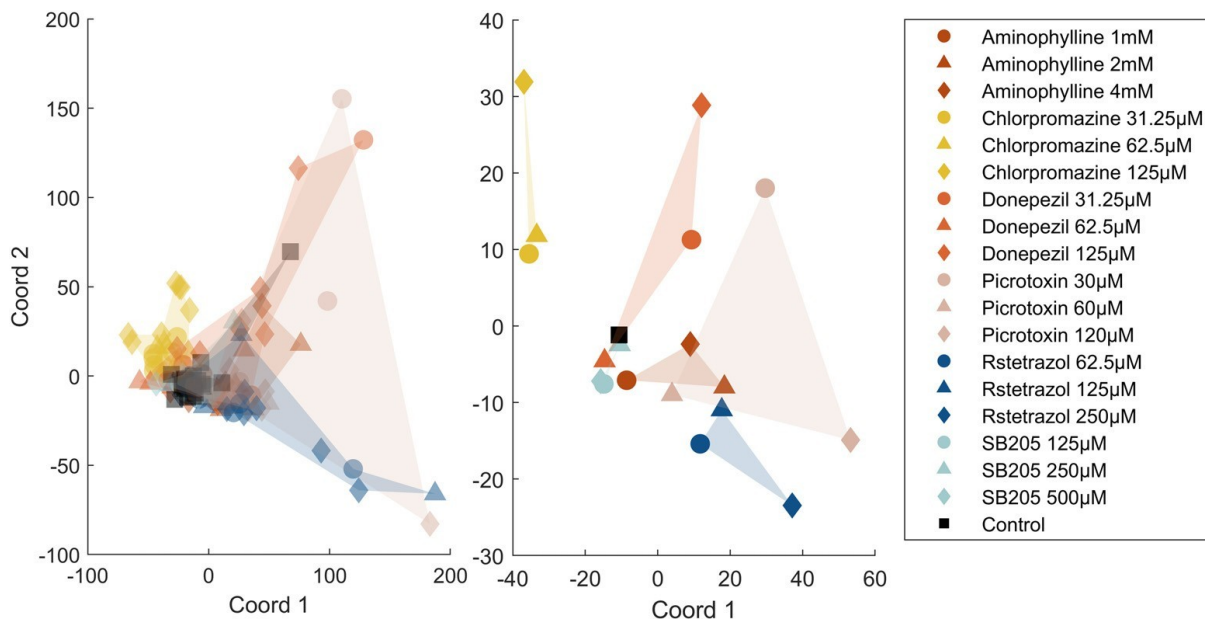


**Figure 3.7:** Multi-dimensional scaling (MDS) of the normalized power spectra. Left-hand image, A scatter graph of the first two co-ordinates produced after classical MDS of each individual larva. In both plots, the circles represent the lowest concentration, the triangles the middle concentration, and the diamonds the highest concentration used for each treatment group. The black square represents the control group. Right-hand image, A scatter graph of the first two coordinates produced after classical MDS of the mean normalized power spectra of each treatment group (see Fig. 6B).

preceding seizure in EEG traces recorded clinically (Fisher et al., 2014b). Similarly, the high-amplitude, high-frequency, discharges observed in the representative traces for the intermediate exposure concentrations for both donepezil and RST share similarities with intracerebral stereo-EEG recordings of seizures reported in mammals (Fisher et al., 2014b). These discharges also contained very high-frequency (80–500 Hz) components similar to examples of



seizures reported previously in mammals (Gliske et al., 2017; Jiruska et al., 2017, 2013; Mackenzie et al., 2002; Shiri et al., 2015). The representative traces for the highest concentration of aminophylline, in addition to that seen for the lowest and highest concentrations of donepezil, appear consistent with electrocromental EEG patterns, a electrophysiological phenotype commonly seen preceding seizure in EEG traces recorded clinically (Fisher et al., 2014b).

Qualitative comparisons of representative traces for the highest concentration of aminophylline, donepezil, and picrotoxin in our study, with traces of spontaneous ictal and interictal activity identified by (Griffin et al., 2021) in their recording of LFPs in zebrafish (where they were screening for potentially seizurogenic genetic modifications), showed strong similarities. Moreover, the traces for the medium and high concentrations of RST appeared similar to their definition of an ictal-type waveform. These similarities support a good degree of consistency between drug induced seizures and spontaneous seizures, although a more extensive comparison would be necessary to confirm this. Compared with behavioral and imaging-based assessments of seizures in zebrafish (Afrikanova et al., 2013; Alfaro et al., 2011; Baraban et al., 2013b; Burgstaller et al., 2019; Winter et al., 2021, 2017, 2008), *in vivo* LFP recordings provide a direct measure of the electrographic response of model organisms to neuroactive drug treatment. This is important as the data generated more readily allows comparisons between model species (Table 3.3), a feature which is crucial for evaluating the translational power of the zebrafish as a surrogate for understanding the effects of neuroactive drugs in higher vertebrates, including humans.

#### 3.4.2 *Trace amplitude and seizure*

Given that seizures are high-amplitude events, measuring the change in the average AUC induced by the different compounds was initially undertaken. Notably the largest increase in AUC was observed after exposure to picrotoxin which is commonly used in animal models as a seizure precipitant (Baraban, 2013; Fan et al., 2019; Ridler et al., 2018; Winter et al., 2008). This is consistent with previous studies in zebrafish exposed to picrotoxin that reported the presence of high-amplitude events (Baraban, 2013). Interestingly, however, the NMDA-receptor agonist RST, which is also a

well-known model convulsant, induced no change in AUC despite inducing changes in other measured parameters. It is worth noting that seizure like states are often characterized by periods of bursting activity with intermittent quiescence (Barnett et al., 2013). In this context, it is possible that periods of seizure-like activity induced via RST are bursting in nature, with long intervals in between and, and thus not best detected using our protocol. In support of this, on a more detailed analysis of the spectral components of its electrographic signature, the resultant data suggested that RST exposure was associated with elevated neural activity in specific frequency bands, rather

Compound	Effects observed in 4-dpf zebrafish LFP recordings undertaken in this study	Effects reported from EEG recordings undertaken in mammals
Aminophylline	Increase in the amount of $\beta$ and $\gamma$ oscillations (Fig. 6) and the presence of electrodecremental type preictal discharges (Fig. 3).	Little frequency domain analysis of EEG exists for aminophylline; however, visual assessment of EEG traces from rats exposed to high doses of aminophylline show epileptiform discharges of high amplitude and frequency (Chu, 1981).
Chlorpromazine (antipsychotic)	We observed a significant reduction in all of the frequency bands >15 Hz on exposure to chlorpromazine (Fig. 6).	Antipsychotic medications haloperidol and clozapine significantly reduce $\gamma$ power (Olszewski et al., 2013; Sun et al., 2020).
Donepezil	Apparent increase in theta oscillations (the largest mean difference of all the compounds) although it did not reach statistical significance (Fig. 6). Events with a large $\theta$ component (Fig. 3).	Rats exposed to Donepezil show increases in cortical EEG oscillations in the $\theta$ frequency band (Ahnaou et al., 2014).
Picrotoxin	Significant increases in gamma, fast $\gamma$ activity, and high-frequency oscillation amplitude (Fig. 6). This is consistent with studies showing high-frequency bursting type LFPs (Baraban, 2013).	Picrotoxin increases $\gamma$ oscillations in the olfactory bulb, an effect that could be suppressed via inhibition of ionotropic glutamate receptors (Lepousez and Lledo, 2013). Mouse brain slices show induction of HFOs via picrotoxin exposure (Shiri et al., 2015).
RST	Significant increases in $\gamma$ and fast $\gamma$ activity (Fig. 6).	In rats, NMDA agonists induce acetylcholine release and affect an increase in both beta and $\gamma$ oscillations in the basal forebrain (Fournier et al., 2004).
SB205607	Few effects of SB205607 on LFP in zebrafish.	No studies found for the electrophysiology of SB205607 in mammals.

**Table 3.3** Summary of information comparing the effect of selected drugs on EEG in mammals from published data with the data obtained for zebrafish in this study.

than showing a more generalized elevated activity. In a previous study using  $\text{Ca}^{2+}$  imaging (Winter et al., 2021), a relative absence of oscillatory activity after exposure to RST (and the pharmacologically similar NMDA) was also reported. Given that here we saw elevated activity only in the >15-Hz frequency range (see below), and notwithstanding the sensitivity of  $\text{Ca}^{2+}$  dye-based imaging, it is possible that in the previous study, the temporal resolution of the imaging-based approach used was insufficient to capture such rapid

oscillations thus highlighting the relative advantages and disadvantages of each type of approach when studying drug-induced neuronal events.

### 3.4.3 *Neural oscillations of zebrafish versus mammals*

The binning of generated frequency spectra into specific frequency bands is a commonly used approach in the analysis of mammalian electrophysiological data (Başar et al., 2001). We adopted this approach primarily to directly compare neural activity signatures between 4 dpf larval zebrafish and mammalian models of drug-induced seizures. It should be noted that we consider the changes seen in the different frequency bands for all drugs to be as

a result of bursts of rhythmic activity. This means there are both periodic and aperiodic contributions to the frequency spectra. We believe this is the case, because the event detection algorithm utilized here identified bursts of rhythmic activity whose spectra were consistent with the frequency spectra performed on the full recordings. Moreover, the number of these events was not adequate to constitute the full traces. As such our analyses suggested that drug exposure resulted in transient bursts of rhythmic activity that altered the overall spectral profile of the recordings, as opposed to sustained oscillatory activity.

In multiple EEG studies undertaken in mice, the antipsychotic medications haloperidol and clozapine have been shown to significantly reduce  $\gamma$  power (Olszewski et al., 2013; Sun et al., 2020). Here, we also observed a significant reduction in all of the frequency bands of  $>15\text{Hz}$  on exposure to chlorpromazine. Both chlorpromazine and haloperidol broadly reduce monoamine signaling, a neurotransmitter subgroup that is highly conserved between larval zebrafish and mammals in both their molecular underpinnings and behavioral functionality (Maximino et al., 2016). Indeed, haloperidol has been shown to induce locomotor impairments in zebrafish, an effect mirrored in the common side effects in humans (e.g., drowsiness, dizziness, and neuromuscular dysfunction; Giacomini et al., 2006). Chlorpromazine has also been shown to induce significant alterations in 4 dpf larval brain functional connectivity (Winter et al., 2021), and our data here also show comparable oscillatory activity induced by this antipsychotic compound between zebrafish and mammals. The confirmation here of shared brain oscillatory changes, in

addition to the aforementioned similar behavioral manifestations, suggests that the established links between neural frequency bands and mammalian behavior may have some translatability to zebrafish.

Exposure to the acetylcholinesterase inhibitor donepezil increased power in the  $\theta$  frequency bands in larval zebrafish. In mammals,  $\theta$  and  $\gamma$  oscillations are associated with successful memory recall (Barnett et al., 2013). Notably, a mechanistically similar compound and cholinesterase inhibitor, physostigmine, has been shown to reverse scopolamine-induced learning impairment in zebrafish, suggesting effectiveness in reversing impaired cognition (Kim et al., 2010a). In this context it would be interesting to assess the behavioral response of zebrafish to donepezil specifically given the apparent enhancement of  $\theta$  oscillations in the electrophysiology data we present here. Indeed, observation of donepezil-induced cognitive enhancement in larval zebrafish would provide further evidence of a similar relationship between brain oscillatory patterns and behavioral manifestations in larval zebrafish as those observed in mammals.

Perturbations in oscillations in the  $\gamma$  and high  $\gamma$  ranges are common across a variety of psychiatric disorders, including attention deficit hyperactivity disorder, schizophrenia and, of particular relevance here, epilepsy (Herrmann and Demiralp, 2005). Epilepsy specifically is associated with an increase in  $\gamma$  oscillations likely because of cortical excitation (Herrmann and Demiralp, 2005). Indeed, in human EEGs, oscillations in the  $\gamma$  and fast  $\gamma$  range precede interictal epileptiform spikes in the seizure onset zone (Jiruska et al., 2013). Similarly, in the nucleus accumbens of rats, there are increases in  $\gamma$  power when seizure kindling is induced using kainic acid (Ma and Leung, 2010). Here, we observed significant increases in  $\gamma$  and fast  $\gamma$  activity after exposure to the two seizure precipitants picrotoxin and RST, in addition to aminophylline. Previously published work in mice has shown that treatment with picrotoxin has been shown to increase  $\gamma$  oscillations in the olfactory bulb, an effect that could be suppressed via inhibition of ionotropic glutamate receptors (Lepousez and Lledo, 2013). In addition, in rats, NMDA agonists induce acetylcholine release and affect an increase in both  $\beta$  and  $\gamma$  oscillations in the basal forebrain (Fournier et al., 2004). In our study, both picrotoxin and RST appeared to induce abnormal electrographic events, similar to those recorded in previous studies in zebrafish

(Afrikanova et al., 2013; Baraban et al., 2005; Copmans et al., 2019; Hortopan et al., 2010; Löscher, 2017) and consistent with seizures observed in human EEG (Fisher et al., 2014b). Notably our data suggest that these events, much like in humans and rats, were characterized by an increase in  $\gamma$  and high- $\gamma$  frequency oscillations. The fact that chlorpromazine appeared to uniquely reduce  $\gamma$  and high  $\gamma$  oscillations is interesting and raises the issue of primary versus secondary pharmacological activity and dosing levels. Certainly, chlorpromazine is known to have potent sedative effects linked to its well-known  $H_1$  activity (von Coburg et al., 2009) and is typically associated with a seizure-threshold lowering effect rather than a direct seizurogenic effect as measured using our exposure method (Chi et al., 2017).

The highest frequency band we measured, in the range between 150 and 500 Hz, contained HFOs (Wang et al., 2020). HFOs are strongly correlated with the epileptogenic zone and have been implicated as a useful biomarker of epilepsy (Lévesque and Avoli, 2019), although their use to prospectively define the epileptogenic zone is not clear (Jacobs et al., 2018). Indeed, fast ripples (250–500 Hz) appear to be highly indicative of epileptic tissue in both human conditions and animal models (Jiruska et al., 2013). HFOs are believed to occur as a result of the synchronization of fast firing within populations of interconnected neurons generating high-frequency population spikes which, when recorded extracellularly, present as an HFO event (Jiruska et al., 2013). Individual pyramidal neurons cannot fire fast enough to account for oscillations higher than 300 Hz, thus, fast ripple oscillations have been proposed to be generated via the action of synchronized, but out-of-phase, neurons (Jiruska et al., 2013). Here, a significant increase in the magnitude of HFOs was observed after exposure to aminophylline, picrotoxin, and RST, while chlorpromazine appeared to reduce the magnitude of HFOs. This is consistent with studies in mouse brain slices showing induction of HFOs via picrotoxin exposure (Shiri et al., 2015). Moreover, automated event detection designed to categorize events unique from baseline identified several events across these compounds that contained HFOs, including after exposure to donepezil, RST, and picrotoxin across all concentrations.

#### 3.4.4 *Study limitations*

Exposure to the d-opioid agonist, SB205607, showed little evidence of altered brain electrophysiology despite showing significantly elevated activity in multiple brain regions at 500 nM (the top concentration used here) in an imaging-based assessment undertaken in 4 dpf zebrafish (Winter et al., 2021). Other studies have reported insensitivity of the larval zebrafish to specific d-OR agonists such as SNC80 (Rodriguez and Gonzalez-Nunez, 2006) although this does not explain why previous work with SB205607 suggested some degree of neuroactivity (Winter et al., 2021). One possible reason for this could be explained by the relative strengths and weaknesses of electrophysiological versus imaging-based neural functional assessments. Electrophysiological assessment offers unparalleled levels of temporal resolution, whereas the imaging-based approach offer much greater spatial coverage. Given the LFP approach used here measures electrical activity in a small population of neurons in one part of the brain it is possible that this region was not activated by SB205607 exposure. Certainly, this would be supported by the data from our Ca21 imaging work (Winter et al., 2021), which suggested comparatively low levels of activity in midbrain regions compared with the hind brain. This could be investigated further by the use of multielectrode arrays to allow for greater spatial coverage during LFP recordings (Hong et al., 2016).

Despite the existence of notable similarities between the LFPs recorded in zebrafish and mammalian electrophysiology data, there are limitations to the larval zebrafish as a model. Specifically, *in vitro* LFP recordings taken in mammals are often performed on specific anatomic structures which in the case of seizure and epilepsy research are recognized as hyper-excitatory in nature, such as the hippocampus. In zebrafish larvae, recording from specific brain structures is extremely challenging due the small size of the brain, thus recordings are generally taken from the midbrain or the forebrain with little ability to differentiate between specific sub regions of higher or lower relevance. In this respect, the use of genetically modified models in which specific neural circuits or populations are labelled may prove useful and allow more precise placement of electrodes in structures that have been identified as especially appropriate for measuring the type of brain activity being investigated.

In summary, *in vivo* LFP-mediated assessment of neural activity in 4 dpf zebrafish larvae revealed responsiveness to seizurogenic compounds that act via a range of pharmacological mechanisms of action. Furthermore, the resultant electrographic profiles exhibited by 4 dpf zebrafish larvae exposed to multiple these compounds show clear differences in their characteristics and in some cases share notable similarities with the signatures exhibited by mammalian, including human, electrophysiological profiles. The data generated here add to the body of data supporting the use of the larval zebrafish as a complimentary and potentially alternative model for the study of seizures and epilepsy and also provide further insight into the electrophysiological characteristics of seizures generated in non-mammalian species.

## Chapter 4: The development and application of a within animal control-based approach for improving the sensitivity and specificity of functional brain imaging in larval zebrafish.

### 4.1 Introduction

The methodology used in Chapter 1 revealed the responsiveness of the 4 dpf larval zebrafish to a wide range of chemicals known to induce neural network hyperactivity (seizure-like electrical activity) in other non-clinical animal models, or in some cases (for small number of marketed drugs) after use in a clinical setting. In this work we were able to identify spatiotemporal patterns of activity common to specific drug mechanisms and relate these to current understanding of zebrafish physiology. Moreover, we were able to measure changes in brain functional connectivity identifying the presences of brain hyper-connectivity for multiple seizurogenic compounds.

However, there was a great deal of variability within the data generated, particularly with regard to the GCaMP expression and resultant fluorescence. The experimental design used in the studies in Chapter 2 relied upon the upfront application of the test chemicals to animals across a range of concentrations predefined from pilot work to define MTC, followed by light sheet microscope imaging. The set up for the light sheet microscope initially precluded the use of a within animal experimental design due to the necessity to use a capillary tube for mounting larva. As such animals would be insulate from *in situ* drug addition by t the glass walls of the capillary tube. Therefore, separate (untreated) control animal groups were used, against which drug exposed animal responses were assessed. Some initial investigations were carried out for conducting within animal controls with this original system (based on Ahrens et al., 2013) by pushing animals out of the end of the capillary tube in a syringe-like manner. This was unsuccessful as this process appeared to result in poor fish health which was reflected by the functional imaging outputs.

We then developed a new approach using an m-squared aurora system. This system has the advantage that the sample (the larva) is loaded onto a flat surface in agarose, rather in a glass capillary, and therefore an initial (baseline)



assessment of neural function can be obtained followed by application of the tests chemical and the assessment of post exposure activity in the same animals. This approach is considered optimal in experiments involving drug application, although data in zebrafish in the literature following this approach are extremely limited. In mammalian models however, baseline recordings are the norm to assess physiological brain function prior to chemical application (Ridler et al., 2018).

The purpose of this chapter was to build upon the methodology developed in Chapter 2, with the goal of improving and refining our approach to  $\text{Ca}^{2+}$  imaging in larval zebrafish. By using a selection of the same compounds used in chapters 1 and 2, it was possible to compare directly between electrographic and imaging-based approaches for assessing drug induced neural signatures, allowing for cross-validation of the two different approaches. Moreover, we aimed to improve the sensitivity and specificity of the approach by comparing baseline with post-exposure outputs in the same animals. Furthermore, the use of the m-squared aurora system facilitated a doubling of the temporal resolution achievable with the same imaging conditions. This allowed gathering a 10-z-slice whole brain volume in around 800 ms, enabling investigation of the impact of increased acquisition speed on the profile of activity obtained. The same image processing template was used as previously, in which brain regions were anatomically derived, and ROI-specific GCaMP fluorescence data extracted, in addition, functional connectivity analysis was undertaken with additional graph theoretical network measures.

Overall, and as before, the aim was to better understand how seizurogenic drugs pharmacodynamics manifest in the larval zebrafish brain. Further, the aim was also to assess if the effect of drug action on fluorescence correlated with the current understanding of larval zebrafish physiology, in particular with regard to drug receptor location. The final aim was to understand the effect of seizurogenic compounds on measures of brain network activity, and to assess if these correlated with similar effects of the drugs tested in mammals.

## 4.2 Methods

### 4.2.1 *Experimental animals*

For this work, 4 dpf transgenic zebrafish, of unknown sex, with a pan-neuronal Ca<sup>2+</sup> sensor (*elavl3:GCaMP6s*) were used. 4 dpf larval zebrafish were selected for use as these are not considered protected vertebrates under European animal legislation and as such are ethically preferable to the use of older, protected, animals. The use of 4 dpf larval zebrafish also enabled the use of neuromuscular blocking agents and for Ca<sup>2+</sup> recordings to be performed in the absence of a potentially confounding general anaesthetic.

Adult *elavl3:GCaMP6s* broodstock were held in dechlorinated mains tap water (culture water), which was routinely monitored for water quality parameters. Fertilized eggs were collected shortly after spawning and transferred to Petri dishes which were filled with culture water and held at 28 ± 1°C until use in experiments at 4 dpf (for full details, see Winter et al., 2017). All work was undertaken under project and personal licences granted by the United Kingdom Home Office under the United Kingdom Animals (Scientific Procedures) Act.

### 4.2.2 *Test compounds and concentration range selection*

Test compounds were selected based on their known seizurogenic potential in mammals, including humans, as defined by case studies of seizure incidence and assays in model organisms as outlined in Table 4.1. Appropriate exposure concentration ranges ensuring CNS responsiveness without generalized toxicity were also selected based on previously published data (Chapter 2:, Winter et al., 2021). The exposure conditions adopted are summarized in Table 4.1. All compounds were dissolved in culture water and pH adjusted to ~7.5 before use. For each compound, there were three exposure concentrations, and for each experimental group, seven to eight larvae were used per concentration. Controls were performed daily in order to have controls representative of all spawning groups and daily experimental conditions. A total of 43 control larvae were imaged. All test chemicals and other reagents were obtained from Sigma-Aldrich or Tocris.

Compound Name	Pharmacodynamics	Concentrations used	Seizure liability
Aminophylline	Adenosine receptor antagonist and phosphodiesterase inhibitor	1, 2, 4 mM	Various cases of seizure in humans, and evidence of kindling in rats (Albertson et al., 1983; Schwartz and Scott, 1974)
Chlorpromazine	Dopamine, serotonin, histamine, Muscarinic and $\alpha_1$ and $\alpha_2$ -adrenergic receptor antagonist	31.25, 62.5, 125 $\mu$ M	Increased risk of seizure in patients receiving anti-psychotic drug (APD) treatment, particularly polytherapy; seizure risk 5-fold higher in individuals receiving low/medium potency APDS such as chlorpromazine (Albertson et al., 1983; Druschky et al., 2019)
Donepezil	Acetylcholinesterase inhibitor	125, 62, 31 $\mu$ M	Among the top 10 drugs most commonly associated with seizures in World Health Organization adverse drug reaction database (Kumlien and Lundberg, 2010)
Picrotoxin	GABA <sub>A</sub> receptor antagonist	30, 60, 120 $\mu$ M	Commonly used convulsant compound used for modelling seizures (Mackenzie et al., 2002)
PTZ	GABA <sub>A</sub> receptor antagonist	5, 2.5, 1.25mM	Commonly used seizure precipitant (Samokhina E & Samokhin A., 2018 )
(RS)-(tetrazol-5-yl)glycine	NMDA receptor agonist	62.5, 125, 250 $\mu$ M	Convulsant compound used for modelling seizures (Schoepp et al., 1991)
SB205607 (TAN- 67)	$\delta$ -Opioid receptor agonist	125, 250, 500 $\mu$ M	Increases incidence of convulsions in bicuculline kindled rats (Yajima et al., 2000)

**Table 4.1:** Test compounds and exposure concentration ranges used for *in vivo* Ca<sup>2+</sup> light sheet imaging, in addition to evidence of seizure liability as reported from the literature sources listed. Reproduced and expanded from (Pinion et al., 2022).

#### 4.2.3 *In vivo* Ca<sup>2+</sup> light sheet imaging

The aim was to generate equally sized datasets of  $n = 8$  animals per treatment in our exposures. These were run over at least four separate days with the same number of batches of larvae. The nicotinic acetylcholine antagonist tubocurarine was selected as a neuromuscular blocker in part due to its stable and long duration of action (Appiah-Ankam and Hunter, 2004) and was applied at a concentration of 4 mM in order to paralyse fish and prevent movement artefacts as in previous functional imaging studies (Favre-Bulle et al., 2018; Miyazawa et al., 2018; Tao et al., 2011; Vanwalleghem et al., 2020). Each larva was transferred to an aqueous mixture of tubocurarine (4 mM) until muscle tone

was lost (typically ~1 min), then moved to tubocurarine in 1% low melting point agarose and positioned on a bespoke 3d printed epoxy recording chamber labelled as **(a)** in Figure 4.1. The larva was repositioned to be at a 45-degree angle in the dorsal-ventral plane. This was to position the larva such that the camera objective **(b)** was perpendicular to the top of the larva, and the laser objective **(c)** was perpendicular to the side of the larva. After positioning, 3ml of culture water was added to the stage, immersing the larva. Larvae were positioned on the light sheet microscope, and the angle of the larva in relation to the camera objective was further optimised using a bespoke 3d printed ball joint tilt stage **(d)**. Dorsal-ventral optical sectioning was then undertaken (10 equidistant Z-slices across 220 $\mu$ m taken in 0.8s, repeated 400 times) to gather a baseline activity profile. After this baseline recording, test compound (or in the case of controls, water) was added to the recording chamber in an appropriate volume to ensure the final desired concentration in the recording chamber was achieved, and mixed by pipetting up and down with a 1ml pipette. There was then a further period with no imaging to allow compound to diffuse into the larva. This time period was defined using uptake data gathered in previous studies such that where low uptake was observed, longer exposure periods were adopted (see Table 2.1). After this period, a second round of imaging was performed with identical parameters (10 equidistant Z-slices across 220 $\mu$ m taken in 0.8s, repeated 400 times) to obtain images of brain function during compound exposure. After this imaging period the larva was removed and killed in benzocaine.

#### *4.2.4 Image processing*

Images were processed identically to that described in the previous chapter section 2.2.6, except processing was performed across 800 image stacks as opposed to 200. Of these 800 image stacks, the first 400 were from the pre-compound baseline period and the second 400 from the compound exposure period. Control fish were treated identically to compound exposed fish except they were not exposed to drug. Image analysis was performed on all image stacks in one processing run such that image analysis was performed identically on both baseline and exposure time periods. Image analysis produced 43 timeseries, each representing the fluorescent intensity overtime of

a different anatomical region of interest. An example timeseries is illustrated in Figure 4.2a.

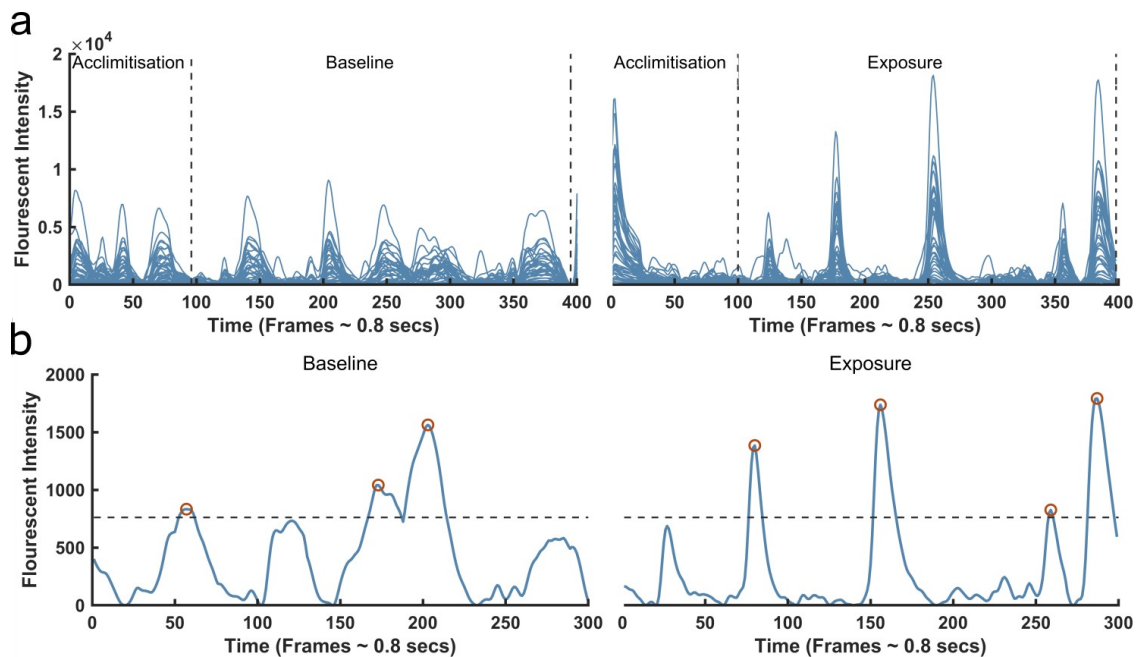


**Figure 4.2 (a)** Timeseries data from a single donepezil (125µM) exposed fish. Text labels and dashed lines indicate the acclimatisation, baseline and exposure periods. There are 43 timeseries on each axis, representing the 43 different ROIs. Baseline and Exposure period are 300 frames each. **(b)** Timeseries data from a single ROI (Rostral hypothalamus) of a donepezil (125µM) exposed fish. Red circles indicate peaks identified by the peak detection algorithm. The dashed line represents the threshold used to identify peaks, which is two times the standard deviation of the baseline.

#### 4.2.5 Data Analysis: Peak and Functional Connectivity Analysis

A 300 time point-long subsections of timeseries was selected from the full timeseries for baseline period and exposure period each. This approach was adopted to remove from analysis any images that were taken when the larva was acclimatising to the laser being initially switched on or off. Typically, during these periods there was a large amount of fluorescence seen immediately after the laser was initially switched on due to overstimulation of visual centres of the brain. This can be seen clearly in the post-exposure acclimatisation period (Figure 4.2a), where for the first 25 frames the  $\text{Ca}^{2+}$  fluorescence is declining from a large initial spike. Peaks were identified to quantify the oscillatory nature

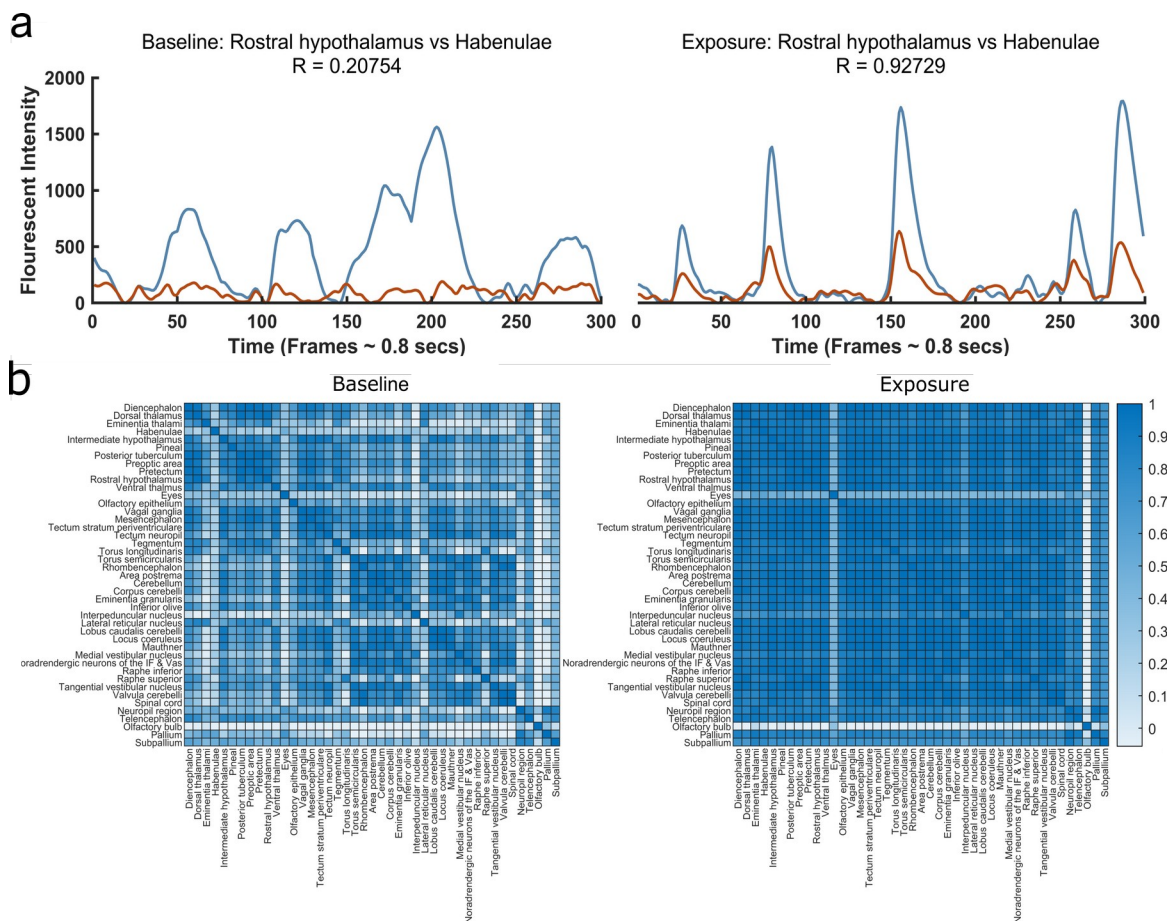


**Figure 4.3 (a)** Two example timeseries from different ROIs in the same fish (donepezil 125uM) across the baseline and exposure periods. The R-values, as calculated by Pearson's correlation coefficient, and the ROI names, for the two timeseries are indicated in the title of each axis. **(b)** Heatmaps of the R-values for the pairwise comparisons of every ROI for the baseline and exposure periods of a single fish (donepezil 125uM). The axes are labelled with the name of each region. The colorbar on the right-hand side shows the R-values in relation to the colour gradient.

of the timeseries. Peaks that were larger than  $2\sigma$  of the baseline period were identified (Figure 4.2b) and their magnitude was recorded. The number of peaks in the baseline and exposure periods was also recorded.

Functional connectivity, in the context of neuroimaging, refers to the similarity between the neuronal activity patterns of anatomically separate brain regions. This relationship is thought to reflect the level of communication between these regions (van den Heuvel and Hulshoff Pol, 2010). Typically, these are represented by measures of correlation that can elucidate changes in networks

responding to stimulation, in this case mediated by the action of seizurogenic compounds. As such, pairwise comparisons of each ROI using Pearson's correlation coefficient were performed, for the baseline and the exposure periods of each larva, in order to measure their functional connectivity e.g. Figure 4.3b. Pearson's correlation co-efficient provides a magnitude normalised measure of the similarity between two vectors, this is visualised in Figure 4.3a.

#### 4.2.6 Data Analysis: Mean Fluorescence Intensity

In order to identify if compound exposure had an effect on overall GCaMP-indicated neural activity for each larva, the mean fluorescence intensity across all ROIs was calculated for the baseline and the exposure period. The baseline was then subtracted from the exposure period in order to identify the change in fluorescence intensity over time (Df). This value was calculated for all larvae and subsequently averaged (mean) across all control larvae and all larvae exposed to each compound. Analysis was performed on the two highest concentrations combined, in addition to each concentration separately, as these were considered the concentration ranges most likely to elicit a seizurogenic response.

The mean of each compound was compared to the control using a Wilcoxon rank sum test, and statistical significance was  $p < 0.05$ . Comparisons were made between the mean baseline subtracted values and control as it was hypothesised that photobleaching and the effect of laser exposure over time may affect the fluorescence emitted by larva. This unpaired test on baseline-normalised values was opted for to allow comparison with control larvae, thus controlling for the effects of laser exposure over time. The results of these analyses are summarised in Figure 4.4.

#### 4.2.7 Data Analysis: Peak Analysis

Peaks were selected as described previously in this thesis, in section 4.2.5. For each larva, the number and mean height of peaks for each ROI were calculated for the exposure period, and separately for the baseline period. For each ROI, the corresponding baseline period was then subtracted from the exposure period. The baseline subtracted mean of each ROI was then calculated separately across all control fish and the two highest concentrations of each

compound as above. The peak numbers and mean heights were then compared between control and each treatment group for each ROI using a Wilcoxon rank sum test, corrected for multiple comparisons using the Benjamini and Hochberg method (Benjamini and Hochberg, 1995).

In order to visualise the differences between concentrations of different compounds, in terms of their peak profiles, multidimensional scaling was performed. As above, for each ROI of each larva the baseline subtracted peak number and peak height was calculated. These were then averaged across different concentrations of each compound and across all controls. This produced a vector of baseline subtracted means for each ROI, and for each treatment group. The Euclidean distances between these vectors were then calculated, and the relative distances were used to map these vectors into a 2-dimensional feature space. The eigenvalues for the first two coordinates accounted for >87% of the sum of all the eigenvalues for the peak heights, and >86% for peak numbers. The mean peak heights and peak numbers were analysed separately as they are continuous, and discrete, data respectively.

#### *4.2.8 Data Analysis: Functional Connectivity*

As described in section 4.2.5, functional connectivity analysis was performed on each larva, generating a single R-value (Pearson's correlation) for each pairwise comparison of ROIs. This totalled 741 R-values for the baseline, and a further 741 values for the exposure period for every larva. The baseline R-values were subtracted from the corresponding exposure values for each larva. The means of these values were calculated across the two highest concentrations for each compound and across the control larva. The means were then compared between each compound and the control using a Wilcoxon rank sum test, corrected for multiple comparisons using the Benjamini and Hochberg method (Benjamini and Hochberg, 1995). Furthermore, the mean baseline subtracted R-values across all connections for each treatment group was also calculated. The means were then compared with control using a Wilcoxon rank sum test. In addition, the mean baseline subtracted R-value, across all the connections for each ROI were calculated. These means were compared between each compound and the control using a Wilcoxon rank sum



test, corrected for multiple comparisons using the Benjamini and Hochberg method (Benjamini and Hochberg, 1995).

#### 4.2.9 Data Analysis: Graph Measures

In addition to direct comparison of changes in functional connectivity, the intention was also to describe the effects of seizurogenic compounds on network structure to better understand changes in the nature of the brain networks. In order to achieve this, we used graph theory measures to identify changes in the network upon exposure to the selected compounds. Graph theoretical analysis is used to measure the nature of networks in graph theory each ROI would be a node and the connections between these ROIs are edges. Graph theory focuses on network topology, for example, how many edges a node has, whether there are subgroupings of nodes and how many edges are needed to connect two nodes. Graph theory has been used for decades to analyse the outputs of fMRI scans and specific graph measures are understood to be associated with certain neurological states (De Vico Fallani et al., 2014)

For this, Pearson's correlation coefficient was calculated pairwise between all the ROIs for the baseline and the exposure period of each larva. These connections were thresholded by removing connections that had an R value of  $<0.25$ . This threshold was selected in order to remove spurious connections and is in line with thresholds used previously (Burgstaller et al., 2019). A weighted graph network was then generated from the remaining connections wherein ROIs represent nodes, and connections between them represent edges. The largest connected component was then identified and the clustering coefficient, maximised modularity, path length, small worldness and betweenness centrality were then calculated for the nodes of this component.

The clustering coefficient describes the fraction of a node's neighbours that are neighbours of each other (Wasserman and Faust, 1994a). The global level of clustering in a network is the mean of the local clustering coefficients of all the nodes. As the connections were weighted, the clustering coefficient of each node was calculated by identifying all nodes connected to the node. The sum of the connections shared between all of these adjacent nodes was calculated and then divided by the total number of possible connections between these nodes.

*Maximised modularity* describes a subdivision of the network into groups of nodes that maximises modularity. Modularity measures the strength of a partition by taking into account its degree distribution (Chang et al., 2012). The method achieves this by taking the weight of a connection between two nodes and subtracting this from its expected weight. The expected weight of a connection is the product of the two nodes it connects, divided by two times the total number of connections in the network.

The subdivision of nodes that maximises modularity was identified using simulated annealing (Danon et al., 2005). This was performed by initially randomly selecting nodes and dividing them into two groups. The modularity for this distribution was calculated, and then a node randomly switched between groups. The modularity was calculated again and the difference between the original and the new modularity values is calculated. If the modularity has increased, the change is accepted, but if the modularity has decreased the change is either accepted or rejected. Whether a decrease in modularity is accepted depends on how many iterations of the above loop, the algorithm has calculated. Simulated annealing is designed such that the likelihood of a negative change being accepted is higher at the beginning of the process and lower at the end of the process. This is undertaken in order to reduce the chance of the algorithm getting 'stuck' in local minima or maxima. A negative change is accepted if the exponent of the difference in modularity divided by  $T$  is larger than a random number between 0 and 1. The value of  $T$  changes each iteration, starting at 0.5 and reducing in size by 0.001 until it reaches zero. As such, this slowly reduces the probability of a negative step being accepted. Simulated annealing was used to repeatedly maximise modularity on different numbers of modules in order to identify the maximised modularity.

*Characteristic path length* is the minimum magnitude of edges between two nodes in the network (Wasserman and Faust, 1994b). It is a measure of functional integration, with shorter paths implying a stronger potential for integration. As shorter paths imply stronger connections, one minus the R-value was used such that highly correlated nodes had a small value that linked them. For example, an R-value of 0.95 becomes 0.05, by subtracting 0.95 from one. The minimum sum of R-values that connected two nodes was identified for

each connection. The mean of this value across all possible connections was calculated, giving the characteristic path length of each network.

*Small worldness* is a property of networks that are highly clustered yet have small characteristic path lengths. Small-world networks possess high local, as well as global, efficiency in signal processing. Here small-worldness was computed as the fraction of the mean clustering co-efficient, and the mean characteristic path length of each network. Human brains are categorised by their tendency towards small-worldness as it allows increased communication efficiency while using less energy (Uehara et al., 2014).

*Betweenness centrality* is a measure of the centrality based on shortest paths and represents the degree to which nodes stand between each other. In order to calculate betweenness centrality on a weighted graph, the shortest path is calculated as outlined above (Wasserman and Faust, 1994c). The centrality for a node  $v$  is calculated by counting the number of times  $v$  occurs in the shortest path between every possible pair of all the other nodes. This value was calculated for each node and scaled between 0 and 1, by dividing by the number of possible pairs of other nodes. Betweenness centrality is useful for identifying nodes that are hubs in networks and are, therefore, particularly important in connecting nodes to one another.

For each larva the graph measures for the baseline were subtracted from the exposure period. Next, the means were calculated across the controls and the two highest concentrations of each compound. These means were compared between each compound and the control using a Wilcoxon rank sum test.

## **4.3 Results**

### *4.3.1 Mean fluorescent intensity*

All compounds tested showed a significant change in the baseline corrected mean fluorescent intensity when averaged across the top concentrations, with the exception of SB205607. Notably, PTZ had the largest increase in average fluorescence, while chlorpromazine exposure was the only compound that resulted in a reduced overall fluorescent intensity (Figure 4.4a). When compounds were averaged across individual concentrations (Figure 4.4b), only the highest concentration of RST and the two highest concentrations of

donepezil had a statistically significant difference in fluorescent intensity. This being the case, it was decided that the majority of subsequent analyses would be performed on a combination of the upper two concentrations.

#### *4.3.2 Peak Parameters*

Of the compounds tested, aminophylline, chlorpromazine, donepezil and PTZ had significantly different peak heights compared to control, see Figure 4.5a. Donepezil exposure resulted in increased average peak height across every ROI, reflecting a ubiquitous increase in neurotransmission across the zebrafish brain. Chlorpromazine was again distinct, as exposure to it typically resulted in a reduced peak height on average, suggesting depression of brain activity. The most frequently affected region were the noradrenergic neurons of the interfascicular and vagal areas, which had significant changes under exposure to donepezil, chlorpromazine and PTZ. SB205607 and RST had no significant changes in peak height.

Of the compounds tested, aminophylline, donepezil, picrotoxin, PTZ, RST and SB205607 exposure all resulted in a significantly different number of peaks, in at least one ROI, compared to control see Figure 4.5a. PTZ and picrotoxin exposure resulted in the greatest increase in the number peaks across ROIs and had the most significant changes in number of peaks, suggesting an increase in the frequency of  $\text{Ca}^{2+}$  oscillations. Chlorpromazine was again distinct in the read out seen, with an apparent reduced number of peaks on average, however this was not statistically significant. This may have been due to the fact that control larvae also had a slightly reduced average peak number. Peak number changed in the vagal ganglia, upon exposure to a compound, more frequently than for any other region.

#### *1.1.1 Multidimensional scaling of peak parameters*

When peak heights across ROIs were scaled across two dimensions (Figure 4.5b), the lower concentrations of most compounds, with the exception of picrotoxin and chlorpromazine, were co-located with control within the multi-feature space. Notably, the different concentrations (low, middle and high) of SB205607, aminophylline and donepezil were closely collocated, the higher concentrations locating progressively further away from control. Chlorpromazine

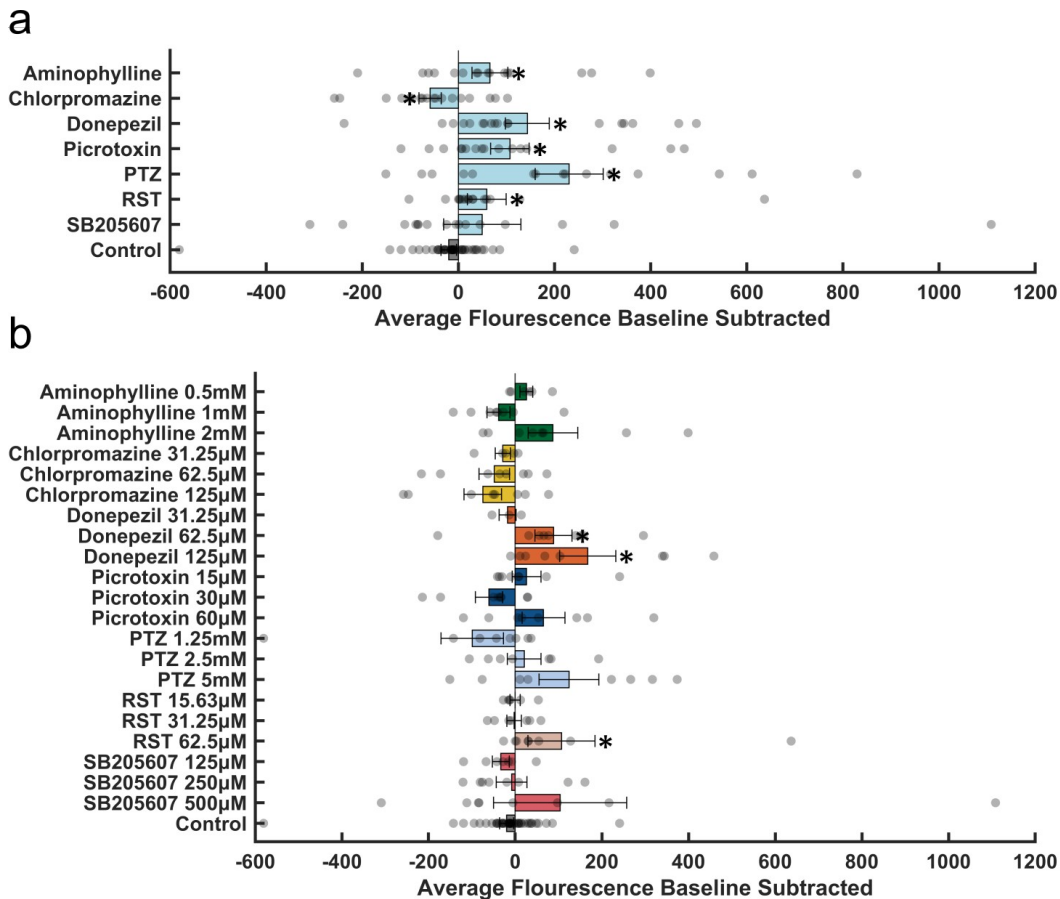


**Figure 4.4 (a)** The baseline subtracted mean fluorescent intensity across all ROIs, averaged across treatment groups. For compound exposed fish this is the mean across the two highest concentrations for each compound. Grey circles represent individual fish. Error bars are standard error of the mean (n=15-43). Asterisks indicate a statistically significant difference from control ( $p < 0.05$ ) as defined by a Wilcoxon rank sum test. **(b)** The baseline subtracted mean fluorescent intensity across all ROIs, averaged across individual concentrations. Grey circles represent individual fish. Error bars are standard error of the mean (n=7-43). Asterisks indicate a statistically significant difference from control ( $p < 0.05$ ) as defined by a Wilcoxon rank sum test.

and RST also appeared to co-locate, although to a lesser degree and with a more random distribution of concentrations. Both GABA<sub>A</sub> antagonists, picROTOXIN and PTZ had large spreads between concentrations while being typically located furthest from control.

When peak numbers across ROIs were scaled across two dimensions (Figure 4.5b), the low concentrations of most compounds with the exception donepezil and SB205607, were closely co-located with control. All of the donepezil

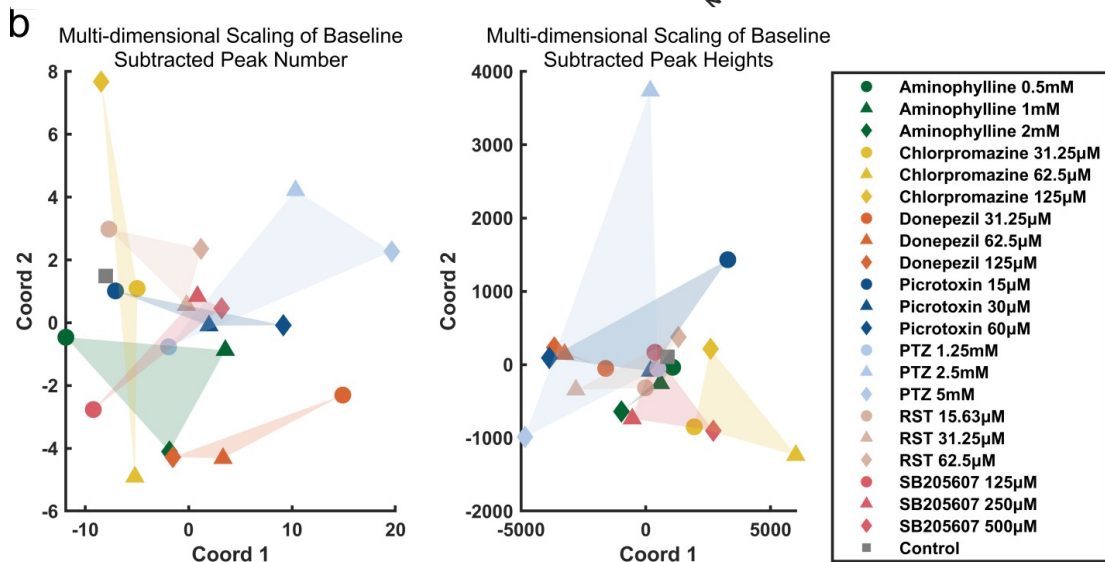
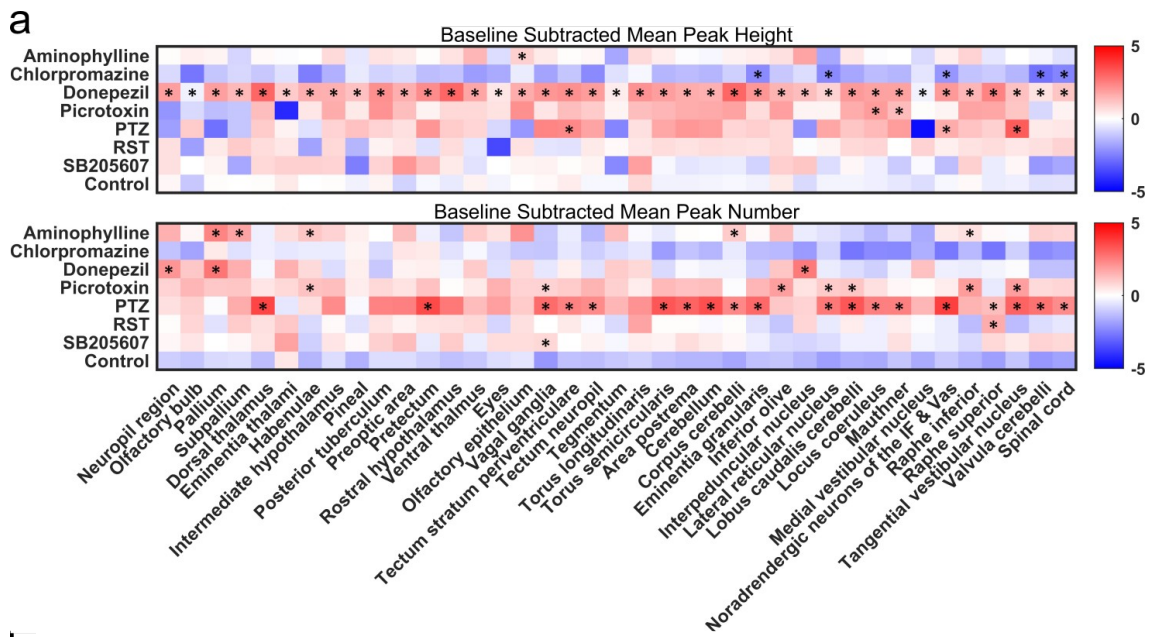


**Figure 4.5 (a)** The mean baseline subtracted peak height and number for each ROI. For compound exposed fish this is the mean across the two highest concentrations for each compound. Peak heights are scaled such that the absolute mean of each column (ROI) of the heatmap is equal to one in order to allow better visualisation across ROIs. Asterisks indicate a statistically significant difference from control ( $p < 0.05$ ) as defined by a Wilcoxon rank sum test, corrected for multiple comparisons using the Benjamini and Hochberg method (Benjamini and Hochberg, 1995) ( $n = 14-43$ ). **(b)** A scatter graph of the first two coordinates produced after classical multi-dimensional scaling of the mean baseline subtracted peak height and number across all ROIs. In both plots, the circles represent the lowest concentration, the triangles the middle concentration, and the diamonds the highest concentration used for each treatment group. The grey square represents the control group.

treatment groups were co-located and were away from the control group. PTZ, aminophylline, picrotoxin and RST were located progressively further away from control as the concentrations increased. Chlorpromazine, was the most disparate between concentrations, with the medium and high concentrations located at opposite ends of the graph.

#### *4.3.3 Functional connectivity changes in individual connections*

Of the compounds tested, only exposure to picrotoxin and donepezil resulted in significant changes in functional connectivity for any individual ROI, after correction for multiple comparisons (Figure 4.6a). Donepezil exposure resulted in an increase in functional connectivity for the vast majority of connections measured, implying a highly synchronised state across all ROIs (Figure 4.6b). For donepezil, ROIs with the fewest significant connections were the noradrenergic neurons of the interfascicular and vagal areas, the eminentia granularis and the interpeduncular nucleus. Picrotoxin exposure also resulted in a large number of significant changes, in particular in the habenulae and the pineal gland, suggesting these regions were highly synchronised with other regions. Moreover, much like for donepezil, the largest changes in magnitude were seen in connections between the spinal cord, the raphe superior and valvula cerebelli.

#### *4.3.4 Changes in Mean Functional connectivity*

When R-values were averaged across each ROI, there were significant increases in at least one ROI, for larvae exposed to aminophylline, donepezil, picrotoxin PTZ and RST (Figure 4.7b). The mean functional connectivity per ROI was significantly increased across all ROIs after exposure to donepezil. Picrotoxin and aminophylline exposure also resulted in a large number of significant increases in functional connectivity. Picrotoxin, aminophylline and donepezil exposure all resulted in increases in GCAMP fluorescence in the eminentia thalami, the habenulae, the pineal and the interpeduncular nucleus. Interestingly, exposure to RST, like that for picrotoxin and donepezil, resulted in significantly increased functional connectivity in the Raphe Superior, suggesting that other ROIs become more synchronised with the Raphe superior upon exposure to convulsant drugs. This may imply increased communication between the Raphe superior and other ROIs. Both chlorpromazine and



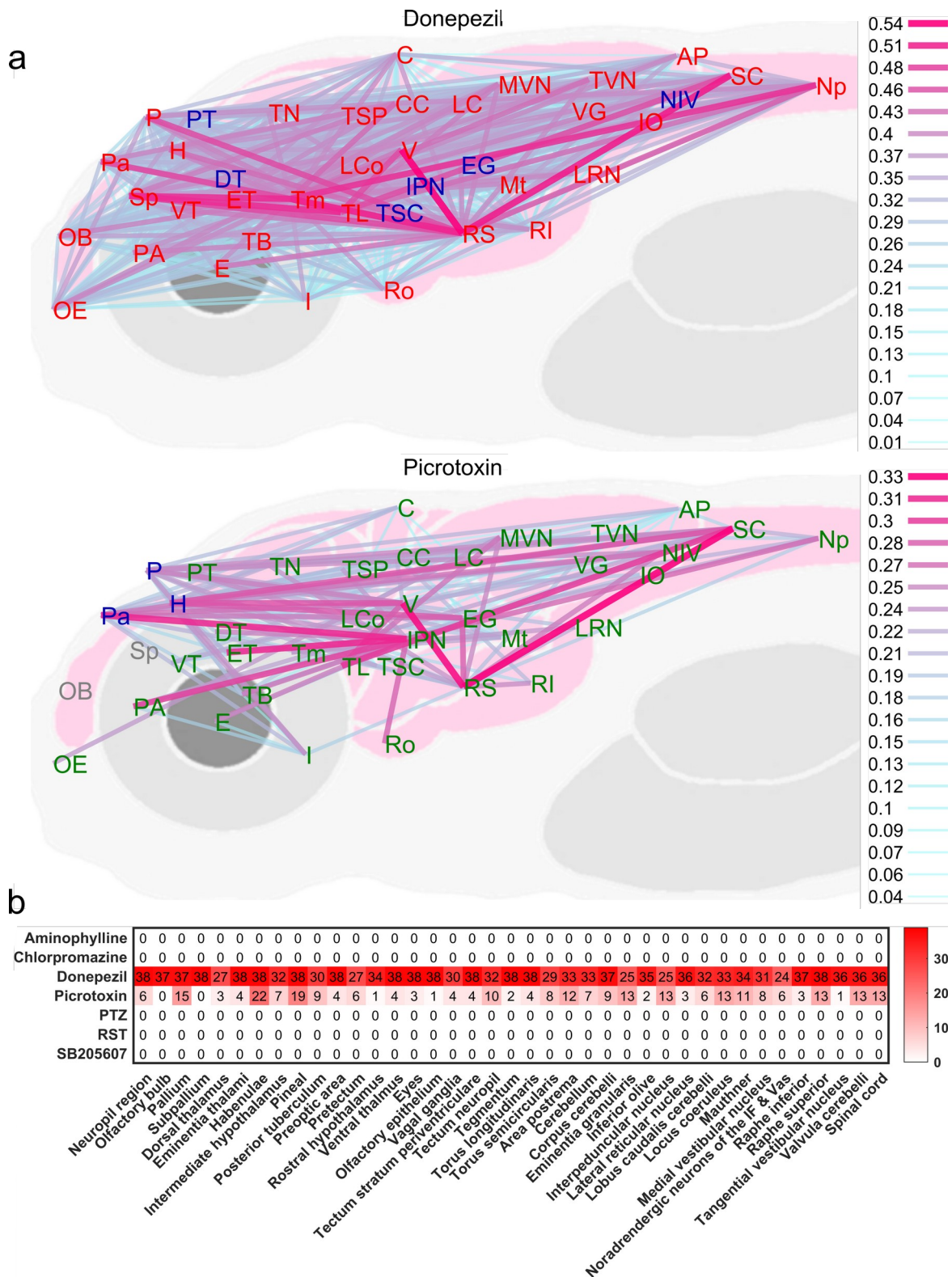


**Figure 4.6:** (a) The baseline subtracted functional connectivity between different ROIs. Lines are drawn if the calculated r-value is significantly different from control ( $p < 0.05$ ) as defined by a Wilcoxon rank sum test, corrected for multiple comparisons using the Benjamini and Hochberg method (Benjamini and Hochberg, 1995) ( $n = ?$ ). The



colour and thickness of the lines represents the magnitude of the difference in functional connectivity from baseline, as defined by the adjacent colorbar. Abbreviated brain regions are as follows: area postrema (AP); cerebellum (C); corpus cerebelli (CC); dorsal thalamus (DT); eyes (E); eminentia granularis (EG); eminentia thalami (ET); habenulae (H); intermediate hypothalamus (I); inferior olive (IO); interpeduncular nucleus (IPN); lobus caudalis cerebelli (LC); locus coeruleus (LCo); lateral reticular nucleus (LRN); Mauthner (Mt); medial vestibular nucleus (MVN); noradrenergic neurons of the interfascicular and vagal areas (NIV); spinal cord neuropil (Np); olfactory bulb (OB); olfactory epithelium (OE); pineal (P); preoptic area (PA); pallium (pa); pretectum (PT); raphe inferior (RI); rostral hypothalamus (Ro); raphe superior (RS); spinal cord (SC); subpallium (Sp); posterior tuberculum (TB); torus longitudinalis (TL); tegmentum (tm); tectum neurophil (TN); torus semicircularis (TSC); tectum stratum periventriculare (TSP); tangential vestibular nucleus (TVN); Valvula cerebelli (V); vagal ganglia (VG); ventral thalamus (VT). Note: Positions of regions approximate to allow spacing of nodes and visualisation of connections. **(b)** The number of significant changes in functional connectivity, per ROI, as defined above in (a).

SB205607 were not significantly different from control across any of the ROIs measured. In terms of mean changes in the magnitude of functional connectivity across all connections (Figure 4.7a), exposure to donepezil, picrotoxin and aminophylline resulted in significantly elevated mean R-values, suggesting an increase in overall synchronicity between ROIs. Notably, exposure to chlorpromazine appeared to result in reduced functional connectivity, relative to control, while PTZ and RST also appeared to increase connectivity overall, however none of these impacted functional connectivity to a significant degree. SB205607, was also not different from control, in terms of over functional connectivity.

#### 4.3.5 Graph measures

There were very few significant changes in betweenness centrality across ROIs (Figure 4.8). The only compound with significant changes in betweenness centrality was PTZ, wherein centrality was significantly reduced in the vagal ganglia and increased in the Eminentia thalami. This implies that the eminentia thalami was more important in transferring information between ROIs and that the amount of information passing through the vagal ganglia was decreased.

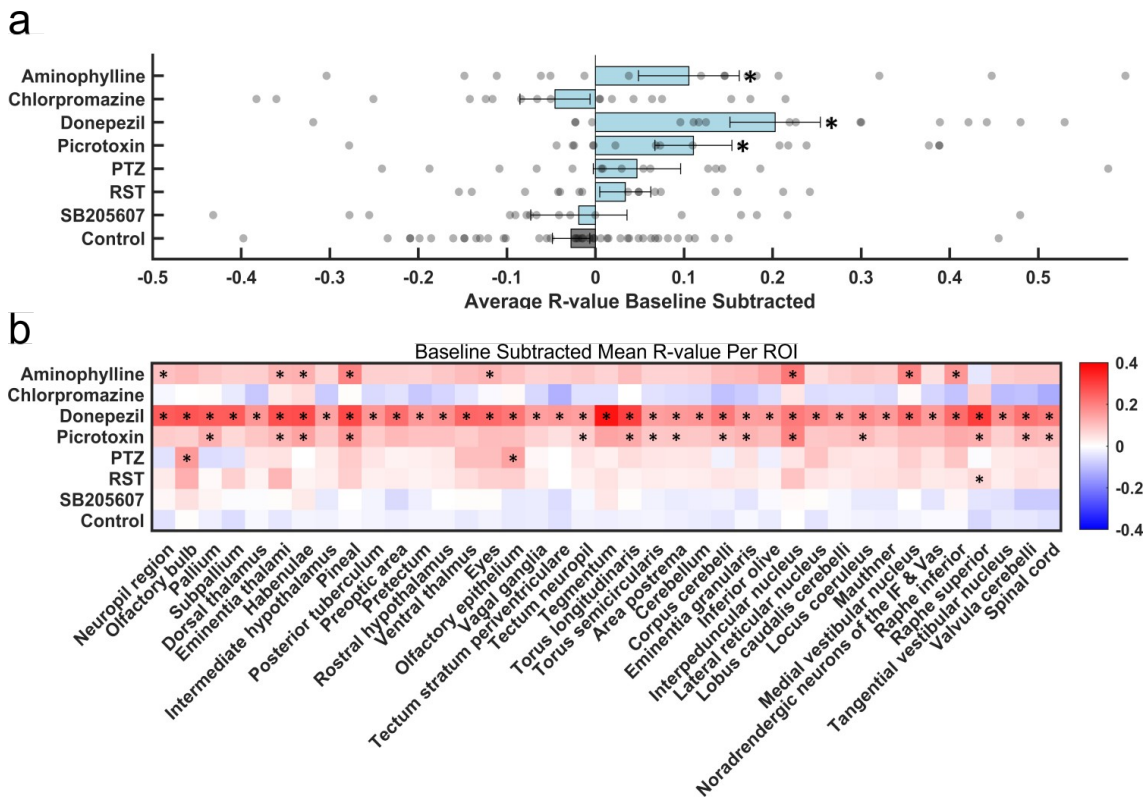


**Figure 4.7 (a)** The baseline subtracted mean functional connectivity across all ROIs, averaged across treatment groups. For compound exposed fish this is the mean across the two highest concentrations for each compound. Grey circles represent individual fish. Error bars are standard error of the mean ( $n=7-43$ ). Asterisks indicate a statistically significant difference from control ( $p<0.05$ ) as defined by a Wilcoxon rank sum test. **(b)** The mean baseline subtracted R-value for each ROI. For compound exposed fish this is the mean across the two highest concentrations for each compound. Asterisks indicate a statistically significant difference from control ( $p<0.05$ ) as defined by a Wilcoxon rank sum test, corrected for multiple comparisons using the Benjamini and Hochberg method (Benjamini and Hochberg, 1995).

Notably, there were some relatively large increases in betweenness in the tangential nucleus upon exposure to PTZ. Moreover, the posterior tuberculum of Donepezil, PTZ and SB205607 also had large increases in betweenness centrality, although not to a significant degree. Also of note, the tectum neuropil exhibited large changes in betweenness after exposure to donepezil, PTZ, picrotoxin and SB205607. There were significant changes in all of the global graph measures applied to both aminophylline and donepezil exposed larvae (Figure 4.9). Aminophylline and donepezil exposure both resulted in increased

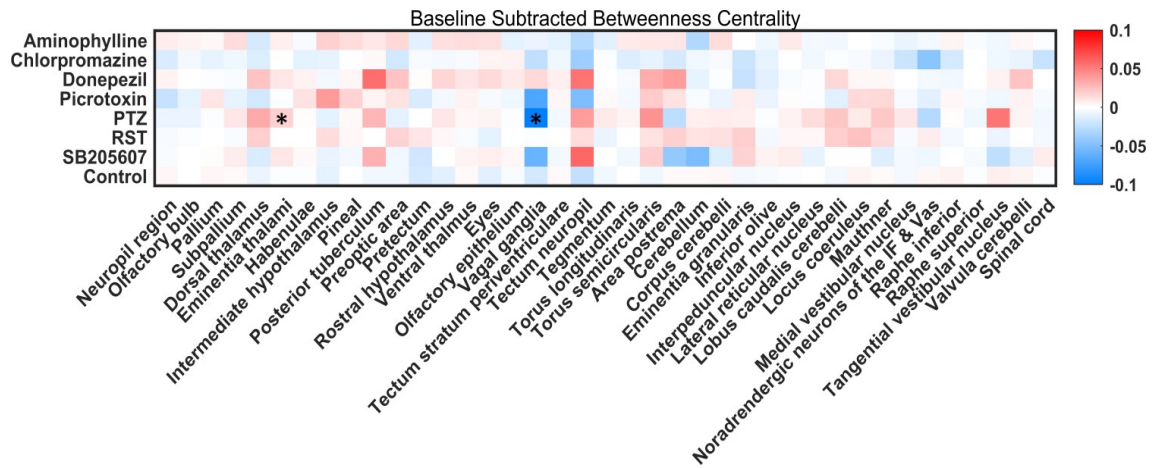


**Figure 4.8** Baseline subtracted betweenness centrality for each ROI. For compound exposed fish this is the mean across the two highest concentrations for each compound. Asterisks indicate a statistically significant difference from control ( $p < 0.05$ ) as defined by a Wilcoxon rank sum test, corrected for multiple comparisons using the Benjamini and Hochberg method (Benjamini and Hochberg, 1995) ( $n=7-43$ ).

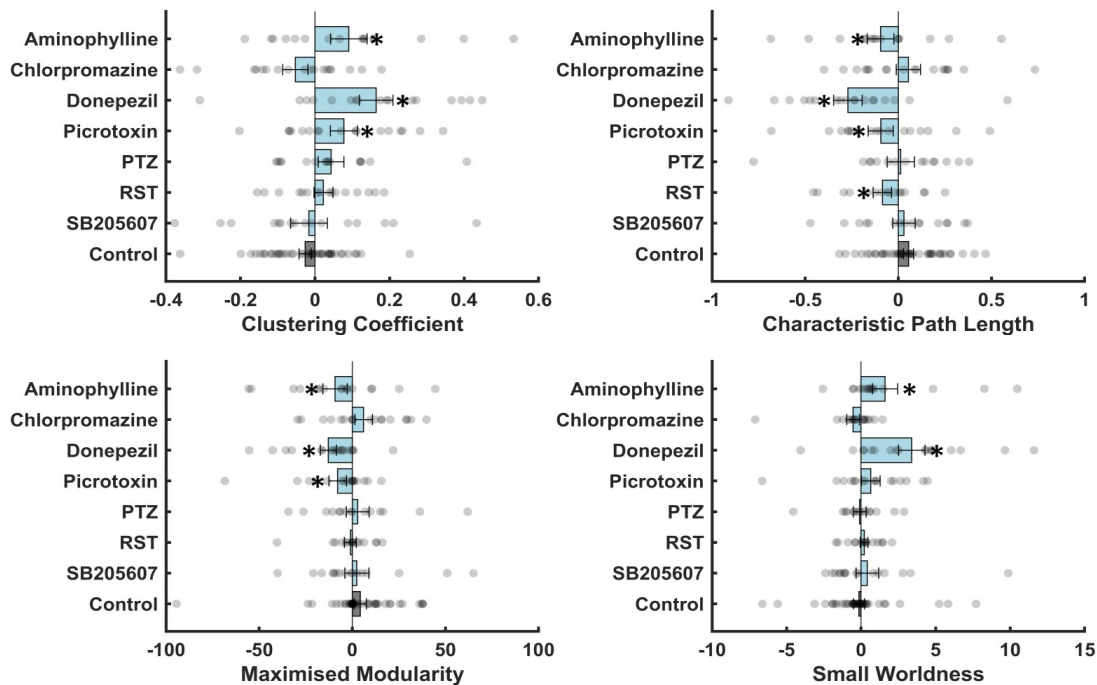


**Figure 4.9** The baseline subtracted mean clustering coefficient, path length, small worldness and maximised modularity. Grey circles represent the baseline corrected values for individual fish. Error bars are standard error of the mean ( $n=7-43$ ). Asterisks indicate a statistically significant difference from control ( $p < 0.05$ ) as defined by a Wilcoxon rank sum test.

clustering coefficients, while reducing path lengths and maximised modularity. This suggests an increase in the speed and efficiency of information transfer as regions become more interconnected and the paths between ROIs become smaller. Moreover, like aminophylline and donepezil, picrotoxin exposed larvae had significantly reduced path lengths, modularities and increased clustering coefficients, however this did not result in significantly increased small worldness. Suggesting an increased speed of information transfer and transition towards more interconnection, but at greater energetic cost, as small worldness is associated with increased efficiency of information transfer (Uehara et al., 2014). In addition, RST exposed larva had reduced path lengths, but RST had little effect on any of the other measures.

#### **4.4 Discussion**

Using high speed light sheet microscopy to record  $\text{Ca}^{2+}$  dynamics *in vivo*, the responsiveness of the larval zebrafish CNS, to a range of seizurogenic compounds, was demonstrated. Moreover, due to the ability to image brain-wide, we were able to elucidate the effect of compounds on multiple and specific anatomical regions in parallel, allowing us to identify effects on functional connectivity and network dynamics. Furthermore, use of a new light sheet system allowed advancement from previous work by incorporating drug free baseline controls and doubling temporal resolution. This improved methodology was tested using a subset of the compounds used in chapter two and selected to include a diverse range of pharmacologies and indications of seizurogenicity.

Of the compounds tested, exposure to aminophylline (an adenosine antagonist), chlorpromazine (a phenothiazine antipsychotic), donepezil (an acetylcholinesterase inhibitor), picrotoxin (a GABAAR antagonist) and PTZ (a GABAAR antagonist) produced the most significant changes across the variables measured. SB205607 exposure resulted in the least differences compared with untreated control animals, with exposure only being associated with a small increase in peak height, which wasn't significant. Moreover, neither overall fluorescent intensity or functional connectivity changed to a significant degree. This is perhaps unsurprising given that synthetic opioids such as U69,593, DPDPE and DAMGO have been reported as having low sensitivity to zebrafish  $\kappa$ -opioid,  $\delta$ -opioid or  $\mu$ -opioid receptors respectively (Rodriguez and

Gonzalez-Nunez, 2006). As such, this suggests that zebrafish lack sensitivity to highly selective opioid ligands, despite these compounds having high potency against mammalian receptors.

Curiously, however, our previous  $\text{Ca}^{2+}$  imaging study (Chapter 2), using the non-baseline normalised, lower temporal resolution light sheet methodology/system, 4 dpf larvae showed significant changes in CNS activity following exposure to SB205607, with changes in both fluorescent intensity (Figure 2.3, Winter et al., 2021) and functional connectivity recorded (Figure 2.4, Winter et al., 2021). Indeed, SB205607 was conspicuously effective in affecting neural activity amongst the opioid agonists tested during this work, despite all showing relatively high levels of uptake over comparable exposure periods (Figure S1). Interestingly, RST also had a much less prominent effect on  $\text{Ca}^{2+}$  dynamics when compared with our previous study (section 5, Winter et al., 2021). In this case, the analyses (Figure 2.3), showed a large number of significant increases in fluorescent intensity as a result of RST exposure, and while in this chapter (using the baseline-corrected higher temporal resolution approach) there was a significant increase in fluorescent intensity overall, the number and height of peaks typically did not change relative to control larvae. This incongruence between studies is difficult to explain, it is possible that diffusion of the compound into the fish was less efficient, due to the fish being immobilised in agarose, compared to the previous study wherein fish were able to swim freely in drug solution. Moreover, fish were also exposed to the laser and encased in agarose for longer which may have resulted in a greater degradation in fish health. Despite these caveats, as an NMDA receptor agonist (Schoepp et al., 1991), one would expect RST exposure to result in large increases in neural activity as reported by increased fluorescent intensity, as ionotropic NMDA receptors act on  $\text{Ca}^{2+}$  channels (Paoletti et al., 2013). While RST exposure did cause significant increases in fluorescent intensity, it was among the smallest changes seen across the compounds tested and did not translate to significant changes in peak height or number in any of the registered brain regions.

In addition to measures of fluorescent intensity, the work undertaken using the previous system (Chapter 2) revealed significant changes (to some degree) in functional connectivity upon exposure to all of the compounds tested in this chapter. However, in this chapter only exposure to donepezil and picrotoxin

resulted in significant changes in individual functional connections. Despite this, when individual connections were averaged across ROIs or whole larva many of the compounds tested here were different from control.

Among the more active compounds tested, exposure to the adenosine receptor antagonist aminophylline resulted in increased overall fluorescent intensity, in addition to causing significant increases in fluorescence intensity in multiple specific ROIs. In aminophylline exposed larva, both the habenulae, and raphe inferior showed significant increases in the number of peaks identified and the strength of functional connectivity, in terms of the sum of the R-values of all connections, a finding consistent with our previous study (section 5, Winter et al., 2021). Moreover, this is particularly notable as caffeine, also a methyl xanthine and a similar compound to aminophylline both structurally and functionally, has been shown to increase glucose metabolism in the habenula of rats, even at relatively low concentrations (Nehlig et al., 1984). Furthermore, the raphe nucleus, of which the raphe inferior is a part, has a high concentration of serotonergic neurons. Aminophylline and other methylxanthines increase brain tryptophan and thus serotonin turnover (Fernando and Curzon, 1976). It is therefore possible that aminophylline increases activity in this area in particular by increasing serotonin synthesis and consequently activating serotonergic neurons.

In addition, aminophylline exposure caused an increase in multiple graph measures, including clustering coefficient and small worldness, while reducing both path length and modularity.

Similarly, graph measures calculated from the coherence of EEG recordings in healthy adults exposed to caffeine showed similar changes upon caffeine exposure, detecting reductions in modularity and increases in the clustering coefficient (Kim et al., 2021). Moreover, increases in small worldness and clustering coefficient and reductions in characteristic path length, was associated with an improvement in measures of cognitive ability (Kim et al., 2021). This is notable as there is evidence that caffeine also has cognitive benefits for zebrafish (Ruiz-Oliveira et al., 2019). It seems therefore, that methylxanthine exposure in both humans and zebrafish, correlates with cognitive enhancement and similar associated changes in brain networks.

Notably, donepezil exposure also resulted in increases in clustering coefficient and small worldness while reducing path length. Donepezil is an acetylcholinesterase inhibitor which can slow decline of cognitive function in dementia patients (Birks and Harvey, 2018), although it has limited efficacy improving cognition in healthy individuals (Tricco et al., 2013). Future studies looking into the effect of donepezil on cognitive function could help to elucidate the connection between changes in network parameters and cognition.

In this study and in previous work (section 5, Winter et al., 2021), donepezil exposure resulted in a very large increase in functional connectivity overall, which was ubiquitous across all ROIs. This activity could easily be described as hypersynchronous, which is one of the descriptive hallmarks of a seizure (Fisher et al., 2014a). Indeed, in clinical practice donepezil use is associated with an increased risk of seizure (Kumlien and Lundberg, 2010), however, the neurological status of patients typically prescribed donepezil is a significant confounding factor. Moreover, donepezil exposure resulted in large increases in fluorescent intensity here, manifested in the increased magnitude of  $\text{Ca}^{2+}$  oscillations across all ROIs. The combination of both hypersynchronicity and dramatically increased  $\text{Ca}^{2+}$  activity highlights the powerful effect of donepezil in the larval zebrafish. Indeed, the presence of acetylcholine in early developmental stages suggests it may play an important role in early development (Arenzana et al., 2005), which may explain donepezil's apparent potency at 4 dpf. Another possible explanation is that donepezil's agonism of the  $\sigma$ -1 receptor drives  $\text{Ca}^{2+}$  movement in and out of the cell (Maurice and Su, 2009). The  $\sigma$ -1 receptor has been implicated as an important modulator of the intracellular mobilisation of  $\text{Ca}^{2+}$  (Crouzier et al., 2021). Moreover, in *scn1a* mutant zebrafish,  $\sigma$ -1 agonism abolishes the antiepileptiform activity of fenfluramine (Sourbron et al., 2017), suggesting that  $\sigma$ -1 activation itself has a seizurogenic effect.

In addition to marketed drugs, two classical seizure precipitant compounds, PTZ and picrotoxin, were also tested. Both of these compounds act by inhibiting  $\text{GABA}_A$  receptors, thus reducing inhibitory neurotransmission and increasing the likelihood of neural network hyperexcitation. Despite having similar mechanisms of action there were some notable differences in the response of larvae between the two compounds. Exposure to picrotoxin appeared to modulate functional

connectivity to a greater degree than PTZ, causing a large number of changes in connections to the habenula in particular. This is pertinent as GABA and glutamate co-release controls habenula output in rodents (Shabel, 2014). It, therefore, follows that inhibition of GABA<sub>A</sub> receptors may dysregulate this process and cause increased excitation that perpetuates to other brain regions. Indeed, in rodents GABAergic fibres can be traced from the habenulae to the pineal gland (Møller and Baeres, 2002), another ROI to which a large amount of connectivity was observed in response to picrotoxin exposure. This suggests GABA<sub>A</sub> inhibition results in increased synchronicity along the habenular-pineal axis, which may have implications for seizuregenesis by this mechanism of action. Similarly, when larvae were exposed to PTZ, both the olfactory epithelium and the olfactory bulb showed significant increases in functional connectivity to other regions. Given the complete lack of GABAergic cells in the olfactory epithelium, it is possible this is driven by the adjacent olfactory bulb, which contains a large amount of GABAergic cells (Mueller et al., 2006), or by descending GABAergic neurons transmitting to the olfactory apparatus.

Both PTZ and picrotoxin exposure was associated with a large increase in fluorescence intensity and increases in the number of peaks detected. This would suggest that GABA<sub>A</sub> inhibition in larval zebrafish increases the frequency and magnitude of Ca<sup>2+</sup> oscillations detectable by GCaMP6s. This is unsurprising given that GABA is the primary inhibitory neurotransmitter in the brain, and GABA<sub>A</sub> activation inhibits the ability of cells to produce action potentials by hyperpolarising the neuron via influx of Cl<sup>-</sup> ions (Johnston, 1996). As Ca<sup>2+</sup> is a proxy of neuronal activity, increase in Ca<sup>2+</sup> upon exposure to PTZ and picrotoxin are likely reflective of a reduction in these inhibitory processes.

However, in addition to being reflective of generalised excitation Ca<sup>2+</sup> oscillations may be reflective of a direct effect on Ca<sup>2+</sup> channels. In adult rodents, GABA<sub>A</sub> inhibition by PTZ induces excitation, that can be shown in some part to be dependent on voltage gated Ca<sup>2+</sup> channels (VGCCs) (Weiergräber et al., 2006). Indeed, GABAergic inhibition either via hyperpolarisation or shunting of synaptic depolarisation reduces the opening probability of NMDA receptors and VGCCs (Higley, 2014). As such GABA<sub>A</sub> inhibition may increase Ca<sup>2+</sup> influx via NMDA, which may be a contributor to increased peak frequency and overall fluorescence in larval zebrafish.



In contrast with all of the other treatment groups, chlorpromazine exposure resulted in reduced overall fluorescent intensity, and reduced peak height in multiple ROIs. This is perhaps unsurprising as chlorpromazine is an antagonist of a variety of typically excitatory receptors including serotonin, dopamine and noradrenaline receptors (Shen, 1999). Despite this there are numerous reports of chlorpromazine correlated seizures, with use associated with an increased incidence of more than 50% (Bloechliger et al., 2015) . However, it should be noted that these were cases in patients with affective disorder, schizophrenia and dementia, and thus with neurological pathologies that increase the risk of seizure (Bloechliger et al., 2015). By contrast, chlorpromazine exposure in larval zebrafish appears to have an inhibitory effect, particularly in brain regions with high concentrations of monoamines. For example, in zebrafish, the raphe inferior is densely populated with serotonergic neurons which project toward the lateral reticular nucleus, eminentia granularis and the spinal cord (Maximino et al., 2013a). All these regions showed significantly reduced peak heights after chlorpromazine exposure, possibly due to serotonin inhibition. Moreover, the presence of monamine oxidase in the valvula cerebelli implies the presence of monaminergic neurons in this region, an area that was also inhibited by chlorpromazine exposure (Anichtchik et al., 2006). Similarly, the noradrenergic neurons of the interfascicular and vagal areas were also inhibited by chlorpromazine, likely as a result of its inhibition of alpha1 and alpha2 adrenergic receptor subtypes (Shen, 1999).

The eminentia granularis is part of the vestibular lobe of the cerebellum and extends into the cerebellar crest (Wullimann et al., 1996). The valvula cerebelli (although not likely fully differentiated at 4 dpf) and lateral reticular nucleus (Wullimann et al., 1996) are also part of the cerebellum. The lateral reticular nucleus is responsible for connecting the cerebellum to the sensory neurons in the spinal cord (Alstermark and Ekerot, 2013). All of these regions exhibited significantly reduced peak heights in response to chlorpromazine exposure, suggesting that chlorpromazine causes a cascade of inhibition through specific areas in the cerebellum, to connections with sensory neurons in the spinal cord. With all of this in mind, it is feasible that chlorpromazine's association with seizure isn't as a result of a direct excitatory mechanism, but rather (paradoxically) the opposite. There are many examples of drugs that are inhibitory in nature and that are associated with seizure, such as barbituates,

benzodiazapines and alcohol (Sellers, 1988). These drugs do not cause seizure acutely, rather chronic use induces a physiological change in neuronal inhibitory/excitatory homeostasis known as drug tolerance. Drug tolerance occurs typically when the number of target receptors of a pharmacological stimulus change in the brain in an attempt to return to a baseline homeostasis (Poulos and Cappell, 1991). With inhibitory compounds this would mean either an increase in excitatory receptors or a reduction in inhibitory receptors. Thus, if the pharmacological input of the compound is removed or reduced, the individual is put into a profoundly excitatory state, and the risk of seizure dramatically increased. It is possible, therefore that chlorpromazine sensitises patients to seizure via this mechanism, by causing upregulation of monoamines overtime due to chronic exposure, although this hasn't been confirmed in animal studies.

In summary, we find that larval zebrafish are sensitive to a range of pharmacological agents and that this is reflected by  $\text{Ca}^{2+}$  dynamics detectable via a genetically encoded GCaMP6 reporter. Moreover, we find that changes in  $\text{Ca}^{2+}$  dynamics typically occur in anatomical regions containing receptors targeted by the exposure compound, with evidence of cascades of altered  $\text{Ca}^{2+}$  dynamics transitioning between anatomically connected regions. In addition, we found changes in brain networks properties that are indicative of cognitive enhancement and that correlate with the use of cognitive enhancing compounds. In distinction to the previous chapter, here the use of baseline control recordings could be applied to normalise for drug effect in the same individual larva. Development of this methodology opens up the opportunity to record the transition to seizure induced by convulsant drugs. However, despite the obvious logistical and technical advantages this updated approach did not appear more sensitive to the effects of drug exposure. Regardless, with further optimisation and development it is likely that this approach offers significant benefit over previous methodology. In particular use of updated and faster decaying GCaMP to match the improved temporal resolution, and use of a remotely controlled 6-axis stage, to improve speed and consistency of larva orientation, may well help improve this approach. The data generated here add to the body of data supporting the use of the larval zebrafish as a complimentary and potentially alternative model for the study of compound pharmacodynamics and seizure liability testing.

## Chapter 5: Behavioural Profiling of Seizurogenic Compounds

### 5.1 Introduction

The previous chapters have focused on approaches to assess drug effect using methods that measure brain activity either directly (e.g. local field potential recordings) or via a directly linked surrogate method (e.g.  $\text{Ca}^{2+}$  imaging). Behaviour profiling is another approach for assessing drug effects, including the behavioural manifestation of seizures (e.g. convulsions), and has been used in mammals for many decades (Fonck et al., 2015; Irwin, 1968). Behavioural analysis aims to elucidate compound effects by assessing the behaviours of animals exposed to said compound. Such behaviours include exploratory behaviour, freezing and twitching and specific behaviours are thought to be associated with specific psychoactive or toxicological effects.

There have been several published studies adopting behavioural pharmacological assays in larval zebrafish, including some assessing the behavioural consequences of exposure to pro-convulsive/seizurogenic drugs (Afrikanova et al., 2013; McCarroll et al., 2019; Rihel et al., 2010; Winter et al., 2008). Behavioural profiling has a particular advantage over local field potential recordings (LFP) and  $\text{Ca}^{2+}$  recording in that it typically enables higher throughput, with the ability to record from multiple larva at once (Winter et al., 2008). Such high throughput platforms typically utilise automated systems for tracking larval behaviour and as such are relatively easy to perform, potentially ensuring a greater degree of consistency in application.

Behavioural profiling, is often used in concert with other approaches as a way of corroborating outputs from other methodologies (Baraban et al., 2013a; Sourbron et al., 2017). However, behavioural profiling has been used effectively in some preliminary studies for screening both seizurogenic (Winter et al., 2008) and anti-epileptic drugs (Berghmans et al., 2007). In both studies, the locomotor activity of multiple 7 days post fertilisation (dpf) zebrafish larvae was recorded simultaneously allowing for high throughput testing. Berghmans *et al.* achieved a detection rate of 93% for anti-epileptic drugs, while Winter *et al.* achieved 72%

predictivity for seizurogenic compounds. These studies highlight the promise of behavioural

profiling as a methodology for seizure liability assessment, particularly when applied in conjunction with direct brain recordings. However, both of these screening studies used univariate statistics on a single behavioural parameter to assess seizure state, despite the availability of multiple measure of locomotion. Improvements to this analytical methodology could be made by using machine learning approaches, which have already shown great potential in a variety of contexts for building classification models of animal behaviour (Valletta et al., 2017). Machine learning models are well suited to identifying patterns within highly multivariate datasets with often unknown interactions and correlations between variables. In particular machine learning classifiers such as logistic regression, support vector machines and neural networks are highly effective at discriminating between categories of data such as a seizurogenic behavioural profile vs non-seizurogenic behavioural profile (Valletta et al., 2017).

To date, machine learning approaches have not been applied to behavioural data from larval zebrafish with the aim of allowing discrimination between seizurogenic and non-seizurogenic phenotypes. As such, the purpose of this chapter was to use high-throughput behavioural profiling to identify seizurogenic compounds, using a machine learning classification algorithm. To this end, we used behavioural profiles from the same compounds tested in Chapter 3: and Chapter 4: to make comparisons between behavioural outputs and brain imaging/electrophysiological outputs reported in those chapters.

## **5.2 Methods**

### *5.2.1 Model Organism*

For all of the experiments described in this chapter, 7 dpf WIK-strain zebrafish larvae were used. WIK broodstock were held in dechlorinated mains tap water (culture water), which was routinely monitored for water quality parameters. Fertilized eggs were collected shortly after spawning and transferred to Petri

dishes which were filled with culture water and held at  $28 \pm 1^\circ\text{C}$  until 6 dpf (for full details, see Winter et al., 2017).

### 5.2.2 *Experimental methodology*

Experiments were performed identically to a previous study (Winter et al., 2008), as outlined briefly below. The day before behavioural tracking was due to be performed, petri dishes containing 6 dpf zebrafish larva were cleaned in order to remove debris that could interfere with tracking. Larva were subsequently transferred into a Corning Costar 24 well plate along with 600ml of culture water, a single larva per well. For each compound, 4 x 24 well plates were used, which allowed for 6 different drug treatment concentrations to be used in addition to a vehicle control (2% dimethylsulphoxide or DMSO) and a positive control (PTZ 5mM) with  $n=12$  for each treatment group. Drug treatment concentrations (outlined in Table 5.1) and controls were distributed randomly across rows of each plate. Animals were not fed from this point to prevent introduction of material that may interfere with tracking. On the day experiments were performed (7 dpf), the viewpoint video tracking system was turned on at least an hour before commencing experiments to allow for warm up time. During this time, compounds were dissolved in 2% DMSO and pH adjusted to between 7 and 8 before experiments were due to be performed. Assays were performed at approximately the same time each day to prevent potential confounds as a result of circadian rhythm. Video tracking was performed using VideoTrack for Zebrafish™ (Version 2.5 with background subtraction, Viewpoint, France). The system consisted of a video camera (maximum 25 frames per second) to capture movements within predefined tracking areas (one area=one well of the microplate, internal diameter approximately 15 mm), and software to analyse data to give numbers of movements, distances travelled and total durations of movements, within 3 predefined 'speed' categories. These 3 speed categories were: low-medium speed movements of  $<5$  mm/s; medium speed movements of between 5 and 20 mm/s; and high-speed movements of  $>20$  mm/s. In addition to speed-based tracking, the number of larval rotations was also analysed. Each of the variables and their corresponding abbreviations are outlined in Table 5.2. Once plates were placed into the tracking system, a 5 minute baseline recording was performed to

ensure tracking was occurring correctly. After the baseline recordings and tracking were checked and considered to be performing appropriately, the plates were removed, and test compound added. The test compound was added by removing 500ml of water from each well and replacing it with an appropriate amount of test compound, or culture water in control wells. Once all treatments have been added to the plates, plates were placed back in the video tracking system and recorded for an hour. The mean of each variable measured over the hour time period was then binned into 10-minute intervals. The mean timeseries obtained for each treatment group are shown in Figure 5.1.

Compound	Concentrations
Aminophylline	1000µM, 500µM, 250µM, 125µM, 63µM, 31µM
Chlorpromazine	125µM, 62µM, 31µM, 16µM, 8µM, 4µM
Donepezil	62µM, 31µM, 16µM, 8µM, 4µM, 2µM
Picrotoxin	120µM, 60µM, 30µM, 15µM, 8µM, 3µM
PTZ	1000µM, 500µM, 250µM, 125µM, 63µM, 31µM
RST	1000µM, 500µM, 250µM, 125µM, 63µM, 31µM
SB205607	500µM, 250µM, 125µM, 62.5µM, 31µM, 16µM

**Table 5.1:** Compounds and concentration ranges used.

Abbreviations	Description
inact	number of movements (< 5mm/sec)
inadur	amount of time spent (< 5mm/sec)
inadist	distance travelled (< 5mm/sec)
smlct	number of movements (5mm/sec < x < 20mm/sec)
smldur	amount of time spent (5mm/sec < x < 20mm/sec)
smldist	distance travelled at (5mm/sec < x < 20mm/sec)
larct	number of movements (> 20mm/sec)
lardur	amount of time spent below (> 20mm/sec)
lardist	distance travelled at (> 20mm/sec)
rotation	Number of rotations

### 5.2.3 Data Analysis

All data analysis was performed in Python using the sklearn, scipy, panda, numpy, and matplotlib toolboxes downloaded under the Anaconda distribution 2021.11 (2021).

## 5.2.4 Data Preparation

Plotting the timeseries of the mean swimming distances at high speed for larvae in each treatment group revealed that high speed swimming occurred in peaks of activity over the duration of the test period. This is unsurprising as high-speed swimming is fatiguing, so it would likely be followed by periods of rest. This can be clearly observed across many of the treatment groups, as seen in Figure 5.1. In order to reduce the dimensionality of the data and produce a single measurement for each variable, all analysis was performed on “peak time point means”, which we defined as the mean of the two time points for each larva, for which the variable being measured was greatest. Selecting these higher-value data points ensured that analysis was performed for the more pertinent timepoints in the timeseries, and limited the introduction of noise from consequential time points. This analysis approach is advantageous as it takes into account the variable onset time of different compound mechanism in

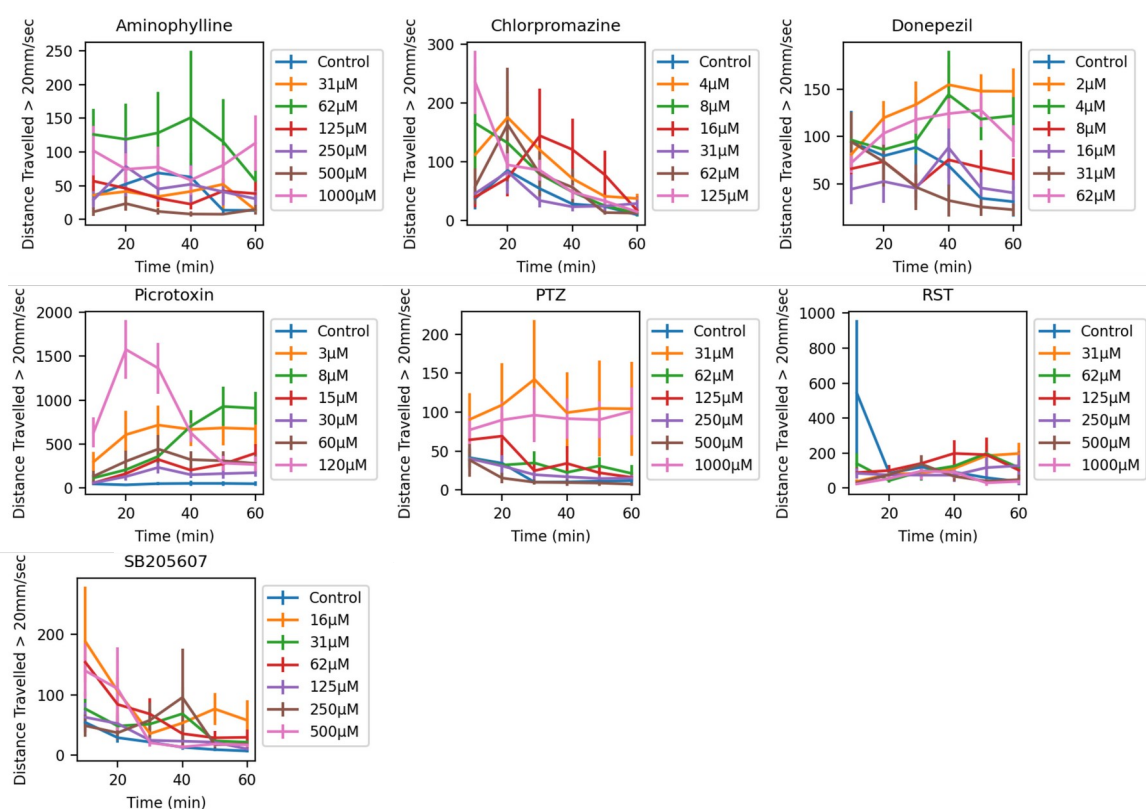


**Figure 5.1:** The mean timeseries of the high speed swimming distance (lardist) for each treatment group (with positive control exempted for ease of visualisation, as it was much higher than other groups). Error bars are standard error of the mean, n=12.

different individual fish. Moreover, it takes into account that the behavioural effect of the drug may wane over time if larva succumb to fatigue.

#### 5.2.5 Data Analysis: PTZ vs Control (Positive Control vs Negative Control)

Each dataset for an individual test compound contained 12 control and 12 PTZ-exposed animals. As there were 8 test compounds, this amounted to  $n=84$  for both PTZ and control larva. Each behavioural parameter was normalised by dividing each larva by the mean of that variable across all 168 control and PTZ exposed larvae. Next, the mean and standard error of the mean (SEM) was calculated for each variable across the PTZ and control treatment groups (Figure 5.2). Each variable was compared between PTZ and control using a Mann Whitney U-test in order to establish if behavioural parameters measured in zebrafish larvae were altered after application of PTZ. The p-values were corrected for multiple comparisons using the Benjamini and Hochberg method (Benjamini and Hochberg, 1995). These initial analyses were performed to establish behavioural parameters that appeared sensitive to convulsant drug exposure and to confirm the optimal parameters with which to perform regression analyses.

#### 5.2.6 Data Analysis: Polynomial Linear Regression

The regression analyses were performed on swimming distance at high speed, as this variable showed the largest normalised mean difference between PTZ and control (Figure 5.2). The independent variable for regression analyses was the concentration of each compound, and the predictor variable was the swimming distance at high speed (Figure 5.3). The regression line was fitted to the data using a gradient descent algorithm designed to minimise the sum of the squared residuals between the line and the data points. The order of the regression equation polynomial was optimised for fit by finding the minimum bayes information criterion (Neath and Cavanaugh, 2012), although the maximum order was set at 2. This was due to the large gap between the highest and second highest concentration causing aberrant predictions with higher order polynomials. The quality of the fit of the regression line was measured using the  $R^2$  value for the fitted line and the F-statistic for the line which resulted in a p-value (Huang and Che, 2008).



### 5.2.7 Data Analysis: Logistic Regression

In order to make predictions about the seizure status of individual larvae exposed to the selected compounds, a logistic regression model was trained to classify PTZ exposed fish vs water control fish. This model was chosen to provide a probability measure for classification in the case of binary outcomes. In order to train and test the model, the positive control (PTZ) and solvent control data were used. This dataset was then split into a training set (80% of the data) and a test set (20%) so that the trained model could be tested on unseen dataset and the accuracy and generalisability could be assessed. The high-speed distance (*lardist*) and high-speed count (*larct*) variables were selected as features for performing the logistic regression as they had the largest difference from control in the univariate analysis (Figure 5.2). The high-speed duration variable was not included as it was considered that this variable would be directly correlated with the high-speed distance measurement. Feature selection was performed to reduce the amount of noise introduced to the model. Multidimensional scaling was used to illustrate the reduction in noise achieved by reducing the number of variables (Figure 5.4).

A logistic regression model is similar to linear regression, in that a regression line is fit to the predictor (*lardist* and *larct*) and independent variables. This involves iteratively optimising the coefficients of the regression line equation to minimise the squared distance between the regression line, and the points in the training dataset (Manogaran and Lopez, 2018). The coefficients in this case were optimised using gradient descent in order to find the regression line with the best fit (Ruder, 2016). The logistic regression equation was sigmoidal, as a sigmoid function produces a line that fits binary outcomes (Manogaran and Lopez, 2018). Once the logistic regression model was trained, we tested it against the test data set (20% of the data). All 34 of the test data points were correctly classified by the model, the separation for which is visualised in Figure 5.5. As this model was highly discriminatory between PTZ and water exposed fish behavioural profiles, an additional logistic regression model was trained on the full PTZ and solvent control dataset, using all 168 data points. This model was used to make predictions about the other compounds in the dataset and to identify larvae exhibiting PTZ-like behavioural phenotypes (Figure 5.6).

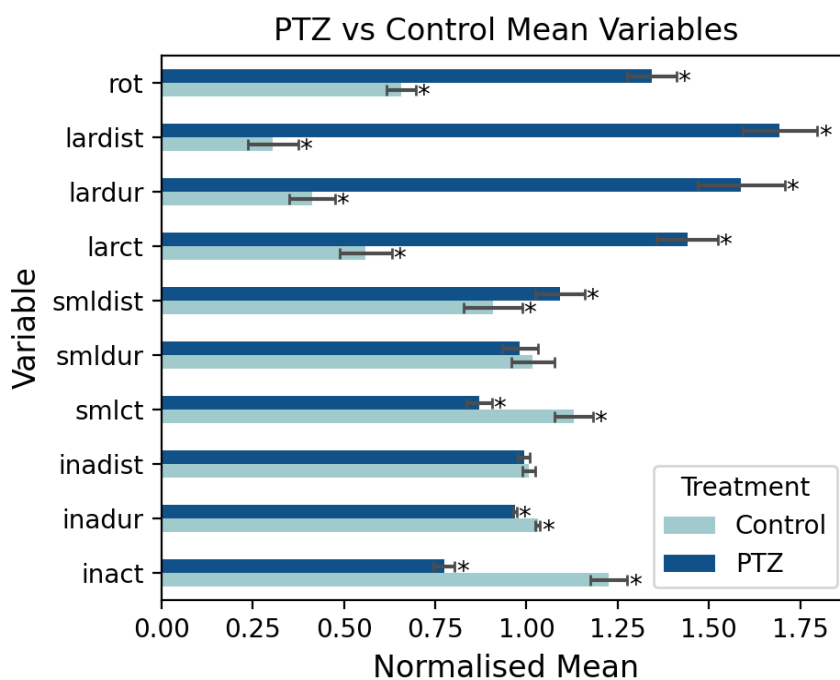


**Figure 5.2:** Bar chart showing the normalised mean of each variable for control larva and PTZ exposed larva. The mean of the two timepoints at which the variable peaks are used. Error bars are standard error of the mean, n=84. Asterisks indicate a statistically significant difference between PTZ 5mM and control ( $p < 0.05$ ) as defined by a Mann Whitney U-test, corrected for multiple comparisons using the Benjamini and Hochberg method (Benjamini and Hochberg, 1995).

As PTZ is a potent convulsant compound these behavioural phenotypes are considered indicative of seizure. Larvae in this case were identified as PTZ like if they had a classification probability of 0.95.

### 5.3 Results

#### 5.3.1 PTZ vs Control

For each compound tested, we used a positive (PTZ 5mM) and negative control (2% DMSO). When 5mM PTZ-exposed larvae were compared with water for each of the behavioural variables tested, there were significant differences in all parameters with the exceptions of medium swim speed duration and low speed swimming distance (Figure 5.2). By far the largest differences were observed in the high speed swimming variables, providing evidence that high speed swimming is associated with seizurogenesis induced by PTZ in larval zebrafish,

a finding consistent with previous studies (Winter et al., 2008). This information was used to inform feature selection in subsequent regression analyses.

### 5.3.2 Polynomial Linear Regression

As high-speed swimming was associated with seizurogenesis, regression analysis was performed to model the relationship between compound concentration and the high speed swimming distance. Of the compounds tested picrotoxin had the strongest association between drug concentration and high-speed movement, with a  $R^2$  value of 0.23 and p-value of  $< 0.05$  (Figure 5.3).

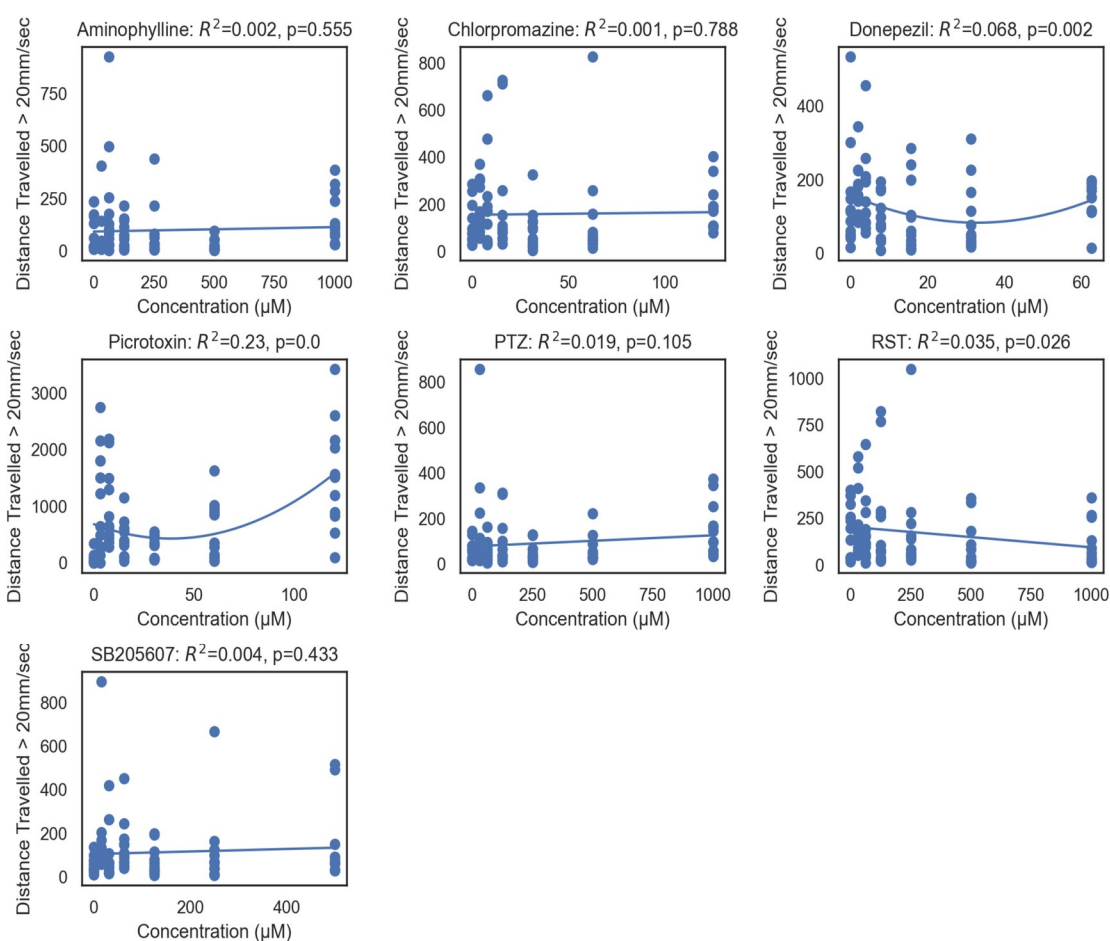


**Figure 5.3:** Regression analyses of each compound with concentration on the x-axis and distance at high speed on the y-axis. Points on graph represent individual larva. Lines on graph are regression lines representing the association between drug exposure concentration and distance moved at high speed.  $R^2$  values and F-statistic p-values are in the title alongside compound name.

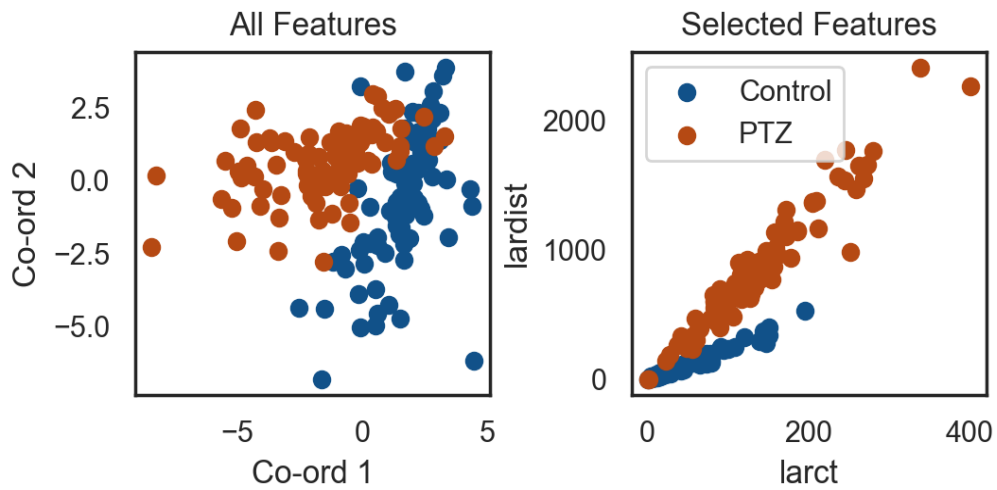


**Figure 5.4:** Multidimensional scaling of all variables (left) vs just the selected variables (right). The selected variables in this case were High speed distance and high-speed count.

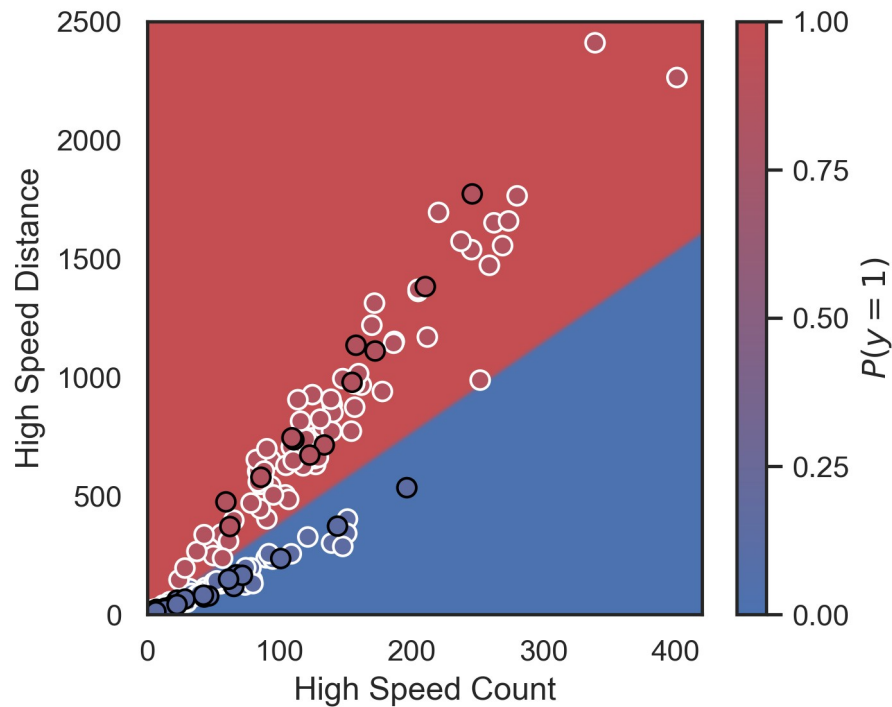


**Figure 5.5** Illustration of logistic regression model where larvae whose points are in the red part of the graph are predicted as PTZ-like and larvae whose points are in the blue part of the graph are untreated controls. The colour bar on the right-hand side shows the colour of the probability distribution of the logistic regression. All red points plotted on the graph are PTZ exposed larva and all blue points are water control larva. The points with a white outline are test group data points and points with a black outline are training group points.

Higher concentrations of picrotoxin were generally associated with an increase in high-speed movement. The line of best fit was slightly curved suggesting that the lowest concentrations had a slightly greater impact on high-speed movement than middle concentrations. It may be that picrotoxin has a milder stimulant effect at lower concentration and induces seizure activity at the highest concentration and that both states manifest in increased high-speed movement. Similarly to picrotoxin, donepezil induced greater increases in high-speed movement at lower and higher concentrations, as compared to the middle concentrations. Finally, the concentration of RST had a linearly negative association with distance moved at high speed. This result was unexpected, as RST is a convulsant compound and would perhaps be expected to increase high speed swimming.

### 5.3.3 *Logistic Regression*

The logistic regression model was 100% accurate when assessed against the test dataset. Data points plotted over the background of the logistic regression model, shown in Figure 5.5, illustrate the clear separation of 5mM PTZ-exposed and control larvae along the regression line. From this, it was clear that high speed swimming distance and the number of bouts of high-speed swimming were strong predictors for the effect of 5mM PTZ exposure.

When seizurogenic compound-treated larvae were classified using logistic regression, those exposed to aminophylline, chlorpromazine, donepezil, PTZ, RST and picrotoxin were classified as PTZ-like. Picrotoxin-treated larva were by far the most frequently categorised as PTZ-like (29 out of 72 larvae).

Notably, after exposure to lower concentrations of PTZ (1mM) only one PTZ exposed larva was classified as PTZ-like suggesting a considerable difference in the response and phenotype in animals exposed to 5mM versus 1mM PTZ. Multiple donepezil and chlorpromazine exposed larva were categorised as PTZ-like but only for the lower concentrations. By contrast, RST exposure resulted in PTZ-like categorised larva across the full test concentration range.

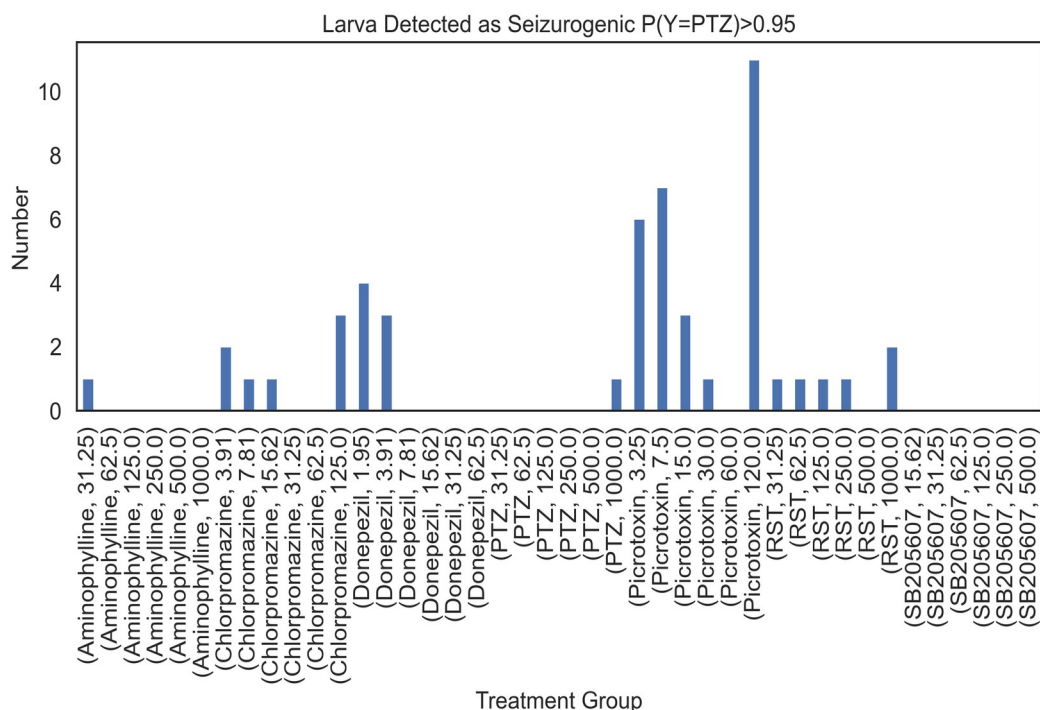


**Figure 5.6:** Bar chart showing the number of larvae classified as PTZ-like with a probability of more than 0.95 for each treatment group.

#### 5.4 Discussion

Using behavioural tracking and swimming speed-based analysis, we demonstrated the responsiveness of 7 dpf larval zebrafish to a variety of seizurogenic compounds. Moreover, a highly discriminatory logistic regression model was trained to classify PTZ-exposed larvae based on their behavioural profiles. This approach was then used to detect seizurogenic compounds, where we demonstrated that at least one larva per compound had a PTZ-like behavioural profile (with the only exception of SB205607). PTZ is a compound with well established seizurogenic properties (Samokhina and Samokhin, 2018), and thus PTZ-like behavioural profiles of the test compounds are comparatively indicative of seizurogenesis.

Due to the ability to record multiple larvae simultaneously and vastly higher throughput, behavioural screening has an advantage over electrophysiological and light sheet-based seizure profiling. Behavioural data are therefore conducive to the use of machine learning models, which typically benefit from higher n-numbers in order to be generalizable and accurate (Jordan and Mitchell, 2015). However, the use of machine learning models in this context

has been extremely limited. Previous approaches have mostly utilised univariate inferential statistics, focussing either on high speed distance (Winter et al., 2008) or total distance travelled (Berghmans et al., 2007). Machine learning models have obvious advantages in this regard, as they allow for combinations of variables to be used as predictors of specific outcomes. There is a variety of behavioural outputs that can be measured beyond swimming activity: for example, a previous study using kainate injected fish measured a variety of different endpoints, such as convulsions and spasmodic muscular contractions (Alfaro et al., 2011).

There is significant potential for a lack of specificity in studies relying on swimming distance and speed-based measures. While a high speed movement and distance travelled have been shown to be effective predictors of seizurogenesis (Baraban et al., 2013b; Winter et al., 2008), there has also been reported motor stimulation in zebrafish after exposure to a variety of non-seizurogenic compounds, such as naproxen, ethambutol and lead acetate (Ali et al., 2012; Winter et al., 2008). Increased locomotion is a behavioural outcome that could be associated with any number of stimulant or irritant compounds, seizurogenic or not.

In contrast, behavioural profiling for identification of seizure in rodents categorises multiple behavioural traits such as (1) freezing, staring, mouth, or facial movements; (2) head nodding or isolated twitches, rigid posture; (3) tail extension, unilateral–bilateral forelimb clonus; (4) rearing, in which the mice sit in an immobile state on their rear haunches with one or both forepaws extended; (5) clonic seizures, loss of posture, jumping, and forepaws extended; (6) tonic seizures with hind limb extension (Tsverava et al., 2019). Many of these behavioural traits result in reduced movement, as opposed to increased, while still being considered indicative of seizure. This suggests that zebrafish behavioural profiling of distance travelled or high-speed movements may lack the sensitivity to identify all types of seizures or ictal responses.

Introducing a larger set of variables fitted to a logistic regression model, as described in this study, may help improve the generalizability of the models to different compounds and/or seizure causes. However, in order for behavioural analysis to remain high throughput, automated ways of identifying such

behaviour would need to be developed, as behavioural profiling of rodents is typically performed by expert practitioners closely observing the behaviour of individual rodents. In addition, generalizability could be further achieved by training the model using a wider variety of seizure precipitants/models, such as seizure phenotype transgenic fish that imitate genetically caused seizure states such as Dravet syndrome (Griffin et al., 2021).

Despite the scope for improvement, the model we present here compares well with other approaches described in this thesis. In both the electrophysiological (Chapter 3:) and light sheet based approaches (Chapter 4:), the most active compounds (defined by electrographic events and imaging-based endpoints) were donepezil, picrotoxin, RST and PTZ. This aligns with the behavioural data wherein donepezil, picrotoxin and RST were among the most active. Similarly, SB205607 and aminophylline were typically less responsive across all methodologies. The relatively low activity of PTZ in the 1mM and below concentration range is likely related to the dose of compound. Indeed, seizure modelling studies in zebrafish typically use between 5mM and 15mM of PTZ (Liu and Baraban, 2019; Turrini et al., 2017; Winter et al., 2017). Furthermore, light sheet microscopy data suggests PTZ at 1.25mM doesn't have a significant effect on overall brain activity (Figure 4.4). As such it seems 1mM PTZ isn't a sufficient dose to induce seizures detectable either by light sheet or behavioural assays, however, may prove to be an optimal dose for seizure kindling studies.

To summarise, high speed movement is strongly discriminatory between PTZ exposed and control fish. As such, high speed movement is a good indicator of seizurogenesis, with sensitivity to compounds other than PTZ including picrotoxin, RST and donepezil. However, the generalisability and specificity of this approach to behavioural seizure profiling would benefit from additional measures.



## Chapter 6: General Discussion

The overall aim of this thesis was to evaluate the potential utility of non-protected larval zebrafish (<5 days post fertilisation, or dpf), with a variety of different methodologies, for drug seizure liability assessment and screening. In order to achieve this, the work sought to address a series of different hypotheses (1.7). The first hypothesis asked whether there were distinct spatio-temporal patterns of neural activity, indicated by changes in  $\text{Ca}^{2+}$  levels, that occur in the larval zebrafish brain upon exposure to compounds with specific mechanisms of action. Further to this, the aim was to ascertain if these profiles were indicative of the seizurogenicity of the test compounds. This initial hypothesis was formulated as it was considered that a good assay of seizure liability would provide information about whether a compound was seizurogenic, and if so which compound mechanisms of action were at play.

In order to assess spatiotemporal patterns of activation, we adapted the methods used in fMRI analysis Chalovich and Eisenberg (2007), and this generated functional connectomes for individual larva. Functional connectivity of EEG has been shown to be highly predictive of epilepsy diagnosis (Lee et al., 2014) and has also been applied for localising epileptogenic regions within the brain (van Mierlo et al., 2014). In resting larval zebrafish, functional connections were strongest between regions associated with homeostatic control, sensory processing and motor activity, which aligned well with the expected light response, and agreed with data from previous imaging studies (Ahrens et al., 2012). Hierarchical cluster analysis performed on the mean connectome from larvae exposed to each compound revealed that monoaminergic and cholinergic compounds in particular group closely based on functional connectivity profiles. Moreover, increases in functional connectivity were strongly associated with seizurogenic compounds, with the exception of pilocarpine and bicuculline. This aligns with previous research showing functional connectivity increases in larval zebrafish as a result of PTZ exposure (Liu and Baraban, 2019; Turrini et al., 2022). Furthermore, increases in overall fluorescence and, by proxy, overall brain activity, were correlated with more seizurogenic compounds.

Seizures are typically characterised by both hypersynchronous and excessive brain activity. Our results similarly indicate drug-induced hyperexcitation, as evidenced through increases in functional connectivity, as well as global increases in fluorescence correlated with seizurogenic compounds. In addition, there was a clear correlation between some drug mechanisms of action, and the spatiotemporal profiles generated after exposure. It was hypothesised that pharmaco-specific spatiotemporal patterns of activation were likely to be the result of drug-target specific receptor distribution, with the locations of activated receptor types correlating with the ROIs activated, based on the  $\text{Ca}^{2+}$  imaging data. In the case of monoaminergic compounds, there was strong evidence in favour of this hypothesis. In addition to colocalising during clustering, monoaminergic compounds appeared to increase connectivity between regions known to be connected by noradrenergic, dopaminergic and adrenergic pathways in zebrafish (and mammal). By contrast, GABAergic compounds, which have a less punctate and more widely dispersed receptor distribution, had disparate functional connectivity profiles. For example, gabazine and bicuculline both cause reductions in functional connectivity in multiple connections, while picrotoxin, bemegride and PTZ tended to increase functional connectivity.

These results gave a good indication of the potential of  $\text{Ca}^{2+}$  imaging of zebrafish larva for assessing compound seizure liability and revealing information about the likely mechanism(s) of action. However, the experimental methodology we used had multiple limitations, predominantly, the inability to perform drug-free baseline recordings prior to compound exposure, due to the fact that the larva were encased in a capillary tube. This meant it was not possible to account for any variation in GCaMP expression between individual animals which ultimately contributed to the variability in response observed within each dataset. In order to address this, a new light sheet microscope system was adapted. With modifications to the imaging stage, and to the method used for agarose embedding, this new system allowed the addition of compounds *in situ*, while also improving speed and dynamic range. In this approach, the need to perform baseline and exposure periods increased the duration and significantly reduced throughput of the experiments. This reduction in throughput may be a limiting factor for the application of this

method in early stages of drug development, where many compounds need to be tested, and thus the throughput of any deployed assay is critical. As such this updated approach offered a compromise, between throughput and faster imaging with baseline recordings. In future, were automated and highly consistent larva-laser orientation software employed multiple larva could potentially be run concurrently greatly increasing throughput, as larva could be removed from the stage during compound exposure and subsequently replaced without the concern of the larval orientation.

Using this modified light sheet imaging method, a subset of compounds was assessed from the original full set of compounds used in Chapter 1. Compounds were selected to have varied pharmacology while also being associated with seizurogenesis, either clinically or in mammalian research. As before, all seizurogenic compounds resulted in at least some increases in fluorescence, with the exception of chlorpromazine, which reduced fluorescence across the majority of brain regions in the original light sheet system method as well (Chapter 2). A possible reason for the lack of response with chlorpromazine was that this drug is a monoamine antagonist and might be expected to reduce neurotransmission overall. When comparing the outputs from the two systems, the overall fluorescence intensity produced in response to compound exposure was broadly similar across treatment groups. Moreover, both systems also detected large increases in functional connectivity upon exposure to donepezil and picrotoxin. Donepezil in particular resulted in a state of hypersynchronicity quantitatively considerably greater than any other compound, a finding consistent between the two approaches. This dramatic response induced by donepezil is unique to donepezil, and was not mirrored by the other cholinesterase inhibitors, which indicates that it is likely that to be independent of this mechanism. An alternative mechanism can be proposed to be mediated by the  $\sigma_1$  receptor, a receptor highly concentrated in the nervous system which modulates intracellular  $\text{Ca}^{2+}$  signalling through the IP3 receptor (Maurice and Su, 2009). Donepezil is a potent agonist of the  $\sigma_1$  receptor (Maurice and Su, 2009), so it is possible that the hypersynchronous  $\text{Ca}^{2+}$  transients detected in larval zebrafish result from intracellular  $\text{Ca}^{2+}$  signalling, as opposed to hypersynchronous neurotransmission. This hypothesis is imminently testable using multi-electrode arrays in conjunction with coherence or functional

connectivity analysis to assess if hyper-synchronicity of neurotransmission is truly present. If this hypothesis was confirmed, it would reveal some of the inherent flaws with using  $\text{Ca}^{2+}$  as a reporter of synaptic transmission, as  $\text{Ca}^{2+}$  has many roles outside of signalling neurotransmitter release and its levels can be influenced by drugs in a variety of ways.

Future imaging studies could use genetically encoded voltage indicators (e.g. zArchon1-GFP) as an alternative to GCaMP (Miyazawa et al., 2018), which would provide a more direct measure of brain activity, that may be less sensitive to the influence of  $\text{Ca}^{2+}$ -level related pharmacology. Genetically encoded voltage indicators have already been successfully used to observe activity in spinal cord neurons in visually stimulated larval zebrafish (Böhm et al., 2022). Using this technique, Böhm et al were able to detect oscillations at timescales comparable to electrophysiology from multiple neurons simultaneously.

While exposure to picrotoxin and donepezil resulted in changes in functional connectivity, using the second 'within animal' based light sheet imaging approach, aminophylline, chlorpromazine, PTZ, RST and SB205607 did not. This was surprising as all of these compounds resulted in changes in functional connectivity using the previous methodology. It's difficult to explain why this approach appears less sensitive with regard to identifying changes in functional connectivity, however, there are some possible explanations. Primarily, there may have been additional variability introduced due to an increase in the inconsistency of larva orientation. Efforts were made to have larva orientated as identically as possible, however, this was more challenging than in the previous assay. One potential solution to this would be to utilise a computer controlled 6-axis stage and use automated image analysis to control the orientation of the larva such that it optimises in a relation to a reference image set. This would be a challenging approach to implement but would improve the reproducibility of results while also making light sheet imaging in zebrafish more accessible (in terms of skill) and higher throughput. Moreover, if such a system was substantially faster than manual orientation, it would reduce laser exposure to the larva, reducing the potential for photobleaching or phototoxicity.

In addition to  $\text{Ca}^{2+}$  imaging, we performed LFP recordings on the same subset of compounds in order to assess concordance between functional imaging

responses to drugs, and direct electrophysiological measurement of network hyperexcitability. This allowed confirmation of the electrographic basis of observed  $\text{Ca}^{2+}$  activity and provided data to help translate to a more established measure of seizurogenesis. Broadly speaking, the electrophysiological measures aligned well with functional imaging outputs. SB205607 was relatively inactive using both measures, while picrotoxin, RST and aminophylline were all relatively active, increasing fluorescent intensity and voltage amplitude in multiple frequency bands. Notably, donepezil was considerably less active in local field potential recordings compared with functional imaging. Donepezil exposure resulted in no significant changes in amplitude in any of the frequency bands, although it did result in an increase in the number of events detected and induced some characteristic waveforms. By comparison,  $\text{Ca}^{2+}$  imaging revealed large, hypersynchronous oscillations throughout the zebrafish brain. Given the large oscillations present in  $\text{Ca}^{2+}$  imaging, the presence of large oscillations and resultant increases in amplitude could be expected in the electrophysiological recordings, however this was not the case. This aligns with the aforementioned hypothesis that  $\text{Ca}^{2+}$  oscillations are driven by the  $\sigma_1$  receptor, as opposed to generalised neurotransmission, which highlights a disparity between  $\text{Ca}^{2+}$  reporters and neurotransmission in certain pharmacological contexts. Chlorpromazine, by contrast had comparable electrophysiological and functional imaging phenotypes, specifically, exposure resulted in reduced amplitude in multiple frequency bands in a concentration-dependent manner while also reducing average fluorescence in a concentration-dependent manner.

Overall, we found that  $\text{Ca}^{2+}$  imaging represents a good indirect measure of brain activity, and that  $\text{Ca}^{2+}$  imaging of seizurogenic compounds correlates qualitatively with electrophysiological phenotypes, with the caveat that compounds with pharmacodynamics influencing intracellular  $\text{Ca}^{2+}$  directly (as opposed to via action potentials) may appear to have disparate phenotypes between the two methods. This is due to an intracellular  $\text{Ca}^{2+}$  release resulting from the direct pharmacological effect of a compound, as opposed to neurotransmission, meaning that  $\text{Ca}^{2+}$  imaging results become less reflective of brain activity.

Electrophysiological recordings are widely used in both non-clinical models of seizures (Fonck et al., 2015) and as a diagnostic tool in clinical practice (Jaiswal and Banka, 2018). As such, performing electrophysiological recordings provides an ideal opportunity to compare larval zebrafish with more established animal models as well as humans. In doing so, we hoped to improve understanding of the larval zebrafish as a model for seizure liability testing.

When comparing representative traces from larval zebrafish exposed to seizurogenic compounds with EEG recordings from epilepsy patients (Fisher et al., 2014b) there were multiple qualitative similarities. Specifically, chlorpromazine, donepezil, RST and picrotoxin all had representative traces with either pre-ictal, inter-ictal or ictal like waveforms based on classifications from mammalian EEG data. In addition, frequency band analysis revealed multiple similarities between larval zebrafish and mammalian EEGs. Indeed, increases in the  $\gamma$  and high  $\gamma$  frequency bands, are a feature of epilepsy in humans, possibly due to cortical excitation, (Herrmann and Demiralp, 2005) and were consistently altered by the convulsant compounds RST and picrotoxin implying similarities in pathophysiology. Moreover, exposure to NMDA agonists (Herrmann and Demiralp, 2005) and picrotoxin (Herrmann and Demiralp, 2005) has been shown to result in increases in  $\gamma$  activity in studies in mammalian models, as was the case here in larval zebrafish. Similarly, chlorpromazine resulted in a distinctive reduction in high frequency oscillations here, similar to findings after dosing with antipsychotic medications in rats (Olszewski et al., 2013).

In addition to performing direct recordings of brain activity we also utilised swimming speed analysis to assess behavioural changes induced by different pharmacological agents. By modelling swimming speed patterns using regression analysis, we showed a clear indication that 5mM PTZ exposure results in increased bouts of high-speed swimming as has previously been reported (e.g. Winter *et al.*, 2008). Moreover, a logistic regression model was trained on high-speed swimming parameters and shown to be highly discriminatory between 5mM PTZ-exposed and with control larvae. Behavioural analysis aligned well with the imaging and electrophysiological assays, identifying donepezil, RST and picrotoxin as the most active compounds, and thus cross-validating these assays. While behavioural analyses were

advantageous due to being vastly higher throughput, they had multiple limitations. Specifically, it seems likely that compounds need to be powerfully seizurogenic in order to elicit a response, as shown previously in studies assessing a wider range of seizurogenic compounds (Winter et al., 2008). Moreover, compounds that are perhaps not seizurogenic, but have stimulant properties may be misclassified. This would likely be mitigated by using more specific measures of zebrafish behaviour such as convulsions and measures of posture. Sophisticated image analysis approaches using convolutional neural networks already exist for this purpose, and could be implemented to improve our methodology (Huang et al., 2021).

One of the primary approaches that would address a potential lack of sensitivity of behavioural profiling, and could be used to heighten the sensitivity of all of the above assays, is using kindling protocols to pre-sensitise larvae. Seizure kindling typically involves exposure to sub-seizure threshold doses of PTZ, prior to application of the test compound (Samokhina and Samokhin, 2018). From our experiments in larval zebrafish, a suggested exposure concentration of PTZ would be approximately 1mM. This approach may be more optimal for identifying compounds that don't typically cause seizures in isolation, but may occasionally cause seizures under particular circumstances, such as in combination with other drugs or in individuals with an increased susceptibility to seizures. Compounds like aminophylline and donepezil are still used clinically, and do have seizures as an associated risk, but they aren't direct seizure precipitants in the traditional sense. Rather, they are drugs with pharmacodynamics that may encourage seizure generation in predisposed individuals. Indeed, our assays of both of these compounds align to this classification. Given that the goal is to develop a seizure liability assay, it is necessary to also identify compounds that do not cause seizures on their own, and in these cases a seizure kindling model would likely help.

To further improve the efficacy of functional imaging approaches for detecting seizure, a higher resolution ROI selection approach could be used. Our current approach using anatomical ROI selection, while ideal for making comparisons with the literature and validating the model, would benefit from having a greater number of ROIs covering more precise (and smaller) brain regions. Indeed, the anatomical ROIs used were derived from a dataset extracted from 7 dpf larva,

which are significantly more developed. As we have generated a large imaging dataset for control larvae, there is an ideal opportunity to develop a new ROI selection protocol based on the functional imaging phenotypes, and thus have a ROI selection criterion more directly applicable to the assay. Indeed, deep learning algorithms have been used for image segmentation in pathology detection and have been effective in rapidly speeding up clinical diagnoses (Wang et al., 2019). It is possible that such approaches could be applied in larval zebrafish for generating an improved ROI mask for 4 dpf larval zebrafish.

Taken together, the work presented in this thesis shows that larval zebrafish offer an excellent opportunity to develop alternative approaches to drug-induced seizure detection. Functional imaging approaches in particular are highly informative about drug mechanism of action. While local field potential recordings offer the best insight into seizure dynamics, and behavioural profiling offers by far the highest throughput. However, further innovations, including but not limited to, using seizure kindling models, genetically encoded voltage indicators and more developed image analysis could potentially improve the ability of functional imaging to detect seizurogenicity in drugs. Without doubt the potential of this approach is enormous and with continued advancements in imaging technology and image analysis, it has the potential to be a standardised approach for assessing drug induced seizure in early drug development.



## Bibliography

- Accardi M V., Pugsley MK, Forster R, Troncy E, Huang H, Authier S (2016) The emerging role of in vitro electrophysiological methods in CNS safety pharmacology. *J Pharmacol Toxicol Methods* 81:47–59.
- Afrikanova T, Serruys A-SK, Buenafe OEM, Clinckers R, Smolders I, de Witte PAM, Crawford AD, Esguerra C V. (2013) Validation of the Zebrafish Pentylentetrazol Seizure Model: Locomotor versus Electrographic Responses to Antiepileptic Drugs. *PLoS One* 8:e54166.
- Ahmad F, Noldus LPJJ, Tegelenbosch RAJ, Richardson MK (2012) Zebrafish embryos and larvae in behavioural assays. *Behaviour* 149:1241–1281.
- Ahnaou A, Huysmans H, Jacobs T, Drinkenburg WHIM (2014) Cortical EEG oscillations and network connectivity as efficacy indices for assessing drugs with cognition enhancing potential. *Neuropharmacology* 86:362–377.
- Ahrens MB, Freeman J, Phillip K, Looger LL, Yang C, Bennett D, Kawashima T, Mu Y, Vladimirov N (2014) Light sheet functional imaging in fictively behaving zebrafish. *Nat Methods* 11:883–884.
- Ahrens MB, Li JM, Orger MB, Robson DN, Schier AF, Engert F, Portugues R (2012) Brain-wide neuronal dynamics during motor adaptation in zebrafish. *Nature* 485:471–477.
- Ahrens MB, Orger MB, Robson DN, Li JM, Keller PJ (2013) Whole-brain functional imaging at cellular resolution using light sheet microscopy. *Nat Methods* 10:413–420.
- Akerboom J, Rivera JDV, Rodríguez Guilbe MM, Malavé ECA, Hernandez HH, Tian L, Hires SA, Marvin JS, Looger LL, Schreier ER (2009) Crystal structures of the GCaMP calcium sensor reveal the mechanism of fluorescence signal change and aid rational design. *J Biol Chem* 284:6455–6464.
- Albertson TE, Stark LG, Joy RM, Bowyer JF (1983) Aminophylline and kindled seizures. *Exp Neurol* 81:703–713.
- Alexander SPH et al. (2019a) THE CONCISE GUIDE TO PHARMACOLOGY 2019/20: G protein-coupled receptors. *Br J Pharmacol* 176:S21–S141.

- Alexander SPH et al. (2019b) THE CONCISE GUIDE TO PHARMACOLOGY 2019/20: Enzymes. *Br J Pharmacol* 176:S297–S396.
- Alexander SPH et al. (2019c) THE CONCISE GUIDE TO PHARMACOLOGY 2019/20: Transporters. *Br J Pharmacol* 176:S397–S493.
- Alexander SPH et al. (2019d) THE CONCISE GUIDE TO PHARMACOLOGY 2019/20: Ion channels. *Br J Pharmacol* 176:S142–S228.
- Alfaro JM, Ripoll-Gómez J, Burgos JS (2011) Kainate administered to adult zebrafish causes seizures similar to those in rodent models. *Eur J Neurosci* 33:1252–1255.
- Alhaque S, Themis M, Rashidi H (2018) Three-dimensional cell culture: From evolution to revolution. *Philos Trans R Soc B Biol Sci* 373.
- Ali S, Champagne DL, Richardson MK (2012) Behavioral profiling of zebrafish embryos exposed to a panel of 60 water-soluble compounds. *Behav Brain Res* 228:272–283.
- Alstermark B, Ekerot CF (2013) The lateral reticular nucleus: A precerebellar centre providing the cerebellum with overview and integration of motor functions at systems level. A new hypothesis. *J Physiol* 591:5453–5458.
- Ambrosini A, Bresciani L, Fracchia S, Brunello N, Racagni G (1995) Metabotropic glutamate receptors negatively coupled to adenylate cyclase inhibit N-methyl-D-aspartate receptor activity and prevent neurotoxicity in mesencephalic neurons in vitro. *Mol Pharmacol* 47.
- Anichtchik O, Sallinen V, Peitsaro N, Panula P (2006) Distinct Structure and Activity of Monoamine Oxidase in the Brain of Zebrafish (*Danio rerio*). *J Comp Neurol* 498:593–610.
- Appiah-Ankam J, Hunter JM (2004) Pharmacology of neuromuscular blocking drugs. *Contin Educ Anaesthesia, Crit Care Pain* 4:2–7.
- Arenzana FJ, Clemente D, Sánchez-González R, Porteros Á, Aijón J, Arévalo R (2005) Development of the cholinergic system in the brain and retina of the zebrafish. *Brain Res Bull* 66:421–425.
- Armstrong D, Migeon J, Rolf MG, Bowes J, Crawford M, Valentin JP (2007)

Secondary Pharmacodynamic Studies and In Vitro Pharmacological Profiling. *Preclin Dev Handb Toxicol* 581–609.

Arnold J, O'Connor P, Riddell J, Harron D, Shanks R, McDevitt D (1985) Effects of the beta 2-adrenoceptor antagonist ICI 118,551 on exercise tachycardia and isoprenaline-induced beta-adrenoceptor responses in man. *Br J Clin Pharmacol* 19:619–630.

Ashford JW (1998) Seizures in Patients Receiving Concomitant Antimuscarinics and Acetylcholinesterase Inhibitor. *Case Reports* 5–8.

Avoli M, Jefferys JGR (2016) Models of drug-induced epileptiform synchronization in vitro. *J Neurosci Methods* 260:26–32.

Bandara SB, Carty DR, Singh V, Harvey DJ, Vasylieva N, Pressly B, Wulff H, Lein PJ (2020) Susceptibility of larval zebrafish to the seizurogenic activity of GABA type A receptor antagonists. *Neurotoxicology* 76:220–234.

Baraban SC (2013) Forebrain Electrophysiological Recording in Larval Zebrafish. *J Vis Exp* 71:2–5.

Baraban SC, Dinday MT, Castro PA, Chege S, Guyenet S, Taylor MR (2007) A Large-scale Mutagenesis Screen to Identify Seizure-resistant Zebrafish. *Epilepsia* 48:1151–1157.

Baraban SC, Dinday MT, Hortopan GA (2013a) Drug screening in Scn1a zebrafish mutant identifies clemizole as a potential Dravet syndrome treatment. *Nat Commun* 4.

Baraban SC, Dinday MT, Hortopan GA (2013b) Drug screening in Scn1a zebrafish mutant identifies clemizole as a potential Dravet syndrome treatment. *Nat Commun* 4:1–10.

Baraban SC, Taylor MR, Castro PA, Baier H (2005) Pentylentetrazol Induced Changes in Zebrafish Behaviour, Neural Activity and C-Fos Expression. *Neuroscience* 131:759–768.

Baran H, Gramer M, Hönack D, Löscher W (1995) Systemic administration of kainate induces marked increases of endogenous kynurenic acid in various brain regions and plasma of rats. *Eur J Pharmacol* 286:167–175.

- Barker-Haliski M, White HS (2015) Glutamatergic mechanisms associated with seizures and epilepsy. *Cold Spring Harb Perspect Med* 5:a022863.
- Barnett W, O'Brien G, Cymbalyuk G (2013) Bistability of silence and seizure-like bursting. *J Neurosci Methods* 220:179–189.
- Barone P, DeBartolomeis A, Tedeschi E, Campanella G (1991) Dopamine D1 and D2 receptors mediate opposite functions in seizures induced by lithium-pilocarpine 195:157–162.
- Barykina N V., Sotskov VP, Gruzdeva AM, Wu YK, Portugues R, Subach OM, Chefanova ES, Plusnin V V., Ivashkina OI, Anokhin K V., Vlaskina A V., Korzhenevskiy DA, Nikolaeva AY, Boyko KM, Rakitina T V., Varizhuk AM, Pozmogova GE, Subach F V. (2020) FGCaMP7, an improved version of fungi-based ratiometric calcium indicator for in vivo visualization of neuronal activity, *International Journal of Molecular Sciences*.
- Başar E, Başar-Eroglu C, Karakaş S, Schürmann M (2001) Gamma, alpha, delta, and theta oscillations govern cognitive processes. *Int J Psychophysiol* 39:241–248.
- Bassett L, Troncy E, Pouliot M, Paquette D, Ascah A, Authier S (2014) Telemetry video-electroencephalography (EEG) in rats, dogs and non-human primates: Methods in follow-up safety pharmacology seizure liability assessments. *J Pharmacol Toxicol Methods* 70:230–240.
- Beagle A, Darwish S, Ranasinghe K, Karageorgiou A, Vossel K (2017) Relative Incidence of Seizures and Myoclonus in Alzheimer's Disease, Dementia with Lewy Bodies, and Frontotemporal Dementia. *Physiol Behav* 176:139–148.
- Becker PL, Fay FS (1987) Photobleaching of fura-2 and its effect on determination of calcium concentrations. *Am J Physiol - Cell Physiol* 253:613–618.
- Begley CE, Durgin TL (2015) The direct cost of epilepsy in the United States: A systematic review of estimates. *Epilepsia* 56:1376–1387.
- Benjamini Y, Hochberg Y (1995) Controlling the False Discovery Rate: A Practical and Powerful Approach to Multiple Testing. *J R Stat Soc* 57:289–

300.

- Berghmans S, Butler P, Goldsmith P, Waldron G, Gardner I, Golder Z, Richards FM, Kimber G, Roach A, Alderton W, Fleming A (2008) Zebrafish based assays for the assessment of cardiac, visual and gut function - potential safety screens for early drug discovery. *J Pharmacol Toxicol Methods* 58:59–68.
- Berghmans S, Hunt J, Roach A, Goldsmith P (2007) Zebrafish offer the potential for a primary screen to identify a wide variety of potential anticonvulsants. *Epilepsy Res* 75:18–28.
- Bettler B, Kaupmann K, Mosbacher J, Gassmann M (2004) Molecular structure and physiological functions of GABAB receptors. *Physiol Rev* 84:835–867.
- Betzel RF (2019) Organizing principles of whole-brain functional connectivity in zebrafish larvae. *Netw Neurosci* 1–23.
- Bianco IH, Wilson SW (2009) The habenular nuclei: A conserved asymmetric relay station in the vertebrate brain. *Philos Trans R Soc B Biol Sci* 364:1005–1020.
- Birks JS, Harvey RJ (2018) Donepezil for dementia due to Alzheimer's disease. *Cochrane Database Syst Rev* 40.
- Bloechliger M, Rüegg S, Jick SS, Meier CR, Bodmer M (2015) Antipsychotic Drug Use and the Risk of Seizures: Follow-up Study with a Nested Case-Control Analysis. *CNS Drugs* 29:591–603.
- Boehmier W, Obrecht-Pflumio S, Canfield V, Thisse C, Thisse B, Levenson R (2004) Evolution and expression of D2 and D3 dopamine receptor genes in zebrafish. *Dev Dyn* 230:481–493.
- Boehmler W, Carr T, Thisse C, Thisse B, Canfield VA, Levenson R (2007) D4 Dopamine receptor genes of zebrafish and effects of the antipsychotic clozapine on larval swimming behaviour. *Genes, Brain Behav* 6:155–166.
- Böhm UL, Kimura Y, Kawashima T, Ahrens MB, Higashijima S ichi, Engert F, Cohen AE (2022) Voltage imaging identifies spinal circuits that modulate locomotor adaptation in zebrafish. *Neuron* 110:1211-1222.e4.

- Boison D (2016) The biochemistry and epigenetics of epilepsy: Focus on adenosine and glycine. *Front Mol Neurosci* 9:1–7.
- Bradley JA, Luithardt HH, Metea MR, Strock CJ (2018) In vitro screening for seizure liability using microelectrode array technology. *Toxicol Sci* 163:240–253.
- Bregola G, Zucchini S, Rodi D, Binaschi A, D'Addario C, Landuzzi D, Reinscheid R, Candeletti S, Romualdi P, Simonato M (2002) Involvement of the neuropeptide nociceptin/orphanin FQ in kainate seizures. *J Neurosci* 22:10030–10038.
- Brown D (2018) Regulation of neural ion channels by muscarinic receptors. *Neuropharmacology* 136:383–400.
- Brown RE, Stevens DR, Haas HL (2001) The physiology of brain histamine. *Prog Neurobiol* 63:637–672.
- Burgstaller J, Hindinger E, Donovan J, Maschio MD, Kist AM, Gesierich B, Portugues R, Baier H (2019) Light sheet imaging and graph analysis of antidepressant action in the larval zebrafish brain network. *bioRxiv* 618843.
- Burrows DRW, Samarut, Liu J, Baraban SC, Richardson MP, Meyer MP, Rosch RE (2020) Imaging epilepsy in larval zebrafish. *Eur J Paediatr Neurol* 24:70–80.
- Butour JL, Moisand C, Mazarguil H, Mollereau C, Meunier JC (1997) Recognition and activation of the opioid receptor-like ORL1 receptor by nociceptin, nociceptin analogs and opioids. *Eur J Pharmacol* 321:97–103.
- Cassar S, Adatto I, Freeman JL, Gamse JT, Iturria I, Lawrence C, Muriana A, Peterson RT, Van Cruchten S, Zon LI (2020) Use of Zebrafish in Drug Discovery Toxicology. *Chem Res Toxicol* 33:95–118.
- Chalovich JM, Eisenberg E (2007) Assessing Functional Connectivity in the Human Brain by fMRI. *Magn Reson Imaging* 25:1347–1357.
- Chang P, Augustin K, Boddum K, Williams S, Sun M, Hardege D, Chen PE, Walker MC, Terschak JA, Williams RSB (2016) Seizure control by decanoic acid through direct AMPA receptor inhibition 431–443.

- Chang YT, Leahy RM, Pantazis D (2012) Modularity-based graph partitioning using conditional expected models. *Phys Rev E - Stat Nonlinear, Soft Matter Phys* 85:1–17.
- Chen HY, Albertson TE, Olson KR (2016) Treatment of drug-induced seizures. *Br J Clin Pharmacol* 81:412–419.
- Chen PE, Wyllie DJA (2006) Pharmacological insights obtained from structure-function studies of ionotropic glutamate receptors. *Br J Pharmacol* 147:839–853.
- Chi SH, Jeong HG, Lee S, Oh SY, Kim SH (2017) Effects of psychotropic drugs on seizure threshold during electroconvulsive therapy. *Psychiatry Investig* 14:647–655.
- Cho S-J, Byun D, Nam T-S, Choi S-Y, Lee B-G, Kim M-K, Kim S (2017) Zebrafish as an animal model in epilepsy studies with multichannel EEG recordings. *Sci Rep* 7:3099.
- Chu N (1981) Caffeine- and Aminophylline-Induced Seizures. *Epilepsia* 22:85–94.
- Chu Sin Chung P, Boehrer A, Stephan A, Matifas A, Scherrer G, Darcq E, Befort K, Kieffer BL (2015) Delta opioid receptors expressed in forebrain GABAergic neurons are responsible for SNC80-induced seizures. *Behav Brain Res* 278:429–434.
- Cocco A, Rönnerberg AMC, Jin Z, André GI, Vossen LE, Bhandage AK, Thörnqvist PO, Birnir B, Winberg S (2017) Characterization of the  $\gamma$ -aminobutyric acid signaling system in the zebrafish (*Danio rerio* Hamilton) central nervous system by reverse transcription-quantitative polymerase chain reaction. *Neuroscience* 343:300–321.
- Copmans D, Kildgaard S, Rasmussen SA, Ślęzak M, Dirx N, Partoens M, Esguerra C V., Crawford AD, Larsen TO, De Witte PAM (2019) Zebrafish-based discovery of antiseizure compounds from the north sea: Isoquinoline alkaloids TMC-120A and TMC-120B. *Mar Drugs* 17:1–20.
- Corcoran ME (1988) Characteristics of accelerated kindling after depletion of noradrenaline in adult rats. *Neuropharmacology* 27:1081–1084.

- Cox JA, Kucenas S, Voigt MM (2005) Molecular characterization and embryonic expression of the family of N-methyl-D-aspartate receptor subunit genes in the zebrafish. *Dev Dyn* 234:756–766.
- Crouzier L, Denus M, Richard EM, Maurice T, Delprat B, Tavernier A, Diez C, Cubedo N (2021) Sigma-1 receptor is critical for mitochondrial activity and unfolded protein response in larval zebrafish. *Int J Mol Sci* 22.
- Curtis MJ, Alexander S, Cirino G, Docherty JR, George CH, Giembycz MA, Hoyer D, Insel PA, Izzo AA, Ji Y, MacEwan DJ, Sobey CG, Stanford SC, Teixeira MM, Wonnacott S, Ahluwalia A (2018) Experimental design and analysis and their reporting II: updated and simplified guidance for authors and peer reviewers. *Br J Pharmacol* 175:987–993.
- Cymerblit-Sabba A, Schiller Y (2012) Development of hypersynchrony in the cortical network during chemoconvulsant-induced epileptic seizures in vivo. *J Neurophysiol* 107:1718–1730.
- Dana H, Chen TW, Hu A, Shields BC, Guo C, Looger LL, Kim DS, Svoboda K (2014) Thy1-GCaMP6 transgenic mice for neuronal population imaging in vivo. *PLoS One* 9.
- Dana H, Sun Y, Mohar B, Hulse B, Hasseman J, Tsegaye G, Tsang A, Wong A, Patel R, Macklin J, Chen Y, Konnerth A, Jayaraman V, Looger L, Schreiter E, Svoboda K, Kim D (2018) High-performance GFP-based calcium indicators for imaging activity in neuronal populations and microcompartments. *bioRxiv* 434589.
- Dani JA, Bertrand D (2007) Nicotinic Acetylcholine Receptors and Nicotinic Cholinergic Mechanisms of the Central Nervous System. *Annu Rev Pharmacol Toxicol* 47:699–729.
- Daniel MQ (1987) Acetylcholinesterase: enzyme structure, reaction dynamics, and virtual transition states. *Chem Rev* 87:955–979.
- Danon L, Díaz-Guilera A, Duch J, Arenas A (2005) Comparing community structure identification. *J Stat Mech Theory Exp* 09008:219–228.
- Davenport AP (2012) *Receptor Binding Techniques*, Third. ed, *Methods in Molecular Biology*. Cambridge: Springer.



- David A, Vassilvitskii S (2007) SODA '07: Proceedings of the Eighteenth Annual ACM-SIAM Symposium on Discrete Algorithms. In: The Advantages of Careful Seeding. , pp1027–1035.
- De Vico Fallani F, Richiardi J, Chavez M, Achard S (2014) Graph analysis of functional brain networks: Practical issues in translational neuroscience. *Philos Trans R Soc B Biol Sci* 369.
- de Vito G, Turrini L, Müllenbroich C, Ricci P, Sancataldo G, Mazzamuto G, Tiso N, Sacconi L, Fanelli D, Silvestri L, Vanzi F, Pavone FS (2022) Fast whole-brain imaging of seizures in zebrafish larvae by two-photon light sheet microscopy. *Biomed Opt Express* 13:1516.
- Delgado L, Schmachtenberg O (2008) Immunohistochemical localization of GABA, GAD65, and the receptor subunits GABA $\alpha$ 1 and GABAB1 in the zebrafish cerebellum. *Cerebellum* 7:444–450.
- Demin KA, Kolesnikova TO, Khatsko SL, Meshalkina DA, Efimova E V., Morzherin YY, Kalueff A V. (2017) Acute effects of amitriptyline on adult zebrafish: Potential relevance to antidepressant drug screening and modeling human toxidromes. *Neurotoxicol Teratol* 62:27–33.
- Diaz Verdugo C, Myren-Svelstad S, Aydin E, Van Hoeymissen E, Deneubourg C, Vanderhaeghe S, Vancraeynest J, Pelgrims R, Cosacak MI, Muto A, Kizil C, Kawakami K, Jurisch-Yaksi N, Yaksi E (2019) Glia-neuron interactions underlie state transitions to generalized seizures. *Nat Commun* 10:1–13.
- Divito CB, Underhill SM (2014) Excitatory amino acid transporters: Roles in glutamatergic neurotransmission. *Neurochem Int* 73:172–180.
- Druschky K, Bleich S, Grohmann R, Engel RR, Neyazi A, Stübner S, Toto S (2019) Seizure rates under treatment with antipsychotic drugs: Data from the AMSP project. *World J Biol Psychiatry* 20:732–741.
- Dulhunty AF (2006) Excitation-contraction coupling from the 1950s into the new millennium. *Clin Exp Pharmacol Physiol* 33:763–772.
- Easter A, Bell ME, Damewood JR, Redfern WS, Valentin JP, Winter MJ, Fonck C, Bialecki RA (2009) Approaches to seizure risk assessment in preclinical

drug discovery. *Drug Discov Today*.

Easter A, Sharp TH, Valentin JP, Pollard CE (2007) Pharmacological validation of a semi-automated in vitro hippocampal brain slice assay for assessment of seizure liability. *J Pharmacol Toxicol Methods* 56:223–233.

Edwards JG, Michel WC (2003) Pharmacological characterization of ionotropic glutamate receptors in the zebrafish olfactory bulb. *Neuroscience* 122:1037–1047.

Eid T, Tu N, Lee TSW, Lai JCK (2013) Regulation of astrocyte glutamine synthetase in epilepsy. *Neurochem Int*.

Eimon PM, Ghannad-Rezaie M, De Rienzo G, Allalou A, Wu Y, Gao M, Roy A, Skolnick J, Yanik MF (2018) Brain activity patterns in high-throughput electrophysiology screen predict both drug efficacies and side effects. *Nat Commun* 9.

Elhwuegi AS (2004) Central monoamines and their role in major depression. *Prog Neuro-Psychopharmacology Biol Psychiatry* 28:435–451.

Engel J (1996) Introduction to temporal lobe epilepsy. *Epilepsy Res* 26:141–150.

Erlander MG, Tobin AJ (1991) The structural and functional heterogeneity of glutamic acid decarboxylase: A review. *Neurochem Res* 16:215–226.

Esler MD, Hasking GJ, Willett IR, Leonard PW, Jennings GL (1985) Noradrenaline release and sympathetic nervous system activity. *J Hypertens*.

Falco-Walter JJ, Scheffer IE, Fisher RS (2018) The new definition and classification of seizures and epilepsy. *Epilepsy Res* 139:73–79.

Fan J, Thalody G, Kwagh J, Burnett E, Shi H, Lewen G, Chen SJ, Levesque P (2019) Assessing seizure liability using multi-electrode arrays (MEA). *Toxicol Vitr* 55:93–100.

Favre-Bulle IA, Vanwalleghem G, Taylor MA, Rubinsztein-Dunlop H, Scott EK (2018) Cellular-Resolution Imaging of Vestibular Processing across the Larval Zebrafish Brain. *Curr Biol* 28:3711-3722.e3.

- Fernando JCR, Curzon G (1976) Effect of Aminophylling on Tryptophan and Other Aromatic AminoAcids in Plasma, Brain and Other Tissues and on Brain 5-Hydroxytryptamine Metabolism. *Br J Pharmacol* 58:533–545.
- Feron FJM, Hendriksen JGM, Nicolai J, Vles JSH (2008) New-Onset Seizures: A Possible Association With Clonidine? *Pediatr Neurol* 38:147–149.
- Filip M, Bader M (2009) Overview on 5-HT receptors and their role in physiology and pathology of the central nervous system. *Pharmacol Reports* 61:761–777.
- Fisher RS et al. (2014a) ILAE Official Report: A practical clinical definition of epilepsy. *Epilepsia* 55:475–482.
- Fisher RS (2013) Deep brain stimulation for epilepsy. *Handb Clin Neurol* 116:217–234.
- Fisher RS, Scharfman HE, DeCurtis M (2014b) How Can We Identify Ictal and Interictal Abnormal Activity? *Epilepsia* 55:3–23.
- Fonck C, Cohen BN, Nashmi R, Whiteaker P, Wagenaar DA, Rodrigues-Pinguet N, Deshpande P, McKinney S, Kwoh S, Munoz J, Labarca C, Collins AC, Marks MJ, Lester HA (2005) Novel seizure phenotype and sleep disruptions in knock-in mice with hypersensitive  $\alpha 4^*$  nicotinic receptors. *J Neurosci* 25:11396–11411.
- Fonck C, Pietras MR, Bialecki RA, Easter A (2015) CNS adverse effects: From functional observation battery/Irwin tests to electrophysiology, *Handbook of Experimental Pharmacology*.
- Fournier GN, Materi LM, Semba K, Rasmusson DD (2004) Cortical acetylcholine release and electroencephalogram activation evoked by ionotropic glutamate receptor agonists in the rat basal forebrain. *Neuroscience* 123:785–792.
- Friedman A, Behrens CJ, Heinemann U (2007) Cholinergic dysfunction in temporal lobe epilepsy. *Epilepsia* 48:126–130.
- Friedrich J, Yang W, Soudry D, Mu Y, Ahrens MB, Yuste R, Peterka DS, Paninski L (2017) Multi-scale approaches for high-speed imaging and analysis of large neural populations. *PLoS Comput Biol* 13:1–24.

- Fung M, Thornton A, Mybeck K, Wu JHH, Hornbuckle K, Muniz E (2001) Evaluation of the Characteristics of Safety Withdrawal of Prescription Drugs from Worldwide Pharmaceutical Markets-1960 to 1999. *Ther Innov Regul Sci* 35:293–317.
- Furukawa H, Singh SK, Mancusso R, Gouaux E (2005) Subunit arrangement and function in NMDA receptors. *Nature* 438:185–192.
- Gabazine free base | C<sub>15</sub>H<sub>17</sub>N<sub>3</sub>O<sub>3</sub> - PubChem [WWW Document] (n.d.). URL <https://pubchem.ncbi.nlm.nih.gov/compound/107896#section=Top> (accessed 7.16.18).
- Gangarossa G, Benedetto M Di, O’Sullivan GJ, Dunleavy M, Alcacer C, Bonito-Oliva A, Henshall DC, Waddington JL, Valjent E, Fisone G (2011) Convulsant doses of a dopamine D1 receptor agonist result in erk-dependent increases in Zif268 and Arc/Arg3.1 expression in mouse dentate gyrus. *PLoS One* 6.
- Gao M, Igata H, Takeuchi A, Sato K, Ikegaya Y (2017) Machine learning-based prediction of adverse drug effects: An example of seizure-inducing compounds. *J Pharmacol Sci* 133:70–78.
- Ghannad-Rezaie M, Eimon PM, Wu Y, Yanik MF (2019) Engineering brain activity patterns by neuromodulator polytherapy for treatment of disorders. *Nat Commun* 10.
- Gharedaghi MH, Seyedabadi M, Ghia JE, Dehpour AR, Rahimian R (2014) The role of different serotonin receptor subtypes in seizure susceptibility. *Exp Brain Res* 232:347–367.
- Giacomini ACVV, Bueno BW, Marcon L, Scolari N, Genario R, Demin KA, Kolesnikova TO, Kalueff A V., de Abreu MS (2020) An acetylcholinesterase inhibitor, donepezil, increases anxiety and cortisol levels in adult zebrafish. *J Psychopharmacol* 34:1449–1456.
- Giacomini NJ, Rose B, Kobayashi K, Guo S (2006) Antipsychotics produce locomotor impairment in larval zebrafish. *Neurotoxicol Teratol* 28:245–250.
- Gliske S V., Stacey WC, Lim E, Holman KA, Fink CG (2017) Emergence of Narrowband High Frequency Oscillations from Asynchronous, Uncoupled

Neural Firing. *Int J Neural Syst* 27:1–11.

Goldsmith P, Golder Z, Hunt J, Berghmans S, Jones D, Stables JP, Murphree L, Howden D, Newton PE, Richards FM (2007) GBR12909 possesses anticonvulsant activity in zebrafish and rodent models of generalized epilepsy but cardiac ion channel effects limit its clinical utility. *Pharmacology* 79:250–258.

Gonzalez-Nunez V, Gonzalez-Sarmiento R, Rodríguez RE (2003) Cloning and characterization of a full-length pronociceptin in zebrafish: Evidence of the existence of two different nociceptin sequences in the same precursor. *Biochim Biophys Acta - Gene Struct Expr* 1629:114–118.

Gonzalez-Nuñez V, Marrón Fernández de Velasco E, Arsequell G, Valencia G, Rodríguez RE (2007) Identification of dynorphin a from zebrafish: A comparative study with mammalian dynorphin A. *Neuroscience* 144:675–684.

Gonzalez Nuñez V, Gonzalez Sarmiento R, Rodríguez RE (2003) Characterization of zebrafish proenkephalin reveals novel opioid sequences. *Mol Brain Res* 114:31–39.

Goodfellow M, Rummel C, Abela E, Richardson MP, Schindler K, Terry JR (2016) Estimation of brain network ictogenicity predicts outcome from epilepsy surgery. *Sci Rep* 6:1–13.

Greene DL, Hoshi N (2017) Modulation of Kv7 channels and excitability in the brain. *Cell Mol Life Sci* 74:495–508.

Grienberger C, Konnerth A (2012) Imaging Calcium in Neurons. *Neuron* 73:862–885.

Griffin A, Carpenter C, Liu J, Paterno R, Grone B, Hamling K, Moog M, Dinday MT, Figueroa F, Anvar M, Ononuju C, Qu T, Baraban SC (2021) Phenotypic analysis of catastrophic childhood epilepsy genes. *Commun Biol* 4.

Griffin A, Hamling KR, Knupp K, Hong SG, Lee LP, Baraban SC (2017) Clemizole and modulators of serotonin signalling suppress seizures in Dravet syndrome. *Brain* 140:669–683.

- Griffin AL, Jaishankar P, Grandjean J-M, Olson SH, Renslo AR, Baraban SC (2019) Zebrafish studies identify serotonin receptors mediating antiepileptic activity in Dravet syndrome. *Brain Commun* 1:1–14.
- Guy Edwards J, Glen-Bott M (1987) Nomifensine and Convulsive Seizures. *Hum Exp Toxicol* 6:247–249.
- Hamilton S, Loose M, Qi M, Levey A, Nathanson N (1997) Disruption of the m1 receptor gene ablates muscarinic receptor-dependent M current regulation and seizure. *Proc Natl Acad Sci United States of America* 94:13311–13316.
- Hanada T (2020) Ionotropic Glutamate Receptors in Epilepsy: A Review Focusing on AMPA and NMDA Receptors.
- Hardingham GE, Chawla S, Johnson CM, Bading H (1997) Distinct functions of nuclear and cytoplasmic calcium in the control of gene expression. *Nature* 385:260–265.
- Haumesser JK, Kühn J, Güttler C, Nguyen D, Beck MH, Kühn AA, Riesen C Van (2017) Acute In Vivo Electrophysiological Recordings of Local Field Potentials and Multi-unit Activity from the Hyperdirect Pathway in Anesthetized Rats 1 . Construction of Epidural Ag / AgCl Epidural Electrodes 1–8.
- Haut SR, Seinfeld S, Pellock J (2016) Benzodiazepine use in seizure emergencies: A systematic review. *Epilepsy Behav* 63:109–117.
- Heikamp K, Bajorath J (2014) Support vector machines for drug discovery. *Expert Opin Drug Discov* 9:93–104.
- Herrmann CS, Demiralp T (2005) Human EEG gamma oscillations in neuropsychiatric disorders. *Clin Neurophysiol* 116:2719–2733.
- Higashijima SI, Mandel G, Fetcho JR (2004) Distribution of prospective glutamatergic, glycinergic, and gabaergic neurons in embryonic and larval zebrafish. *J Comp Neurol* 480:1–18.
- Higley MJ (2014) Localized GABAergic inhibition of dendritic Ca<sup>2+</sup> signalling. *Nat Rev Neurosci* 15:567–572.

- Hillman EM, Voleti V, Patel K, Li W, Yu H, Perez-Campos C, Benezra SE, Bruno RM, Galwaduge PT (2018) High-speed 3D imaging of cellular activity in the brain using axially-extended beams and light sheets. *Curr Opin Neurobiol* 50:190–200.
- Hillman EMC, Voleti V, Li W, Yu H (2019) Light sheet Microscopy in Neuroscience. *Annu Rev Neurosci* 42:295–313.
- Hogberg HT, Bal-Price AK (2011) Domoic acid-induced neurotoxicity is mainly mediated by the AMPA/KA receptor: Comparison between immature and mature primary cultures of neurons and glial cells from rat cerebellum. *J Toxicol* 2011.
- Hong SG, Lee P, Baraban SC, Lee LP (2016) A Novel Long-term, Multi-Channel and Non-invasive Electrophysiology Platform for Zebrafish. *Sci Rep* 6:1–10.
- Hoppmann V, Wu JJ, Søviknes AM, Helvik JV, Becker TS (2008) Expression of the eight AMPA receptor subunit genes in the developing central nervous system and sensory organs of zebrafish. *Dev Dyn* 237:788–799.
- Horita A, Weber J (1960) Dephosphorylation of Psilocybin to Psilocin by Alkaline Phosphatase. *Proc Soc Exp Biol Med* 32–34.
- Hortopan GA, Dinday MT, Baraban SC (2010) Zebrafish as a model for studying genetic aspects of epilepsy. *DMM Dis Model Mech* 3:144–148.
- Horzmann KA, Freeman JL (2016) Zebrafish get connected: Investigating neurotransmission targets and alterations in chemical toxicity. *Toxics*.
- Hu C, Flecknell PA, Liles JH (1992) Fentanyl and medetomidine anaesthesia in the rat and its reversal using atipamazole and either nalbuphine or butorphanol. *Lab Anim* 26:15–22.
- Huang LS, Che J (2008) Analysis of variance, coefficient of determination and F-test for local polynomial regression. *Ann Stat* 36:2085–2109.
- Huang ZJ, He XX, Wang FJ, Shen Q (2021) A Real-Time Multi-Stage Architecture for Pose Estimation of Zebrafish Head with Convolutional Neural Networks. *J Comput Sci Technol* 36:434–444.

- Huisken J (2012) Slicing embryos gently with laser light sheets. *BioEssays* 34:406–411.
- Hunyadi B, Siekierska A, Sourbron J, Copmans D, de Witte PAM (2017) Automated analysis of brain activity for seizure detection in zebrafish models of epilepsy. *J Neurosci Methods* 287:13–24.
- Huot P, Fox SH, Brotchie JM (2015) Monoamine reuptake inhibitors in parkinson's disease. *Parkinsons Dis* 2015.
- Irons TD, MacPhail RC, Hunter DL, Padilla S (2010) Acute neuroactive drug exposures alter locomotor activity in larval zebrafish. *Neurotoxicol Teratol* 32:84–90.
- Irwin S (1968) Comprehensive Observational Assessment: Ia. A Systematic, Quantitative Procedure for Assessing the Behavioral and Physiologic State of the Mouse. *Psychopharmacologia* 13:222–257.
- Jacobs J, Wu JY, Perucca P, Zelmann R, Mader M, Dubeau F, Mathern GW, Schulze-Bonhage A, Gotman J (2018) Removing high-frequency oscillations: A prospective multicenter study on seizure outcome. *Neurology* 91:1040–1052.
- Jaiswal AK, Banka H (2018) Epileptic seizure detection in EEG signal using machine learning techniques. *Australas Phys Eng Sci Med* 41:81–94.
- Jiménez-Jiménez D, Nekkare R, Flores L, Chatzidimou K, Bodi I, Honavar M, Mullatti N, Elwes RDC, Selway RP, Valentín A, Alarcón G (2015) Prognostic value of intracranial seizure onset patterns for surgical outcome of the treatment of epilepsy. *Clin Neurophysiol* 126:257–267.
- Jin Z (2011) Muscarine, imidazole, oxazole, and thiazole alkaloids. *Nat Prod Rep* 28:1143–1191.
- Jiruska P, Alvarado-Rojas C, Schevon CA, Staba R, Stacey W, Wendling F, Avoli M (2017) Update on the mechanisms and roles of high-frequency oscillations in seizures and epileptic disorders. *Epilepsia* 58:1330–1339.
- Jiruska P, de Curtis M, Jefferys JGR, Schevon CA, Schiff SJ, Schindler K (2013) Synchronization and desynchronization in epilepsy: Controversies and hypotheses. *J Physiol* 591:787–797.



- Johannessen Landmark C, Henning O, Johannessen SI (2016) Proconvulsant effects of antidepressants — What is the current evidence? *Epilepsy Behav* 61:287–291.
- Johnston GAR (2013) Advantages of an antagonist: Bicuculline and other GABA antagonists. *Br J Pharmacol* 169:328–336.
- Johnston GAR (1996) GABA<sub>A</sub> receptor pharmacology. *Pharmacol Ther* 69:173–198.
- Jordan MI, Mitchell TM (2015) Machine learning: Trends, perspectives, and prospects. *Science* (80- ) 349:255–260.
- Jutkiewicz EM, Baladi MG, Folk JE, Rice KC, Woods JH (2006) The convulsive and electroencephalographic changes produced by nonpeptidic  $\delta$ -opioid agonists in rats: Comparison with pentylentetrazol. *J Pharmacol Exp Ther* 317:1337–1348.
- Kalueff A V., Stewart AM, Gerlai R (2014) Zebrafish as an emerging model for studying complex brain disorders. *Trends Pharmacol Sci* 35:63–75.
- Kamendi HW, Brott DA, Chen Y, Litwin DC, Lengel DJ, Fonck C, Bui KH, Gorko MA, Bialecki RA (2010) Combining radio telemetry and automated blood sampling: A novel approach for integrative pharmacology and toxicology studies. *J Pharmacol Toxicol Methods* 62:30–39.
- Kamour A, Crichton S, Cooper G, Lupton DJ, Eddleston M, Vale JA, Thompson JP, Thomas SHL (2017) Central nervous system toxicity of mefenamic acid overdose compared with other NSAIDs: an analysis of cases reported to the United Kingdom National Poisons Information Service. *Br J Clin Pharmacol* 83:855–862.
- Kandratavicius L, Balista P, Cleiton L-A, Rafael R, Eduardo U, Norberto G-C, Lezio B-J, Joao L (2014) Animal models of epilepsy: Use and limitations [WWW Document]. Dove Press. URL <https://psycnet.apa.org/record/2014-38471-001> (accessed 4.29.22).
- Kaslin J, Panula P (2001) Comparative anatomy of the histaminergic and other aminergic systems in zebrafish (*Danio rerio*). *J Comp Neurol* 440:342–377.
- Katarova Z, Sekerková G, Prodan S, Mugnaini E, Szabó G (2000) Domain-

restricted expression of two glutamic acid decarboxylase genes in midgestation mouse embryos. *J Comp Neurol* 424:607–627.

Kelava I, Lancaster MA (2016) Dishing out mini-brains: Current progress and future prospects in brain organoid research. *Dev Biol* 420:199–209.

Khan KM, Collier AD, Meshalkina DA, Kysil E V., Khatsko SL, Kolesnikova T, Morzherin YY, Warnick JE, Kalueff A V., Echevarria DJ (2017) Zebrafish models in neuropsychopharmacology and CNS drug discovery. *Br J Pharmacol* 174:1925–1944.

Kim H, Kang SH, Kim Soon Ho, Kim Seong Hwan, Hwang J, Kim JG, Han K, Kim J Bin (2021) Drinking coffee enhances neurocognitive function by reorganizing brain functional connectivity. *Sci Rep* 11:1–11.

Kim YH, Lee Y, Kim D, Jung MW, Lee CJ (2010a) Scopolamine-induced learning impairment reversed by physostigmine in zebrafish. *Neurosci Res* 67:156–161.

Kim YH, Lee Y, Lee K, Lee T, Kim YJ, Lee CJ (2010b) Reduced neuronal proliferation by proconvulsant drugs in the developing zebrafish brain. *Neurotoxicol Teratol* 32:551–557.

Kim YJ, Nam RH, Yoo YM, Lee CJ (2004) Identification and functional evidence of GABAergic neurons in parts of the brain of adult zebrafish (*Danio rerio*). *Neurosci Lett* 355:29–32.

Kimura KT, Asada H, Inoue A, Kadji FMN, Im D, Mori C, Arakawa T, Hirata K, Nomura Y, Nomura N, Aoki J, Iwata S, Shimamura T (2019) Structures of the 5-HT 2A receptor in complex with the antipsychotics risperidone and zotepine. *Nat Struct Mol Biol* 26:121–128.

Kirla KT, Groh KJ, Steuer AE, Poetzsch M, Banote RK, Stadnicka-Michalak J, Eggen RIL, Schirmer K, Kraemer T (2016) Zebrafish larvae are insensitive to stimulation by cocaine: Importance of exposure route and toxicokinetics. *Toxicol Sci* 154:183–193.

Kitanaka J, Kitanaka N, Hall FS, Uhl GR, Asano H, Chatani R, Hayata S, Yokoyama H, Tanaka KI, Nishiyama N, Takemura M (2012) Pretreatment with nomifensine or nomifensine analogue 4-phenyl-1,2,3,4-

- tetrahydroisoquinoline augments methamphetamine-induced stereotypical behavior in mice. *Brain Res* 1439:15–26.
- Koenderink JJ, van Doorn AJ (1992) Surface shape and curvature scales. *Image Vis Comput* 10:557–564.
- Koziół E, Józwiak K, Budzyńska B, de Witte PAM, Copmans D, Skalicka-woźniak K (2021) Comparative antiseizure analysis of diverse natural coumarin derivatives in zebrafish. *Int J Mol Sci* 22.
- Kreir M, Van Deuren B, Versweyveld S, De Bondt A, Van den Wyngaert I, Van der Linde H, Lu HR, Teuns G, Gallacher DJ (2018) Do in vitro assays in rat primary neurons predict drug-induced seizure liability in humans? *Toxicol Appl Pharmacol* 346:45–57.
- Kumar SS, Bacci A, Kharazia V, Huguenard JR (2002) A developmental switch of AMPA receptor subunits in neocortical pyramidal neurons. *J Neurosci* 22:3005–3015.
- Kumlien E, Lundberg PO (2010) Seizure risk associated with neuroactive drugs: Data from the WHO adverse drug reactions database. *Seizure* 19:69–73.
- Lawson K (2017) A brief review of the pharmacology of amitriptyline and clinical outcomes in treating fibromyalgia. *Biomedicines* 5.
- Lea IV PM, Custer SJ, Vicini S, Faden AI (2002) Neuronal and glial mGluR5 modulation prevents stretch-induced enhancement of NMDA receptor current. *Pharmacol Biochem Behav* 73:287–298.
- Lee HW, Arora J, Papademetris X, Tokoglu F, Negishi M, Scheinost D, Farooque P, Blumenfeld H, Spencer DD, Constable RT (2014) Altered functional connectivity in seizure onset zones revealed by fMRI intrinsic connectivity. *Neurology* 83:2269–2277.
- Leite J, Bortolotto A, Cavalheiro A (1990) Spontaneous Recurrent Seizures in Rats: An Experimental Model of Partial Epilepsy. *Neurosci Biobehav Rev* 14:511–517.
- Lepousez G, Lledo P-M (2013) Odor Discrimination Requires Proper Olfactory Fast Oscillations in Awake Mice. *Neuron* 80:1010–1024.

- Leira J (2006) Kainate receptor physiology. *Curr Opin Pharmacol* 6:89–97.
- Lévesque M, Avoli M (2019) High-frequency oscillations and focal seizures in epileptic rodents. *Neurobiol Dis* 124:396–407.
- Levin ED, Chen E (2004) Nicotinic involvement in memory function in zebrafish. *Neurotoxicol Teratol* 26:731–735.
- Li P, Shah S, Huang L, Carr AL, Gao Y, Thisse C, Thisse B, Li L (2007) Cloning and spatial and temporal expression of the zebrafish dopamine D1 receptor. *Dev Dyn* 236:1339–1346.
- Libersat F, Pflueger HJ (2004) Monoamines and the Orchestration of Behavior. *Bioscience*.
- Liechti ME (2017) Modern Clinical Research on LSD. *Neuropsychopharmacology* 42:2114–2127.
- Lilley E, Stanford SC, Kendall DE, Alexander SPH, Cirino G, Docherty JR, George CH, Insel PA, Izzo AA, Ji Y, Panettieri RA, Sobey CG, Stefanska B, Stephens G, Teixeira M, Ahluwalia A (2020) ARRIVE 2.0 and the British Journal of Pharmacology: Updated guidance for 2020. *Br J Pharmacol* 177:3611–3616.
- Lin X, Duan X, Jacobs C, Ullmann J, Chan CY, Chen S, Cheng SH, Zhao WN, Poduri A, Wang X, Haggarty SJ, Shi P (2018) High-throughput brain activity mapping and machine learning as a foundation for systems neuropharmacology. *Nat Commun* 9:1–12.
- Liu J, Baraban SC (2019) Network properties revealed during multi-scale calcium imaging of seizure activity in Zebrafish. *eNeuro* 6.
- Lopes MA, Perani S, Yaakub SN, Richardson MP, Goodfellow M, Terry JR (2019) Revealing epilepsy type using a computational analysis of interictal EEG. *Sci Rep* 9:1–10.
- Löscher W (2017) Animal Models of Seizures and Epilepsy: Past, Present, and Future Role for the Discovery of Antiseizure Drugs. *Neurochem Res* 42:1873–1888.
- Lundt A, Wormuth C, Siwek ME, Müller R, Ehninger D, Henseler C, Broich K,

- Papazoglou A, Weiergräber M (2016) EEG radiotelemetry in small laboratory rodents: A powerful state-of-the art approach in neuropsychiatric, neurodegenerative, and epilepsy research. *Neural Plast* 2016:10–12.
- Ma HC, Dohi S, Wang YF, Ishizawa Y, Yanagidate F (2001) The antinociceptive and sedative effects of carbachol and oxycodone administered into brainstem pontine reticular formation and spinal subarachnoid space in rats. *Anesth Analg* 92:1307–1315.
- Ma J, Leung LS (2010) Kindled seizure in the prefrontal cortex activated behavioral hyperactivity and increase in accumbens gamma oscillations through the hippocampus. *Behav Brain Res* 206:68–77.
- Mackenzie L, Medvedev A, Hiscock JJ, Pope KJ, Willoughby JO (2002) Picrotoxin-induced generalised convulsive seizure in rat: Changes in regional distribution and frequency of the power of electroencephalogram rhythms. *Clin Neurophysiol* 113:586–596.
- MacRae CA, Peterson RT (2015) Zebrafish as tools for drug discovery. *Nat Rev Drug Discov* 14:721–731.
- Madsen U, Stensbol T, Krogsgaard-Larsen P (2012) Inhibitors of AMPA and Kainate Receptors. *Curr Med Chem* 8:1291–1301.
- Maehara S, Hikichi H, Satow A, Okuda S, Ohta H (2008) Antipsychotic property of a muscarinic receptor agonist in animal models for schizophrenia. *Pharmacol Biochem Behav* 91:140–149.
- Maia GH, Brazete CS, Soares JI, Luz LL, Lukoyanov N V. (2017) Serotonin depletion increases seizure susceptibility and worsens neuropathological outcomes in kainate model of epilepsy. *Brain Res Bull* 134:109–120.
- Mann KD, Hoyt Carlton, Feldman Shaina, Blunt Lachelle, Raymond Aaron, Page-mccaw PS, Kd M, Hoyt C, Feldman S, Blunt L, Raymond A (2010) Cardiac response to startle stimuli in larval zebrafish: sympathetic and parasympathetic components. *Am J Physiol* 1288–1297.
- Manogaran G, Lopez D (2018) Health data analytics using scalable logistic regression with stochastic gradient descent. *Int J Adv Intell Paradig*

10:118–132.

Markgraf CG, DeBoer E, Zhai J, Cornelius L, Zhou YY, MacSweeney C (2014) Assessment of seizure liability of Org 306039, a 5-HT<sub>2c</sub> agonist, using hippocampal brain slice and rodent EEG telemetry. *J Pharmacol Toxicol Methods* 70:224–229.

Martin SC, Heinrich G, Sandell JH (1998) Sequence and expression of glutamic acid decarboxylase isoforms in the developing zebrafish. *J Comp Neurol* 396:253–266.

MATLAB signal processing toolbox 8.4 (2020) R2020a The Mathworks Inc., Natick, Massachusetts.

MATLAB version 9.8.0 (2020) R2020a The Mathworks Inc., Natick, Massachusetts.

MATLAB wavelet toolbox 5.4 (2020) R2020a The Mathworks Inc., Natick, Massachusetts.

Maurice T, Su TP (2009) The pharmacology of sigma-1 receptors. *Pharmacol Ther* 124:195–206.

Maximino C, Gomes M, Araujo J, Oliveira KRM, Herculano AM, Stewart AM, Kyzar EJ, Cachat J, Kalueff A V. (2013a) The serotonergic system of zebrafish: Genomics, neuroanatomy and neuropharmacology. *Serotonin Biosynthesis, Regul Heal Implic* 53–67.

Maximino C, Herculano AM (2010) A review of monoaminergic neuropsychopharmacology in zebrafish. *Zebrafish* 7:359–378.

Maximino C, P. Costa B, G. Lima M (2016) A Review of Monoaminergic Neuropsychopharmacology in Zebrafish, 6 Years Later: Towards Paradoxes and their Solution. *Curr Psychopharmacol* 5:96–138.

Maximino C, Puty B, Benzecry R, Araújo J, Lima MG, De Jesus Oliveira Batista E, Renata De Matos Oliveira K, Crespo-Lopez ME, Herculano AM (2013b) Role of serotonin in zebrafish (*Danio rerio*) anxiety: Relationship with serotonin levels and effect of buspirone, WAY 100635, SB 224289, fluoxetine and para-chlorophenylalanine (pCPA) in two behavioral models. *Neuropharmacology* 71:83–97.

- McCarroll MN, Gendele L, Kinser R, Taylor J, Bruni G, Myers-Turnbull D, Helsell C, Carbajal A, Rinaldi C, Kang HJ, Gong JH, Sello JK, Tomita S, Peterson RT, Keiser MJ, Kokel D (2019) Zebrafish behavioural profiling identifies GABA and serotonin receptor ligands related to sedation and paradoxical excitation. *Nat Commun* 10.
- McIntyre DC, Edson N (1982) Effect of norepinephrine depletion on dorsal hippocampus kindling in rats. *Exp Neurol* 77:700–704.
- McLean DL, Fetcho JR (2004) Ontogeny and innervation patterns of dopaminergic, noradrenergic, and serotonergic neurons in larval zebrafish. *J Comp Neurol* 480:38–56.
- Mégevand P, Quairiaux C, Lascano AM, Kiss JZ, Michel CM (2008) A mouse model for studying large-scale neuronal networks using EEG mapping techniques. *Neuroimage* 42:591–602.
- Migault G, van der Plas TL, Trentesaux H, Panier T, Candelier R, Proville R, Englitz B, Debrégeas G, Bormuth V (2018) Whole-Brain Calcium Imaging during Physiological Vestibular Stimulation in Larval Zebrafish. *Curr Biol* 28:3723-3735.e6.
- Miyazawa H, Okumura K, Hiyoshi K, Maruyama K, Kakinuma H, Amo R, Okamoto H, Yamasu K, Tsuda S (2018) Optical interrogation of neuronal circuitry in zebrafish using genetically encoded voltage indicators. *Sci Rep* 8:1–10.
- Mochizuki T, Yamatodani A, Okakura K, Takemura M, Inagaki N, Wada H (1991) In vivo release of neuronal histamine in the hypothalamus of rats measured by microdialysis. *Naunyn Schmiedeberg's Arch Pharmacol* 343:190–195.
- Moffett SX, O'Malley SM, Man S, Hong D, Martin J V. (2017) Dynamics of high frequency brain activity. *Sci Rep* 7:4–8.
- Møller M, Baeres FM (2002) The anatomy and innervation of the mammalian pineal gland. *Cell Tissue Res* 309:139–150.
- Møller MF (1993) A scaled conjugate gradient algorithm for fast supervised learning. *Neural Networks* 6:525–533.

- Moser VC (2000) Observational batteries in neurotoxicity testing. *Int J Toxicol* 19:407–411.
- Moser VC, Becking GC, Macphail RC, Kulig BM (1997) The IPCS collaborative study on neurobehavioral screening models. *Fundam Appl Toxicol* 35:143–151.
- Mueller T, Vernier P, Wullimann MF (2006) A phylotypic stage in vertebrate brain development: GABA cell patterns in zebrafish compared with mouse. *J Comp Neurol* 494:620–634.
- Nabinger DD, Altenhofen S, Bonan CD (2020) Zebrafish models: Gaining insight into purinergic signaling and neurological disorders. *Prog Neuro-Psychopharmacology Biol Psychiatry* 98.
- Nakai J, Ohkura M, Imoto K (2001) A high signal-to-noise  $ca^{2+}$  probe composed of a single green fluorescent protein. *Nat Biotechnol* 19:137–141.
- Nam RH, Kim W, Lee CJ (2004) NMDA receptor-dependent long-term potentiation in the telencephalon of the zebrafish. *Neurosci Lett* 370:248–251.
- Nasr GE, Badr EA, Joun C (2002) Cross Entropy Error Function in Neural Networks: Forecasting Gasoline Demand. *FLAIRS Conf* 381–384.
- Neath AA, Cavanaugh JE (2012) The Bayesian information criterion: Background, derivation, and applications. *Wiley Interdiscip Rev Comput Stat* 4:199–203.
- Neher E, Sakaba T (2008) Multiple Roles of Calcium Ions in the Regulation of Neurotransmitter Release. *Neuron* 59:861–872.
- Nehlig A, Lucignani G, Kadekaro M, Porrino LJ, Sokoloff L (1984) Effects of Acute Administration of Caffeine on Local Cerebral Glucose Utilization in the Rat. *Eur J Pharmacol* 101:91–100.
- Nichols D, Nichols C (2008) Serotonin Receptors. *Chem Rev* 1614–1641.
- Olszewski M, Piasecka J, Goda SA, Kasicki S, Hunt MJ (2013) Antipsychotic compounds differentially modulate high-frequency oscillations in the rat



nucleus accumbens: A comparison of first- and second-generation drugs. *Int J Neuropsychopharmacol* 16:1009–1020.

Onakpoya IJ, Heneghan CJ, Aronson JK (2016) Post-marketing withdrawal of 462 medicinal products because of adverse drug reactions: A systematic review of the world literature. *BMC Med* 14:1–11.

Ota T, Shinotoh H, Fukushi K, Kikuchi T, Sato K, Tanaka N, Shimada H, Hirano S, Miyoshi M, Arai H, Suhara T, Irie T (2010) Estimation of plasma IC<sub>50</sub> of donepezil for cerebral acetylcholinesterase inhibition in patients with Alzheimer disease using positron emission tomography. *Clin Neuropharmacol* 33:74–78.

Ozawa S, Kamiya H, Tsuzuki K (1998) Glutamate receptors in the mammalian central nervous system. *Prog Neurobiol* 54:581–618.

Panula P, Sallinen V, Sundvik M, Kolehmainen J, Torkko V, Tiittula A, Moshnyakov M, Podlasz P (2006) Modulatory neurotransmitter systems and behavior: Towards zebrafish models of neurodegenerative diseases. *Zebrafish* 3:235–247.

Paoletti P, Bellone C, Zhou Q (2013) NMDA receptor subunit diversity: Impact on receptor properties, synaptic plasticity and disease. *Nat Rev Neurosci* 14:383–400.

Pardo-Peña K, Medina-Ceja L, Morales-Villagrán A (2014) Serotonin modulates fast ripple activity in rats with spontaneous recurrent seizures. *Brain Res* 1583:211–219.

Patten SA, Ali DW (2007) AMPA receptors associated with zebrafish Mauthner cells switch subunits during development. *J Physiol* 581:1043–1056.

Paulson C, Chien D, Lin F, Seidlits S, Cai Y, Sargolzaei S, Harris NG, Giza CC (2018) A Novel Modular Headmount Design for non-invasive Scalp EEG Recordings in Awake Animal Models. *Conf Proc . Annu Int Conf IEEE Eng Med Biol Soc IEEE Eng Med Biol Soc Annu Conf* 2018:5422–5425.

Peitsaro N, Sundvik M, Anichtchik O V, Kaslin J, Panula P (2007) Identification of zebrafish histamine H<sub>1</sub>, H<sub>2</sub> and H<sub>3</sub> receptors and effects of histaminergic ligands on behavior. *Biochem Pharmacol* 73:1205–1214.

- Perucca P, Dubeau F, Gotman J (2014) Intracranial electroencephalographic seizure-onset patterns: Effect of underlying pathology. *Brain* 137:183–196.
- Pesola GR, Avasarala J (2002) Bupropion seizure proportion among new-onset generalized seizures and drug related seizures presenting to an emergency department. *J Emerg Med* 22:235–239.
- Pinal-Seoane N, Martin IR, Gonzalez-Nuñez V, Fernandez de Velasco EM, Alvarez FA, Sarmiento RG, Rodriguez RE (2006) Characterization of a new duplicate  $\delta$ -opioid receptor from zebrafish. *J Mol Endocrinol* 37:391–403.
- Pinion J, Walsh C, Goodfellow M, Randall AD, Tyler CR, Winter MJ (2022) Differential Electrographic Signatures Generated by Mechanistically-Diverse Seizurogenic Compounds in the Larval Zebrafish Brain. *Eneuro* 9:ENEURO.0337-21.2022.
- Pitrone PG, Schindelin J, Stuyvenberg L, Preibisch S, Weber M, Eliceiri KW, Huisken J, Tomancak P (2013) OpenSPIM: An open-access light sheet microscopy platform. *Nat Methods* 10:598–599.
- Polster T (2019) Individualized treatment approaches: Fenfluramine, a novel antiepileptic medication for the treatment of seizures in Dravet syndrome. *Epilepsy Behav* 91:99–102.
- Postlethwait J, Amores A, Force A, Yan YL (1999) The zebrafish genome. *Methods Cell Biol* 60:149–163.
- Poulos CX, Cappell H (1991) Homeostatic Theory of Drug Tolerance: A General Model of Physiological Adaptation. *Psychol Rev* 98:390–408.
- Preller KH, Burt JB, Ji JL, Schleifer CH, Adkinson BD, Stämpfli P, Seifritz E, Repovs G, Krystal JH, Murray JD, Vollenweider FX, Anticevic A (2018) Changes in global and thalamic brain connectivity in LSD-induced altered states of consciousness are attributable to the 5-HT<sub>2A</sub> receptor. *Elife* 7:1–31.
- Prescott MJ, Lidster K (2017) Improving quality of science through better animal welfare: The NC3Rs strategy. *Lab Anim (NY)* 46:152–156.
- Ram CVS (2010) Beta-blockers in hypertension. *Am J Cardiol* 106:1819–1825.

- Reichert C, Reichert P, Monnet-Tschudi F, Kupferschmidt H, Ceschi A, Rauber-Lüthy C (2014) Seizures after single-agent overdose with pharmaceutical drugs: Analysis of cases reported to a poison center. *Clin Toxicol* 52:629–634.
- Renier C, Faraco JH, Bourgin P, Motley T, Bonaventure P, Rosa F, Mignot E (2007) Genomic and functional conservation of sedative-hypnotic targets in the zebrafish. *Pharmacogenet Genomics* 17:237–253.
- Renner U, Oertel R, Kirch W (2005) Pharmacokinetics and pharmacodynamics in clinical use of scopolamine. *Ther Drug Monit* 27:655–665.
- Reynaud EG, Peychl J, Huisken J, Tomancak P (2014) Guide to light sheet microscopy for adventurous biologists. *Nat Methods* 12:30–34.
- Richetti SK, Blank M, Capiotti KM, Piato AL, Bogo MR, Vianna MR, Bonan CD (2011) Quercetin and rutin prevent scopolamine-induced memory impairment in zebrafish. *Behav Brain Res* 217:10–15.
- Rickli A, Liakoni E, Hoener MC, Liechti ME (2018) Opioid-induced inhibition of the human 5-HT and noradrenaline transporters in vitro: link to clinical reports of serotonin syndrome. *Br J Pharmacol* 175:532–543.
- Rico EP, de Oliveira DL, Rosemberg DB, Mussulini BH, Bonan CD, Dias RD, Wofchuk S, Souza DO, Bogo MR (2010) Expression and functional analysis of Na<sup>+</sup>-dependent glutamate transporters from zebrafish brain. *Brain Res Bull* 81:517–523.
- Ridler T, Matthews P, Phillips KG, Randall AD, Brown JT (2018) Initiation and slow propagation of epileptiform activity from ventral to dorsal medial entorhinal cortex is constrained by an inhibitory gradient. *J Physiol* 596:2251–2266.
- Rihel J, Prober DA, Arvanites A, Lam K, Zimmerman S, Jang S, Haggarty SJ, Kokel D, Rubin LL, Peterson RT, Schier AF (2010) Zebrafish behavioral profiling links drugs to biological targets and rest/wake regulation. *Science* (80-) 327:348–351.
- Rijkers K, Moers-Hornikx VMP, Hemmes RJ, Aalbers MW, Temel Y, Vles JSH, Hoogland G (2015) Sustained Reduction of Cerebellar Activity in

- Experimental Epilepsy. Biomed Res Int 2015.
- Ritter J, Flower R, Henderson G, Loke Y, MacEwan D, Rang H (2018) Rang and Dale's Pharmacology, Ninth. ed. Elsevier.
- Rodriguez RE, Gonzalez-Nunez V (2006) Characterization of Opioid-binding sites in zebrafish brain. *J Pharmacol Exp Ther* 316:900–904.
- Rosch R, Hunter P, Friston K, Meyer M (2018) Calcium imaging and dynamic causal modelling reveal brain-wide changes in effective connectivity and synaptic dynamics during epileptic seizures. *PLoS One* 160259.
- Ross JF (2000) ECOs, FOBs, and UFOs: Making Sense of Observational Data. *Toxicol Pathol* 28:132–136.
- Rossi LF, Kullmann DM, Wykes RC (2018) The enlightened brain: Novel imaging methods focus on epileptic networks at multiple scales. *Front Cell Neurosci* 12:1–8.
- Ruder S (2016) An overview of gradient descent optimization algorithms 1–14.
- Ruffmann C, Bogliun G, Beghi E (2006) Epileptogenic drugs: A systematic review. *Expert Rev Neurother* 6:575–589.
- Ruiz-Oliveira J, Silva PF, Luchiarini AC (2019) Coffee time: Low caffeine dose promotes attention and focus in zebrafish. *Learn Behav* 47:227–233.
- Ruuskanen Jori O, Peitsaro N, Kaslin JVM, Panula P, Scheinin M (2005) Expression and function of  $\alpha_2$ -adrenoceptors in zebrafish: drug effects, mRNA and receptor distributions. *J Neurochem* 94:1559–1569.
- Ruuskanen Jori O., Peitsaro N, Kaslin JVM, Panula P, Scheinin M (2005) Expression and function of  $\alpha_2$ -adrenoceptors in zebrafish: Drug effects, mRNA and receptor distributions. *J Neurochem* 94:1559–1569.
- Sacconi L, Silvestri L, Rodríguez EC, Armstrong GAB, Pavone FS, Shrier A, Bub G (2022) KHz-rate volumetric voltage imaging of the whole Zebrafish heart. *Biophys Reports* 2:100046.
- Sadek B, Saad A, Latac G, Kuder K, Olejarz A, Karcz T, Stark H, Kieć-Kononowicz K (2016) Non-imidazole-based histamine H3 receptor antagonists with anticonvulsant activity in different seizure models in male

- adult rats. *Drug Des Devel Ther* 10:3879–3898.
- Saitoh A, Tominaga H, Ogawa Y, Irukayama-Tomobe Y, Yamada M, Yanagisawa M, Nagase H (2018) Effects of the delta opioid receptor agonist KNT-127 on electroencephalographic activity in mice. *Pharmacol Reports* 70:350–354.
- Sakaguchi H, Kadoshima T, Soen M, Narii N, Ishida Y, Ohgushi M, Takahashi J, Eiraku M, Sasai Y (2015) Generation of functional hippocampal neurons from self-organizing human embryonic stem cell-derived dorsomedial telencephalic tissue. *Nat Commun* 6.
- Sakata T, Yoshimatsu H, Kurokawa M (1997) Hypothalamic neuronal histamine: Implications of its homeostatic control of energy metabolism. *Nutrition* 13:403–411.
- Samokhina E, Samokhin A (2018) Neuropathological profile of the pentylenetetrazol (PTZ) kindling model. *Int J Neurosci* 128:1086–1096.
- Sanchez-Simon FM, Rodriguez RE (2008) Developmental expression and distribution of opioid receptors in zebrafish. *Neuroscience* 151:129–137.
- Scharfman HE (2007) The neurobiology of epilepsy. *Curr Neurol Neurosci Rep* 7:348–354.
- Scherkl R, Hashem A, Frey HH (1991) Histamine in brain - its role in regulation of seizure susceptibility. *Epilepsy Res* 10:111–118.
- Schoepp DD, Smith CL, Lodge D, Millar JD, Leander JD, Sacaan AI, Lunn WHW (1991) D,L-(Tetrazol-5-yl) glycine: a novel and highly potent NMDA receptor agonist. *Eur J Pharmacol* 203:237–243.
- Scholtes F, Renier W, Meinardi H (1996) Non-convulsive status epilepticus: Causes, treatment, and outcome in 65 patients. *J Neurol Neurosurg Psychiatry* 61:93–95.
- Schwartz M, Scott D. (1974) Aminophylline-Induce Seizures. *Epilepsia* 15:501–505.
- Schwartzkroin PA (1994) Role of the hippocampus in epilepsy. *Hippocampus* 4:239–242.

- Schweitzer J, Driever W (2009) Development of the dopamine systems in Zebrafish. *Adv Exp Med Biol* 651:1–14.
- Schweitzer J, Löhr H, Filippi A, Driever W (2012) Dopaminergic and noradrenergic circuit development in zebrafish. *Dev Neurobiol* 72:256–268.
- Sellers EM (1988) Alcohol, barbiturate and benzodiazepine withdrawal syndromes: Clinical management. *Cmaj* 139:113–120.
- Sette WF (1989) Adoption of new guidelines and data requirements for more extensive neurotoxicity testing under FIFRA. *Toxicol Ind Health* 5:181–194.
- Shabel SJ (2014) antidepressant treatment 1494.
- Shang Y, Filizola M (2015) Opioid receptors: Structural and mechanistic insights into pharmacology and signaling. *Eur J Pharmacol* 763:206–213.
- Shemesh OA et al. (2020) Precision Calcium Imaging of Dense Neural Populations via a Cell-Body-Targeted Calcium Indicator. *Neuron* 107:470-486.e11.
- Shen WW (1999) A history of antipsychotic drug development. *Compr Psychiatry* 40:407–414.
- Shigemoto R, Kinoshita A, Wada E, Nomura S, Ohishi H, Takada M, Flor PJ, Neki A, Abe T, Nakanishi S, Mizuno N (1997) Differential presynaptic localization of metabotropic glutamate receptor subtypes in the rat hippocampus. *J Neurosci* 17:7503–7522.
- Shiri Z, Manseau F, Lévesque M, Williams S, Avoli M (2015) Interneuron activity leads to initiation of low-voltage fast-onset seizures. *Ann Neurol* 77:541–546.
- Sieghart W (1994) Pharmacology of benzodiazepine receptors: An update. *J Psychiatry Neurosci* 19:24–29.
- Simonato M, Romualdi P (1996) Dynorphin and epilepsy. *Prog Neurobiol* 50:557–583.
- Smith RS, Araneda RC (2010) Cholinergic Modulation of Neuronal Excitability in the Accessory Olfactory Bulb 2963–2974.

- Snead OC (1986) Opiate-induced seizures: A study of  $\mu$  and  $\delta$  specific mechanisms. *Exp Neurol* 93:348–358.
- Snell LD, Su-Jin Yi, Johnson KM (1988) Comparison of the effects of MK-801 and phencyclidine on catecholamine uptake and NMDA-induced norepinephrine release. *Eur J Pharmacol* 145:223–226.
- Soderpalm B, Engel J (1988) Biphasic effects of clonidine on conflict behavior: involvement of different alpha-adrenoceptors. *Pharmacol Biochem Behav* 30:471–477.
- Sourbron J, Smolders I, de Witte P, Lagae L (2017) Pharmacological analysis of the anti-epileptic mechanisms of fenfluramine in *scn1a* mutant zebrafish. *Front Pharmacol* 8:1–13.
- Sperk G (1994) Kainic acid seizures in the rat. *Prog Neurobiol* 42:1–32.
- Staley K (2015) Molecular mechanisms of epilepsy. *Nat Neurosci* 18:367–372.
- Starr M (1996) The role of dopamine in epilepsy. *Synapse* 159–194.
- Stefanescu RA, Shivakeshavan RG, Talathi SS (2012) Computational models of epilepsy. *Seizure* 21:748–759.
- Steidl EM, Neveu E, Bertrand D, Buisson B (2006) The adult rat hippocampal slice revisited with multi-electrode arrays. *Brain Res* 1096:70–84.
- Stein C, Hassan AHS, Lehrberger K, Stein C, Giefing J, Yassouridis A (1993) Local analgesic effect of endogenous opioid peptides. *Lancet* 342:321–324.
- Stevens CF, Wesseling JF (1998) Activity-dependent modulation of the rate at which synaptic vesicles become available to undergo exocytosis. *Neuron* 21:415–424.
- Subach OM et al. (2020) Novel genetically encoded bright positive calcium indicator *ncamp7* based on the mneongreen fluorescent protein. *Int J Mol Sci* 21:1–24.
- Südhof TC (2012) Calcium control of neurotransmitter release. *Cold Spring Harb Perspect Biol* 4.

- Sumiyoshi A, Riera JJ, Ogawa T, Kawashima R (2011) A mini-cap for simultaneous EEG and fMRI recording in rodents. *Neuroimage* 54:1951–1965.
- Sun D, Kermani M, Hudson M, He X, Unnithan RR, French C (2020) Effects of antipsychotic drugs and potassium channel modulators on cognition-related local field potential spectral properties in mouse hippocampus and frontal cortex. *bioRxiv*.
- Sundvik M, Kudo H, Toivonen P, Rozov S, Chen Y, Panula P (2011) The histaminergic system regulates wakefulness and orexin / hypocretin neuron development via histamine receptor H1 in zebrafish. *FASEB J* 5:4338–4347.
- Suryanto ME, Audira G, Uapipatanakul B, Hussain A, Saputra F, Siregar P, Chen KHC, Hsiao C Der (2021) Antidepressant screening demonstrated non-monotonic responses to amitriptyline, amoxapine and sertraline in locomotor activity assay in larval zebrafish. *Cells* 10.
- Swanson GT, Sakai R (2009) Marine Toxins as Research Tools, *Marine Toxins as Research Tools*.
- Talos DM, Chang M, Kosaras B, Fitzgerald E, Murphy A, Folkerth RD, Jensen FE (2013) Antiepileptic effects of levetiracetam in a rodent neonatal seizure model. *Pediatr Res* 73:24–30.
- Tao KM (2002) A closer look at the radial basis function (RBF) networks 401–405.
- Tao L, Lauderdale JD, Sornborger AT (2011) Mapping functional connectivity between neuronal ensembles with larval zebrafish transgenic for a ratiometric calcium indicator. *Front Neural Circuits* 5:1–11.
- Tay TL, Ronneberger O, Ryu S, Nitschke R, Driever W (2011) Comprehensive catecholaminergic projectome analysis reveals single-neuron integration of zebrafish ascending and descending dopaminergic systems. *Nat Commun* 2.
- Thomas AJ, Hailey DW, Stawicki TM, Wu P, Coffin AB, Rubel EW, Raible DW, Simon JA, Ou HC (2013) Functional mechanotransduction is required for



- cisplatin-induced hair cell death in the zebrafish lateral line. *J Neurosci* 33:4405–4414.
- Thundiyil JG, Kearney TE, Olson KR (2007) Evolving epidemiology of drug-induced seizures reported to a Poison Control Center System. *J Med Toxicol* 3:15–19.
- Thurman DJ, Logroscino G, Beghi E, Hauser WA, Hesdorffer DC, Newton CR, Scorza FA, Sander JW, Tomson T (2017) The burden of premature mortality of epilepsy in high-income countries: A systematic review from the Mortality Task Force of the International League Against Epilepsy. *Epilepsia* 58:17–26.
- Todd AJ, Watt C, Spike RC, Sieghart W (1996) Colocalization of GABA, glycine, and their receptors at synapses in the rat spinal cord. *J Neurosci* 16:974–982.
- Tortella F, Echevarria E, Robles L, Mosberg H, Holaday J (1988) Anticonvulsant Effects of Mu (DAGO) and Delta (DPDPE) Enkephalins in Rats. *Peptides* 9:1177–1181.
- Tortella F, Mosberg H, Robles L (1987) Evidence for Mu Opioid Receptor Mediation of Enkephalin-Induced Electroencephalographic Seizures. *J Pharmacol Exp Ther* 240:571–577.
- Tran S, Fulcher N, Nowicki M, Desai P, Tsang B, Facciol A, Chow H, Gerlai R (2017) Time-dependent interacting effects of caffeine, diazepam, and ethanol on zebrafish behaviour. *Prog Neuro-Psychopharmacology Biol Psychiatry* 75:16–27.
- Tricco AC, Soobiah C, Berliner S, Ho JM, Ng CH, Ashoor HM, Chen MH, Hemmelgarn B, Straus SE (2013) Efficacy and safety of cognitive enhancers for patients with mild cognitive impairment: A systematic review and meta-analysis. *Cmaj* 185:1393–1401.
- Tsverava L, Kandashvili M, Margvelani G, Lortkipanidze T, Gamkrelidze G, Lepsveridze E, Kokaia M, Solomonias R (2019) Long-Term Effects of Myoinositol on Behavioural Seizures and Biochemical Changes Evoked by Kainic Acid Induced Epileptogenesis. *Biomed Res Int* 2019.

- Tukker AM, Van Kleef RGDM, Wijnolts FMJ, De Groot A, Westerink RHS (2020) Towards animal-free neurotoxicity screening: Applicability of hiPSC-derived neuronal models for in vitro seizure liability assessment. *ALTEX* 37:121–135.
- Turrini L, Fornetto C, Marchetto G, Müllenbroich MC, Tiso N, Vettori A, Resta F, Masi A, Mannaioni G, Pavone FS, Vanzi F (2017) Optical mapping of neuronal activity during seizures in zebrafish. *Sci Rep* 7:1–12.
- Turrini L, Sorelli M, de Vito G, Credi C, Tiso N, Vanzi F, Pavone FS (2022) Multimodal Characterization of Seizures in Zebrafish Larvae. *Biomedicines* 10:1–16.
- Twele F, Bankstahl M, Klein S, Kerstin R (2015) The AMPA receptor antagonist NBQX exerts anti-seizure but not antiepileptogenic effects in the intrahippocampal kainate mouse model of mesial temporal lobe epilepsy. *Neuropharmacology* 1–9.
- Uehara T, Yamasaki T, Okamoto T, Koike T, Kan S, Miyauchi S, Kira JI, Tobimatsu S (2014) Efficiency of a small-world brain network depends on consciousness level: A resting-state fMRI study. *Cereb Cortex* 24:1529–1539.
- Usman SM, Khalid S, Akhtar R, Bortolotto Z, Bashir Z, Qiu H (2019) Using scalp EEG and intracranial EEG signals for predicting epileptic seizures: Review of available methodologies. *Seizure* 71:258–269.
- Valletta JJ, Torney C, Kings M, Thornton A, Madden J (2017) Applications of machine learning in animal behaviour studies. *Anim Behav* 124:203–220.
- van den Heuvel MP, Hulshoff Pol HE (2010) Exploring the brain network: A review on resting-state fMRI functional connectivity. *Eur Neuropsychopharmacol* 20:519–534.
- van der Walt S, JL S, J N-I, F B, JD W, N Y, E G, T Y (2014) scikit-image: image processing in Python. *PeerJ*.
- van Koert RR, Bauer PR, Schuitema I, Sander JW, Visser GH (2018) Caffeine and seizures: A systematic review and quantitative analysis. *Epilepsy Behav* 80:37–47.

- van Mierlo P, Papadopoulou M, Carrette E, Boon P, Vandenberghe S, Vonck K, Marinazzo D (2014) Functional brain connectivity from EEG in epilepsy: Seizure prediction and epileptogenic focus localization. *Prog Neurobiol* 121:19–35.
- Vanwalleghem G, Schuster K, Taylor MA, Favre-Bulle IA, Scott EK (2020) Brain-wide mapping of water flow perception in zebrafish. *J Neurosci* 40:4130–4144.
- Vermoesen K, Serruys AK, Loyens E, Afrikanova T, Massie A, Schallier A, Michotte Y, Crawford AD, Esguerra C V, Witte PAM De, Smolders I, Clinckers R (2011) Assessment of the convulsant liability of antidepressants using zebrafish and mouse seizure models. *Epilepsy Behav* 22:450–460.
- Volkman K, Rieger S, Babaryka A, Köster RW (2008) The zebrafish cerebellar rhombic lip is spatially patterned in producing granule cell populations of different functional compartments. *Dev Biol* 313:167–180.
- von Coburg Y, Kottke T, Weizel L, Ligneau X, Stark H (2009) Potential utility of histamine H3 receptor antagonist pharmacophore in antipsychotics. *Bioorganic Med Chem Lett* 19:538–542.
- Wang S, Yang DM, Rong R, Zhan X, Xiao G (2019) Pathology Image Analysis Using Segmentation Deep Learning Algorithms. *Am J Pathol* 189:1686–1698.
- Wang Y, Zhou D, Yang X, Xu X, Ren L, Yu T, Zhou W, Shao X, Yang Z, Wang S, Cao D, Liu C, Kwan SY, Xiang J (2020) Expert consensus on clinical applications of high-frequency oscillations in epilepsy. *Acta Epileptol* 2.
- Waring MJ, Arrowsmith J, Leach AR, Leeson PD, Mandrell S, Owen RM, Pairaudeau G, Pennie WD, Pickett SD, Wang J, Wallace O, Weir A (2015) An analysis of the attrition of drug candidates from four major pharmaceutical companies. *Nat Rev Drug Discov* 14:475–486.
- Wasserman S, Faust K (1994a) *Social Network Analysis: Methods and Applications*.
- Wasserman S, Faust K (1994b) *Social Network Analysis: Methods and*

Applications.

Wasserman S, Faust K (1994c) *Social Network Analysis: Methods and Applications*.

Weiergräber M, Henry M, Krieger A, Kamp M, Radhakrishnan K, Hescheler J, Schneider T (2006) Altered seizure susceptibility in mice lacking the Cav2.3 E-type Ca<sup>2+</sup> channel. *Epilepsia* 47:839–850.

Weinshenker D, Szot P (2002) The role of catecholamines in seizure susceptibility: New results using genetically engineered mice. *Pharmacol Ther* 94:213–233.

Wilcoxon rank sum test - MATLAB ranksum - MathWorks United Kingdom [WWW Document] (n.d.). URL <https://uk.mathworks.com/help/stats/ranksum.html> (accessed 7.29.21).

Williams FE, Messer WS (2004) Muscarinic acetylcholine receptors in the brain of the zebrafish (*Danio rerio*) measured by radioligand binding techniques. *Comp Biochem Physiol - C Toxicol Pharmacol* 137:349–353.

Winter MJ, Pinion J, Tochwin A, Takesono A, Ball JS, Grabowski P, Metz J, Trznadel M, Tse K, Redfern WS, Hetheridge MJ, Goodfellow M, Randall AD, Tyler CR (2021) Functional brain imaging in larval zebrafish for characterising the effects of seizurogenic compounds acting via a range of pharmacological mechanisms. *Br J Pharmacol* 9:1–19.

Winter MJ, Redfern WS, Hayfield AJ, Owen SF, Valentin J, Hutchinson TH (2008) Validation of a larval zebrafish locomotor assay for assessing the seizure liability of early-stage development drugs. *J Pharmacol Toxicol Methods* 57:176–187.

Winter MJ, Windell D, Metz J, Matthews P, Pinion J, Brown JT, Hetheridge MJ, Ball JS, Owen SF, Redfern WS, Moger J, Randall AD, Tyler CR (2017) 4-Dimensional Functional Profiling in the Convulsant-Treated Larval Zebrafish Brain. *Sci Rep* 7:1–16.

Wokosin DL, Loughrey CM, Smith GL (2004) Characterization of a Range of Fura Dyes with Two-Photon Excitation. *Biophys J* 86:1726–1738.

Wullimann MF, Rupp B, Reichert H (1996) *Neuroanatomy of the Zebrafish* [224]

Brain: A Topological Atlas, 1st ed. Birkhauser.

- Wyart C, Bene F Del, Warp E, Scott EK, Trauner D, Baier H, Isacoff EY (2009) Optogenetic dissection of a behavioural module in the vertebrate spinal cord. *Nature* 461:407–410.
- Wykes RC, Khoo HM, Caciagli L, Blumenfeld H, Golshani P, Kapur J, Stern JM, Bernasconi A, Dedeurwaerdere S, Bernasconi N (2019) WONOEP appraisal: Network concept from an imaging perspective. *Epilepsia* 60:1293–1305.
- Yajima Y, Narita M, Takahashi-Nakano Y, Misawa M, Nagase H, Mizoguchi H, Tseng LF, Suzuki T (2000) Effects of differential modulation of  $\mu$ -,  $\delta$ - and  $\kappa$ -opioid systems on bicuculline-induced convulsions in the mouse. *Brain Res* 862:120–126.
- Yang Y, Liu N, He Y, Liu Y, Ge L, Zou L, Song S, Xiong W, Liu X (2018) Improved calcium sensor GCaMP-X overcomes the calcium channel perturbations induced by the calmodulin in GCaMP. *Nat Commun* 9.
- Yokoi R, Shibata M, Odawara A, Ishibashi Y, Nagafuku N, Matsuda N, Suzuki I (2021) Analysis of signal components < 500 Hz in brain organoids coupled to microelectrode arrays: A reliable test-bed for preclinical seizure liability assessment of drugs and screening of antiepileptic drugs. *Biochem Biophys Reports* 28:101148.
- Zalesky A, Fornito A, Bullmore ET (2010) Network-based statistic: Identifying differences in brain networks. *Neuroimage* 53:1197–1207.
- Zarowny L, Aggarwal A, Rutten VMS, Kolb I, Patel R, Huang HY, Chang YF, Phan T, Kanyo R, Ahrens MB, Allison WT, Podgorski K, Campbell RE (2020) Bright and High-Performance Genetically Encoded Ca<sup>2+</sup>Indicator Based on mNeonGreen Fluorescent Protein. *ACS Sensors* 5:1959–1968.
- Zhang H, Li W, Xie Y, Wang WJ, Li LL, Yang SY (2011) Rapid and accurate assessment of seizure liability of drugs by using an optimal support vector machine method. *Toxicol Vitr* 25:1848–1854.
- Zou L, Xue Y, Jones M, Heinbockel T, Ying M, Zhan X (2018) The Effects of Quinine on Neurophysiological Properties of Dopaminergic Neurons.

Neurotox Res 34:62–73.